Modeling properties of the vapor-liquid interface using classical density functional theory and density gradient theory

Von der Fakultät Energie-, Verfahrens- und Biotechnik der Universität Stuttgart zur Erlangung der Würde eines Doktors der Ingenieurwissenschaft (Dr.-Ing.) genehmigte Abhandlung

Vorgelegt von

Jonas Mairhofer

aus Stuttgart

Hauptberichter: Prof. Dr.-Ing. Joachim Groß
Mitberichter: Prof. Dr. habil. rer. nat. Sabine Enders

Tag der mündlichen Prüfung: 19.11.2018

Institut für Technische Thermodynamik und Thermische Verfahrenstechnik der Universität Stuttgart

2018

Eidesstattliche Erklärung zu meiner Dissertation mit dem Titel:

Modeling properties of the vapor-liquid interface using classical density functional theory and density gradient theory

Hiermit erkläre ich, dass ich die beigefügte Dissertation selbstständig verfasst und keine anderen als die angegebenen Hilfsmittel genutzt habe. Alle wörtlich oder inhaltlich übernommenen Stellen habe ich als solche gekennzeichnet.

Ich versichere außerdem, dass ich die beigefügte Dissertation nur in diesem und keinem anderen Promotionsverfahren eingereicht habe und dass diesem Promotionsverfahren keine endgültig gescheiterten Promotionsverfahren vorausgegangen sind.

Ort, Datum	Unterschrift

Contents

List of symbols

a	Helmholtz energy density
A	Helmholtz energy
AAD	average absolute deviation
B	approximation of inverse of Jacobian in quasi Newton methods
c	influence parameter of DGT
d	temperature dependent segment diameter, PCP-SAFT
D	size of computation domain
D	sum of functional derivatives, modified iSAFT
f	norm of the residual
F	residual
F'	Jacobian
Δh^{lv}	enthalpy of evaporation
I	integral expressions, modified iSAFT
k	Boltzmann constant
k_{ij}	binary interaction parameter between component i and j
m	segment number, PCP-SAFT
m	number of old iterations used in current solution update
M	molecular mass
n	weighted density of Fundamental Measure Theory
N	number of components in the system
NS	number of segments in the system
$n_{grid},\ n_s,\ n_z$	number of discretization steps
p	pressure
$\mathbf{r}$	coordinate vector
s	variable of path function algorithm for DGT
T	temperature
Q	quadrupole moment
V	volume
V	external potential
y	cavity correlation function
z	spatial coordinate perpendicular to the interface

Greek letters

α	numerical parameter of Anderson mixing method
α	variable of path function algorithm for DGT
α	index for weighted densities of Fundamental Measure Theory
β	numerical parameter of Anderson mixing method
β_{ij}	binary interaction parameter for the cross influence parameter between component i and j
$\beta_{\alpha\beta}$	group-group interaction parameter between groups of type α and β, GC-PCP-SAFT
γ	surface tension
Γ	set of all association sites on a component or segment, PCP-SAFT
ϵ	depth of pair potential, PCP-SAFT
ϵ	numerical parameter in inexact Newton method
$\epsilon^{A_iB_i}$	association energy of association sites on molecule i, PCP-SAFT
η	forcing term in inexact Newton method
$\kappa^{A_iB_i}$	effective association volume of association sites on molecule i, PCP-SAFT
λ	average density at contact-distance
λ	damping parameter for solution update
Λ	De Broglie wavelength
μ	chemical potential
μ	dipole moment
ξ	moments of density, PCP-SAFT
ρ	density
σ	segment diameter, PCP-SAFT
τ_T	relaxation constant of thermostat
τ_p	relaxation constant of barostat
ϕ	individualization parameter, GC-PCP-SAFT
χ	fraction of non-bonded association sites, PCP-SAFT
ψ	parameter of Helmholtz energy functional for dispersive interactions
ω	acentric factor
ω	weight functions of Fundamental Measure Theory
$\Delta\omega$	grand potential energy density difference
Ω	grand potential energy

Subscripts

0	evaluated for homogeneous fluid
1	reference component
α	index of weighted densities of Fundamental Measure Theory
c	value at critical point
i, j, k	indices for components
is, ks	indices for segments
r	reduced variable

Superscripts

0	initial guess
$assoc$	association contribution, PCP-SAFT
$bulk$	evaluated for bulk phase
$calc$	calculated value
$chain$, HC	chain contribution, PCP-SAFT
$contact$	evaluated at contact distance
$dipole$, dd	dipolar contribution, PCP-SAFT
$disp$	dispersive contribution, PCP-SAFT
dq	dipolar-quadrupolar contribution, PCP-SAFT
hs	hard sphere contribution, PCP-SAFT
ig	ideal gas contribution
k	value at iteration k
l, liq	liquid phase
min	minimum value
new	value at current grid point
old	value at previous grid point
$polar$	all polar contributions, PCP-SAFT
qq	quadrupolar contribution, PCP-SAFT
res	residual part
v, vap	vapor phase

Kurzzusammenfassung

Für die Modellierung vielzähliger Prozesse der chemischen Industrie ist die genaue Vorhersage von Grenzflächeneigenschaften eine wichtige Voraussetzung. In dieser Arbeit werden sowohl die klassische Dichtefunktionaltheorie, als auch die Dichtegradiententheorie verwendet, um die Oberflächenspannung sowie die Dichteprofile über die Phasengrenzfläche für eine Vielzahl von Systemen zu bestimmen. Grenzen der Anwendbarkeit beider Modelle sowie Aspekte wie die effiziente Lösung des nichtlinearen Gleichungssystems zur Bestimmung der Gleichgewichtsdichteprofile mit der klassischen Dichtefunktionaltheorie und der praktische Nutzen eines binären Korrekturparameters in der Kombinationsregel des Kreuzeinflussparameters für die Dichtegradiententheorie werden behandelt. Der Anwendungsbereich der klassischen Dichtefunktionaltheorie wird erweitert auf Stoffe, deren thermodynamischen Eigenschaften nur über Gruppenbeitragsmethoden zugänglich sind. Hierfür wird ein Helmholtzenergiefunktional entwickelt, welches konsistent zum heterosegment-basierten Gruppenbeitragsmodell der PCP-SAFT Zustandsgleichung ist. Die Ergebnisse dieser Arbeit zeigen, dass die Vorhersage der Oberflächenspannung aus der klassischen Dichtefunktionaltheorie für die meisten Systeme so genau ist - oder sogar genauer - als Ergebnisse der Dichtegradiententheorie mit an experimentelle Oberflächenspannungsdaten angepasstem Einflussparameter.

Summary

The accurate prediction of interfacial properties is an important requirement in modeling many processes of chemical industry. In this thesis, classical density functional theory and density gradient theory are applied to determine surface tension and the interfacial density profiles for a variety of systems. Limitations of both models are addressed and aspects such as the efficient solution of the non-linear system of equations to obtain the equilibrium density profiles by classical density functional theory as well as the practical utility of a binary correction parameter in the combining rule for the cross-influence parameter of density gradient theory are presented. Furthermore, the range of applicability of classical density functional theory is extended to compounds whose thermodynamic properties can only be obtained by group-contribution methods. This is achieved by developing a Helmholtz energy functional consistent with the heterosegmented group-contribution PCP-SAFT equation of state. Results of this work show that for most systems, surface tension predicted by classical density functional theory is as accurate, or even more accurate, as values obtained from density gradient theory with the component specific influence parameters adjusted to experimental surface tension data.

Journal publications

This thesis led to the following publications:

- Chapter 2: Mairhofer, Gross: Modeling of interfacial properties of multicomponent systems using density gradient theory and PCP-SAFT, Fluid Phase Equilibria, 439, 2017, 31-42

- Chapter 3: Mairhofer, Gross: Numerical aspects of classical density functional theory for one-dimensional vapor-liquid interfaces, Fluid Phase Equilibria, 444, 2017, 1-12

- Chapter 4: Mairhofer, Gross: Modeling properties of the one-dimensional vapor-liquid interface: Application of classical density functional and density gradient theory, Fluid Phase Equilibria, 458, 2018, 243-252

- Chapter 5: Mairhofer, Xiao, Gross: A classical Density Functional Theory for Vapor-Liquid Interfaces consistent with the heterosegmented group-contribution Perturbed-Chain Polar Statistical Associating Fluid Theory, Fluid Phase Equilibria, 472, 2018, 117-127

- Chapter 6: Mairhofer, Gross: Identifying pure component parameters of an analytic equation of state using experimental surface tension or molecular simulations with a transferable force field, Industrial & Engineering Chemistry Research, 2018, submitted

The chapters 2 to 6 present literal quotes of the published work. Any addition with respect to the published work is marked. Any deletion is indicated with square brackets as ‚[...]'. Cross-references between chapters of this thesis, which are added to the published version of the text to increase readability, are marked by square brackets. The Supporting Informations to the single chapters are presented in the Appendix of this thesis.

Acknowledgements

First and foremost, I would like to express my gratitude to Joachim Groß for his supervision and motivation during my work on this thesis. I very much appreciate the chance you gave me to work on this interesting topic and also your encouragement to explore and follow my research interests. In the four years of working with you, I learned a lot more than what is written on the following pages.
I would also like to thank everybody else of the ITT team for creating this great atmosphere at the institute that made the work on this thesis all the more fun!
Furthermore, thank you to all the partners involved in the MoDeNa project for this interesting collaboration. And of course I am indebted to my friends and family and especially my wife Deysi for their support and understanding during the last four years.

Chapter 1

Introduction

Processes, where phenomena occurring at the interface between a vapor and a liquid phase have a determining impact on the overall process performance, are ubiquitous in the chemical industry. Interfacial properties such as surface tension play a governing role for the hydrodynamics of multi-phase flow e.g. in distillation columns, film reactors, evaporators and condensers and thus strongly impact the central step of these applications: the interfacial heat and mass transfer. Determination of surface tension is thus a crucial step in understanding, modeling and optimizing these processes.
The experimental determination of surface tension is tedious and expensive. Furthermore, the interfacial density profiles, which reveal details at the molecular level e.g. the accumulation of certain components at the interface, can only be determined indirectly and with great uncertainty by experimental methods. The models applied and developed in this thesis aim at providing surface tension as well as information on the vapor-liquid interface at the molecular length scale. The knowledge gained from their predictions can then be used for optimization at the process level.

1.1 Phenomenology of the vapor-liquid interface

In a heterogeneous system at equilibrium, consisting of a liquid and its coexisting vapor, the thermodynamic properties are constant within the liquid and the gas phase and both phases are separated by an interface. Properties such as density may change drastically across interfaces. From a macroscopic perspective, these changes appear as sharp jumps. However, for the vapor-liquid interface, it was already postulated by Laplace and Poisson in the early 19th century [1] that density changes continuously across the interface. Josiah Willard Gibbs, in the time around 1876, wrote his influential article-series *On the Equilibrium of Heterogeneous Substances* that is based on continuous transitions of thermodynamic properties across an interface on the microscopic scale. This was confirmed experimentally more than a century later using optical reflectivity measurements

[2, 3, 4]. This implies that a transition layer exists where density changes from the value of the liquid phase to the value of the gas phase. The forces acting on molecules inside this layer differ significantly from the forces acting on molecules in the liquid or vapor bulk phases far away from the interface. Interactions between molecules can be split in a short-range repulsive contribution which determines the structure of dense fluids and a longer-ranged attractive part which forms a uniform background potential [5]. In bulk phases, molecules are surrounded isotropically by other molecules and the resulting force vector on the molecules averaged over time is zero [6]. Interfaces, on the other hand, are not isotropic. Within the range of the attractive interactions, there are more molecules to the liquid side of the interface than to the vapor side. There is thus a net force vector acting on molecules in the transition layer and work must be done to move molecules from the bulk liquid to the interface. The macroscopic equivalent of this energy required to increase the interface is called surface tension γ and its value is a direct measure for the forces acting on the molecular level.

A thermodynamic definition of γ follows from the fundamental equations, e.g. the Gibbs energy G,

$$dG = -S\mathrm{d}T + V\mathrm{d}p + \sum \mu_i \mathrm{d}N_i + \left(\frac{\partial G}{\partial A}\right)_{T,p,N_i} \mathrm{d}A \tag{1.1}$$

with entropy S, temperature T, pressure p, volume V, chemical potential and particle number of component i, μ_i and N_i, respectively, as well as interfacial area A, as $\gamma = \left(\frac{\partial G}{\partial A}\right)_{T,p,N_i}$. Surface tension is thus defined as the change of Gibbs energy related to a change in interfacial area at constant T, p and N_i.

For a system at equilibrium, G is minimal and for a given value of surface tension γ, the system will minimize its interfacial area A. The same follows from the remaining fundamental equations for systems at equilibrium for specified conditions other than p and T.

The definition of surface tension γ given by eq. 1.1 is valid for the planar interfaces studied in this work. A definition of γ for the more general case of curved interfaces can be found in the study of Rehner and Gross [7].

1.2 Measuring interfacial properties

1.2.1 Surface tension

Experimental methods for surface tension can be classified as static or dynamic. From static methods, the value of surface tension is obtained for a system which has reached its equilibrium state. Dynamic methods measure the course of surface tension over time while the system approaches its equilibrium state, e.g. while large surface-active substances

are still diffusing towards their preferred location at the interface. In this thesis, only equilibrium surface tension results are of concern.

Many different static methods exist. Widely applied is the *method of capillary rise*, where surface tension is determined from the rise of a liquid in a narrow capillary tube. It is considered the simplest and most accurate method for liquids which do not form an appreciable capillary-liquid contact angle [8]. From the Young-Laplace equation for the pressure difference across a curved surface and the condition of mechanical equilibrium, surface tension γ is obtained as [9]

$$\gamma = \frac{rhg\Delta\rho}{2\cos\theta} \tag{1.2}$$

where r and h denote the radius of the capillary and the rise of the liquid in the capillary, respectively, g is the acceleration of gravity, θ is the fluid-capillary contact angle and $\Delta\rho$ is the density difference between the liquid and the coexisting vapor phase.

The *pendant drop method* uses information of the shape of a droplet hanging from a capillary [10]. The shape of the droplet is recorded optically and surface tension can be obtained by solving a set of differential equations arising from the Young-Laplace equation as well as the influence of gravitational forces on the droplet shape. Further alternative methods include the method of weight of a drop, ring detachment methods or the method of maximum bubble pressure [11]. Large sets of experimental surface tension for many compounds and mixtures can be found in the compilation of Jasper [8] and the book of Lechner et al. [11] or in databases such as the Design Institute for Physical Properties (DIPPR) [12] or the Dortmund Data Bank [13].

1.2.2 Interfacial density profiles

Optical measurement techniques such as reflectivity measurements can be applied to obtain information on the structure of interfaces such as the thickness of the interface and the interfacial density profiles. First results are due to Webb an coworkers [2, 3, 4]. The general procedure can be outlined as follows [3]: one first assumes a certain functional form for the interfacial density profiles $\rho(z)$, where z denotes the direction normal to the interface. Plausible candidates are for example a hyperbolic form

$$\rho(z) = \frac{1}{2}(\rho^{liq} + \rho^{vap}) + \frac{1}{2}(\rho^{liq} - \rho^{vap})\tanh\left(2z/L\right) \tag{1.3}$$

the error function

$$\rho(z) = \frac{1}{2}(\rho^{liq} + \rho^{vap}) + \frac{1}{2}(\rho^{liq} - \rho^{vap})\mathrm{erf}\left(\pi^{1/2}z/L\right) \tag{1.4}$$

an exponential form

$$\rho(z) = \begin{cases} \rho^{vap} + \frac{1}{2}(\rho^{liq} - \rho^{vap})\exp\left(2z/L\right), & z < 0 \\ \rho^{vap} - \frac{1}{2}(\rho^{liq} - \rho^{vap})\exp\left(-2z/L\right), & z \geq 0 \end{cases} \tag{1.5}$$

or a profile proposed by Fisk and Widom [14]

$$\rho(z) = \frac{1}{2}(\rho^{liq} + \rho^{vap}) + \frac{\frac{1}{2}(\rho^{liq} - \rho^{vap})\sqrt{2}\tanh\left(6^{1/2}z/L\right)}{\left(3 - \left(\tanh\left(6^{1/2}z/L\right)\right)^2\right)^{1/2}} \tag{1.6}$$

where ρ^{liq} and ρ^{vap} denote the liquid and vapor bulk densities, respectively. The value of the parameter L may be defined in several ways to ensure comparability of the different ansatz functions [3]. The assumption is made that the indices of refraction $n(z)$ at any given location in the interface are proportional to the local density $\rho(z)$. It is then possible to calculate the interfacial normal incidence reflectivity profiles of the assumed model functions for $\rho(z)$. Comparing these calculated reflectivity profiles to measured values, the best ansatz function can be identified and a good guess of the actual density profile is obtained. Results for sulphur hexafluoride [4] and the binary mixture methanol-cyclohexane [3] show that the error function (eq. 1.4) and the function of Fisk and Widom (eq. 1.6) are in better agreement with the measured reflectivity profiles than eqs. 1.3 and 1.5. Alternative measurement techniques to study interfaces in detail include specular neutron reflection [15] or X-ray reflection [16]. Furthermore, infrared-visible sum-frequency analysis [17, 18] can be applied to study the orientation of polar molecules such as alcohols at the interface.

1.3 Engineering models for surface tension

Many simple engineering models to determine surface tension have been proposed. Probably the oldest one is the so called parachor method of Macleod and Sudgen [19, 20]. In its final form, surface tension γ is determined from the value of the parachor P and the densities of the corresponding liquid and vapor phases, ρ^{liq} and ρ^{vap}, respectively, as

$$\gamma(T) = \left[P\left(\rho^{liq}(T) - \rho^{vap}(T)\right)\right]^4 \tag{1.7}$$

The value of P is calculated as the sum of the single contributions from the structural groups that make up the molecule. Parachor values for a large number of structural groups adjusted to surface tension data of the DIPPR database can be found in the work of Knotts et al. [21]. Several extensions of the parachor method to mixtures exist [22, 23, 24] which differ in the mixing rules applied to the parachor and the value of the scaling exponent (in the original form of the parachor method, the scaling exponent is 4, eq. 1.7). However, one fundamental problem arises when the parachor method is applied

to mixtures [6]: the composition in the interface may be very different from the composition in the bulk phases. Mixing rules weighting the contributions of the single components based on the vapor and liquid compositions therefore often produce unsatisfactory results.

Corresponding state theory offers an alternative to determine surface tension. Based on the work of van der Waals, Guggenheim [25] proposed the relationship

$$\gamma(T) = k_0 \left(1 - \frac{T}{T_c}\right)^r \tag{1.8}$$

where $r = 11/9$, $k_0 = (V_c)^{2/3/T_c}$ [6] and T_c and V_c denote the critical temperature and volume, respectively. However, accurate results can only be obtained for very simple molecules such as argon, nitrogen or oxygen [25]. In a different approach based on the corresponding state principle, Hirschfelder et al. [26] introduced the concept of reference fluids. The surface tension of a given compound i is then obtained as

$$\gamma_i(T) = \left(\frac{T_c^i}{T_c^{ref}}\right) \left(\frac{V_c^{ref}}{V_c^i}\right)^{2/3} \gamma^{ref} \left(\frac{T \cdot T_c^{ref}}{T_c^i}\right) \tag{1.9}$$

The superscript ref indicates properties that have to be evaluated for the reference fluid. Several modifications of eq. 1.9 have been proposed [27, 28, 29] to overcome the limited number of compounds which can accurately be described by eq. 1.9. However, the problem of choosing a suitable reference fluid remains.

Besides equations based on quantitative structure–property relationship such as the parachor method or expressions derived from the corresponding state principle, a great variety of empirical correlations for surface tension exists in the literature [30, 31, 32, 33, 34, 35]. A common drawback of most simple engineering equations for surface tension is their need for liquid and vapor densities or critical properties as input. These properties have to be known experimentally or obtained by auxiliary methods. Furthermore, their predictive capabilities for mixtures are very limited. Additionally, these simple equations can only provide values for surface tension but no information on microscopic properties such as the interfacial density profiles.

1.4 Perturbed-Chain Polar Statistical Associating Fluid Theory

The Perturbed-Chain Polar Statistical Associating Fluid Theory (PCP-SAFT) [36, 37, 38, 39, 40] is applied in this thesis to determine the equilibrium properties of coexisting vapor and liquid phases. Furthermore, the models to determine interfacial properties presented in section 1.5 also apply or are developed to be consistent with PCP-SAFT.

The development of PCP-SAFT is based on the repetitive application of a perturbation approach. The goal of perturbation theory is to obtain the thermodynamic properties of a target fluid which interacts via the potential U^{target} from a reference fluid with well known properties and interaction potential U^{ref}. The difference between both potentials represents the perturbation $U^{pert} = U^{target} - U^{ref}$. For pairwise additive and spherically symmetric perturbing potentials $U^{pert} = \sum_{i>j} u^{pert}(r_{ij})$, where r_{ij} denotes the distance between particles i and j, Zwanzig [41] developed the so called high-temperature expansion which leads to the following expression for the Helmholtz energy A of the target fluid [42]

$$\frac{A^{target}}{NkT} = \frac{A^{ref}}{NkT} + \frac{A^{pert}}{NkT} = \frac{A^{ref}}{NkT} + \frac{1}{2}\beta\rho \int u^{pert}(r) g^{ref}(r) \mathrm{d}r + \mathcal{O}(\beta^2) \tag{1.10}$$

where $\beta = 1/kT$ with temperature T and Boltzmann's constant k, $\rho = N/V$ denotes the number density and $g^{ref}(r)$ is the pair correlation function of the reference fluid. Contributions beyond the first-order term generally also require higher-order correlation functions of the reference fluid. The expansion given by eq. 1.10 converges the quicker, the more the correlation functions of the reference and the target fluid agree. A successful application of perturbation theory for target and reference fluids where this is not the case is the Thermodynamic Perturbation Theory (TPT) of Wertheim [43, 44, 45, 46]: TPT allows to treat fluids with highly directional attractive forces using the hard-sphere model as the reference fluid. Depending on the strength of these attractive forces, they can model hydrogen bonding or cause complete polymerization of the hard-sphere monomers to chain-fluids. In both cases, the correlation functions of the target fluid and the hard-sphere reference fluid differ significantly [47].

Based on Wertheim's results, Chapman et al. [48, 49] and Jackson et al. [50] developed the Statistical Associating Fluid Theory (SAFT) which results in Helmholtz energy contributions for the formation of repulsive chains from hard-sphere segments [48, 51], A^{HC}, and association (hydrogen bonding) between segments [51, 52], A^{Assoc}. The Helmholtz energy of the hard-sphere reference fluid, A^{HS}, can be obtained from the accurate equation of state presented by Boublik [53] and Mansoori et al. [54].

In PCP-SAFT, the contribution to the Helmholtz energy due to dispersive interactions between the chain molecules, A^{Disp}, are treated as a perturbation to the hard-chain reference fluid using the second-order perturbation theory of Barker and Henderson [42, 55] which does not require higher-order correlation functions of the reference fluid beyond the pair correlation function. The perturbing potential is of Lennard-Jones type. The integrals over the pair correlation function of the reference fluid and the perturbing potential in the expansion of the perturbation (as shown for the first-order term in eq. 1.10) are approximated as power-series in density and the coefficients of these power-series are adjusted to experimental vapor pressure and PvT data of n-alkanes [36].

The Helmholtz energy contributions of dipolar-dipolar, A^{dd}, quadrupolar-quadrupolar, A^{qq}, and dipolar-quadrupolar, A^{dq}, interactions were developed by Gross [39], Gross and Vrabec [38] and Vrabec and Gross [40] using a third-order perturbation presented by Stell et al. [56, 57] to the two-center Lennard-Jones fluid. The integrals over the correlation functions of the reference fluid and the polar perturbing potential are approximated as power-series in density with parameters which depend on the elongation of the molecule and constants that are adjusted to results of molecular simulations.
The final expression for the residual Helmholtz energy of PCP-SAFT $A^{res} \equiv A(T, \rho, x) - A^{IG}(T, \rho, x)$, where A^{IG} denotes the Helmholtz energy of an ideal gas, is given by the sum

$$A^{res} = A^{HS} + A^{HC} + A^{Disp} + A^{Assoc} + A^{dd} + A^{qq} + A^{dq} \tag{1.11}$$

A non-associating, non-polar compound i is characterized by three parameters in PCP-SAFT: the segment number m_i, the segment diameter σ_i and the dispersive energy parameter ϵ_i. To include associative interactions, two additional parameters are required: the energy parameter $\epsilon_{A_iB_i}$ characterizing the association strength and the association volume $\kappa_{A_iB_i}$. Here, A and B denote association sites located on compound i. The aforementioned parameters are usually regressed to experimental vapor pressure and liquid density data. For polar compounds, also the dipolar and/or quadrupolar moments, μ_i and Q_i, need to be specified. For both, literature values can be used. For mixtures, appropriate combining rules have to be applied to the pure-component parameters [36, 37].
A group-contribution PCP-SAFT (GC-PCP-SAFT) has been developed by Gross et al. [58] and Sauer et al. [59]. The core idea of group-contribution methods is to assume that the properties of a molecule can be determined as a function of the functional groups which make up the molecule. Only parameters for the distinct functional groups are then required and component-specific equation of state parameters are obsolete.

1.5 Fundamentals of classical Density Functional Theory and Density Gradient Theory

The shortcomings of simple engineering models for surface tension presented in section 1.3 clearly reveal the need for more predictive and comprehensive models. Classical density functional theory (DFT) and density gradient theory (DGT) are two approaches that meet these requirements. Both approaches do not rely on auxiliary models and allow to obtain not only the value of surface tension but also the interfacial density profiles. In this section, the basic equations of DFT and DGT are summarized. Both approaches are applied to study the one-dimensional vapor-liquid interface of a system of N components. The value of temperature T is specified and by choosing a suitable computational domain,

which has to accommodate the interface, the volume V of the system is also known. Only systems at thermodynamic equilibrium are considered, i.e. the chemical potential μ_i of every component i is constant throughout the system. The equilibrium properties of the coexisting vapor and liquid phases are determined by a preceding flash calculation.

Volume, temperature and chemical potential are the natural variables of the grand potential Ω, which, in the absence of an external field, is defined as

$$\Omega[\{\rho_k\}] = A[\{\rho_k\}] - \sum_i^N \int \mu_i \rho_i(\mathbf{r}) \mathrm{d}\mathbf{r} \tag{1.12}$$

where $A[\{\rho_k\}]$ is the intrinsic Helmholtz energy of the system. The square brackets make the functional dependency of Ω and A on the density profiles explicit, the curly brackets denote the dependency on all species-density profiles $\rho_i(\mathbf{r})$ and k is a generic component index. For brevity, the dependencies of Ω and A on T, μ_i and V are omitted. For the imposed variables $\{\mu_k, T, V\}$, the density profiles ρ_k are internal degrees of freedom of the considered system. In equilibrium, $\Omega[\{\rho_k\}]$ reaches its minimum value and the functional derivatives with respect to the systems internal degrees of freedom, i.e. the species-density profiles $\rho_k(\mathbf{r})$, vanish

$$\frac{\delta\Omega]\{\rho_k\}}{\delta\rho_i(\mathbf{r})} = \frac{\delta A[\{\rho_k\}]}{\delta\rho_i(\mathbf{r})} - \mu_i = 0, \quad i = 1, ..., N. \tag{1.13}$$

From eqs. 1.12 and 1.13, the working equations of DFT and DGT are derived. Both approaches only differ in the way the intrinsic Helmholtz energy $A[\{\rho_k\}]$ is determined. This said, it should be pointed out that the classification of DFT and DGT as two distinct models is not clear-cut as shown by Evans [60]. Rather, density functional theory can be seen as a generalization of density gradient theory.

1.5.1 Density Gradient Theory

Density gradient theory dates back to the work of van der Waals [61] and was later reformulated by Cahn and Hilliard [62]. In DGT, the local Helmholtz energy density a of the inhomogeneous fluid at position $\mathbf{r}$ is developed as an expansion about the local density approximation $a_0(\{\rho_k\})$ truncated after the square density gradient term. Odd terms in the expansion, such as the first order term, vanish, which is understood because the Helmholtz energy has to be invariant towards the orientation of the coordinate system. The value of a is then obtained as the sum of the Helmholtz energy density of a hypothetical homogeneous fluid with density $\rho_k = \rho_k(\mathbf{r})$ and a correction term to account for the inhomogeneity [62]

$$a\left(\{\rho_k\},\{\nabla\rho_k\}\right) = a_0(\{\rho_k\}) + \frac{1}{2}\sum_i^N\sum_j^N c_{ij}\nabla\rho_i\nabla\rho_j \tag{1.14}$$

with the local density gradient $\nabla\rho_i$ and the influence parameter c_{ij}. Density gradient theory thus only requires the value of the local Helmholtz energy density of the homogeneous fluid $a_0(\{\rho_k\})$, which can be obtained from a bulk equation of state, as well as a value for the influence parameter c_{ij}. The equation, of course, is an approximation, if c_{ij} is treated as a function of temperature only, because higher order terms are neglected (or if c_{ij} is even assumed constant altogether, as usually done in DGT applications). Theoretically derived expressions exist to calculate the influence parameter from the direct correlation function of the homogeneous fluid [60, 63, 64]. However, the direct correlation function is tedious to obtain and in practical application, the value of the pure-component values, c_{ii}, are usually regressed to experimental surface tension data. This procedure to determine c_{ii} is also adopted in this thesis and PCP-SAFT is applied to calculate $a_0(\{\rho_k\})$. With eq. 1.14 and eq. 1.12, the grand potential of the system is given by

$$\Omega = \int\left(a_0(\{\rho_k\}) + \frac{1}{2}\sum_i^N\sum_j^N c_{ij}\nabla\rho_i\nabla\rho_j - \sum_i^N\mu_i\rho_i\right)\mathrm{d}\mathbf{r} \tag{1.15}$$

The equilibrium density profiles minimize Ω. For variational problems of the type given by eq. 1.15, where the integrand $\mathcal{L}$ is of the form $\mathcal{L} = \mathcal{L}\left(\mathbf{r},\{\rho_k(\mathbf{r})\},\nabla\{\rho_k(\mathbf{r})\}\right)$, the optimal solution has to satisfy the Euler-Lagrange equations [65]

$$\frac{\partial\mathcal{L}}{\partial\rho_i} - \nabla\cdot\frac{\partial\mathcal{L}}{\partial\nabla\rho_i} = 0, \quad i = 1,...,N \tag{1.16}$$

for every component i at any location $\mathbf{r}$. It is common practice in DGT to assume density-independent and temperature-independent influence parameters. For density-independent and symmetric ($c_{ij} = c_{ji}$) influence parameters, the Euler-Lagrange equations for the equilibrium density profiles for a flat vapor-liquid interface, where properties vary only along the z-axis normal to the interface, take the form

$$\frac{\partial a_0(\{\rho_k\})}{\partial\rho_i} - \mu_i - \sum_j^N c_{ij}\frac{\partial^2\rho_j}{\partial z^2} = 0, \quad i = 1,...,N. \tag{1.17}$$

The system is thought to expand towards the liquid bulk phase for $z\to\infty$ and towards the vapor bulk phase for $z\to-\infty$. The boundary conditions of eq. 1.17 are thus $\rho_i(z\to\infty) = \rho_i^{liq}$, $\rho_i(z\to-\infty) = \rho_i^{vap}$. Several approaches have been developed to solve this system of non-linear second-order partial differential equations: the frequently applied reference component approach and the path function approach of Liang et al. [66] reduce eq. 1.17 to a set of algebraic equations by introducing a reference function which

changes monotonically across the interface and requiring the cross-influence parameter to be calculated by the geometric combining rule $\left(c_{ij} = \sqrt{c_{ii}c_{jj}}\right)$. In the stabilized DGT algorithm of Qiao and Sun [67], an artificial time-dependency is introduced in eq. 1.17 and the resulting set of equations is discretized in time and space. The solution to eq. 1.17 is then obtained by performing the integration in quasi-time until the steady-state solution has been reached. This approach allows to introduce an adjustable binary correction parameter β_{ij} in the calculation of the cross-influence parameter $\left(c_{ij} = \sqrt{c_{ii}c_{jj}}(1-\beta_{ij})\right)$. This additional degree of flexibility comes at the prize of substantially higher computation time compared to the reference component or path function approach. In Chapters 1 and 3, these three approaches to solve eq. 1.17 will be presented in detail and applied to determine interfacial density profiles and surface tensions of a variety of systems.

1.5.2 Classical Density Functional Theory

Density functional theory was developed by Hohenberg and Kohn [68] as well as Mermin [69] to study the inhomogeneous electron gas. First applications to classical systems are due to Ebner et al. [70, 71]. In contrast to the expansion about the local density approximation of density gradient theory, the Helmholtz energy of the inhomogeneous system, $A[\{\rho_k\}]$, is developed as the sum of Helmholtz energy functionals according to the PCP-SAFT model in the density functional theory applied in this work

$$A[\{\rho_k\}] = A^{IG}[\{\rho_k\}] + A^{HS}[\{\rho_k\}] + A^{HC}[\{\rho_k\}] + A^{Disp}[\{\rho_k\}] + A^{Assoc}[\{\rho_k\}] + A^{dd}[\{\rho_k\}] + A^{qq}[\{\rho_k\}] + A^{dq}[\{\rho_k\}] \quad (1.18)$$

Furthermore, DFT requires no adjustable parameter such as the influence parameter of density gradient theory. Interfacial properties are determined in a completely predictive manner. The development of the individual contributions of eq. 1.18 follows similar lines as the development of the Helmholtz energy contributions of PCP-SAFT, eq. 1.11. Starting point is again Wertheim's TPT, which does not only apply to homogeneous bulk systems but also to the more general case of inhomogeneous fluids. In the derivation, the pair distribution function of the inhomogeneous hard-sphere reference fluid $g^{hs}(\mathbf{r}_1, \mathbf{r}_2)$ is required. Rigorous and accurate approaches to obtain $g^{hs}(\mathbf{r}_1, \mathbf{r}_2)$ are computationally demanding [72]. Thus, simple approximations based on the pair distribution function of the homogeneous hard-sphere fluid are commonly applied. A list of frequently found approximations is presented in [72].

In this thesis, two DFT approaches are applied, one consistent with PCP-SAFT, the other consistent with heterosegmented group-contribution PCP-SAFT. Consistency in this context requires the developed Helmholtz energy functional $A[\{\rho_k\}]$ to reduce to

the expression for the Helmholtz energy $A(\{\rho_k\})$ of the corresponding equation of state when applied to a homogeneous system. Besides the underlying equation of state, the fundamental difference between both approaches are the entities for which density profiles are determined: in the former approach, one density profile per specie is calculated while in the latter approach, density profiles are obtained for the individual functional groups which make up the molecules (the generic index k thus identifies individual groups instead of molecules in this approach). This results in a significant increase of computation time but also in a more detailed picture of the interface.

DFT consistent with PCP-SAFT The hard-sphere contribution, $A^{HS}[\{\rho_k\}]$, of the DFT consistent with PCP-SAFT is determined from Rosenfeld's Fundamental Measure Theory (FMT) [73] in the modified form of Roth et al. [74] and Yu and Wu [75]. Chain formation, $A^{HC}[\{\rho_k\}]$, is treated using the iSAFT functional developed by Tripathi and Chapman [76] with the adaptations of Gross [77] and Klink and Gross [78]. The weighted-density approximation developed by Sauer and Gross [79] is applied for dispersive ($A^{Disp}[\{\rho_k\}]$) as well as polar contributions ($A^{dd}[\{\rho_k\}]$, $A^{qq}[\{\rho_k\}]$, $A^{dq}[\{\rho_k\}]$). In this approach, the local Helmholtz energy density at a position in the interface $\mathbf{r}$ is obtained from the corresponding Helmholtz energy contributions of PCP-SAFT, eq. 1.11, evaluated at a density which is averaged over an interaction volume around $\mathbf{r}$. Finally, the functional of Bymaster et al. [80], a modification of the work of Segura et al. [81], is adopted for associative interactions, i.e. hydrogen bonding. A detailed description of the single functionals of this DFT is presented in Chapter 2.

DFT consistent with GC-PCP-SAFT In the DFT consistent with heterosegmented GC-PCP-SAFT, the same functionals as in the DFT consistent with PCP-SAFT are applied for the hard-sphere and association contributions, $A^{HS}[\{\rho_k\}]$ and $A^{Assoc}[\{\rho_k\}]$. The dispersive and polar terms are again obtained from the weighted-density approximation of Sauer and Gross [79]. However, the local Helmholtz energy density is now obtained from the corresponding Helmholtz energy contributions of heterosegmented GC-PCP-SAFT. $A^{HC}[\{\rho_k\}]$ is obtained from the modified iSAFT functional of Jain et al. [82]. This functional is a modification of the work of Tripathi and Chapman [76] with corrected description of the stoichiometry of chain formation from the single segments. The detailed expressions of these functional are given in Chapter 4.

Most functionals have a similar structure. For illustrative purposes, this is presented for the hard-sphere contribution of the DFT consistent with PCP-SAFT:

$$A^{HS}[\{\rho_k\}] = \int a^{HS}\left(n_\alpha[\{\rho_k(\mathbf{r})\}]\right) \mathrm{d}\mathbf{r} \tag{1.19}$$

Here, a^{HS} is the local Helmholtz energy density of a hard-sphere fluid, which is a function of a set of weighted densities n_α (the index α runs over different types of weighted densities) which themselves are functionals of the density profiles. The prototype form of a weighted density n_α is

$$n_\alpha[\{\rho_k(\mathbf{r})\}] = \sum_i^N m_i \int \rho_i(\mathbf{r'})\omega_{i,\alpha}(\mathbf{r}-\mathbf{r'})\mathrm{d}\mathbf{r'} \tag{1.20}$$

The weight functions $\omega_{i,\alpha}$ determine the volume around $\mathbf{r}$ over which the local densities $\rho_i(\mathbf{r})$ are averaged into the weighted density n_α at $\mathbf{r}$ as well as the weight of the local densities in this averaging step. Typical weight functions applied in DFT lead to an averaging of local densities within a sphere of given radius around $\mathbf{r}$ or on a spherical shell of given distance to $\mathbf{r}$.

For the planar vapor-liquid interface studied in this work, densities vary only in the dimension normal to the interface. Introducing two cylindrical coordinate systems according to Fig. 1.1 with z and $\hat{z}$ as the coordinates normal to the interface, the three-dimensional integral (eq. 1.20) can be reduced to one dimension.

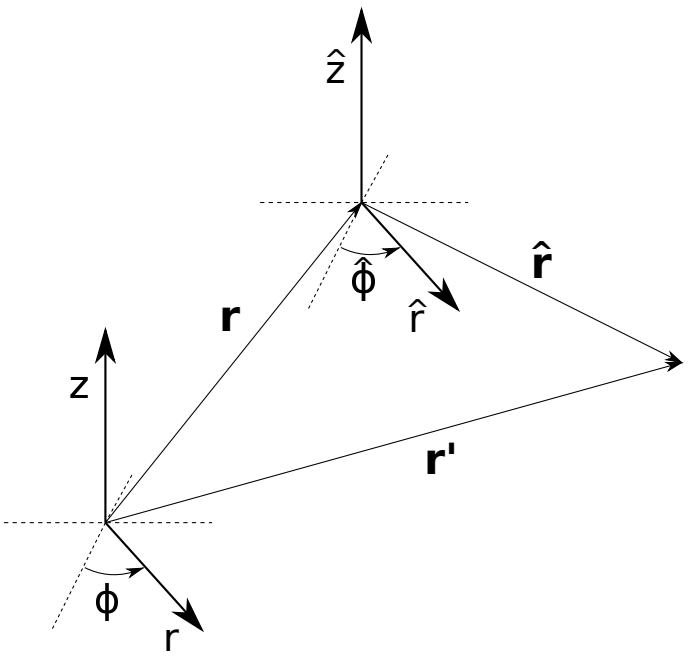

Figure 1.1: Illustration of the two coordinate systems used to carry out the integrations e.g. for the weighted densities n_α. The origin of the coordinate system (r, ϕ, z) is space-fixed while the origin of the coordinate system $(\hat{r}, \hat{\phi}, \hat{z})$ moves with $\mathbf{r}$.

For one of the weighted-densities of FMT, n_3, this procedure is demonstrated here: with the weight function $\omega_{i,3} = \Theta(R_i - |\mathbf{r}-\mathbf{r'}|)$, where Θ denotes the Heaviside step function and $R_i = \sigma_i/2$, n_3 is obtained as

$$n_3[\{\rho_k(\mathbf{r})\}] = \sum_i^N m_i \int \rho_i(\mathbf{r'})\Theta(R_i - |\mathbf{r} - \mathbf{r'}|)\mathrm{d}\mathbf{r'} \tag{1.21}$$

This integration is most conveniently performed in the coordinate system $(\hat{r}, \hat{\phi}, \hat{z})$ with origin at $\mathbf{r}$, see Fig. 1.1. From $\hat{\mathbf{r}} = \mathbf{r'} - \mathbf{r}$ and because the integration is performed for a fixed value of $\mathbf{r}$, it follows $\mathrm{d}\hat{\mathbf{r}} = \mathrm{d}\mathbf{r'}$. In this coordinate system, n_3 reads

$$n_3[\{\rho_k(\mathbf{r})\}] = \sum_i^N m_i \int \rho_i(\mathbf{r} + \hat{\mathbf{r}})\Theta(R_i - |\hat{\mathbf{r}}|)\mathrm{d}\hat{\mathbf{r}} \tag{1.22}$$

In coordinate system $(\hat{r}, \hat{\phi}, \hat{z})$, $\hat{\mathbf{r}}$ is given as

$$\hat{\mathbf{r}} = \begin{pmatrix} \hat{r}\cos\hat{\phi} \\ \hat{r}\sin\hat{\phi} \\ \hat{z} \end{pmatrix} \tag{1.23}$$

with $\hat{r} = |\hat{\mathbf{r}}| = \sqrt{\hat{r}^2 + \hat{z}^2}$ and $\mathrm{d}\hat{\mathbf{r}} = \hat{r}\mathrm{d}\hat{r}\mathrm{d}\hat{\phi}\mathrm{d}\hat{z}$. For densities which vary only in z-direction, the resulting integrals in cylindrical coordinates read

$$n_3[\{\rho_k(z)\}] = 2\pi \sum_i^N m_i \int\int \rho_i(z + \hat{z})\Theta(R_i - \sqrt{\hat{r}^2 + \hat{z}^2})\hat{r}\mathrm{d}\hat{r}\mathrm{d}\hat{z} \tag{1.24}$$

where the multiplication by 2π follows from the integration over $\hat{\phi}$. The integration bounds for $\hat{r}(\hat{z})$ as well as for $\hat{z}$ follow from the definition of the Heaviside function Θ which is non-zero only for $R_i - \sqrt{\hat{r}^2 + \hat{z}^2} > 0$ and thus $\hat{r}(\hat{z}) < \sqrt{R_i^2 - \hat{z}^2}$ and $-R_i < \hat{z} < R_i$. The final result is then

$$n_3[\{\rho_k(z)\}] = 2\pi \sum_i^N m_i \int_{-R_i}^{R_i} \int_0^{\sqrt{R_i^2 - \hat{z}^2}} \rho_i(z+\hat{z})\hat{r}\mathrm{d}\hat{r}\mathrm{d}\hat{z} = \pi \sum_i^N m_i \int_{-R_i}^{R_i} \rho_i(z+\hat{z}) \left(R_i^2 - \hat{z}^2\right) \mathrm{d}\hat{z} \tag{1.25}$$

Once the complete Helmholtz energy functional is established, the equilibrium density profiles are obtained by minimizing the grand potential Ω of the system. The minimization procedure applied in classical density functional theory differs from the route taken in density gradient theory: in DGT, the local grand potential density ω at position $\mathbf{r}$ depends only on local densities and density gradients (eq. 1.15). The local optimality conditions for the density profiles $\rho_i(\mathbf{r})$ are given by the Euler-Lagrange equations, eq. 1.17, which also only depend on the values of $\{\rho_k\}$ and $\nabla\{\rho_k\}$ at $\mathbf{r}$. Thus, the set of Euler-Lagrange equations for different locations are not coupled.

In DFT, the local Helmholtz energy density and consequently the local density of the grand potential $\omega[\{\rho_k\}] = a[\{\rho_k\}] - \sum_i^N \mu_i\rho_i(\mathbf{r})$ depend not only on local variables but

are functionals of the density profiles. The simple Euler-Lagrange formalism to obtain the local optimality conditions for the equilibrium density profiles, eq. 1.16, thus no longer applies. Instead, the minimal value of Ω is determined directly from eq. 1.13, i.e. by identifying the density profiles $\rho_i(\mathbf{r})$ for which the functional derivatives of Ω with respect to all $\rho_i(\mathbf{r})$ vanish. The local optimality conditions are obtained by discretizing eq. 1.13 on a one-dimensional grid. In contrast to the Euler-Lagrange equations of DGT, where the set of equations of dimension N for every point in the interface $\mathbf{r}$ can be solved independently, the non-local information required to evaluate $a[\{\rho_k\}]$ leads to a spatially coupled system of non-linear equations of dimension $n_{grid} \cdot N$, where n_{grid} denotes the number of grid points used in the discretization.

The step of calculating functional derivatives is presented exemplary again for the hard-sphere contribution and the weighted density n_3:

$$\frac{\delta A^{HS}[\{\rho_k\}]}{\delta \rho_i(z')} = \int \frac{\delta a^{HS}(n_\alpha\{\rho_k(z)\}])}{\delta \rho_i(z')} \mathrm{d}z = \int \sum_\alpha \frac{\partial a^{HS}(n_\alpha\{\rho_k(z)\}])}{\partial n_\alpha} \frac{\delta n_\alpha[\{\rho_k(z)\}]}{\delta \rho_i(z')} \mathrm{d}z \tag{1.26}$$

In general, the functional derivative of a functional $F[f_1(x), f_2(x), ..., f_n(x)] = F[\{f_k(x)\}]$ with respect to the function $f_i(x)$ at position x' can be obtained as

$$\frac{\delta F[\{f_k(x)\}]}{\delta f_i(x')} = \lim_{\epsilon \to 0} \frac{F[\{f_{k\neq i}(x)\}, f_i(x) + \epsilon\delta(x - x')] - F[\{f_k(x)\}]}{\epsilon} \tag{1.27}$$

with the Dirac function δ. For the weighted density n_3, eq. 1.25, this results in

$$\begin{aligned}
\frac{\delta n_3[\{\rho_k(z)\}]}{\delta \rho_i(z')} &= \lim_{\epsilon \to 0} \frac{\pi}{\epsilon} \left[\sum_{j \neq i}^{N} m_j \int_{-R_j}^{R_j} \rho_j(z + \hat{z}) \left(R_j^2 - \hat{z}^2\right) \mathrm{d}\hat{z} \right. \\
&\quad + m_i \int_{-R_i}^{R_i} (\rho_i(z + \hat{z}) + \epsilon\delta(\hat{z} - z')) \left(R_i^2 - \hat{z}^2\right) \mathrm{d}\hat{z} \\
&\quad \left. - \sum_{j}^{N} m_j \int_{-R_j}^{R_j} (\rho_j(z + \hat{z}))) \left(R_j^2 - \hat{z}^2\right) \mathrm{d}\hat{z} \right] \\
&= \lim_{\epsilon \to 0} \frac{1}{\epsilon} \pi m_i \int_{-R_i}^{R_i} \epsilon\delta(\hat{z} - z') \left(R_i^2 - \hat{z}^2\right) \mathrm{d}\hat{z} \\
&= \pi m_i \left(R_j^2 - (z')^2\right)
\end{aligned} \tag{1.28}$$

where the last step follows from the sifting property of the Dirac function $\int f(x)\delta(x' - x)\mathrm{d}x = f(x')$.

1.6 Outline of this thesis

In Chapter 2, interfacial properties of multicomponent mixtures, which are prototypes of reservoir fluids, are studied using DGT with the simple reference component approach to solve eq. 1.17. Limitations of this approach for mixtures of components with strongly differing attractive interactions, such as alkane-alcohol mixtures, are discussed and a measure of its applicability based on the values of the activity coefficients at infinite dilution is proposed.

Chapter 3 is dedicated to identifying efficient algorithms to solve the resulting equations of DFT for the one-dimensional vapor-liquid interface, i.e the discretized form of eq. 1.13. The performance of five algorithms is evaluated for several test systems: Picard iterations, Anderson mixing, a restarted quasi Newton method as well as two versions of the matrix-free inexact Newton method, one using analytical the other using numerically approximated directional derivatives. Aspects such as suitable stopping criteria and parallelization are addressed as well.

Interfacial properties for a variety of non-polar, non-associating as well as polar and associating pure components and mixtures are studied in Chapter 4 using the purely predictive DFT consistent with PCP-SAFT and DGT with influence parameters adjusted to experimental surface tension data. Here, the path function approach of Liang et al. [66] and the stabilized DGT algorithm of Qiao and Sun [67] are applied to solve the optimality conditions of DGT, eq. 1.17. The practical utility of a binary interaction parameter β_{ij} in the combining rule of the cross-influence parameters c_{ij} is assessed and discussed.

A DFT consistent with heterosegmented group-contribution PCP-SAFT is developed in Chapter 5. In a preliminary step, GC-PCP-SAFT results for vapor pressure and mixture vapor-liquid equilibria (VLE) are improved by introducing and adjusting a component specific parameter to experimental vapor pressure data as well as transferable group-group interaction parameters to experimental VLE results of binary mixtures. Interfacial properties obtained from the presented DFT are evaluated for many pure components and mixtures including polar and associating compounds. Special attention is given to systems where a group-contribution approach is particularly desirable such as biodiesel systems and long alkane molecules.

In Chapter 6, the capability of DFT to predict interfacial properties is exploited and experimental surface tension data is included in the adjustment of pure-component PCP-SAFT parameters. Results obtained with parameters adjusted to experimental surface tension and liquid density for bulk properties such as vapor pressure and enthalpy of evaporation are evaluated and compared to results obtained with parameters adjusted to results of molecular simulations.

Bibliography

[1] A. Rüger, "Die molekularhypothese in der theorie der kapillarerscheinungen (1805–1873)," *Centaurus*, vol. 28, no. 3, pp. 244–276, 1985.

[2] G. Gilmer, W. Gilmore, J. Huang, and W. Webb, "Diffuse interface in a critical fluid mixture," *Physical Review Letters*, vol. 14, no. 13, p. 491, 1965.

[3] J. Huang and W. Webb, "Diffuse interface in a critical fluid mixture," *The Journal of Chemical Physics*, vol. 50, no. 9, pp. 3677–3693, 1969.

[4] E. Wu and W. Webb, "Critical liquid-vapor interface in SF6. I. thickness of the diffuse transition layer," *Physical Review A*, vol. 8, no. 4, p. 2065, 1973.

[5] H. C. Andersen, D. Chandler, and J. D. Weeks, "Roles of repulsive and attractive forces in liquids: The equilibrium theory of classical fluids," *Adv. Chem. Phys*, vol. 34, p. 105, 1976.

[6] K. Birdi, *Surface and colloid chemistry: principles and applications*. CRC press, 2009.

[7] P. Rehner and J. Gross, "Surface tension of droplets and tolman lengths of real substances and mixtures from density functional theory," *The Journal of Chemical Physics*, vol. 148, no. 16, p. 164703, 2018.

[8] J. J. Jasper, "The surface tension of pure liquid compounds," *Journal of physical and chemical reference data*, vol. 1, no. 4, pp. 841–1010, 1972.

[9] R. Pashley and M. Karaman, *Applied colloid and surface chemistry*. John Wiley & Sons, 2005.

[10] T. Wadewitz, *Flüssige Grenzphasensysteme: Struktur, optische und Grenzflächeneigenschaften*. PhD thesis, University of Halle Wittenberg, 1999.

[11] M. Lechner, C. Wohlfarth, and B. Wohlfarth, *Surface tension of pure liquids and binary liquid mixtures*. Springer, 2015.

[12] Design Institute for Physical Properties, 2017, www.aiche.org/dippr.

[13] Dortmund Data Bank, 2015, www.ddbst.com.

[14] S. Fisk and B. Widom, "Structure and free energy of the interface between fluid phases in equilibrium near the critical point," *The Journal of Chemical Physics*, vol. 50, no. 8, pp. 3219–3227, 1969.

[15] J. Penfold and R. Thomas, "The application of the specular reflection of neutrons to the study of surfaces and interfaces," *Journal of Physics: Condensed Matter*, vol. 2, no. 6, p. 1369, 1990.

[16] S. Roser, R. Felici, and A. Eaglesham, "Energy dispersive x-ray reflection from a liquid-liquid interface," *Langmuir*, vol. 10, no. 10, pp. 3853–3856, 1994.

[17] R. Superfine, J. Huang, and Y. Shen, "Nonlinear optical studies of the pure liquid/vapor interface: Vibrational spectra and polar ordering," *Physical review letters*, vol. 66, no. 8, p. 1066, 1991.

[18] C. Stanners, Q. Du, R. Chin, P. Cremer, G. Somorjai, and Y.-R. Shen, "Polar ordering at the liquid-vapor interface of n-alcohols (c1-c8)," *Chemical physics letters*, vol. 232, no. 4, pp. 407–413, 1995.

[19] D. Macleod, "On a relation between surface tension and density," *Transactions of the Faraday Society*, vol. 19, no. July, pp. 38–41, 1923.

[20] S. Sugden, "VI.—the variation of surface tension with temperature and some related functions," *Journal of the Chemical Society, Transactions*, vol. 125, pp. 32–41, 1924.

[21] T. A. Knotts, W. V. Wilding, J. L. Oscarson, and R. L. Rowley, "Use of the DIPPR database for development of qspr correlations: Surface tension," *Journal of Chemical & Engineering Data*, vol. 46, no. 5, pp. 1007–1012, 2001.

[22] C. F. Weinaug and D. L. Katz, "Surface tensions of methane-propane mixtures," *Industrial & Engineering Chemistry*, vol. 35, no. 2, pp. 239–246, 1943.

[23] S.-T. Lee, M. Chien, *et al.*, "A new multicomponent surface tension correlation based on scaling theory," in *SPE Enhanced Oil Recovery Symposium*, Society of Petroleum Engineers, 1984.

[24] J. Hugill and A. Van Welsenes, "Surface tension: a simple correlation for natural gas + conensate systems," *Fluid Phase Equilibria*, vol. 29, pp. 383–390, 1986.

[25] E. A. Guggenheim, "The principle of corresponding states," *The Journal of Chemical Physics*, vol. 13, no. 7, pp. 253–261, 1945.

[26] J. Hirschfelder, R. B. Bird, and C. F. Curtiss, "Molecular theory of gases and liquids," 1964.

[27] S. Murad, "Generalized corresponding states correlation for the surface tension of liquids and liquid mixtures," *Chemical Engineering Communications*, vol. 24, no. 4-6, pp. 353–358, 1983.

[28] P. Rice and A. S. Teja, "A generalized corresponding-states method for the prediction of surface tension of pure liquids and liquid mixtures," *Journal of Colloid and Interface Science*, vol. 86, no. 1, pp. 158–163, 1982.

[29] A. Queimada, L. Rolo, A. Caço, I. Marrucho, E. H. Stenby, and J. Coutinho, "Prediction of viscosities and surface tensions of fuels using a new corresponding states model," *Fuel*, vol. 85, no. 5, pp. 874–877, 2006.

[30] A. Mulero, I. Cachadiña, and M. Parra, "Recommended correlations for the surface tension of common fluids," *Journal of Physical and Chemical Reference Data*, vol. 41, no. 4, p. 043105, 2012.

[31] G. Somayajulu, "A generalized equation for surface tension from the triple point to the critical point," *International journal of thermophysics*, vol. 9, no. 4, pp. 559–566, 1988.

[32] S. Sastri and K. Rao, "A simple method to predict surface tension of organic liquids," *The Chemical Engineering Journal and the Biochemical Engineering Journal*, vol. 59, no. 2, pp. 181–186, 1995.

[33] J. Straub, N. Rosner, U. Grigull, *et al.*, "A simple equation for the temperature dependence of the surface tension of water," in *Proceedings of the 8th Conference on the Properties of Water and Steam*, p. 1085, 1974.

[34] C. Miqueu, D. Broseta, J. Satherley, B. Mendiboure, J. Lachaise, and A. Graciaa, "An extended scaled equation for the temperature dependence of the surface tension of pure compounds inferred from an analysis of experimental data," *Fluid Phase Equilibria*, vol. 172, no. 2, pp. 169–182, 2000.

[35] G. Di Nicola and M. Moglie, "A generalized equation for the surface tension of refrigerants," *International Journal of Refrigeration*, vol. 34, no. 4, pp. 1098–1108, 2011.

[36] J. Gross and G. Sadowski, "Perturbed-chain SAFT: An equation of state based on a perturbation theory for chain molecules," *Industrial & engineering chemistry research*, vol. 40, no. 4, pp. 1244–1260, 2001.

[37] J. Gross and G. Sadowski, "Application of the perturbed-chain SAFT equation of state to associating systems," *Industrial & engineering chemistry research*, vol. 41, no. 22, pp. 5510–5515, 2002.

[38] J. Gross and J. Vrabec, "An equation-of-state contribution for polar components: Dipolar molecules," *AIChE journal*, vol. 52, no. 3, pp. 1194–1204, 2006.

[39] J. Gross, "An equation-of-state contribution for polar components: Quadrupolar molecules," *AIChE journal*, vol. 51, no. 9, pp. 2556–2568, 2005.

[40] J. Vrabec and J. Gross, "Vapor-liquid equilibria simulation and an equation of state contribution for dipole- quadrupole interactions," *The Journal of Physical Chemistry B*, vol. 112, no. 1, pp. 51–60, 2008.

[41] R. W. Zwanzig, "High-temperature equation of state by a perturbation method. I. nonpolar gases," *The Journal of Chemical Physics*, vol. 22, no. 8, pp. 1420–1426, 1954.

[42] J. A. Barker and D. Henderson, "Perturbation theory and equation of state for fluids: The square-well potential," *The Journal of Chemical Physics*, vol. 47, no. 8, pp. 2856–2861, 1967.

[43] M. Wertheim, "Fluids with highly directional attractive forces. I. statistical thermodynamics," *Journal of statistical physics*, vol. 35, no. 1, pp. 19–34, 1984.

[44] M. Wertheim, "Fluids with highly directional attractive forces. II. thermodynamic perturbation theory and integral equations," *Journal of statistical physics*, vol. 35, no. 1-2, pp. 35–47, 1984.

[45] M. Wertheim, "Fluids with highly directional attractive forces. III. multiple attraction sites," *Journal of statistical physics*, vol. 42, no. 3, pp. 459–476, 1986.

[46] M. Wertheim, "Fluids with highly directional attractive forces. IV. equilibrium polymerization," *Journal of statistical physics*, vol. 42, no. 3, pp. 477–492, 1986.

[47] W. Zmpitas and J. Gross, "Detailed pedagogical review and analysis of wertheim's thermodynamic perturbation theory," *Fluid Phase Equilibria*, vol. 428, pp. 121–152, 2016.

[48] W. G. Chapman, G. Jackson, and K. E. Gubbins, "Phase equilibria of associating fluids: chain molecules with multiple bonding sites," *Molecular Physics*, vol. 65, no. 5, pp. 1057–1079, 1988.

[49] W. G. Chapman, K. E. Gubbins, G. Jackson, and M. Radosz, "SAFT: Equation-of-state solution model for associating fluids," *Fluid Phase Equilibria*, vol. 52, pp. 31–38, 1989.

[50] G. Jackson, W. G. Chapman, and K. E. Gubbins, "Phase equilibria of associating fluids: Spherical molecules with multiple bonding sites," *Molecular Physics*, vol. 65, no. 1, pp. 1–31, 1988.

[51] W. G. Chapman, K. E. Gubbins, G. Jackson, and M. Radosz, "New reference equation of state for associating liquids," *Industrial & Engineering Chemistry Research*, vol. 29, no. 8, pp. 1709–1721, 1990.

[52] S. H. Huang and M. Radosz, "Equation of state for small, large, polydisperse, and associating molecules," *Industrial & Engineering Chemistry Research*, vol. 29, no. 11, pp. 2284–2294, 1990.

[53] T. Boublík, "Hard-sphere equation of state," *The Journal of chemical physics*, vol. 53, no. 1, pp. 471–472, 1970.

[54] G. Mansoori, N. F. Carnahan, K. Starling, and T. Leland Jr, "Equilibrium thermodynamic properties of the mixture of hard spheres," *The Journal of Chemical Physics*, vol. 54, no. 4, pp. 1523–1525, 1971.

[55] J. A. Barker and D. Henderson, "Perturbation theory and equation of state for fluids. ii. a successful theory of liquids," *The Journal of chemical physics*, vol. 47, no. 11, pp. 4714–4721, 1967.

[56] G. Stell, J. Rasaiah, and H. Narang, "Thermodynamic perturbation theory for simple polar fluids, I," *Molecular Physics*, vol. 23, no. 2, pp. 393–406, 1972.

[57] G. Stell, J. Rasaiah, and H. Narang, "Thermodynamic perturbation theory for simple polar fluids. II," *Molecular Physics*, vol. 27, no. 5, pp. 1393–1414, 1974.

[58] J. Gross, O. Spuhl, F. Tumakaka, and G. Sadowski, "Modeling copolymer systems using the perturbed-chain SAFT equation of state," *Industrial & engineering chemistry research*, vol. 42, no. 6, pp. 1266–1274, 2003.

[59] E. Sauer, M. Stavrou, and J. Gross, "Comparison between a homo-and a heterosegmented group contribution approach based on the perturbed-chain polar statistical associating fluid theory equation of state," *Industrial & Engineering Chemistry Research*, vol. 53, no. 38, pp. 14854–14864, 2014.

[60] R. Evans, "The nature of the liquid-vapour interface and other topics in the statistical mechanics of non-uniform, classical fluids," *Advances in Physics*, vol. 28, no. 2, pp. 143–200, 1979.

[61] J. Van der Waals, "Thermodynamische theorie der kapillarität unter voraussetzung stetiger dichteänderung," *Zeitschrift für Physikalische Chemie*, vol. 13, no. 1, pp. 657–725, 1894.

[62] J. W. Cahn and J. E. Hilliard, "Free energy of a nonuniform system. I. interfacial free energy," *The Journal of chemical physics*, vol. 28, no. 2, pp. 258–267, 1958.

[63] V. Bongiorno, L. Scriven, and H. Davis, "Molecular theory of fluid interfaces," *Journal of colloid and interface science*, vol. 57, no. 3, pp. 462–475, 1976.

[64] A. Yang, P. Fleming, and J. Gibbs, "A molecular theory of interfacial phenomena in multicomponent systems," *Journal of Chemical Physics*, vol. 64, pp. 3732–3747, 1976.

[65] R. Courant and D. Hilbert, *Methods of mathematical physics, vol. I.* Interscience Publishers, 1953.

[66] X. Liang, M. L. Michelsen, and G. M. Kontogeorgis, "Pitfalls of using the geometric-mean combining rule in the density gradient theory," *Fluid Phase Equilibria*, vol. 415, pp. 75–83, 2016.

[67] Z. Qiao and S. Sun, "Two-phase fluid simulation using a diffuse interface model with peng–robinson equation of state," *SIAM Journal on Scientific Computing*, vol. 36, no. 4, pp. B708–B728, 2014.

[68] P. Hohenberg and W. Kohn, "Inhomogeneous electron gas," *Physical review*, vol. 136, no. 3B, p. B864, 1964.

[69] N. D. Mermin, "Thermal properties of the inhomogeneous electron gas," *Physical Review*, vol. 137, no. 5A, p. A1441, 1965.

[70] C. Ebner, W. Saam, and D. Stroud, "Density-functional theory of simple classical fluids. I. surfaces," *Physical Review A*, vol. 14, no. 6, p. 2264, 1976.

[71] W. Saam and C. Ebner, "Density-functional theory of classical systems," *Physical Review A*, vol. 15, no. 6, p. 2566, 1977.

[72] P. Lurie-Gregg, J. B. Schulte, and D. Roundy, "Approach to approximating the pair distribution function of inhomogeneous hard-sphere fluids," *Physical Review E*, vol. 90, no. 4, p. 042130, 2014.

[73] Y. Rosenfeld, "Free-energy model for the inhomogeneous hard-sphere fluid mixture and density-functional theory of freezing," *Physical review letters*, vol. 63, no. 9, p. 980, 1989.

[74] R. Roth, R. Evans, A. Lang, and G. Kahl, "Fundamental measure theory for hard-sphere mixtures revisited: the white bear version," *Journal of Physics: Condensed Matter*, vol. 14, no. 46, p. 12063, 2002.

[75] Y.-X. Yu and J. Wu, "Structures of hard-sphere fluids from a modified fundamental-measure theory," *The Journal of chemical physics*, vol. 117, no. 22, pp. 10156–10164, 2002.

[76] S. Tripathi and W. G. Chapman, "Microstructure of inhomogeneous polyatomic mixtures from a density functional formalism for atomic mixtures," *The Journal of chemical physics*, vol. 122, no. 9, p. 094506, 2005.

[77] J. Gross, "A density functional theory for vapor-liquid interfaces using the PCP-SAFT equation of state," *The Journal of chemical physics*, vol. 131, no. 20, p. 204705, 2009.

[78] C. Klink and J. Gross, "A density functional theory for vapor–liquid interfaces of mixtures using the perturbed-chain polar statistical associating fluid theory equation of state," *Industrial & Engineering Chemistry Research*, vol. 53, no. 14, pp. 6169–6178, 2014.

[79] E. Sauer and J. Gross, "Classical density functional theory for liquid–fluid interfaces and confined systems: A functional for the perturbed-chain polar statistical associating fluid theory equation of state," *Industrial & Engineering Chemistry Research*, vol. 56, no. 14, pp. 4119–4135, 2017.

[80] A. Bymaster and W. G. Chapman, "An iSAFT density functional theory for associating polyatomic molecules," *The Journal of Physical Chemistry B*, vol. 114, no. 38, pp. 12298–12307, 2010.

[81] C. J. Segura, W. G. Chapman, and K. P. Shukla, "Associating fluids with four bonding sites against a hard wall: density functional theory," *Molecular Physics*, vol. 90, no. 5, pp. 759–772, 1997.

[82] S. Jain, A. Dominik, and W. G. Chapman, "Modified interfacial statistical associating fluid theory: A perturbation density functional theory for inhomogeneous complex fluids," *The Journal of chemical physics*, vol. 127, no. 24, p. 244904, 2007.

Chapter 2

Modeling of Interfacial Properties of Multicomponent systems using Density Gradient Theory and PCP-SAFT

The content of this chapter is a literal quote of the publication

Mairhofer, Gross, Fluid Phase Equilibria, 439, 2017, 31-42.

In comparison to the published work, the abstract is here omitted. Additions or deletions compared to the published work are marked with angular brackets.

Interfacial properties such as surface tension, surface thickness and interfacial density profiles play an important role in many industrial applications ranging from the design of nanomaterials [1] to the design of destillation columns [2] [3] [4]. Methods to calculate surface tensions such as the Parachor method of Macleod [5] and Sudgen [6], the corresponding-state principle of Guggenheim [7] and more recently of Queimada et al. [8] as well as simple thermodynamic relations such as those of Girifalco and Good [9], Fowkes [10] and Winterfeld et al. [11] have been available for a long time. However, in order to obtain more detailed information about the interface such as density profiles, more predictive and comprehensive models are required.
A viable approach to predict the interface on an atomistic level is using molecular dynamics simulations. Early works focussed on the description of the phase interface of the Lennard-Jones fluid [12] [13] [14] [15] [16] or alkanes [17]. More complex, molecular systems were recently studied including mixtures of alkanes and solvents [18] [19], the Lennard-Jones plus quadrupole fluid [20], ternary aqueous systems [21] [22] and other complex mixtures [23].

The framework of density functional theory (DFT) offers a versatile alternative at lower computational demands. DFT requires an expression of the Helmholtz energy as a functional of the density profile across the interface. The equilibrium density profile is found by minimizing the grand potential energy of the system. For more detail on DFT we refer to introductions [24] [25] and review articles [26] [27] [28] [29]. Recent results for interfacial properties for a broad class of systems including polar components and liquid-liquid equilibria obtained by DFT are available from our group [30] [31] [32].

In this work, we focus on density gradient theory (DGT). This theory was first developed by Van der Waals [33], reformulated by Cahn and Hilliard [34]. Compared to DFT the implementation of DGT is less demanding, the only inputs being the Helmholtz energy density of the homogeneous fluid which can be obtained from a bulk equation of state and the so called influence parameter c_{ii} which is a component specific property (index i). In practical application, the influence parameter is a determining difference to DFT-approaches: DFT is entirely predictive, whereas DGT requires adjusting the influence parameter to (some sort of) experimental interfacial data. Bongiorno et al. [35], Yang et al. [36] as well as later Evans [37] showed that the influence parameter can be obtained from the direct correlation function of the homogeneous fluid. However, this property is tedious to obtain and therefore simpler correlations for c_{ii} have been derived from its theoretical expression. Examples of these correlations can be found in the works of Breure and Peters [38], Cornelisse et al. [39], Miqueu et al. [40], Lin et al. [41] as well as Garrido et al. [42]. Most often however, the influence parameter c_{ii} is regressed to experimental pure component surface tension data.

Density gradient theory has been used with many different equations of state as the model for the Helmholtz energy density. Early studies by Carey et al. [43] and Cornelisse et al. [44] used the Peng-Robinson (PR) equation of state [45] and obtained surface tension results in good agreement with experimental data for hydrocarbons while results for polar components are poor. Volume-corrected cubic equations of state were applied in the works of Miqueu et al. [40] [46] and Lin et al. [41] to non-polar as well as polar pure components and mixtures.

In order to study more complex systems including associating components, Cornelisse et al. [47] used the associated perturbed anisotropic chain theory [48] in their study of mixtures composed of one or more associating components. As a further variation of cubic equations of state, Oliveira et al. [49] used the Cubic-Plus-Association (CPA) equation of state [50] and showed that it can be successfully applied to pure components and binary mixtures of associating components such as alcohols.

Kahl and Enders [51] used the statistical associating fluid theory (SAFT) [52] [53] to investigate the surface properties of non-polar and polar binary mixtures including liquid-liquid equilibria and obtained results in good agreement with experimental surface tension data.

Since then, different SAFT-type equations of state have been employed in density gradient theory. Lafitte et al. [54] and later Miguez et al. [21] as well as Chow et al. [55] used SAFT-VR Mie [56] to study the interfacial properties of aqueous systems of up to three components. PC-SAFT [57] was first applied by Fu and coworkers to systems of pure n-alkanes [58] and later also to polar components and their mixtures [59] [60] [61]. Li et al. [62] studied similar systems using PC-SAFT and Mousazadeh and Faramarzi [63] applied DGT and PC-SAFT to pure molten metals. Furthermore, Breure and Peters [38] achieved good agreement with experimental surface tensions of hydrocarbon mixtures when they applied PC-SAFT and the theoretical approach of Bongiorno et al. [35] to obtain the pure component influence parameters once a correction term had been applied. Vinš et al. [64] showed that the polar extension to PC-SAFT, PCP-SAFT [65] [66] [67], is superior to PC-SAFT in describing surface properties of systems containing polar components. PCP-SAFT was also applied by Schäfer et al. [68] in their study of azeotropic binary mixtures of DMF and n-alkanes. Simplified PC-SAFT, sPC-SAFT [69], was used by Khosharay et al. [70] to calculate surface tensions of aqueous systems.

The studies listed so far all deal with systems of up to three components. Only recently, results have been reported for multicomponent systems. The interfacial properties of multicomponent systems are relevant for example in reservoir modeling where interfacial tension largely influences the necessary effort of oil recovery [71] [72].

The most common approach to apply DGT to mixtures is to define one component to be the reference and to calculate the densities of the remaining components from the known density of this reference component. The only requirement which qualifies a component to be the reference is that its density has to change monotonically between the vapor and the liquid bulk phase, i.e. there cannot be any enrichment of this component in the interface.

Miqueu et al. [73] [74] used DGT with the volume-corrected PR equation to calculate surface tensions of multicomponent systems whereby the reference component was chosen beforehand by the physical argument that the less volatile compounds will not show any enrichment in the interface; therefore, their density profiles should exhibit a monotonic behaviour.

Larsen et al. [75] implemented a computationally efficient method based on a refinement strategy where the density profile is first obtained for a few points in the interface and then refined as needed. This approach also uses a reference component, however, it is not chosen a priori but during execution based on the chemical potential gradient at the vapor side of the interface. The CPA equation of state is used and surface tensions values of many binary systems including strongly associating mixtures are compared to experimental values. A speed up of their algorithm is shown for mixtures of up to eleven components. However, no surface tensions are reported for these mixtures. Kou et al.

[76] report an alternative to the reference component approach by using a linear transformation which reduces the Euler-Lagrange equations. Density profiles and surface tensions are reported for up to five components using the PR equation to calculate the Helmholtz energy density but no comparisons to experimental results are shown.

In this work, we use PCP-SAFT as the model for the Helmholtz energy density and compare the calculated surface tensions of systems of up to twenty components including systems with supercritical and polar components to experimental data. We apply the reference component approach and the physical argument of Miqueu et al. [73] [74] of choosing this reference component.

2.1 Development of the Density Gradient Theory for an N-component mixture

The basics of density gradient theory has been described in detail in the literature [34] [77] [78] and we only repeat the main equations of the theory here. The DGT is developed as an expansion of the Helmholtz energy density of an inhomogeneous fluid about the local density approximation $a_0(\rho_k)$, truncated after the square density gradient term. We consider N components with local species-densities $\rho_i(z)$, varying with some space coordinate z. For the Helmholtz energy density, $a_0(\rho_k)$, we introduce index k as a generic index, representing the full vector of all species-densities and, for brevity, we don't make the dependence on temperature T explicit. The Helmholtz energy density of the inhomogeneous system then has two contributions, the Helmholtz energy density $a_0(\rho_k)$ evaluated at the local density value, i.e. for a hypothetically homogeneous fluid with density $\rho_k = \rho_k(z)$, and a second order (square) gradient correction term to account for the inhomogeneity of the fluid [34]

$$a(\rho_k, \nabla\rho_k) = a_0(\rho_k) + \frac{1}{2}\sum_{i}^{N}\sum_{j}^{N} c_{ij}\nabla\rho_i\nabla\rho_j \tag{2.1}$$

where $\nabla\rho_i$ is the local density gradient of component i and $c_{ij} = (1-\beta_{ij})\sqrt{c_{ii}c_{jj}}$ is the influence parameter. Like in most other DGT-studies, we treat the influence parameters as temperature-independent. From a theoretical standpoint [36], one would expect c_{ij} to vary significantly with temperature and it is thus surprising to observe that DGT-calculations with this assumption give valuable results. In this work, we further use the simple geometric combining rule for c_{ij}, i.e. $\beta_{ij} = 0$, and we use the PCP-SAFT equation of state for $a_0(\rho_k)$.

The equilibrium density profile minimizes the grand potential Ω of the system given by

$$\Omega = \int \left(a(\rho_k, \nabla\rho_k) - \sum_i^N \mu_i \rho_i \right) \mathrm{d}\mathbf{r} \tag{2.2}$$

We regard flat vapor-liquid interfaces in this work, where properties vary only in one direction z of the positional vector $\mathbf{r}$. The vapor and liquid phase are thought to extend towards $z \to -\infty$ and $z \to +\infty$, respectively. The chemical potential μ_i of component i, is for these cases equal to the equilibrium chemical potential of the two bulk phases. Assuming a density-independent influence parameter, the equations for the surface tension γ and the density profile follow from the resulting Euler-Lagrange equation as

$$\mathrm{z}(\rho_1) = \mathrm{z}_0 + \int_{\rho_1(\mathrm{z}_0)}^{\rho_1} \sqrt{\frac{c_{\mathrm{mix}}}{2\Delta\omega_0}} \mathrm{d}\rho_1 \tag{2.3}$$

$$\gamma = \int_{\rho_1^v}^{\rho_1^l} \sqrt{2\Delta\omega_0 c_{\mathrm{mix}}} \mathrm{d}\rho_1 \tag{2.4}$$

where ρ_1, ρ_1^v and ρ_1^l denote the local density, the bulk vapor density, and the bulk liquid density of the reference component, respectively. Furthermore, the mixture influence parameter c_{mix} is given by

$$c_{\mathrm{mix}} = \sum_i^N \sum_j^N c_{ij} \frac{\mathrm{d}\rho_i}{\mathrm{d}\rho_1} \frac{\mathrm{d}\rho_j}{\mathrm{d}\rho_1} \tag{2.5}$$

and $\Delta\omega_0$ denotes the difference of the grand potential energy density of the local homogeneous fluid to its bulk value, $\Delta\omega_0 = a_0(\rho_k) - \sum_i^N \rho_i\mu_i + p$, with equilibrium pressure p of both bulk phases.

At every point in the interface, the local species-densities need to satisfy the Euler-Lagrange equation

$$\sum_j^N c_{ij} \nabla^2 \rho_j = \mu_{i,0}(\rho_k) - \mu_i \qquad i = 1, .., N \tag{2.6}$$

where $\mu_{i,0} = \frac{\partial a_0}{\partial \rho_i}$.

The left hand sides of eq. (2.6) for every pair of components k and l can be eliminated by multiplying the equation of component k by $\sqrt{c_{ll}}$ and the one of component l by $\sqrt{c_{kk}}$ and subsequently subtracting the results. Doing so for all combinations of the reference component ($l = 1$) with all other components leads to a set of *(N-1)* equations for the *(N-1)* unknown species-densities of the non-reference components

$$\sqrt{c_{11}}\,(\mu_{0,k} - \mu_k) = \sqrt{c_{kk}}\,(\mu_{0,1} - \mu_1)\,, \qquad k = 2, ..., N \tag{2.7}$$

The derivative of eq. (2.7) with respect to the reference density ρ_1, taking into account

that at constant temperature and pressure $\mathrm{d}\mu_{0,k} = \sum_n^N \frac{\partial \mu_{0,k}}{\partial \rho_n} \mathrm{d}\rho_n$ and therefore $\frac{\mathrm{d}\mu_{0,k}}{\mathrm{d}\rho_1} = \sum_n^N \frac{\partial \mu_{0,k}}{\partial \rho_n} \frac{\mathrm{d}\rho_n}{\mathrm{d}\rho_1}$ as well as the constant equilibrium chemical potential, i.e. $\frac{\mathrm{d}\mu_k}{\mathrm{d}\rho_1} = 0$, yields a set of *(N-1)* linear equations for the derivatives $\frac{\mathrm{d}\rho_k}{\mathrm{d}\rho_1}$ (for *k=2,...,N*) which are needed to evaluate eq. (2.5)

$$\sqrt{c_{11}} \sum_n^N \frac{\partial \mu_{0,k}}{\partial \rho_n} \frac{\mathrm{d}\rho_n}{\mathrm{d}\rho_1} = \sqrt{c_{kk}} \sum_n^N \frac{\partial \mu_{0,1}}{\partial \rho_n} \frac{\mathrm{d}\rho_n}{\mathrm{d}\rho_1}, \qquad k = 2, ..., N \tag{2.8}$$

This set of equations can be rewritten in matrix form and solved by LU [lower-upper] decomposition.

2.2 Solution procedure

The following steps summarize the algorithm. First, the phase equilibrium state is determined leading to values of the coexisting liquid and vapor bulk densities, ρ_i^l and ρ_i^v, respectively, as well as equilibrium chemical potentials μ_i of all components. Secondly, the bulk density difference of the reference component has to be discretized in n_{grid} steps as $\Delta\rho_1 = \frac{\rho_1^l - \rho_1^v}{n_{\mathrm{grid}}}$. The starting point of the calculation is given by $z = 0$, $\rho_i^{\mathrm{old}} = \rho_i^v$ (for *i=1...,N*) and with derivatives $\frac{\mathrm{d}\rho_k}{\mathrm{d}\rho_1}$ (for *k=2,...,N*) obtained by solving eq. (2.8). The following steps have to be repeated n_{grid} times (i.e. until $\rho_1^{\mathrm{new}} = \rho_1^l$)

1. Update density of reference component: $\rho_1^{\mathrm{new}} = \rho_1^{\mathrm{old}} + \Delta\rho_1$
2. Set initial values for remaining densities: $\rho_k^{\mathrm{new},0} = \rho_k^{\mathrm{old}} + \frac{\mathrm{d}\rho_k}{\mathrm{d}\rho_1}\Delta\rho_1, \quad k = 2, ..., N$
3. Solve the nonlinear system, eq. (2.7), for the remaining densities $\rho_k^{\mathrm{new}}, \quad k = 2, ..., N$
4. Calculate $\Delta\omega_0$ and $\frac{\mathrm{d}\mu_{0,i}}{\mathrm{d}\rho_j}, \quad i, j = 1, ..., N$
5. Solve the linear system, eq. (2.8), for $\frac{\mathrm{d}\rho_k}{\mathrm{d}\rho_1}, \quad k = 2, ..., N$
6. Update z according to eq. (2.3)
7. Set $\rho_i^{\mathrm{old}} = \rho_i^{\mathrm{new}}, \quad i = 1, ..., N$

Once the density profile is known, the value of surface tension can be calculated according to eq. (2.4). We solve the set of nonlinear equations, eq. (2.7), using standard routines from Minpack [79] and for the linear system, eq. (2.8), we use LU decomposition. The derivatives $\frac{\partial \mu_{0,k}}{\partial \rho_l}$ in eq. (2.8) are calculated using automatic differentiation [80]. The number of discretization steps n_{grid} is set depending on the system under study to values between 1,000 and 10,000. Higher numbers are required especially at low pressure, low temperature conditions.

During the calculations we observed that the algorithm shown above sometimes approaches negative species-densities as intermediate values of the iterative procedure, especially in the low pressure, low temperature region. A simple remedy to circumvent problems resulting from negative species-densities is to set the value of the corresponding density to a small positive number. This recipe stabilized our iteration in all cases.
An alternative approach which never approached negative densities during iterative solution in all our calculations is to eliminate the left hand side of eq. (2.6) not only for the combinations of the reference component with the remaining components but for all pairwise combinations. This leads to a set of $\sum_{i=1}^{N-1} i$ equations for the *(N-1)* unknown densities, i.e. the system is overdetermined for $N > 3$. The resulting overdetermined set of linear equations, corresponding to eq. (2.8), can be solved by QR [orthogonal-triangular] decomposition. However, the increased number of equations which need to be solved (mildly) increases the calculation time. Therefore, we used the simple approach of resetting negative densities to a small positive number.

2.3 Results and Discussion

In this section we show that DGT results of multicomponent systems with symmetric or weakly asymmetric interactions are in good agreement with experimental data for surface tension. We evaluate DGT results for alkane and alkane-CO_2 mixtures of up to twenty components. The experimental data is taken from studies of Ng et al. [81] and Danesh et al. [82] where surface tensions of model reservoir fluids have been measured for several isotherms and for a large range of pressures. Some of the components in the systems under study are supercritical at the considered state conditions (if they were pure). Following the results of Amézquita et al. [83], it is assumed that it is still a valid approximation to use the constant influence parameter for these supercritical components. The influence parameters are adjusted to experimental surface tension data of pure fluids and the cross-influence parameters are determined from a geometric combining rule. The values of the influence parameters are presented in the appendix [Tables 2.4, 2.5 and 2.6]. If not indicated otherwise, no binary interaction parameters are used in the combining rules of the PCP-SAFT equation of state.
As presented by Liang et al. [84], no reasonable results can be obtained for the system ethanol-hexane using DGT in combination with the PC-SAFT and CPA equations of state, density independent influence parameters and a geometric combining rule for c_{ij}. In the appendix we show DGT results for this mixture and use results obtained by density functional theory as a reference. This comparison helps to analyze why DGT results for surface tension deviate significantly from experimental values. Furthermore, we suggest the value of the activity coefficient at infinite dilution γ_{ij}^{∞} as an indicator for

the applicability of DGT.

2.3.1 Comparison to experimental data of Ng et al.

Ng et al. [81] report results of four multi-component systems: a seven-component mixture denoted *wet gas*, an eleven-component mixture denoted *associate gas* and both mixtures with additional CO_2. The overall compositions of these mixtures are given in the appendix [Tables 2.2 and 2.3]. Besides surface tension results, the corresponding bulk densities are also reported [81]. That is important, because it allows us to first evaluate whether PCP-SAFT is able to calculate the equilibrium states sufficiently well. Only when this is the case, we can expect meaningful results of the subsequent DGT calculation because bulk densities and equilibrium chemical potentials directly enter the equations of density gradient theory.

Wet Gas results

Fig. 2.1 shows a comparison of calculated results to experimental data for the seven-component mixture denoted *wet gas* and three of the four isotherms reported by Ng et al. [81]. Fig. 2.1a confirms that PCP-SAFT results for the bulk liquid and vapor densities are in very good agreement with experiments. The averaged relative deviation for all reported data points is 3% for both the liquid and vapor bulk densities. Larger deviations only occure at $T = 283.15$ K and $T = 227.59$ K (results not shown in Fig. 2.1) at the highest experimental pressure value where the relative deviation of the liquid bulk density increases to 8%. Results of the DGT for surface tensions follow the experimental values closely, see Fig. 2.1b. Averaged overall results of a given isotherm, absolute deviations decrease with increasing temperature from 1.2 mN/m to 0.002 mN/m.

Wet Gas + CO_2 results

Fig. 2.2a shows that the coexisting bulk densities of the eight-component mixture for all isotherms reported by Ng et al. [81] are very satisfyingly reproduced by PCP-SAFT. The averaged relative deviation of the vapor and liquid bulk densities is 3%. Only at $T = 283.15$ K and the highest experimental pressure, deviations are 14% and 7% for the liquid and vapor density, respectively.

These deviations in bulk densities cause a deviation of the calculated surface tension at this state point, see Fig. 2.2b. The relative deviation of calculated surface tensions at $T = 283.15$ K and the highest experimental pressure value reaches 64%. On the other hand, the agreement between experimental and calculated results is very good for those

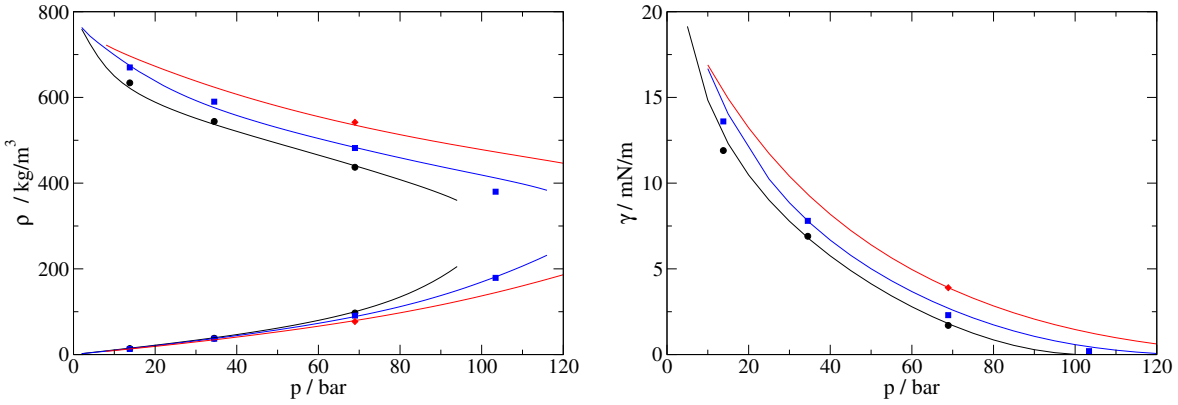

(a) (b)

Figure 2.1: Experimental [81] (symbols) and calculated (lines) results of bulk densities (a) and surface tensions (b) of the seven-component mixture *wet gas* at $T = 255.37$ K (black), $T = 283.15$ K (blue) and $T = 310.93$ K (red).

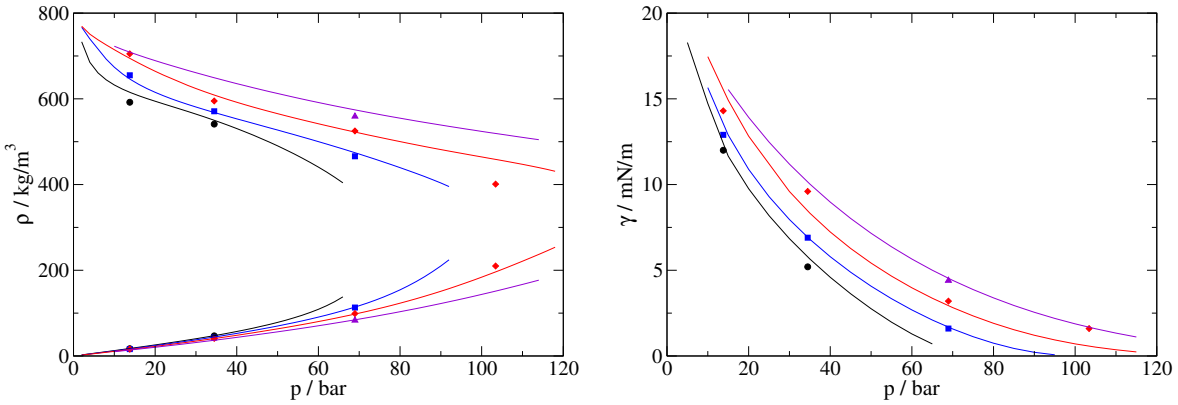

(a) (b)

Figure 2.2: Experimental [81] (symbols) and calculated (lines) results of bulk densities (a) and surface tensions (b) of the eight-component mixture *wet gas* + CO_2 at at $T = 227.59$ K (black), $T = 255.37$ K (blue), $T = 283.15$ K (red) and $T = 255.37$ K (purple).

state points where bulk densities are reproduced with good accuracy, with relative deviations usually well below 10%. The process of injecting CO_2 into oil reservoirs is called carbon dioxide flooding and has the primary goal of increasing oil recovery e.g. by reducing oil viscosity or miscibility effects [85]. Comparing experimental results of [81] shown in figures 2.1b and 2.2b for given values of temperature and pressure shows that, for this model reservoir fluid, adding CO_2 increases surface tension on average by 11%. DGT also predicts an increase of surface tension. However, averaged over the state points where experimental data is available, the predicted increase is only 4%.

Fig. 2.3 shows the species-density profiles of the eight-component mixture at $T = 255.37$ K and $p = 10$ bar. Evidently, there is an accumulation of the light n-alkanes, especially methane, at the interface. CO_2 also exhibits an accumulation, albeit less pronounced. The relative enrichment of one component in a binary mixture has been studied in several

studies using DGT including those of Carey et al. [43] and Amézquita et al. for under-critical and supercritical components [86] [83] and the works of Telo de Gama and Evans [87], Llovel et al. [88] and Klink and Gross [31] using density functional theory. As Fig. 2.3 and also the study of Miqueu et al. [73] show, in the case of multicomponent mixtures, more than one component can accumulate at the interface. The implication of an enriched species at the interface for mass transport is analyzed by Klink et al. [89], who determine the resistance of the interface to heat and (coupled) mass transport through the interface, a phenomena also studied in detail by Glavatskiy and Bedeaux [90] [91].

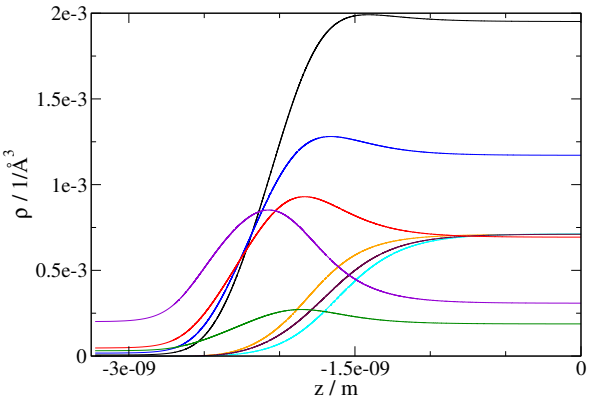

Figure 2.3: Species-density profiles of the eight-component mixture *wet gas* + CO_2 at $T = 255.37$ K and $p = 10$ bar. The components are indicated by colors: butane (black), propane (dark blue), ethane (red), methane (purple), heptane (orange), methylcyclohexane (brown), toluene (light blue) and CO_2 (green).

Associate Gas results

The eleven- and twelve-component mixtures studied by Ng et al. [81], *associate gas* and *associate gas* + CO_2, contain 3-methylnonane. For this compound no experimental surface tension data could be found so that the influence parameter of 3-methylnonane could not be obtained in the same way as for the other components of this work. As shown in Fig. 2.4, the influence parameter of many compounds is a well-behaved function of molecular mass. We note, the value of the influence parameter of several simple branched alkanes closely follows the trend (with molecular mass) as n-alkanes, see Fig. 2.4. Therefore, we approximate the influence parameter of 3-methylnonane by the value of a hypothetical n-alkane of same molecular mass. A least-squares fit of the influence parameters for n-alkanes results in the correlation $c = 3.5980 \cdot 10^{-23} \mathrm{Jm}^5/\mathrm{mol}^2 \cdot (M/(g/mol))^{2.051}$ where M denotes the molecular mass. From this correlation, the influence parameter of 3-methylnonane is obtained as $c = 9.3784 \cdot 10^{-19} \mathrm{Jm}^5/\mathrm{mol}^2$.
For the eleven-component mixture *associate gas*, PCP-SAFT predictions of bulk densities are in very good agreement with experimental results, see Fig. 2.5a. Averaged relative deviations are 2% and 6% for the liquid and vapor phase, respectively. As Fig. 2.5b

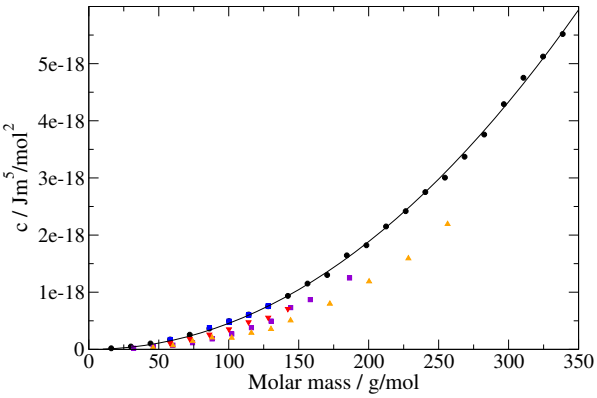

Figure 2.4: Values of the influence parameter, individually adjusted to surface tension data, and displayed against molar mass for n-alkanes (black), branched alkanes (blue), 1-alcohols (purple), carboxylic acids (orange) and 2-ketones (red). The solid line represents a least-squares fit to the results of n-alkane.

shows, DGT results overpredict surface tension for most of the state points especially at lower temperatures. In this case, these deviations cannot be explained by deviations in bulk densities, as was the case for the *associate gas*. With 2% at $T = 310.93$ K and 1% at $T = 366.48$ K, averaged relative deviations of liquid bulk density are similar at both temperatures. For vapor densities, we obtain relative deviations of 4% at the lower and 8% at the higher temperature, i.e. deviations in vapor bulk densities are larger at the isotherm where surface tension values are predicted in better agreement with experiments.

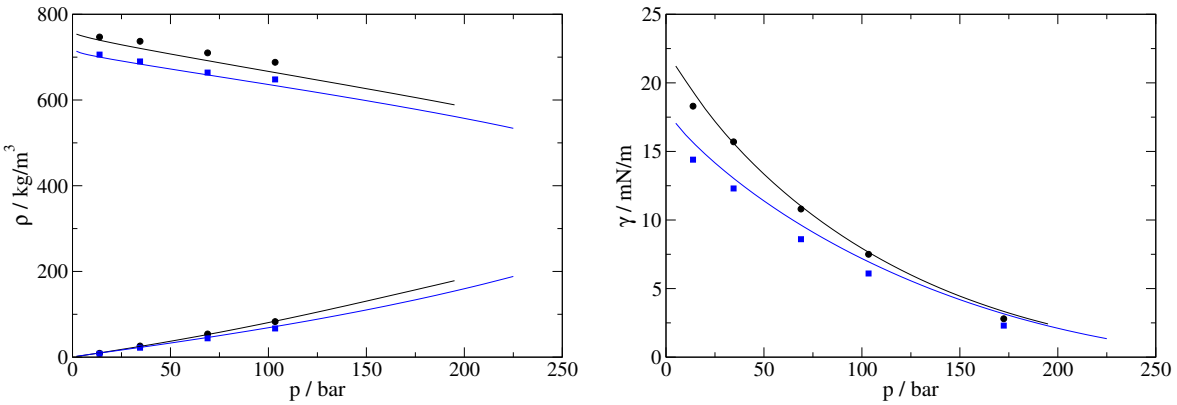

(a) (b)

Figure 2.5: Experimental [81] (symbols) and calculated (lines) results of bulk densities (a) and surface tensions (b) of the eleven-component mixture *associate gas* at $T = 310.93$ K (black) and $T = 366.48$ K (blue).

Associate Gas + CO_2 results

As can be seen from Fig. 2.6a, PCP-SAFT predicts the equilibrium bulk densities of the twelve-component mixture in good agreement to experimental values. Relative deviations of the DGT-results for surface tensions increase with pressure along a given isotherm. Similar to the results of the *associate gas* mixture, surface tension is more prominently overpredicted by DGT at lower temperatures - and more so, than could be explained by deviations in bulk densities. The averaged relative deviations of liquid density at the lower depicted isotherm is 2% and is therefore only slightly larger than for the higher isotherm where the value is 0.9%. However, like in the previous section, for the vapor bulk densities the averaged relative deviation is higher at the isotherm where the agreement of DGT surface tension results with experiments is better (6% at $T = 310.93$ K compared to 8% at $T = 366.48$ K).

For this model reservoir fluid, the effect of adding CO_2 is not uniform. Experimental results of ref. [81] show a maximum increase of surface tension of 23% at the lowest temperature and the highest pressure and a maximum decrease of 8% at the same temperature and intermediate pressure. For most of the state points, DGT predicts the correct sign of the change in surface tension. However, the magnitude of this change is usually underpredicted.

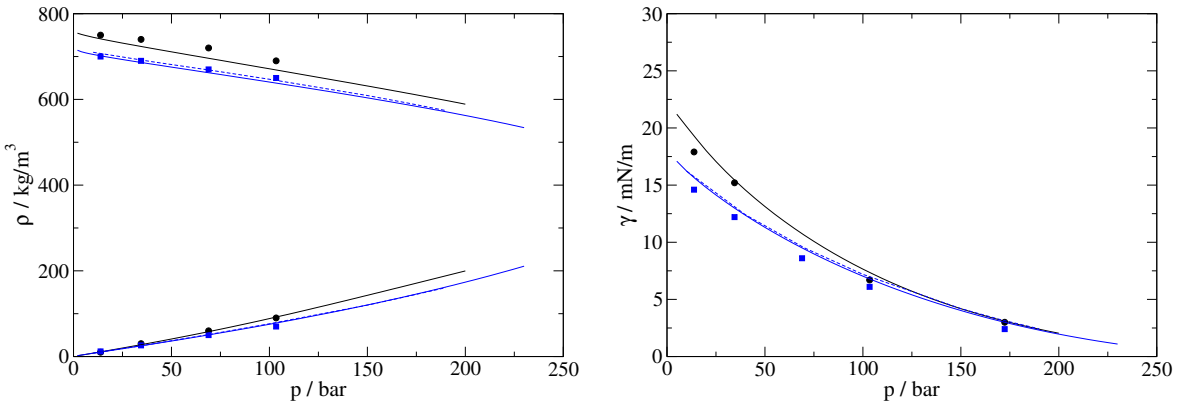

Figure 2.6: Experimental [81] (symbols) and calculated (lines) results of bulk densities (a) and surface tensions (b) of the twelve-component mixture *associate gas* + CO_2 at $T = 310.93$ K (black) and $T = 366.48$ K (blue). Results obtained with the Peng-Robinson equation of state at $T = 366.48$ K are shown for comparison (dashed lines).

2.3.2 Comparison to experimental data of Danesh et al.

Danesh et al. [82] measured surface tensions of two five-component mixtures (denoted *Fluid A* and *Fluid B*) and a twenty-component hydrocarbon system (*Fluid C*). *Fluid B*

is composed of the same five components as *Fluid A* but has a different overall composition. The overall molar compositions of all three mixtures are given in the appendix. No experimental bulk densities are reported. Therefore, the capability of PCP-SAFT to predict the phase equilibrium of these systems cannot be evaluated and only surface tension results of DGT are compared to the reported experimental results.
For the five-component mixture *Fluid A*, experimental results are reported for two isotherms, $T = 313.15$ K and $T = 353.15$ K, and a pressures of up to 30 MPa. Results for *Fluid B* are given for $T = 303.15$ K and $T = 308.15$ K and a similar pressure range as for *Fluid A*. Fig. 2.7b shows surface tension results of *Fluid A* at $T = 353.15$ K and *Fluid B* at $T = 303.15$ K. Calculated results agree very well with the experimental values over the complete pressure range. The averaged absolute deviations for the results depicted in Fig. 2.7b is 0.06 mN/m for *Fluid A* and 0.03 mN/m for *Fluid B*. For *Fluid B* at the second reported isotherm, $T = 308.15$ K, this value reduces to 0.015 mN/m. For *Fluid A*, experimental values are also reported at $T = 313.15$ K. At this temperature, the averaged absolute deviation is 0.2 mN/m. The importance of an accurate reproduction of bulk densities as a prerequisite for a reliable description of interfacial properties is reemphasized by comparing results obtained with PCP-SAFT to results of the Peng-Robinson equation of state for *Fluid B*. Results for bulk densities differ greatly between both equations of state (fig. 2.7a) and it follows that values for surface tension are also different (fig. 2.7b). Since no experimental bulk densities are reported for this system, only the surface tension results can be validated. As fig. 2.7b shows, surface tensions obtained with PCP-SAFT are in very good agreement with the experimental results while results of the Peng-Robinson equation are too low and vanish too early. This suggests that a more accurate description of bulk densities by PCP-SAFT compared with the PR model leads to lower errors of PC-SAFT for surface tensions. For other systems studied in this work both, the PCP-SAFT and the PR model accurately describe bulk densities and, consequently, also surface tension, as shown in fig. 2.6 for the example of a twelve-component mixture *associate gas* + CO_2.

Fluid C is a mixture of twenty n-alkanes. Experimental surface tension values are reported for three isotherms, $T = 338.65$ K, $T = 366.45$ K and $T = 394.25$ K, and three values of pressure in the range of 32 MPa to 35 MPa per isotherm. As was the case for the previous systems, DGT results of surface tension calculated with PCP-SAFT reproduce the experimental values closely. Absolute deviations between DGT calculation and experiment are largest for the lowest and highest temperature and take on values between 0.05 mN/m and 0.08 mN/m. At the intermediate temperature all absolute deviations are below 0.023 mN/m. The results for this isotherm are shown in Fig. 2.8 together with the experimental results of [82].

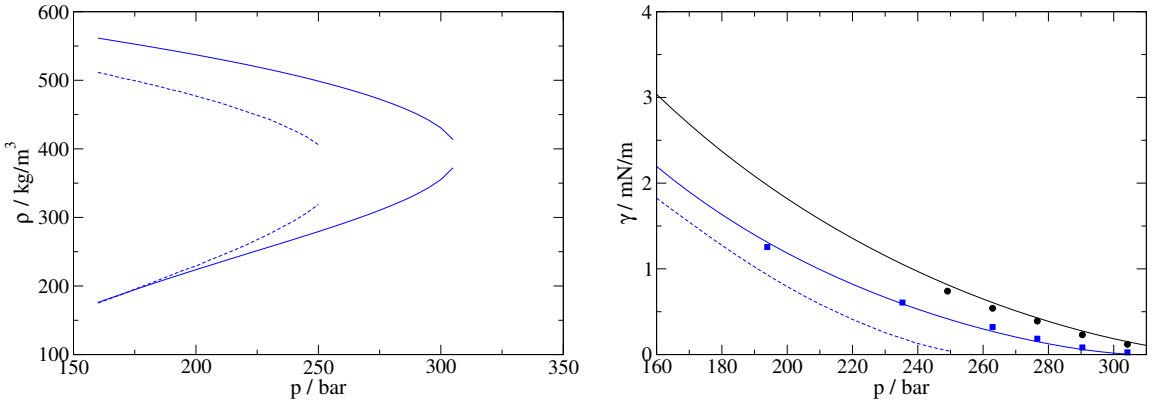

Figure 2.7: (a) Bulk densities of the five-component mixture *Fluid B* at $T = 303.15$ K obtained with PCP-SAFT (solid line) and the Peng-Robinson equation of state (dashed line). (b) Surface tension of both five-component mixtures, *Fluid A* at $T = 353.15$ K (black) and *Fluid B* at $T = 303.15$ K (blue). Comparison of DGT results obtained with PCP-SAFT (solid lines) to experimental data (circles and squares). In addition, DGT results obtained with the Peng-Robinson equation of state for *Fluid B* are shown (dashed line). Experimental results are taken from [82].

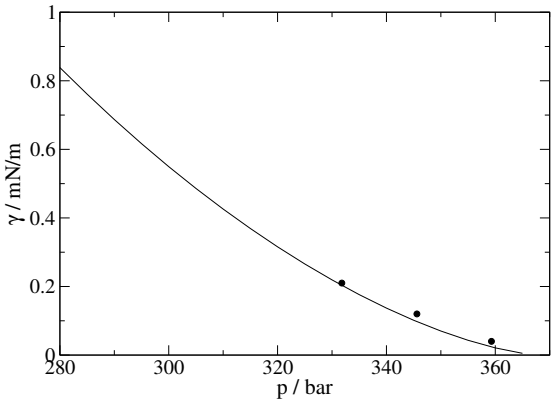

Figure 2.8: Surface tension of the twenty-component mixture *Fluid C* at $T = 366.45$ K. Comparison of DGT results (solid line) to experimental data (circles). Experimental results are taken from [82].

2.4 Conclusion

Interfacial properties of multicomponent mixtures are studied by density gradient theory in combination with PCP-SAFT. The overall agreement of the calculated results for surface tension with experimental data is good for hydrocarbon mixtures as well as for systems including carbon dioxide. The prerequisite for accurate surface tensions is a precise description of the bulk densities. PCP-SAFT is shown to predict bulk densities reliably without adjustable binary interaction parameters.

Appendix

The binary mixture ethanol-hexane

The results of the previous sections showed that density gradient theory is capable of describing the interfacial properties of multicomponent mixtures including molecules that differ significantly in size, e.g. methane and eicosane. Furthermore, other studies show results of systems such as the binary mixtures water and ethanol, water and acetic-acid or water and acetone [75] where both components exhibit associative interactions and/or cross association occurs in the mixture. However, for sufficiently non-ideal mixtures DGT with common assumptions, i.e. density independent influence parameters and geometric combining rule for c_{ij}, fails to give accurate results. The mixtures are particularly non-ideal when substances have very asymmetric attractive interactions, such as the binary mixture consisting of ethanol and hexane or water and hexane. Our hypothesis is thus: DGT with these assumptions gives unreliable results for sufficiently non-ideal mixtures. As a measure for the non-ideality we take the activity coefficient at infinite dilution γ_{ij}^{∞} (with index i: solvent, j: solute). The more $\ln(\gamma_{ij}^{\infty})$-values deviate from zero, the more non-ideal is component j in solvent i.

Table 2.1: Activity cofficients at infinite dilution at $T = 298.15$ K, unless indicated otherwise, taken from refs.[92] and [93]

mixture	$\ln\gamma_{12}^{\infty}$	$\ln\gamma_{21}^{\infty}$
ethanol(1)-hexane(2)	2.4	4.1
water(1)-hexane(2)	11.5	7.6
water(1)-ethanol(2)	1.3	1.06 (at 373K)
water(1)-acetone(2)	2.0	1.9
hexane(1)-hexatriacontane(2)	-0.45 (at 349K)	-0.68 (at 280K)

Table 2.1 lists values of activity coefficient at infinite dilution for several mixtures. The first two mixtures (ethanol-hexane) and (water-hexane) can not reliably be predicted with the DGT, as reported in ref.[84] and they indeed have the highest deviation from $\ln(\gamma_{ij}^{\infty}) = 0$. Other mixtures with more reliable DGT-results, such as water-ethanol and water-acetone have $\ln(\gamma_{ij}^{\infty})$-values much closer to zero. The deviation from ideal behavior ($\ln(\gamma_{ij}^{\infty}) = 0$) is thus mainly caused by asymmetric attractive interactions. Asymmetric molecular size or shape also leads to deviation from ideal behavior, however, to lesser extent as the example of hexane-hexatriacontate (C36) in Table 2.1 shows. The mixture hexane-hexatriacontate was not considered in this work, but was chosen as a representative shape-asymmetic mixture, where values for the activity coefficients at infinite dilution were available in literature[93].

In the case of ethanol-hexane, the influence of a third bulk phase, albeit not physically

present [94], might also affect the results. Liang et al. [84] have studied the mixture ethanol-hexane in detail using the CPA and PC-SAFT equation of state and a path function approach to solve the DGT equations for mixtures. With PC-SAFT, results could be obtained for all compositions, however, the resulting density profiles were unphysical over a wide concentration range. Using the CPA equation of state, convergence could only be achieved at very low and high ethanol concentrations.

As Fig. 2.9a shows, the reference component approach used in this work yields a similar result. Only for low ethanol concentrations physically reasonable surface tensions and density profiles can be obtained. However, even then the DGT severely underpredicts the experimental surface tension. Density functional theory, on the other hand, does not suffer from these shortcomings for the mixture ethanol-hexane, as Fig. 2.9a shows. Surface tensions are in very good agreement with experimental results except at high ethanol concentrations and density profiles look reasonable in the complete concentration range. We reemphasize that DFT does not offer any adjustable parameters for calculating interfacial properties (such as the influence parameter of DGT) so that the DFT calculations are full predictions for both, the pure component results and for the mixture behavior. The different results for surface tension of DFT and DGT can be explained by the density profiles depicted in Fig. 2.9b. By performing this comparison at an ethanol concentration where DFT results for surface tension are in very good agreement to experimental values, we can use the density profiles calculated using DFT as a reference for the density profiles of DGT: while DFT predicts only a slight accumulation of ethanol in the interface, this accumulation is strongly overpredicted by DGT leading to a value of surface tension which is by far too low. The accumulation of ethanol in the interface also shows that it is not always the component having the higher vapor pressure at mixture temperature that will be enriched at the interface as postulated for example in the studies of Amèzquita et al. [86] [83]. Rather, the enrichment of a component at the interface has to be attributed to a general asymmetry in the component properties such as chain lengths or interaction energies as noted by Llovel et al. [88].

For the DFT calculation shown in Fig. 2.9 we used the modified fundamental measure theory functional for the hard sphere contribution to the helmholtz energy [95] [96], a functional of Tripathi and Chapman for chain formation [97] which was made consistent with PC-SAFT [30], a weighted density approach for dispersive interactions from our group and the association functional of Bymaster and Chapman [98].

A more detailed comparison of DGT and DFT is in development in our group.

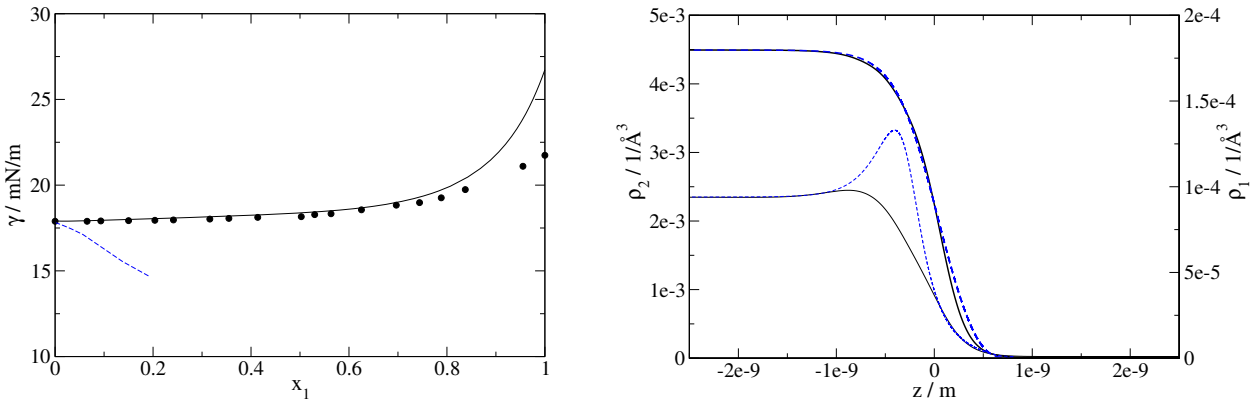

(a) (b)

Figure 2.9: (a) Surface tension of the binary mixture ethanol (1) and hexane (2) at $T = 283.15$ K calculated using DGT (dashed line) and DFT (solid line). Experimental results (symbols) are taken from Jimènez et al. [99]. A binary interaction parameter of $k_{ij} = 0.0285$ which was adjusted to VLE data of Góral et al. [100] was used in the calculations. (b) Comparison of density profiles of ethanol (1, bold lines) and hexane (2, thin lines) obtained with DGT (dashed lines) and DFT (solid lines) at $T = 283.15$ K and $p = 0.24$ bar ($x_1 = 0.02$).

Molar overall compositions of the studied systems

Table 2.2: Molar overall compositions (%) of the systems studied by Ng et al. [81].

Component	*wet gas*	*wet gas* + CO_2	*asso. gas*	*asso. gas* + CO_2
Methane	67.670	64.133	58.68	55.996
Ethane	19.171	15.365	4.98	4.797
Propane	7.683	6.145	1.94	1.87
Butane	3.880	3.080	0.98	0.975
Heptane	0.532	0.426	4.49	4.187
Methylcyclohexane	0.531	0.427	4.42	3.927
Toluene	0.533	0.426	4.74	4.462
Decane	-	-	5.09	4.716
3-Methylnonane	-	-	5.16	4.719
Butyl-Cyclohexane	-	-	5.00	4.716
1,3-Diethylbenzene	-	-	5.00	4.719
CO_2	-	9.997	-	4.917

Table 2.3: Molar overall compositions (%) of the systems studied by Danesh et al. [82].

Component	*Fluid A*	*Fluid B*	*Fluid C*
Methane	82.05	82.32	80.11
Ethane	-	-	8.23
Propane	8.95	8.71	2.11
Butane	-	-	1.07
Pentane	5.00	5.05	0.80
Hexane	-	-	1.20
Heptane	-	-	0.96
Octane	-	-	0.55
Nonane	-	-	0.49
Decane	1.99	1.98	0.48
Undecane	-	-	0.45
Dodecane	-	-	0.44
Tridecane	-	-	0.44
Tetradecane	-	-	0.41
Pentadecane	-	-	0.41
Hexadecane	2.01	1.94	0.39
Heptadecane	-	-	0.38
Octadecane	-	-	0.37
Nonadecane	-	-	0.36
Eicosane	-	-	0.35

Equation of state parameters and influence parameters

The following tables show the parameters for the PCP-SAFT equation of state of all components of this study. Furthermore, the values of the influence parameters as well as the references to the experimental data which was used to adjust the values of c are presented. The average absolute deviation is calculated as $AAD\% = \frac{1}{N}\sum_{i=1}^{N}\frac{|\gamma^{exp}-\gamma^{calc}|}{\gamma^{exp}} \cdot 100\%$

Table 2.4: Values of PCP-SAFT parameters and influence parameters for unpolar and non-associating components.

Component	m	σ/Å	ϵ/k/K	Ref.	$c/10^{-19}/Jm^5/mol^2$	T/K	AAD%	Ref.
Methane	1.0000	3.7039	150.03	[57]	0.1917554	105 - 180	7.07	[101]
Ethane	1.6069	3.5206	191.42	[57]	0.4972791	105 - 285	1.68	[101]
Propane	2.0020	3.6184	208.11	[57]	1.0300755	100 - 340	1.96	[101]
Butane	2.3316	3.7086	222.88	[57]	1.7228683	150 - 390	1.76	[101]
Pentane	2.6896	3.7729	231.20	[57]	2.5651212	160 - 460	5.11	[101]
Hexane	3.0576	3.7983	236.77	[57]	3.6444985	195 - 495	7.07	[101]
Heptane	3.4831	3.8049	238.40	[57]	4.9391699	200 - 500	2.70	[101]
Octane	3.8176	3.8373	242.78	[57]	6.0933095	230 - 560	7.31	[101]
Nonane	4.2079	3.8448	244.51	[57]	7.5417139	235 - 580	7.52	[101]
Decane	4.6627	3.8384	243.87	[57]	9.3629705	260 - 590	3.89	[101]
Undecane	4.9082	3.8893	248.82	[57]	11.508127	273 - 373	0.41	[102] [103]
Dodecane	5.3060	3.8959	249.21	[57]	13.769134	273 - 473	0.44	[102] [104]
Tridecane	5.6877	3.9143	249.78	[57]	16.4519049	273 - 443	0.50	[102] [105]
Tetradecane	5.9002	3.9396	254.21	[57]	18.2103532	273 - 353	0.50	[102]
Pentadecane	6.2855	3.9531	254.14	[57]	21.5025322	273 - 359	0.53	[102] [106]
Hexadecane	6.6485	3.9552	254.70	[57]	24.1825590	273 - 353	0.61	[102]
Heptadecane	6.9809	3.9675	255.65	[57]	27.5240777	273 - 473	0.53	[102] [104]
Octadecane	7.3271	3.9668	256.20	[57]	30.0556228	273 - 443	0.51	[102] [105]
Nonadecane	7.7175	3.9721	256.00	[57]	33.7122254	293 - 353	0.49	[107]
Eicosane	7.9849	3.9869	257.75	[57]	37.5930577	293 - 353	0.70	[108] [107]
Methylcyclohexane	2.6637	3.9993	282.33	[57]	4.1596579	180 - 555	6.25	[109]
Toluene	2.8149	3.7169	285.69	[57]	3.1517615	220 - 570	6.42	[101]
n-Butylcyclohexane	3.6023	4.0637	285.97	[110]	8.5438142	279 - 333	0.14	[111]
m-Diethylbenzene	3.6407	3.9049	287.43	[110]	6.8911789	283 - 373	0.53	[111]
3-Methylnonane	4.4407	3.8840	246.30	[110]	9.3784			

Table 2.5: Values of PCP-SAFT parameters [112] and influence parameters for associating components.

Component	m	σ/Å	ϵ/k/K	$\epsilon^{A_iB_i}/k$/K	$\kappa^{A_iB_i}$	$c/10^{-19}/Jm^5/mol^2$	T/K	AAD%	Ref.
Ethanol	2.3827	3.1771	198.24	2653.4	0.032384	0.5280672	200 - 505	2.96	[113]

Table 2.6: Values of PCP-SAFT parameters and influence parameters for polar components.

Component	m	σ/Å	ϵ/k/K	$\lvert Q\rvert$/DÅ	Ref.	$c/10^{-19}/Jm^5/mol^2$	T/K	AAD%	Ref.
CO2	1.5131	3.1869	163.33	4.4	[65]	0.2419666	230 -290	1.77	[101]

Table 2.7: Equation of state and influence parameters for the Peng-Robinson equation.

Component	T_c/K	p_c/bar	ω	Ref.	$c/10^{-19}/Jm^5/mol^2$	Ref. data
Methane	190.564	45.992	0.01142	[101]	0.164788	[101]
Ethane	305.33	48.718	0.0993	[101]	0.441159	[101]
Propane	369.825	42.4766	0.1524	[101]	0.977851	[101]
Butane	425.125	37.96	0.201	[101]	1.712732	[101]
Pentane	469.7	33.7	0.251	[101]	2.694158	[101]
Heptane	540.13	27.36	0.349	[101]	6.051802	[101]
Decane	617.7	21.03	0.488	[101]	13.52718	[101]
Hexadecane	723	14	0.718	[114]	46.72697	[102]
Methylcyclohexane	572.19	34.71	0.235	[114]	4.505940	[109]
Toluene	591.75	41.08	0.264	[114]	3.655061	[101]
CO_2	304.2	73.74	0.225	[114]	0.294791	[101]
n-Butylcyclohexane	667.0	31.51	0.362	[115]	6.046241	[111]
m-Diethylbenzene	657.0	28.7	0.354	[115]	9.357979	[111]
3-Methylnonane	613.5	21.6	0.465	[115]		

Bibliography

[1] S. Cuenot, C. Frétigny, S. Demoustier-Champagne, and B. Nysten, "Surface tension effect on the mechanical properties of nanomaterials measured by atomic force microscopy," *Physical Review B*, vol. 69, no. 16, p. 165410, 2004.

[2] F. Zuiderweg and A. Harmens, "The influence of surface phenomena on the performance of distillation columns," *Chemical Engineering Science*, vol. 9, no. 2, pp. 89–103, 1958.

[3] R. E. Tsai, P. Schultheiss, A. Kettner, J. C. Lewis, A. F. Seibert, R. B. Eldridge, and G. T. Rochelle, "Influence of surface tension on effective packing area," *Industrial & Engineering Chemistry Research*, vol. 47, no. 4, pp. 1253–1260, 2008.

[4] A. Elgozali, V. Linek, M. Fialova, O. Wein, and J. Zahradnık, "Influence of viscosity and surface tension on performance of gas–liquid contactors with ejector type gas distributor," *Chemical Engineering Science*, vol. 57, no. 15, pp. 2987–2994, 2002.

[5] D. Macleod, "On a relation between surface tension and density," *Trans. Faraday Soc.*, vol. 19, no. July, pp. 38–41, 1923.

[6] S. Sugden, "A relation between surface tension, density, and chemical composition," *Journal of the Chemical Society, Transactions*, vol. 125, pp. 1177–1189, 1924.

[7] E. A. Guggenheim, "The principle of corresponding states," *The Journal of Chemical Physics*, vol. 13, no. 7, pp. 253–261, 1945.

[8] A. Queimada, L. Rolo, A. Caço, I. Marrucho, E. H. Stenby, and J. Coutinho, "Prediction of viscosities and surface tensions of fuels using a new corresponding states model," *Fuel*, vol. 85, no. 5, pp. 874–877, 2006.

[9] L. Girifalco and R. Good, "A theory for the estimation of surface and interfacial energies. I. derivation and application to interfacial tension," *The Journal of Physical Chemistry*, vol. 61, no. 7, pp. 904–909, 1957.

[10] F. M. Fowkes, "Determination of interfacial tensions, contact angles, and dispersion forces in surfaces by assuming additivity of intermolecular interactions in surfaces," *The Journal of Physical Chemistry*, vol. 66, no. 2, pp. 382–382, 1962.

[11] P. Winterfeld, L. Scriven, and H. Davis, "An approximate theory of interfacial tensions of multicomponent systems: Applications to binary liquid-vapor tensions," *AIChE Journal*, vol. 24, no. 6, pp. 1010–1014, 1978.

[12] M. Nijmeijer, A. Bakker, C. Bruin, and J. Sikkenk, "A molecular dynamics simulation of the lennard-jones liquid–vapor interface," *The Journal of chemical physics*, vol. 89, no. 6, pp. 3789–3792, 1988.

[13] C. D. Holcomb, P. Clancy, and J. A. Zollweg, "A critical study of the simulation of the liquid-vapour interface of a lennard-jones fluid," *Molecular Physics*, vol. 78, no. 2, pp. 437–459, 1993.

[14] M. Mecke, J. Winkelmann, and J. Fischer, "Molecular dynamics simulation of the liquid–vapor interface: The lennard-jones fluid," *The Journal of chemical physics*, vol. 107, no. 21, pp. 9264–9270, 1997.

[15] M. Mecke, J. Winkelmann, and J. Fischer, "Molecular dynamics simulation of the liquid–vapor interface: binary mixtures of lennard-jones fluids," *The Journal of chemical physics*, vol. 110, no. 2, pp. 1188–1194, 1999.

[16] A. Trokhymchuk and J. Alejandre, "Computer simulations of liquid/vapor interface in lennard-jones fluids: Some questions and answers," *The Journal of chemical physics*, vol. 111, no. 18, pp. 8510–8523, 1999.

[17] J. G. Harris, "Liquid-vapor interfaces of alkane oligomers: structure and thermodynamics from molecular dynamics simulations of chemically realistic models," *The Journal of Physical Chemistry*, vol. 96, no. 12, pp. 5077–5086, 1992.

[18] E. A. Müller and A. Mejía, "Interfacial properties of selected binary mixtures containing n-alkanes," *Fluid Phase Equilibria*, vol. 282, no. 2, pp. 68–81, 2009.

[19] A. Mejía, M. Cartes, H. Segura, and E. A. Müller, "Use of equations of state and coarse grained simulations to complement experiments: Describing the interfacial properties of carbon dioxide + decane and carbon dioxide + eicosane mixtures," *Journal of Chemical & Engineering Data*, vol. 59, no. 10, pp. 2928–2941, 2014.

[20] S. Werth, M. Horsch, and H. Hasse, "Surface tension of the two center lennard-jones plus quadrupole model fluid," *Fluid Phase Equilibria*, vol. 392, pp. 12–18, 2015.

[21] J. M. Míguez, J. M. Garrido, F. J. Blas, H. Segura, A. Mejía, and M. M. Piñeiro, "Comprehensive characterization of interfacial behavior for the mixture CO2 + H2O + CH4: Comparison between atomistic and coarse grained molecular simulation models and density gradient theory," *The Journal of Physical Chemistry C*, vol. 118, no. 42, pp. 24504–24519, 2014.

[22] F. R. Beierlein, A. M. Krause, C. M. Jäger, P. Fita, E. Vauthey, and T. Clark, "Molecular dynamics simulations of liquid phase interfaces: understanding the structure of the glycerol/water–dodecane system," *Langmuir*, vol. 29, no. 38, pp. 11898–11907, 2013.

[23] S. Eckelsbach and J. Vrabec, "Fluid phase interface properties of acetone, oxygen, nitrogen and their binary mixtures by molecular simulation," *Physical Chemistry Chemical Physics*, vol. 17, no. 40, pp. 27195–27203, 2015.

[24] H. T. Davis, *Statistical mechanics of phases, interfaces, and thin films*. Wiley-VCH, 1996.

[25] R. Evans and D. Henderson, "Fundamentals of inhomogeneous fluids," *New York: Marcel Dekker Chapt*, vol. 3, pp. 85–175, 1992.

[26] J. Wu, "Density functional theory for chemical engineering: From capillarity to soft materials," *AIChE journal*, vol. 52, no. 3, pp. 1169–1193, 2006.

[27] J. Wu and Z. Li, "Density-functional theory for complex fluids," *Annu. Rev. Phys. Chem.*, vol. 58, pp. 85–112, 2007.

[28] C. P. Emborsky, Z. Feng, K. R. Cox, and W. G. Chapman, "Recent advances in classical density functional theory for associating and polyatomic molecules," *Fluid Phase Equilibria*, vol. 306, no. 1, pp. 15–30, 2011.

[29] H. Löwen, "Density functional theory of inhomogeneous classical fluids: recent developments and new perspectives," *Journal of Physics: Condensed Matter*, vol. 14, no. 46, p. 11897, 2002.

[30] J. Gross, "A density functional theory for vapor-liquid interfaces using the pcp-saft equation of state," *The Journal of chemical physics*, vol. 131, no. 20, p. 204705, 2009.

[31] C. Klink and J. Gross, "A density functional theory for vapor–liquid interfaces of mixtures using the perturbed-chain polar statistical associating fluid theory equation of state," *Industrial & Engineering Chemistry Research*, vol. 53, no. 14, pp. 6169–6178, 2014.

[32] C. Klink, B. Planková, and J. Gross, "Density functional theory for liquid–liquid interfaces of mixtures using the perturbed-chain polar statistical associating fluid theory equation of state," *Industrial & Engineering Chemistry Research*, vol. 54, no. 16, pp. 4633–4642, 2015.

[33] J. Van der Waals, "Z. phys. chem., 13, 657. english translation: Rowlinson, js, 1979," *J. statist. Phys*, vol. 20, p. 197, 1894.

[34] J. W. Cahn and J. E. Hilliard, "Free energy of a nonuniform system. I. interfacial free energy," *The Journal of chemical physics*, vol. 28, no. 2, pp. 258–267, 1958.

[35] V. Bongiorno, L. Scriven, and H. Davis, "Molecular theory of fluid interfaces," *Journal of Colloid and Interface Science*, vol. 57, no. 3, pp. 462–475, 1976.

[36] A. J. Yang, P. D. Fleming III, and J. H. Gibbs, "Molecular theory of surface tension," *The Journal of Chemical Physics*, vol. 64, no. 9, pp. 3732–3747, 1976.

[37] R. Evans, "The nature of the liquid-vapour interface and other topics in the statistical mechanics of non-uniform, classical fluids," *Advances in Physics*, vol. 28, no. 2, pp. 143–200, 1979.

[38] B. Breure and C. Peters, "Modeling of the surface tension of pure components and mixtures using the density gradient theory combined with a theoretically derived influence parameter correlation," *Fluid Phase Equilibria*, vol. 334, pp. 189–196, 2012.

[39] P. Cornelisse, C. Peters, and J. de Swaan Arons, "On the fundamentals of the gradient theory of van der waals," *The Journal of chemical physics*, vol. 106, no. 23, pp. 9820–9834, 1997.

[40] C. Miqueu, B. Mendiboure, A. Graciaa, and J. Lachaise, "Modelling of the surface tension of pure components with the gradient theory of fluid interfaces: a simple and accurate expression for the influence parameters," *Fluid phase equilibria*, vol. 207, no. 1, pp. 225–246, 2003.

[41] H. Lin, Y.-Y. Duan, and Q. Min, "Gradient theory modeling of surface tension for pure fluids and binary mixtures," *Fluid phase equilibria*, vol. 254, no. 1, pp. 75–90, 2007.

[42] J. M. Garrido, A. Mejía, M. M. Piñeiro, F. J. Blas, and E. A. Müller, "Interfacial tensions of industrial fluids from a molecular-based square gradient theory," *AIChE Journal*, vol. 62, no. 5, pp. 1781–1794, 2016.

[43] B. Carey, L. Scriven, and H. Davis, "Semiempirical theory of surface tension of binary systems," *AIChE journal*, vol. 26, no. 5, pp. 705–711, 1980.

[44] P. Cornelisse, C. Peters, and J. de Swaan Arons, "Simultaneous prediction of phase equilibria, interfacial tension and concentration profiles," *Molecular Physics*, vol. 80, no. 4, pp. 941–955, 1993.

[45] D.-Y. Peng and D. B. Robinson, "A new two-constant equation of state," *Industrial & Engineering Chemistry Fundamentals*, vol. 15, no. 1, pp. 59–64, 1976.

[46] C. Miqueu, B. Mendiboure, C. Graciaa, and J. Lachaise, "Modelling of the surface tension of binary and ternary mixtures with the gradient theory of fluid interfaces," *Fluid phase equilibria*, vol. 218, no. 2, pp. 189–203, 2004.

[47] P. Cornelisse, M. Wijtkamp, C. Peters, and J. de Swaan Arons, "Interfacial tensions of fluid mixtures with polar and associating components," *Fluid phase equilibria*, vol. 150, pp. 633–640, 1998.

[48] G. Ikonomou and M. Donohue, "Thermodynamics of hydrogen-bonded molecules: The associated perturbed anisotropic chain theory," *AIChE journal*, vol. 32, no. 10, pp. 1716–1725, 1986.

[49] M. Oliveira, I. Marrucho, J. Coutinho, and A. Queimada, "Surface tension of chain molecules through a combination of the gradient theory with the CPA EoS," *Fluid Phase Equilibria*, vol. 267, no. 1, pp. 83–91, 2008.

[50] G. M. Kontogeorgis, E. C. Voutsas, I. V. Yakoumis, and D. P. Tassios, "An equation of state for associating fluids," *Industrial & engineering chemistry research*, vol. 35, no. 11, pp. 4310–4318, 1996.

[51] H. Kahl and S. Enders, "Interfacial properties of binary mixtures," *Physical Chemistry Chemical Physics*, vol. 4, no. 6, pp. 931–936, 2002.

[52] W. G. Chapman, G. Jackson, and K. E. Gubbins, "Phase equilibria of associating fluids: chain molecules with multiple bonding sites," *Molecular Physics*, vol. 65, no. 5, pp. 1057–1079, 1988.

[53] W. G. Chapman, K. E. Gubbins, G. Jackson, and M. Radosz, "New reference equation of state for associating liquids," *Industrial & Engineering Chemistry Research*, vol. 29, no. 8, pp. 1709–1721, 1990.

[54] T. Lafitte, B. Mendiboure, M. M. Pineiro, D. Bessieres, and C. Miqueu, "Interfacial properties of water/co2: a comprehensive description through a gradient theory-

SAFT-VR Mie approach," *The Journal of Physical Chemistry B*, vol. 114, no. 34, pp. 11110–11116, 2010.

[55] Y. F. Chow, D. K. Eriksen, A. Galindo, A. J. Haslam, G. Jackson, G. C. Maitland, and J. M. Trusler, "Interfacial tensions of systems comprising water, carbon dioxide and diluent gases at high pressures: Experimental measurements and modelling with SAFT-VR Mie and square-gradient theory," *Fluid Phase Equilibria*, vol. 407, pp. 159–176, 2016.

[56] T. Lafitte, D. Bessieres, M. M. Piñeiro, and J.-L. Daridon, "Simultaneous estimation of phase behavior and second-derivative properties using the statistical associating fluid theory with variable range approach," *The Journal of chemical physics*, vol. 124, no. 2, p. 024509, 2006.

[57] J. Gross and G. Sadowski, "Perturbed-chain SAFT: An equation of state based on a perturbation theory for chain molecules," *Industrial & engineering chemistry research*, vol. 40, no. 4, pp. 1244–1260, 2001.

[58] D. Fu, X.-S. Li, S. Yan, and T. Liao, "Investigation of critical properties and surface tensions for n-alkanes by perturbed-chain statistical associating fluid theory combined with density-gradient theory and renormalization-group theory," *Industrial & engineering chemistry research*, vol. 45, no. 24, pp. 8199–8206, 2006.

[59] D. Fu, "Investigation of surface tensions for pure associating fluids by perturbed-chain statistical associating fluid theory combined with density-gradient theory," *Industrial & Engineering Chemistry Research*, vol. 46, no. 22, pp. 7378–7383, 2007.

[60] D. Fu and Y. Wei, "Investigation of vapor- liquid surface tension for carbon dioxide and hydrocarbon mixtures by perturbed-chain statistical associating fluid theory combined with density-gradient theory," *Industrial & Engineering Chemistry Research*, vol. 47, no. 13, pp. 4490–4495, 2008.

[61] D. Fu, H. Jiang, B. Wang, and S. Fu, "Investigation of the surface tension of methane and n-alkane mixtures by perturbed-chain statistical associating fluid theory combined with density-gradient theory," *Fluid Phase Equilibria*, vol. 279, no. 2, pp. 136–140, 2009.

[62] X.-S. Li, J.-M. Liu, and D. Fu, "Investigation of interfacial tensions for carbon dioxide aqueous solutions by perturbed-chain statistical associating fluid theory combined with density-gradient theory," *Industrial & Engineering Chemistry Research*, vol. 47, no. 22, pp. 8911–8917, 2008.

[63] M. Mousazadeh and E. Faramarzi, "Calculation of surface tension of metals using density gradient theory and PC-SAFT equation of state," *Fluid Phase Equilibria*, vol. 301, no. 1, pp. 13–17, 2011.

[64] V. Vinš, B. Planková, and J. Hrubỳ, "Surface tension of binary mixtures including polar components modeled by the density gradient theory combined with the PC-SAFT equation of state," *International Journal of Thermophysics*, vol. 34, no. 5, pp. 792–812, 2013.

[65] J. Gross, "An equation-of-state contribution for polar components: Quadrupolar molecules," *AIChE journal*, vol. 51, no. 9, pp. 2556–2568, 2005.

[66] J. Gross and J. Vrabec, "An equation-of-state contribution for polar components: Dipolar molecules," *AIChE journal*, vol. 52, no. 3, pp. 1194–1204, 2006.

[67] J. Vrabec and J. Gross, "Vapor-liquid equilibria simulation and an equation of state contribution for dipole-quadrupole interactions," *The Journal of Physical Chemistry B*, vol. 112, no. 1, pp. 51–60, 2008.

[68] E. Schäfer, G. Sadowski, and S. Enders, "Interfacial tension of binary mixtures exhibiting azeotropic behavior: Measurement and modeling with PCP-SAFT combined with density gradient theory," *Fluid Phase Equilibria*, vol. 362, pp. 151–162, 2014.

[69] N. von Solms, M. L. Michelsen, and G. M. Kontogeorgis, "Computational and physical performance of a modified PC-SAFT equation of state for highly asymmetric and associating mixtures," *Industrial & engineering chemistry research*, vol. 42, no. 5, pp. 1098–1105, 2003.

[70] S. Khosharay, M. Abolala, and F. Varaminian, "Modeling the surface tension and surface properties of (CO2 + h2o) and (H2S + H2O) with gradient theory in combination with sPC–SAFT EOS and a new proposed influence parameter," *Journal of Molecular Liquids*, vol. 198, pp. 292–298, 2014.

[71] R. G. Larson, H. Davis, L. Scriven, *et al.*, "Elementary mechanisms of oil recovery by chemical methods," *Journal of Petroleum Technology*, vol. 34, no. 02, pp. 243–258, 1982.

[72] E. C. Donaldson, G. V. Chilingarian, and T. F. Yen, *Enhanced oil recovery, I: fundamentals and analyses*, vol. 17. Elsevier, 1985.

[73] C. Miqueu, B. Mendiboure, A. Graciaa, and J. Lachaise, "Modeling of the surface tension of multicomponent mixtures with the gradient theory of fluid interfaces," *Industrial & engineering chemistry research*, vol. 44, no. 9, pp. 3321–3329, 2005.

[74] C. Miqueu, B. Mendiboure, A. Graciaa, and J. Lachaise, "Petroleum mixtures: An efficient predictive method for surface tension estimations at reservoir conditions," *Fuel*, vol. 87, no. 6, pp. 612–621, 2008.

[75] P. M. Larsen, B. Maribo-Mogensen, and G. M. Kontogeorgis, "A collocation method for surface tension calculations with the density gradient theory," *Fluid Phase Equilibria*, vol. 408, pp. 170–179, 2016.

[76] J. Kou, S. Sun, and X. Wang, "Efficient numerical methods for simulating surface tension of multi-component mixtures with the gradient theory of fluid interfaces," *Computer Methods in Applied Mechanics and Engineering*, vol. 292, pp. 92–106, 2015.

[77] V. Bongiorno and H. T. Davis, "Modified van der waals theory of fluid interfaces," *Physical Review A*, vol. 12, no. 5, p. 2213, 1975.

[78] P. M. W. Cornelisse, *The Square Gradient Theory Applied*. PhD thesis, TU Delft, 1997.

[79] J. J. Moré, B. S. Garbow, and K. E. Hillstrom, "User guide for minpack-1," tech. rep., CM-P00068642, 1980.

[80] L. Hascoet and V. Pascual, "The tapenade automatic differentiation tool: principles, model, and specification," *ACM Transactions on Mathematical Software (TOMS)*, vol. 39, no. 3, p. 20, 2013.

[81] H. Ng, S. Taylor, H. Schroeder, and D. Sieben, "High pressure gas separation and conditioning," *GPA Research Report, Rep. No. PR-193*, pp. 1–50, 2008.

[82] A. Danesh, A. Dandekar, A. Todd, and R. Sarkar, "A modified scaling law and parachor method approach for improved prediction of interfacial tension of gas-condensate systems," in *SPE Annual Technical Conference and Exhibition*, Society of Petroleum Engineers, 1991.

[83] O. N. Amézquita, S. Enders, P. Jaeger, and R. Eggers, "Interfacial properties of mixtures containing supercritical gases," *The Journal of Supercritical Fluids*, vol. 55, no. 2, pp. 724–734, 2010.

[84] X. Liang, M. L. Michelsen, and G. M. Kontogeorgis, "Pitfalls of using the geometric-mean combining rule in the density gradient theory," *Fluid Phase Equilibria*, vol. 415, pp. 75–83, 2016.

[85] N. Mungan *et al.*, "Carbon dioxide flooding-fundamentals," *Journal of Canadian Petroleum Technology*, vol. 20, no. 01, pp. 87–92, 1981.

[86] O. N. Amézquita, S. Enders, P. Jaeger, and R. Eggers, "Measurement and prediction of interfacial tension of binary mixtures," *Industrial & Engineering Chemistry Research*, vol. 49, no. 2, pp. 592–601, 2009.

[87] M. Telo da Gama and R. Evans, "Theory of the liquid-vapour interface of a binary mixture of lennard-jones fluids," *Molecular Physics*, vol. 41, no. 5, pp. 1091–1112, 1980.

[88] F. Llovell, A. Galindo, F. J. Blas, and G. Jackson, "Classical density functional theory for the prediction of the surface tension and interfacial properties of fluids mixtures of chain molecules based on the statistical associating fluid theory for potentials of variable range," *The Journal of chemical physics*, vol. 133, no. 2, p. 024704, 2010.

[89] C. Klink, C. Waibel, and J. Gross, "Analysis of interfacial transport resistivities of pure components and mixtures based on density functional theory," *Industrial & Engineering Chemistry Research*, vol. 54, no. 45, pp. 11483–11492, 2015.

[90] K. Glavatskiy and D. Bedeaux, "Transport of heat and mass in a two-phase mixture: From a continuous to a discontinuous description," *The Journal of chemical physics*, vol. 133, no. 14, p. 144709, 2010.

[91] K. Glavatskiy and D. Bedeaux, "Resistances for heat and mass transfer through a liquid–vapor interface in a binary mixture," *The Journal of chemical physics*, vol. 133, no. 23, p. 234501, 2010.

[92] J. Gmehling, D. Tiegs, A. Medina, M. Soares, J. Bastos, P. Alessi, I. Kikic, M. Schiller, and J. Menke, "Dechema chemisry data series, volume IX activity coefficients at infinite dilution," *DECHEMA Chemistry Data Series Vol. IX Activity Coefficients at Infinite Dilution*, 1994.

[93] K. Kniaź, "Influence of size and shape effects on the solubility of hydrocarbons: the role of the combinatorial entropy," *Fluid Phase Equilibria*, vol. 68, pp. 35–46, 1991.

[94] B. Widom, "Structure of the $\alpha\gamma$ interface," *The Journal of Chemical Physics*, vol. 68, no. 8, pp. 3878–3883, 1978.

[95] R. Roth, R. Evans, A. Lang, and G. Kahl, "Fundamental measure theory for hard-sphere mixtures revisited: the white bear version," *Journal of Physics: Condensed Matter*, vol. 14, no. 46, p. 12063, 2002.

[96] Y.-X. Yu and J. Wu, "Structures of hard-sphere fluids from a modified fundamental-measure theory," *The Journal of chemical physics*, vol. 117, no. 22, pp. 10156–10164, 2002.

[97] S. Tripathi and W. G. Chapman, "Microstructure of inhomogeneous polyatomic mixtures from a density functional formalism for atomic mixtures," *The Journal of chemical physics*, vol. 122, no. 9, p. 094506, 2005.

[98] A. Bymaster and W. G. Chapman, "An iSAFT density functional theory for associating polyatomic molecules," *The Journal of Physical Chemistry B*, vol. 114, no. 38, pp. 12298–12307, 2010.

[99] E. Jiménez, H. Casas, L. Segade, and C. Franjo, "Surface tensions, refractive indexes and excess molar volumes of hexane + 1-alkanol mixtures at 298.15 k," *Journal of Chemical & Engineering Data*, vol. 45, no. 5, pp. 862–866, 2000.

[100] M. Goral, P. Oracz, A. Skrzecz, A. Bok, and A. Maczyński, "Recommended vapor–liquid equilibrium data. part 1: binary n-alkanol–n-alkane systems," *Journal of Physical and Chemical Reference Data*, vol. 31, no. 3, pp. 701–748, 2002.

[101] E. W. Lemmon, M. O. McLinden, and D. G. Friend, "Thermophysical properties of fluid systems," in *NIST Chemistry WebBook, NIST Standard Reference Database Number 69* (P. J. Linstrom and W. G. Mallard, eds.), Gaithersburg MD, 20899: National Institute of Standards and Technology, 2016. http://webbook.nist.gov, (retrieved July 12, 2016).

[102] J. J. Jasper, E. R. Kerr, and F. Gregorich, "The orthobaric surface tensions and thermodynamic properties of the liquid surfaces of the nalkanes, c5 to c28," *Journal of the American Chemical Society*, vol. 75, no. 21, pp. 5252–5254, 1953. In Dortmund Data Bank, 2015, www.ddbst.com.

[103] P. P. Pugachevich and Y. A. Khvorov, "The surface tensions of heptane, undecane, hexadecane and their mixtures," *Deposited Doc. VINITI*, vol. 3893–77, pp. 1–14, 1977. In Dortmund Data Bank, 2015, www.ddbst.com.

[104] P. P. Pugachevich and B. B. Zhalsabon, "Experimental determination of surface tension of dodecane, heptadecane and tricosane binary and ternary mixtures in a wide temperature and concentration region," *Deposited Doc. VINITI*, vol. 2644–81, pp. 1–17, 1981. In Dortmund Data Bank, 2015, www.ddbst.com.

[105] P. P. Pugachevich and V. A. Dozorov, "Experimental study of surface tension of decane, tridecane, octadecane and their solutions," *Deposited Doc. VINITI*, vol. 1282–81, pp. 1–34, 1981. In Dortmund Data Bank, 2015, www.ddbst.com.

[106] A. I. Vogel, "38. physical properties and chemical constitution. part IX. aliphatic hydrocarbons," *Journal of the Chemical Society (Resumed)*, pp. 133–139, 1946. In Dortmund Data Bank, 2015, www.ddbst.com.

[107] G. Korosi and E. S. Kovats, "Density and surface tension of 83 organic liquids," *Journal of Chemical and Engineering Data*, vol. 26, no. 3, pp. 323–332, 1981. In Dortmund Data Bank, 2015, www.ddbst.com.

[108] A. J. Queimada, A. I. Caco, I. M. Marrucho, and J. A. Coutinho, "Surface tension of decane binary and ternary mixtures with eicosane, docosane, and tetracosane," *Journal of Chemical & Engineering Data*, vol. 50, no. 3, pp. 1043–1046, 2005. In Dortmund Data Bank, 2015, www.ddbst.com.

[109] K. Stephan and H. Hildwein, "Recommended data of selected compounds and binary mixtures," *Chemistry Data Series Vol. IV, Pts. 1+2, DECHEMA*, 1987. In Surface tension of pure liquids and binary liquid mixtures, M.D. Lechner, Ch. Wohlfarth, B. Wohlfarth, 2015, Springer.

[110] G. M. Kontogeorgis and G. K. Folas, *Thermodynamic Models for Industrial Applications: From Classical and Advanced Mixing Rules to Association Theories*. Wiley Online Library, 2009.

[111] J. J. Jasper, "The surface tension of pure liquid compounds," *Journal of physical and chemical reference data*, vol. 1, no. 4, pp. 841–1010, 1972. In Surface tension of pure liquids and binary liquid mixtures, M.D. Lechner, Ch. Wohlfarth, B. Wohlfarth, 2015, Springer.

[112] J. Gross and G. Sadowski, "Application of the perturbed-chain SAFT equation of state to associating systems," *Industrial & engineering chemistry research*, vol. 41, no. 22, pp. 5510–5515, 2002.

[113] A. Mulero, I. Cachadiña, and M. Parra, "Recommended correlations for the surface tension of common fluids," *Journal of Physical and Chemical Reference Data*, vol. 41, no. 4, p. 043105, 2012.

[114] B. E. Poling, J. M. Prausnitz, O. John Paul, and R. C. Reid, *The properties of gases and liquids*, vol. 5. McGraw-Hill New York, 2001.

[115] G. Thomson, "The DIPPR databases," *International journal of thermophysics*, vol. 17, no. 1, pp. 223–232, 1996.

Chapter 3

Numerical aspects of classical Density Functional Theory for one-dimensional vapor-liquid interfaces

The content of this chapter is a literal quote of the publication

Mairhofer, Gross, Fluid Phase Equilibria, 444, 2017, 1-12.

In comparison to the published work, the abstract is here omitted. Additions or deletions compared to the published work are marked with angular brackets.

Classical density functional theory (DFT) is a versatile framework to study the properties of inhomogeneous systems and has been applied to many problems in chemical engineering and material science [1] [2] [3] [4]. It is based on a thermodynamic minimization principle: at equilibrium the grand potential Ω of a system consisting of N components at given values of temperature T, volume V and chemical potentials μ_i $(i = 1, ..., N)$ is minimal with respect to internal degrees of freedom. For inhomogeneous systems, the grand potential is a functional of the spatially varying density. The goal of DFT applications is to determine the equilibrium density profiles $\rho_i(\tilde{\mathbf{r}})$ as an internal degree of freedom iteratively until Ω has reached its minimum. The functional derivatives of Ω with respect to the density profiles are thus zero at equilibrium conditions. Because the density profiles $\rho_i(\tilde{\mathbf{r}})$ are for practical applications discretized on a grid, the condition of vanishing functional derivatives reduces to a set of coupled nonlinear equations.
Most studies on density functional theory are concerned with developing Helmholtz energy functionals for DFT [5] [6] [7] [8] [9] [10] and a simple damped direct substitution method (Picard iteration) is used to solve the resulting system of equations. The development

and comparison of numerical methods has received less attention. Notable exceptions are the studies of Frink and coworkers [11] [12] [13] [14] [15] presenting matrix-based as well as matrix-free Newton methods for atomic and polymeric DFT approaches in confined media of up to three dimensions, also exploring the potential of parallelization and preconditioning. Further studies include the work of Knepley et al. on charged hard sphere particles and the comparison of a Picard iteration with a line search method to Newton iterations [16], the works of Oettel et al. [17] and Härtel et al. [18] on hard spheres in three-dimensional geometries using the direct inversion in the iterative subspace method [19], the review of Roth [20] on hard-sphere models where a simple line search algorithm is presented as well as the work of Edelmann and Roth [21] on hard spheres with attractive interactions in three dimensions applying a limited memory Broyden method. Thus, most of these previous studies on numerical aspects of DFT focus on algorithms to track interfacial phenomena of model fluids in confined media in more than one dimension where restrictions due to memory limitations play an important role. The goal of this work is to compare different algorithms to obtain the interfacial properties of the one-dimensional vapor-liquid interface of real fluids.

The motivation for this study is the integration of DFT in the MoDeNa [Modelling of morphology Development of micro- and Nano Structures] interface [22] for multiscale modeling as a tool to calculate surface tensions. To use DFT for this purpose is appealing because unlike alternative methods such as density gradient theory it does not require any additional parameters beyond those of the equation of state to calculate interfacial properties. To study real fluids, a Helmholtz energy functional suitable for non-spherical molecules and polar or associating interactions needs to be applied. The functional needs to correlate or predict phase equilibrium properties, such as the densities of the corresponding vapor and liquid phases and the equilibrium chemical potential sufficiently well, because these properties enter the DFT calculations. PC-SAFT [23] [24] is an equation of state successfully applied to a wide range of systems. A Helmholtz energy functional consistent with PC-SAFT has been developed by Gross [5] and Gross and Klink [6]. This DFT approach is used here with some modifications: the dispersive contribution is included in a weighted-density approximation presented in [25] and associative interactions are treated in a non-local description using the approaches of Yu and Wu [26] and Bymaster and Chapman [27].

To carry out this work, we use of the *Portable, Extensible Toolkit for Scientific Computing* (PETSc) [28], as a framework that allows to use different algorithms without the need to change the interface between the solver and the application code as well as an efficient and convenient handling of parallel data structures.

In this work, we apply five different algorithms to solve the system of coupled, nonlinear equations arising from DFT for one-dimensional vapor-liquid interfaces: Picard iteration,

Anderson mixing, a restarted quasi Newton method and two matrix-free inexact Newton methods, using analytical and numerical derivatives. We compare the convergence behavior with emphasis on computation time. Furthermore, we compare the Helmholtz energy functionals of Yu and Wu [26] and Bymaster and Chapman [27] to account for associative interactions. The computational speed-up of using a line search method, parallelization and a convergence criterion based on the value of surface tension is discussed.

3.1 Classical density functional theory

This section summarizes the basic equations of classical density functional theory. For a more detailed description of the underlying molecular model of PC-SAFT and the DFT approach used in this work, we refer to the work of Gross [5] and Klink and Gross [6]. For a system of N components in thermodynamic equilibrium at fixed values of temperature T, chemical potentials μ_i $(i = 1, ..., N)$ and volume V, the grand potential Ω is at a minimum with respect to the systems' internal degrees of freedom. This applies to homogeneous systems as well as to inhomogeneous system where the densities $\rho_i(\tilde{\mathbf{r}})$ may vary in space either due to an external potential $V(\tilde{\mathbf{r}})$ or due to a phase interface. We consider fluid-liquid interfaces in absence of an external field so that the grand potential can be expressed as

$$\Omega[\{\rho_k\}] = A[\{\rho_k\}] - \sum_i^N \int \mu_i \rho_i(\tilde{\mathbf{r}}) \mathrm{d}\tilde{\mathbf{r}} \tag{3.1}$$

where $A[\{\rho_k\}]$ is the intrinsic Helmholtz energy of the system which is a functional of the density profiles $\rho_i(\tilde{\mathbf{r}})$. For a compact notation, we don't explicitly show that A and Ω are functions of T and μ_i. The curly brackets denote the dependency on all species-densities. According to the PC-SAFT model, the Helmholtz energy functional $A[\{\rho_k\}]$ can be decomposed into a sum of several contributions

$$A[\{\rho_k\}] = A^{\mathrm{ig}}[\{\rho_k\}] + A^{\mathrm{hs}}[\{\rho_k\}] + A^{\mathrm{chain}}[\{\rho_k\}] + A^{\mathrm{disp}}[\{\rho_k\}] + A^{\mathrm{assoc}}[\{\rho_k\}] \tag{3.2}$$

where the individual contributions to the Helmholtz energy are for the ideal gas, hard sphere interactions, chain formation, dispersion and association (i.e. hydrogen bonding). The ideal gas contribution is given by

$$A^{\mathrm{ig}}[\{\rho_k\}]/kT = \int \sum_{i=1}^N \rho_i(\tilde{\mathbf{r}}) \left(\ln[\rho_i(\tilde{\mathbf{r}}) \Lambda_i^3] - 1 \right) \mathrm{d}\tilde{\mathbf{r}} \tag{3.3}$$

The spatial variable $\tilde{\mathbf{r}}$ is a vector defining the position $\mathbf{r}$ as well as the configuration and orientation of a given molecule. The density $\rho_i(\tilde{\mathbf{r}})$ is a single-particle probability density of finding molecules at a certain $\tilde{\mathbf{r}}$. One has to be careful about the normalization of $\rho_i(\tilde{\mathbf{r}})$.

As described in the work of Klink and Gross [6], the configurational and orientational degrees of freedom can to good approximation be absorbed in the de Broglie wavelength $\Lambda_i(T)$. The de Broglie wavelength appears in two contributions in eq. (3.1) with opposite sign and cancels out. Our goal is thus simply to calculate the density profiles $\rho_i(\mathbf{r})$, i.e. single-molecule (or single molecular segment) number density for the center of mass position $\mathbf{r}$. The remaining ideal gas contribution then reads

$$\tilde{A}^{\mathrm{ig}}[\{\rho_k\}]/kT = \int \sum_{i=1}^{N} \rho_i(\mathbf{r}) \left(\ln[\rho_i(\mathbf{r})] - 1\right) \mathrm{d}\mathbf{r} \tag{3.4}$$

For the hard sphere contribution we apply the Fundamental Measure Theory of Rosenfeld [29] in the modified form of Roth et al. [30] and Yu and Wu [31]

$$A^{\mathrm{hs}}[\{\rho_k\}]/kT = \int \Phi^{\mathrm{hs}}\left(\{n_\alpha(\mathbf{r})\}\right) \mathrm{d}\mathbf{r} \tag{3.5}$$

where the reduced Helmholtz energy density Φ^{hs} is a function of a set of weighted densities $n_\alpha(\mathbf{r})$ which are themselves functionals of density. For more details on Fundamental Measure Theory we refer to the original publications [29, 30, 31]. Expressions for the one-dimensional form of eq. (3.5) as well as for the functional derivative can be found in [5].

A Helmholtz energy functional for the contribution of chain formation $A^{\mathrm{chain}}[\{\rho_k\}]$ for mixtures consistent with PC-SAFT was developed by Tripathi and Chapman [8] and adapted in ref. [5, 6], as

$$\begin{aligned} A^{\mathrm{chain}}[\{\rho_k\}]/kT = &\sum_{i}^{N} (m_i - 1) \int \rho_i(\mathbf{r}) \left\{\ln\left(\rho_i(\mathbf{r})\right) - 1\right\} \mathrm{d}\mathbf{r} \\ &- \sum_{i}^{N} (m_i - 1) \int \rho_i(\mathbf{r}) \left\{\ln\left[y_{ii}^{dd}\left(\{\bar{\rho}_k(\mathbf{r})\}\right)\lambda_i(\mathbf{r})\right] - 1\right\} \mathrm{d}\mathbf{r} \end{aligned} \tag{3.6}$$

where y_{ii}^{dd} denotes the value of the cavity correlation function of a homogeneous fluid at contact distance evaluated at a weighted density $\bar{\rho}(\mathbf{r})$ in order to approximate the value of the inhomogeneous fluid [8] [32] and $\lambda_i(\mathbf{r})$ is the average density at contact-distance. Detailed expressions for these quantities as well as the functional derivative of eq. (3.6) for the one-dimensional case are presented in [6].

Dispersive interactions are treated in a weighted-density approximation [25].

$$A^{\mathrm{disp}}[\{\rho_k\}]/kT = \int \bar{\rho}^{\mathrm{disp}}(\mathbf{r}) a^{pcsaft}(\bar{\rho}^{\mathrm{disp}}(\mathbf{r})) \mathrm{d}\mathbf{r} \tag{3.7}$$

where $a^{pcsaft}(\bar{\rho}^{\text{disp}}(\mathbf{r}))$ is the reduced Helmholtz energy density according to the dispersive term of PC-SAFT evaluated at a weighted density $\bar{\rho}^{\text{disp}}(\mathbf{r})$ given in [25].

We consider two different approaches for the associative contribution of the Helmholtz energy functional which are both modifications of the work of Segura et al. [33]. The first approach is due to Bymaster and Chapman [27], the second due to Yu and Wu [26]. In the approach of Bymaster and Chapman, the contribution of association to the Helmholtz energy functional is

$$A^{\text{assoc}}[\{\rho_k\}]/kT = \int \sum_{i=1}^{N} \rho_i(\mathbf{r}) \sum_{A \in \Gamma^i} \left(\ln \chi_A^i(\mathbf{r}) - \frac{\chi_A^i(\mathbf{r})}{2} + \frac{1}{2} \right) \mathrm{d}\mathbf{r} \tag{3.8}$$

where χ_A^i is the monomer fraction, i.e. the fraction of association sites A on molecule i un-bonded to other association sites. The second sum runs over all association sites on molecule i. The expression for χ_A^i based on Bymaster and Chapman [27] but modified to be consistent with PC-SAFT is given by

$$\chi_A^i(z) = \left(1 + \frac{1}{2} \sum_{j=1}^{N} \kappa_{ij} \sigma_{ij}^2 \int_{z-\sigma_{ij}}^{z+\sigma_{ij}} \rho_j(z') \sum_{B \in \Gamma^j} \chi_B^j(z') \left\{ y_{ij}^{dd}(z, z') \left[\exp(\beta \epsilon_{AiBj}) - 1 \right] \right\} \mathrm{d}z' \right)^{-1} \tag{3.9}$$

Here, σ_{ij}, κ_{ij} and ϵ_{AiBj} denote the segment diameter parameter, association volume and association energy parameter of the mixture, respectively, whose definitions can be found in [23] and [24]. Furthermore, $y_{ij}^{dd}(z, z') = \sqrt{y_{ij}^{dd}(\{\bar{\rho}_k(z)\}) \cdot y_{ij}^{dd}(\{\bar{\rho}_k(z')\})}$ where y_{ij}^{dd} denotes the value of the cavity correlation function of the homogeneous fluid at contact distance evaluated at a weighted density $\bar{\rho}(z)$. The detailed form of y_{ij}^{dd} can be found in [8]. Details on the functional derivative of $A^{\text{assoc}}[\{\rho_k\}]$ and the determination of $\chi_A^i(z)$ are presented in the supporting information of [27].

Yu and Wu [26] proposed a weighted-density approximation for the associative contribution employing the weighted densities of the Fundamental Measure Theory $n_\alpha(\mathbf{r})$ [29] [30] [31]

$$A^{\text{assoc}}[\{\rho_k\}]/kT = \int \Phi^{\text{assoc}}\left(\{n_\alpha(\mathbf{r})\}\right) \mathrm{d}\mathbf{r} \tag{3.10}$$

where the reduced Helmholtz energy density in a form consistent with PC-SAFT is given by [25]

$$\Phi^{\text{assoc}}\left(\{n_\alpha(\mathbf{r})\}\right) = \sum_i^N \frac{n_{0,i}(\mathbf{r})}{m_i}\zeta_i(\mathbf{r}) \sum_{A\in\Gamma^i}\left(\ln\chi_A^i(\mathbf{r}) - \frac{\chi_A^i(\mathbf{r})}{2} + \frac{1}{2}\right) \tag{3.11}$$

In eq. (3.11), $n_{0,i}(\mathbf{r})$ is a component specific weighted density, m_i is the segment number of component i and $\zeta(\mathbf{r})$ is a function of a subset of the weighted densities [26]. The fraction of un-bonded A site $\chi_A^i(\mathbf{r})$ is obtained by solving the set of nonlinear equations

$$\chi_A^i(\mathbf{r}) = \left(1 + \sum_j^N n_{0,j}(\mathbf{r})\zeta_j(\mathbf{r})\kappa_{ij}\sigma_{ij}^3 \sum_{B\in\Gamma^j}\chi_B^j(\mathbf{r})\left\{g_{ij}^{dd}\left[\exp\left(\beta\epsilon_{AiBj}\right) - 1\right]\right\}\right)^{-1} \tag{3.12}$$

with the contact value of a modified hard-sphere pair correlation function $g_{ij}^{dd}\left(\{n_\alpha(\mathbf{r})\}\right)$ [26].

In both approaches, the values of χ_A^i are determined by solving the corresponding equations, eq. (3.9) or eq. (3.12), by a simple damped successive substitution iteration. We solved for χ_A^i values in an inner iteration and didn't investigate a simultaneous procedure, together with solving for a density profile. The important difference between both association terms is, for the approach of Yu and Wu non-local information is only needed for calculating the FMT-weighted-densities $n_\alpha(\mathbf{r})$ whereas the subsequent iterative determination of $\chi_A^i(z)$ requires only the values of variables at position z, i.e. it is a purely local operation. For the approach of Bymaster and Chapman, on the other hand, values of $\chi_A^i(z)$ are coupled to the values at neighbouring grid points z'. Therefore, eq. (3.12) is much easier to solve than eq. (3.9) and a longer solution time can be expected with the approach of Bymaster and Chapman.

In equilibrium the grand potential of the system is minimal and the functional derivatives of Ω with respect to the species-density profiles vanish

$$\frac{\delta\Omega[\{\rho_k\}]}{\delta\rho_i(\mathbf{r})} = \frac{\delta A[\{\rho_k\}]}{\delta\rho_i(\mathbf{r})} - \mu_i = 0 \qquad \forall i \tag{3.13}$$

Eq. (3.13) can be rewritten to yield an expression which can be solved by a fixed-point method

$$\rho_i(\mathbf{r}) = \rho_i^{l,\text{bulk}} \exp\left(\mu_i^{l,\text{res}}/kT - \frac{\delta A^{\text{res}}[\{\rho_k\}]/kT}{\delta\rho_i(\mathbf{r})}\right) \qquad \forall i \tag{3.14}$$

or alternatively for a root finding algorithm

$$0 = \rho_i^{l,\text{bulk}} \exp\left(\mu_i^{l,\text{res}}/kT - \frac{\delta A^{\text{res}}[\{\rho_k\}]/kT}{\delta\rho_i(\mathbf{r})}\right) - \rho_i(\mathbf{r}) \qquad \forall i \tag{3.15}$$

where A^{res} is the residual part of the Helmholtz energy functional $A^{\text{res}} = A - A^{\text{ig}}$ and $\rho_i^{l,\text{bulk}}$ and $\mu_i^{l,\text{res}}$ denote the bulk density of component i in the liquid phase and the residual part

of the equilibrium chemical potential of component i in the liquid phase, respectively. For a planar interface where the inhomogeneity is only one-dimensional, eq. (3.15) can be discretized on a one-dimensional grid and solved by a suitable method. The dimension of the resulting system of coupled nonlinear equations is $n_{\text{grid}} \cdot N$ where n_{grid} is the number of grid points used in the discretization.

3.2 Algorithms

In this section, we briefly summarize the algorithms applied in this work. These are the inexact Newton method, a quasi Newton method, Anderson mixing and Picard iteration. The value of the residual given by the right hand side of eq. (3.15) is, for the k^{th} iteration, denoted $F(\rho^k)$. Further, $F'(\rho^k) = \frac{\partial F(\rho^k)}{\partial \rho^k}$ is the corresponding Jacobian. To simplify notation, ρ^k denotes an array of all species-density profiles at iteration k, i.e. ρ^k has $N \cdot n_{\text{grid}}$ entries where N is the number of components and n_{grid} is the number of grid points.

3.2.1 Line search method

For all algorithms except Anderson mixing the solution at iteration k is updated as

$$\rho^{k+1} = \rho^k + \lambda^k u^k \tag{3.16}$$

where the determination of the update u^k is algorithm specific and the damping factor λ^k has to be determined suitably. That is necessary because taking the whole step $\lambda^k = 1$ may not lead to a decrease of the residual. Furthermore, in applications like DFT where the solution ρ^k is bound by physical arguments to positive values not exceeding a maximum packing fraction, using $\lambda^k = 1$ may lead to unphysical values during the iterative procedure. A line search method searches along the update direction u^k in order to find a suitable value of λ^k. Several line search methods are available in PETSc, some of which can only be used with certain algorithms. For the test cases considered in this work, the different line search methods give very similar results. Therefore, a method is chosen that can be used in combination with all studied algorithms.
This line search method determines values of λ^k by minimizing the square of the norm of the residual $f = \left(||F(\rho^k + \lambda^k u^k)||_2\right)^2$. The minimization is conducted with a Newton scheme. We restrict the solution procedure to one Newton iteration step. Given an initial value $\lambda^{k,0}$, λ^k is determined as

$$\lambda^k = \lambda^{k,0} \pm \left(\left.\frac{\partial f}{\partial \lambda}\right|_{\lambda^{k,0}}\right)\left(\left.\frac{\partial^2 f}{\partial \lambda^2}\right|_{\lambda^{k,0}}\right)^{-1} \tag{3.17}$$

where the second derivative is approximated as

$$\left.\frac{\partial^2 f}{\partial \lambda^2}\right|_{\lambda^{k,0}} \approx \left(\left.\frac{\partial f}{\partial \lambda}\right|_{\lambda^{k,0}} - \left.\frac{\partial f}{\partial \lambda}\right|_{\lambda=0}\right) \Big/ \lambda^{k,0} \tag{3.18}$$

and both first derivates are approximated by a second-order upwind scheme using values of f at $\lambda = 0$, $\frac{1}{2}\lambda^{k,0}$ and $\lambda^{k,0}$. The sign in eq. (3.17) is the opposite of the sign of $\frac{\partial^2 f}{\partial \lambda^2}|_{\lambda^{k,0}}$ to ensure a step in the descent direction of f. In case of a concave function f, where the positive sign in eq. (3.17) applies instead of the negative sign of the regular Newton update, this procedure exhibits the risk of failure, because although the change of sign guarantees a step in the descent direction of f at $\lambda^{k,0}$, the step length is effectively arbitrary. In practical application, however, eq. (3.17) proved robust and no failures were detected for our application.
The advantage of this line search method is that steps $\lambda^k > 1$ are chosen if that accelerates convergence. The values of $\lambda^{k,0}$ are presented in the results section.

3.2.2 Inexact Newton method

Inexact Newton methods [34] solve a system of nonlinear equations by computing a sequence of steps u^k and approximate solutions ρ^k given by

$$||F(\rho^k) + F'(\rho^k)u^k||_2 \leq \eta_k ||F(\rho^k)||_2 \tag{3.19}$$

$$\rho^{k+1} = \rho^k + \lambda^k u^k \tag{3.20}$$

where $||\cdot||_2$ denotes the Euclidean norm and λ^k is a damping parameter which is determined according to the line search method described in section 3.2.1. The forcing term $\eta^k \in [0, 1)$ determines to which accuracy the linear system eq. (3.19) is solved at every Newton iteration k and by setting $\eta^k = 0$ the classical Newton method is recovered. The frequently used method of Eisenstat and Walker [35] where η^k is set depending on the agreement of $F(\rho^k)$ and its linear approximation does not perform better for the systems studied in this work than setting a fixed number of iterations (15 in this work) to solve eq. (3.19). GMRES [generalized minimal residual method] [36] is used as the linear solver. This solver offers the advantage that the resulting method can be used in a matrix-free way [37], i.e. the Jacobian $F'(\rho^k)$ never needs to be formed explicitly nor stored, because Krylov-subspace methods such as GMRES only require the action of the Jacobian on a vector $F'(\rho^k)v$. This matrix-vector product can be calculated using directional derivatives which can be obtained analytically using automatic differentiation or approximated numerically as

$$F'(\rho^k)v \approx \frac{F(\rho^k + \epsilon v) - F(\rho^k)}{\epsilon} \tag{3.21}$$

In this work, two matrix-free approaches are used. The first approach uses automatic differentiation [38] for evaluating $F'(\rho^k)v$ and will be denoted Newton_AD. The second approach (Newton_FD) uses the numerical approximation given in eq. (3.21) where the value of ϵ is set according to

$$\epsilon = \epsilon_{\text{rel}} \cdot \rho_k^T v \frac{1}{||v||_2^2} \qquad |\rho_k^T v| > \rho_{\min}||v||_1 \tag{3.22}$$

$$\epsilon = \epsilon_{\text{rel}} \cdot \rho_{\min} \cdot \text{sign}(\rho_k^T v) \frac{||v||_1}{||v||_2} \qquad \text{otherwise} \tag{3.23}$$

and the PETSc default values $\epsilon_{\text{rel}} = 10^{-8}$ and $\rho_{\min} = 10^{-6}\mathring{A}^{-3}$ are used.

3.2.3 Quasi Newton method

The limited memory Broyden-Fletcher-Goldfarb-Shanno algorithm (L-BFGS) [39] is a quasi Newton method where the system of nonlinear equations $F(\rho)$ is solved using successive updates of the approximation of the inverse of Jacobian $B^k \approx F'(\rho^k)^{-1}$. Given initial values B^0 and ρ^0 the solution ρ^k and the matrix B^k are updated as

$$u^k = -B^k F(\rho^k) \tag{3.24}$$

$$\rho^{k+1} = \rho^k + \lambda^k u^k \tag{3.25}$$

$$s_k = \lambda^k u^k \tag{3.26}$$

$$y_k = F(\rho^{k+1}) - F(\rho^k) \tag{3.27}$$

$$B^{k+1} = \left(\mathbf{I} - \frac{s_k y_k^T}{y_k^T s_k}\right) B^k \left(\mathbf{I} - \frac{y_k s_k^T}{y_k^T s_k}\right) + \frac{s_k s_k^T}{y_k^T s_k} \tag{3.28}$$

In the limited memory version of the algorithm, only the values of B from the last $m^k = \min(m, k)$ iterations are used to construct B^k. In all calculations we set $m = 10$ and $B^0 = \mathbf{I}$ where $\mathbf{I}$ is the identity matrix. For the remaining options PETSc default settings are used, i.e. Shanno scaling [40] is applied and restarts are invoked according to Powell's restart conditions [41]

$$|F(\rho^{k-1})^T F(\rho^k)| > \phi||F(\rho^{k-1})||_2^2 \tag{3.29}$$

with $\phi = 1$. The damping parameter λ^k is again calculated using the line search method of section 3.2.1.

3.2.4 Picard iteration

Picard iteration is a simple fixed-point method where the solution is updated according to

$$\rho^{k+1} = \rho^k + \lambda^k F(\rho^k) \tag{3.30}$$

and λ^k is calculated by a line search method, see section 3.2.1.

3.2.5 Anderson mixing

Anderson mixing [42] is an accelerated fixed-point iteration that computes the new solution ρ^{k+1} as a linear combination of the residuals and solutions of the last m^k iterations. A mixing parameter β determines the weight of the previous solutions and the previous residuals in the calculation of ρ^{k+1}

$$\rho^{k+1} = (1-\beta)\sum_{i=0}^{m^k} \alpha_i^k \rho^{k-m^k+i} + \beta \sum_{i=0}^{m^k} \alpha_i^k G(\rho^{k-m^k+i}) \tag{3.31}$$

where $m^k = \min(m, k)$ and $G(\rho^k) = F(\rho^k) + \rho^k$. The coefficients α_i^k are determined by minimizing the residuals of the last m^k steps

$$\min_{\alpha=(\alpha_0,\ldots,\alpha_{m^k})^T} \sum_{i=0}^{m^k} ||\alpha_i^k F(\rho^{k-m^k+i})||_2 \quad s.t. \quad \sum_{i=0}^{m^k} \alpha_i^k = 1 \tag{3.32}$$

For all calculations we use $m = 50$. Values between $\beta = 0.05$ and $\beta = 0.1$ gave the best results for our test cases. The actual values are given in the results section. The algorithm is here applied without restarting option (according to the PETSc default settings).

3.3 Numerical settings

All calculations are performed on a regular workstation with an Intel Core i5-3570 processor with four CPU cores at 3.4 GHz and the gfortran 4.7.2 compiler. The one-dimensional domain of length $50 \cdot \sigma^{\min}$, where $\sigma^{\min}$ is the minimal segment diameter of all components, is discretized in z-direction using $n_{\text{grid}} = 1000$ equidistant grid points. We don't explore reducing the number of grid points, either by taking a larger grid distance or by reducing the interfacial domain. It is further noteworthy that the numerical routines for calculating the Helmholtz energy and its derivatives are not optimized for computational speed.

Therefore, there is still potential to farther decrease the computation time given in the results section.
All numerical integrations are carried out using cubic spline interpolations and PETSc is configured in non-debug mode. An empirical relation similar to the one presented in [5] is used as the initial density profile $\rho_i^0(z)$ in all calculations

$$\rho_i^0(z) = \frac{1}{2}\left(\rho_i^{l,\text{bulk}} - \rho_i^{v,\text{bulk}}\right)\tanh\left(\frac{z}{\sigma_i}\left(2.4728 - 2.3625\frac{T}{T_c^{\text{calc}}}\right)\right) + \frac{1}{2}\left(\rho_i^{l,\text{bulk}} + \rho_i^{v,\text{bulk}}\right) \tag{3.33}$$

where the origin of the z-coordinate is located in the middle of the computational domain and T_c^{calc} is the critical temperature of the mixture.

3.4 Results and discussion

In this section we compare the performance, especially the calculation time, of the different algorithms for 3 representative test cases. These test systems exhibit different levels of complexity either due to their molecular interactions or number of components. We consider pure n-butane as the first and simplest test system. The second case is the binary mixture ethanol-hexane. This case is studied as an example of a system with asymmetric interactions. Ethanol shows strong associative interactions which are not present for hexane. The association approaches by Bymaster and Chapman [27] and Yu and Wu [26] are compared for this mixture. The last test case is a twenty-component mixture containing all n-alkanes from methane to eicosane. The complexity of this system results from the dimension of the system of equations to be solved. Further aspects such as the performance increase due to the line search method or parallelization are shown exemplarily for some algorithms and test systems only.
We found that all algorithms converge to the same solution for every test system, but at different computational costs. The pure component PC-SAFT parameters used in this study are listed in the appendix.

3.4.1 Test system n-butane

Figure 3.1a shows the results for the surface tension of n-butane. The very good agreement of the DFT predictions to experimental data confirms the DFT formalism is suited for rather simple, non-spherical fluids up to temperatures rather close to the critical point.
The convergence rates of the different algorithms are compared in figure 3.1b. All algorithms show a steady decrease of the norm of the residual and reduce it to the same value. Computation time varies from well below one second for the Anderson mixing method to

five second for the Picard iteration. Both inexact Newton methods converge in three to four iterations.

Newton_FD converges almost as fast as Anderson mixing while the convergence rate of Newton_AD is similar to the one of the L-BFGS method. Thus, for this test system, the analytic calculation of the Jacobian-vector product $F'\left(\rho^k\right) v$ using automatic differentiation is not advantageous regarding computation time or accuracy of the solution.

We emphasize that the good performance of Newton_FD is due to the matrix-free calculation of the approximate value of $F'\left(\rho^k\right) v$ which requires only a single function evaluation (see eq. 3.21). This has to be compared to the approach of approximating the Jacobian using finite-differences which requires up to $N \cdot n_{grid}$ function evaluations (without taking advantage of any structure of the Jacobian) and, therefore, would result in a much longer computation time.

For all calculations with n-butane, an initial value of the damping parameter $\lambda^{k,0} = 1$ is used and $\beta = 0.1$ for Anderson mixing.

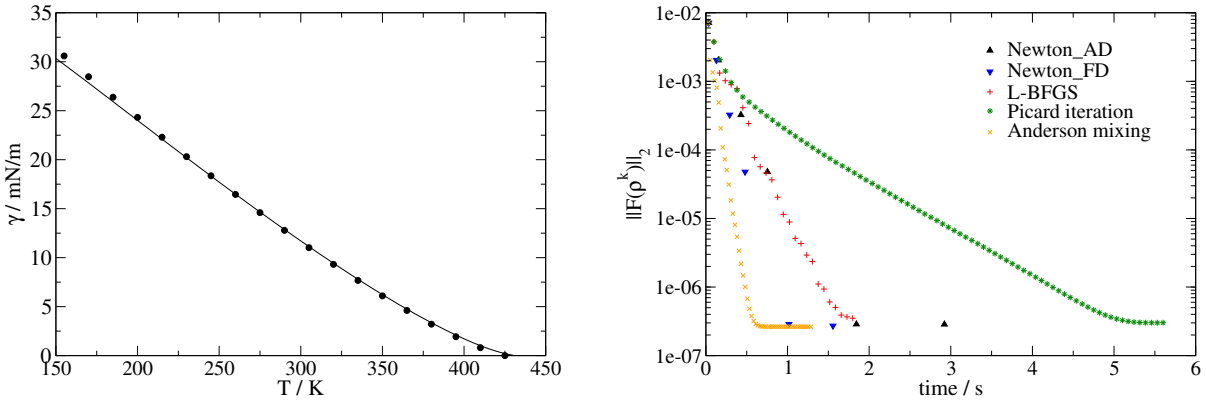

(a) (b)

Figure 3.1: Experimental [43] (symbols) and calculated (lines) results for surface tension of n-butane as a function of temperature (a). Convergence rate of different algorithms for n-butane at $T = 300$ K ($p = 2.59$ bar) (b).

3.4.2 Test system ethanol-hexane

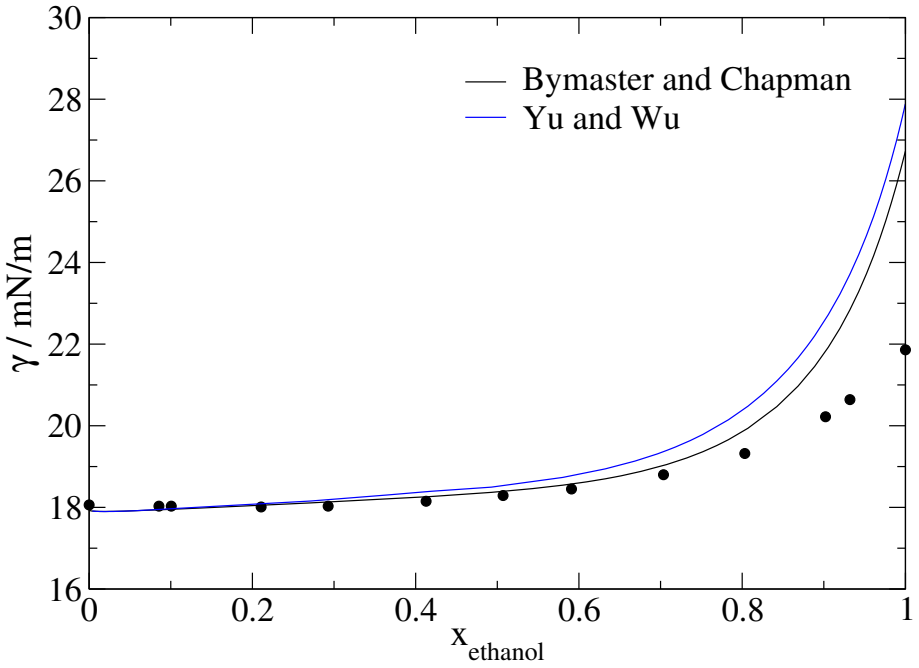

Figure 3.2: Experimental [44] (symbols) and calculated (lines) results for surface tension for the mixture ethanol-hexane at $T = 298.15$ K as a function of the molar composition in the liquid phase using the approaches of Bymaster and Chapman [27] and Yu and Wu [26] for the associative contribution to the Helmholtz energy functional. A binary interaction parameter of $k_{ij} = 0.02854$ was adjusted to experimental VLE data of Zhang et al. [45].

For the mixture ethanol-hexane, the associative contribution to the Helmholtz energy functional $A^{\text{assoc}}[\{\rho_k\}]$ needs to be taken into account because strong hydrogen bonding occurs between the ethanol molecules. The approaches of Yu and Wu [26] and Bymaster and Chapman [27] are applied to calculate $A^{\text{assoc}}[\{\rho_k\}]$. A comparison of predicted results to experimental data is shown in figure 3.2. Results of both association models are practically identical at low ethanol concentrations and agree very well with experiments. With increasing ethanol concentration, results obtained with the approach of Yu and Wu start to overpredict surface tension values slightly while results of the approach of Bymaster and Chapman follow the experiments closely up to $x_{Ethanol} \approx 0.7$. At higher ethanol mole fraction $x_{Ethanol}$, both approaches overpredict surface tension significantly. Results obtained with the approach of Bymaster and Chapman are in better agreement to the experimental data. We suspect that the deviations emerge because the nonisotropic orientational degree of freedom is not captured by the functional.

Figure 3.3 shows the density profiles obtained with both approaches at two values of ethanol concentration. At $x_{ethanol} = 0.057$, where results for surface tension are practically identical for both approaches (fig. 3.2), the density profiles are also very similar. The only difference is the prediction of a slight accumulation of ethanol on the liquid side of the

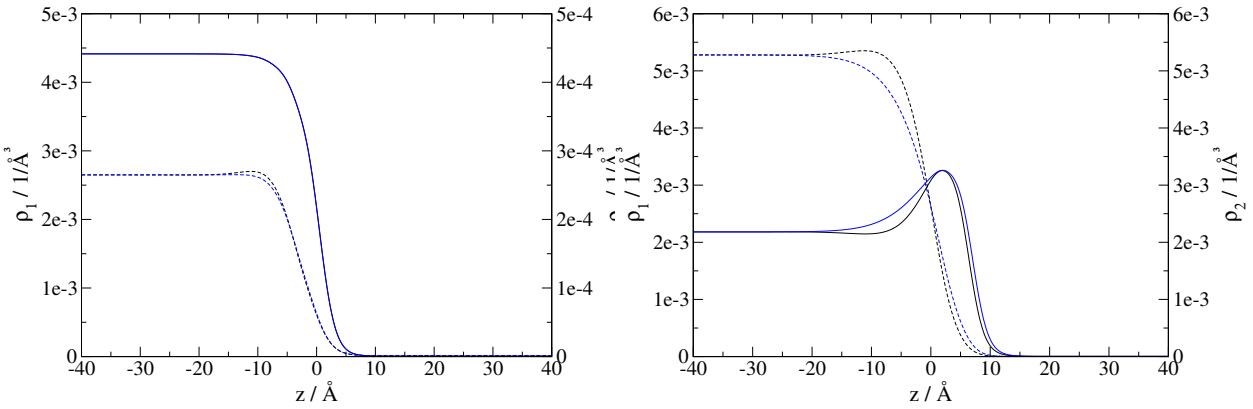

Figure 3.3: Density profiles for hexane (1, solid lines) and ethanol (2, dashed lines) obtained with the approaches of Bymaster and Chapman [27] (black) and Yu and Wu [26] (blue) for the associative contribution to the Helmholtz energy functional at $T = 298.15$ K. The calculations are performed at (a) $x_{ethanol} = 0.057$ ($p = 0.25$ bar) and (b) $x_{ethanol} = 0.708$ ($p = 0.245$ bar).

interface by the approach of Bymaster and Chapman which is not present in the density profile obtained with the approach of Yu and Wu. The density profiles for hexane are non-distinguishable for both approaches. At $x_{ethanol} = 0.708$, the density profiles differ more clearly which explains the different results for surface tension (fig. 3.2). Both approaches predict a pronounced enrichment of hexane in the interface. However, the approach of Bymaster and Chapman also shows a weak accumulation of ethanol and a depletion of hexane on the liquid side of the interface which are not present in the density profiles obtained with the approach of Yu and Wu.

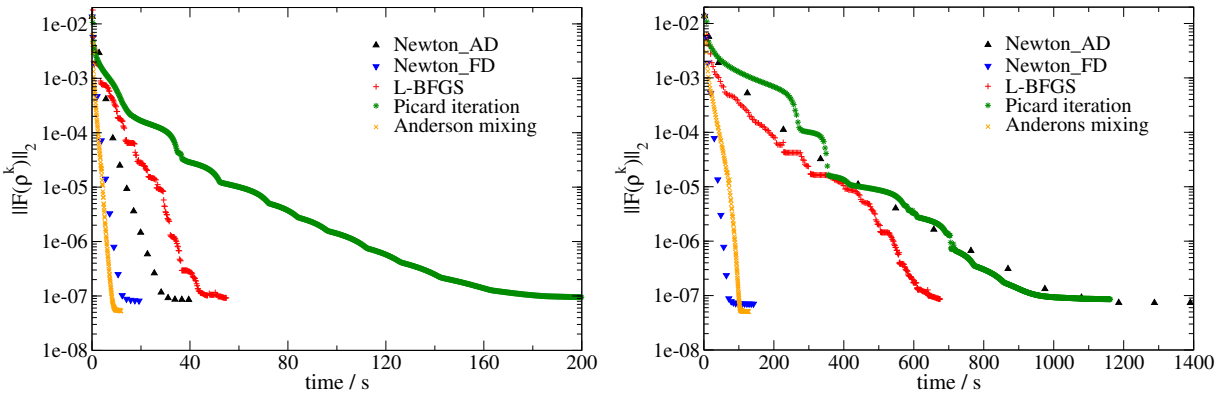

Figure 3.4: Convergence rate of all algorithms for the system ethanol-hexane at $T = 298.15$ K and $x_{Ethanol} = 0.27$ ($p = 0.256$ bar) for (a) the association approach of Yu and Wu [26] and for (b) the association Helmholtz energy functional of Bymaster and Chapman [27].

As figure 3.4 shows, the increased accuracy of the approach of Bymaster and Chapman

comes at the price of much slower convergence rates. All algorithms require much longer computation time for the approach of Bymaster and Chapman as compared to the approach of Yu and Wu. For the two fastest algorithms, Anderson mixing and Newton_FD, the calculation time of both association approaches differs roughly by a factor of ten. As mentioned in section 3.1, the main difference between the two approaches is the calculation of the fraction of free association sites on molecule i $\chi_A^i(\mathbf{r})$. In the approach of Yu and Wu, this is a local operation. Eq. (3.12) couples the value for a specific association site $\chi_A^i(\mathbf{r})$ only to the values of $\chi(\mathbf{r})$ of all other association sites at the same position $\mathbf{r}$. For the approach of Bymaster and Chapman, the integral in eq. (3.9) couples the values of $\chi_A^i(\mathbf{r})$ also to all values of $\chi(\mathbf{r'})$ at neighbouring points of $\mathbf{r}$. Thus, the system of equations given by eq. (3.9) is more complex and time consuming to solve than eq. (3.12) which explains the longer computation time for the approach of Bymaster and Chapman.

For both approaches, Newton_FD and Anderson mixing are again the preferred algorithms and converge at a similar rate. L-BFGS converges more rapidly than the Picard iteration. Newton_AD converges considerably faster than the L-BFGS algorithm and Picard iterations with the approach of Yu and Wu. When the approach of Bymaster and Chapman is applied, however, Newton_AD converges even slower than the Picard iteration. This loss in performance of Newton_AD can be attributed to the analytic calculation of the Jacobian-vector product $F'(\rho^k)v$ using automatic differentiation. In this case, the iterative solution of a system of nonlinear equations for all $\chi_A^i(\mathbf{r})$ *as well as* for the derivatives of all $\chi_A^i(\mathbf{r})$ with respect to all species-densities at every evaluation of $F'(\rho^k)v$ is required. The requirement applies to both association models, however, for the approach of Yu and Wu the resulting system of equations for determining $\chi_A^i(\mathbf{r})$ and its species-density derivatives only contains the local unknowns at $\mathbf{r}$ while in the approach of Bymaster and Chapman also unknowns at neighbouring points $\mathbf{r'}$ have to be considered. The loss in performance of Newton_AD for the model of Bymaster and Chapman stems from the different convergence behaviour of $\chi_A^i(\mathbf{r})$ and its species-density derivatives. While both properties show a similar convergence rate when the approach of Yu and Wu is applied, the species-density derivatives of $\chi_A^i(\mathbf{r})$ converge much slower than $\chi_A^i(\mathbf{r})$ with the approach of Bymaster and Chapman. The significant increase in computational time can thus be attributed to the additional iterations necessary converging the density derivatives of $\chi_A^i(\mathbf{r})$ at every evaluation of $F'(\rho^k)v$. Figure 3.4 also shows that Anderson mixing can reduce the final value of the norm of residual $||F(\rho^k)||_2$ further than the other algorithms. We verified, however, this does not result in different values of surface tension or notable differences in the final density profiles.

In the calculations for the system ethanol-hexane, the following settings are used: $\beta = 0.05$ for Anderson mixing, the initial damping parameter $\lambda^{k,0}$ is set to 1 for both inexact Newton

methods and to 0.4 for the Picard iteration. These values are used for both association approaches. For L-BFGS the initial damping parameter is set to 0.5 for the approach of Yu and Wu and to 0.3 for the approach of Bymaster and Chapman.

3.4.3 Test system twenty-component alkane mixture

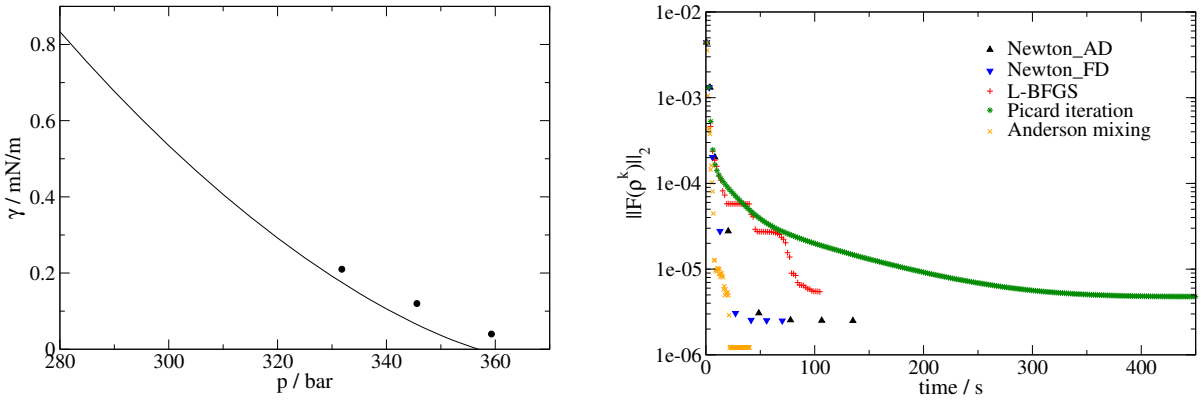

(a) (b)

Figure 3.5: Experimental [46] (symbols) and calculated (lines) results for surface tension for the twenty-component mixture as a function of pressure (a). Convergence rate of the different algorithms for the twenty-component mixture at $T = 366.45$ K and $p = 330$ bar (b).

The experimental surface tension results of this twenty-component mixture which is composed of all n-alkanes from methane to eicosane was determined by Danesh et al. [46]. Figure 3.5b shows the convergence rate of the different algorithms for the twenty-component mixture. Anderson mixing is the fastest algorithm and it reduces the norm of the residuals $||F(\rho^k)||_2$ further than the remaining algorithms. Both inexact Newton methods perform similarly and converge in four iterations. L-BFGS and Picard iteration both converge to levels of $||F(\rho^k)||_2$ significantly higher than the level reached by Anderson mixing and the inexact Newton methods. We verified, however, these differences in the final value of $||F(\rho^k)||_2$ have only a negligible effect on the value of surface tension and the final density profiles so that the results depicted in figure 3.5a are in graphical terms identical for all algorithms: predicted results for surface tension are somewhat lower than experimental data. We still consider the overall agreement to the experimental data, however, as satisfying.

In all calculations, no binary interaction parameters are used in the combining rules of the equation of state and the numerical settings are $\beta = 0.05$ for Anderson mixing and $\lambda^{k,0} = 1$ for the remaining algorithms. The molar overall composition of the mixture is specified in the appendix.

Anderson mixing requires only about $\leq 10\%$ of the computation time required for the

Picard iteration for all considered test systems.

3.4.4 Influence of the line search method

The influence of the line search method is illustrated examplarily for the test system n-butane and the Picard iteration. The Picard iteration is chosen because it is frequently used in DFT applications and often no line search method is applied. Instead, a fixed value λ is used throughout the calculation to scale the update according to eq. (3.16). A constant λ has to be chosen individually for every calculation and it has to be small enough to avoid divergence. On the other hand, if λ is chosen too small, computation time is increased unnecessarily. Figure 3.6 shows this situation for n-butane at two different temperatures. At $T = 300$ K, values of $\lambda > 0.1$ lead to divergence within the first few iterations. For $\lambda = 0.1$, the calculation diverges after an initial decrease of the norm of the residuals. A fixed value of $\lambda = 0.05$ in this case leads to a convergence rate even higher than when the line search method of section 3.2.1 is applied. Reducing the value further to $\lambda = 0.01$ ensures convergence, however, the computation time increases by a factor of four compared to the results with line search. At $T = 160$ K the situation is different. The choice $\lambda = 0.05$ now leads to divergence at the very beginning of the calculation and smaller damping factors such as $\lambda = 0.01$ or $\lambda = 0.005$ are necessary to enforce convergence. That comes at the price of longer computation time compared to the flexible determination of λ^k by a line search method. We came to much appreciate the line search method, because a proper choice of a constant damping factor λ is *a priori* unknown for any system. Suitable values strongly depend on the considered case (substances and state conditions) and need to be determined by trial and error. The line search method largely alleviates this problem. The appeal of the line search method is that it uses large update steps when possible and smaller updates when necessary and therefore makes a trial and error approach to find the optimal fixed value of λ obsolete.

3.4.5 A convergence criterion based on the value of surface tension

In previous sections, the decrease of the norm of the residual $||F(\rho^k)||_2$ is used as the criterion to compare the convergence rate of the different algorithms. In most cases where DFT is applied to the one-dimensional vapor-liquid interface, the calculation of the value of surface tension γ is the main objective. As figure 3.7 shows for the system n-butane and for the mixture ethanol-hexane with the approach of Bymaster and Chapman for the associative contribution to the Helmholtz energy functional, the value of γ converges to a constant value long before $||F(\rho^k)||_2$ reaches its final level. For the systems and algorithms depicted in figure 3.7, using the value of γ instead of $||F(\rho^k)||_2$ as convergence criterion

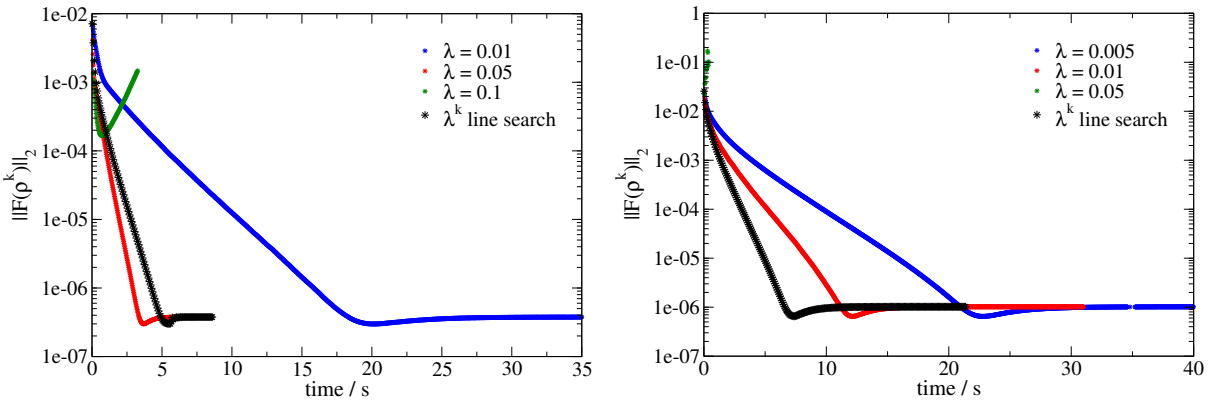

(a) (b)

Figure 3.6: Convergence rate of the Picard iteration for different values of a constant damping parameter λ^k compared to a flexible determination of λ^k by a line search method. Results are shown (a) for the temperatures $T = 300$ K ($p = 2.59$ bar) and (b) for $T = 160$ K ($p = 3.33 \cdot 10^{-4}$ bar) of the system n-butane.

can save more than 50% computation time and similar findings apply to the remaining test systems and algorithms.

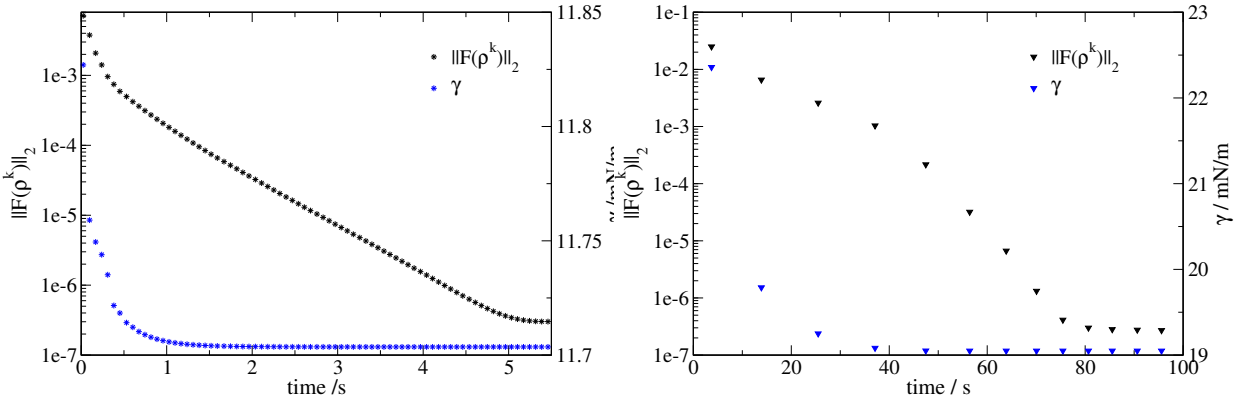

(a) (b)

Figure 3.7: Convergence rate of the norm of the residual $||F(\rho^k)||_2$ (black symbols, left y-axis) and the value of surface tension γ (blue symbols, right y-axis) as a function of computation time. Diagram (a) for the system n-butane at $T = 300$ K ($p = 2.59$ bar) using Picard iterations. Diagram (b) for ethanol-hexane at $T = 298.15$ K and $x_{ethanol} = 0.27$ ($p = 0.256$ bar) using the approach of Bymaster and Chapman [27] for the associative contribution to the Helmholtz energy functional and Newton_MF (b).

Figure 3.8 compares the final density profiles obtained from calculations where both convergence criteria are applied to the systems shown in fig. 3.7. For n-butane (fig. 3.8a), the effort spent on reducing $||F(\rho^k)||_2$ to its final level while the value of γ is already constant has only a minimal effect on the density profile. For the binary mixture ethanol-hexane (fig. 3.8b), the differences in the density profiles are more notable: the profile obtained from a convergence criterion for γ shows a slight enrichment of hexane in the

interface which has vanished once $||F(\rho^k)||_2$ reached its lowest value. Calculations targeting details of the interfacial density distribution should be conducted using $||F(\rho^k)||_2$ as a convergence criterion.

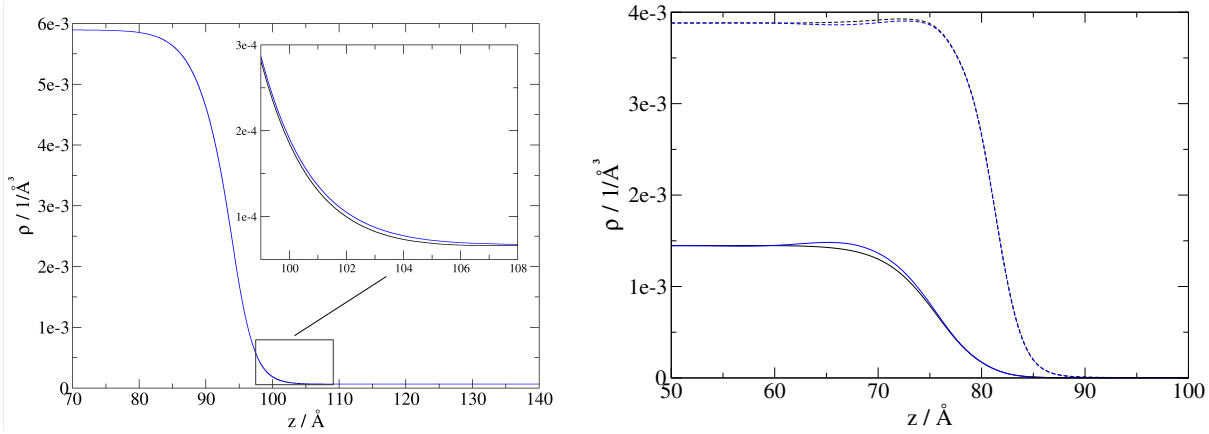

(a) (b)

Figure 3.8: Diagram (a): density profile of n-butane at $T = 300$ K ($p = 2.59$ bar). Calculations are stopped based on the convergence of $||F(\rho^k)||_2$ (black) after 75 Picard iterations (computation time 5.4 s) and based on the convergence of γ (blue) after 22 Picard iterations (computation time 1.5 s). Diagram (b): density profiles of hexane (solid lines) and ethanol (dashed lines) at $T = 298.15$ K and $x_{ethanol} = 0.27$ ($p = 0.256$ bar) using the approach of Bymaster and Chapman [27] for the associative contribution to the Helmholtz energy functional. Calculations are stopped based on the convergence of $||F(\rho^k)||_2$ (black) after 12 Newton_FD iterations (computation time 90 s) and based on the convergence of γ (blue) after 4 Newton_FD iterations (computation time 37 s).

3.4.6 Parallelization

In this section, the reduction of computation time realized by executing the DFT calculation in parallel is presented for the twenty-component alkane mixture as well as for the mixture ethanol-hexane with the approach of Yu and Wu for the associative contribution. The calculations are performed using the same settings as in the previous sections and the same workstation as described in section 3.3. In the parallel case, each processor works only on a subset of the n_{grid} grid points. Due to the spatially coupled nature of the equations, data exchange between the processors is necessary. This parallel data management and inter-processor communication is handled automatically by PETSc.

Figure 3.9 shows the speed-up of computation time $\frac{t(1)}{t(n_p)}$, where $t(n_p)$ is the time required to reach a converged solution based on the value of $||F(\rho^k)||_2$ using n_p processors. For the twenty-component mixture, figure 3.9a, all algorithms show almost exactly the same behaviour: using two processors results in a reduction of computation time of almost 50%. With four processors the time to reach a converged solution can be reduced by almost

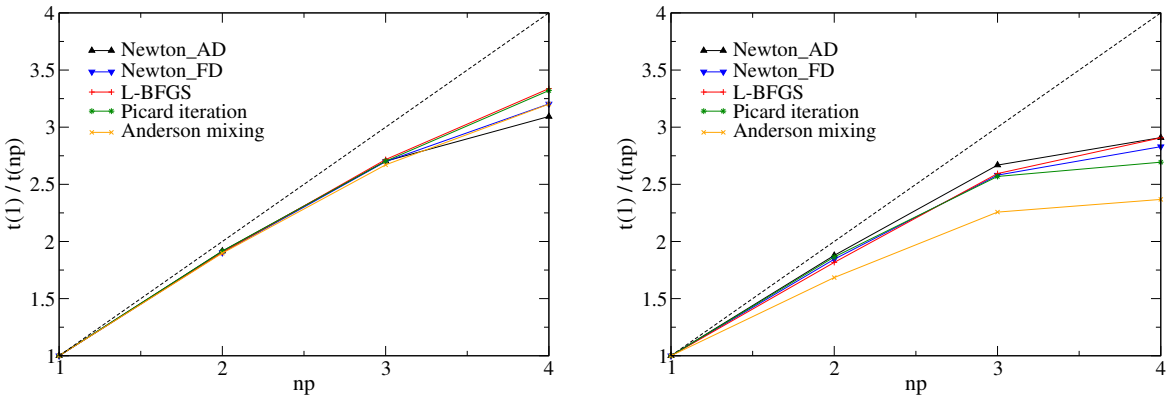

Figure 3.9: Speed-up of computation time $\frac{t(1)}{t(n_p)}$ for varying numbers of processors, n_p, used in the calculation. Diagram (a): twenty-component mixture at $T = 366.45$ K and $p = 330$ bar. Diagram (b): mixture ethanol-hexane at $T = 298.15$ K and $x_{Ethanol} = 0.27$ ($p = 0.256$ bar) using the association model of Yu and Wu [26]. Results are averages of ten calculation runs. The dashed line denotes perfectly linear scaling.

70%. For the mixture ethanol-hexane, figure 3.9b, the results are similar. In this case, the computation time can be reduced by around 60% using four processors. For Anderson mixing the decrease is slightly smaller than for the other algorithms. Considering that parallelization comes at practically no additional effort when a toolkit such as PETSc is used, it poses a good opportunity to speed up DFT calculations.

3.5 Conclusion

Five algorithms are applied to solve the equations of classical DFT for one-dimensional vapor-liquid interfaces and their performance is compared on three test systems. All algorithms converged to the same values for surface tension in all considered cases. Anderson mixing and the matrix-free inexact Newton method with numerically approximated derivatives outperform the remaining algorithms in all calculations. Using analytic derivatives with the matrix-free inexact Newton method does not result in any improvement regarding accuracy or computation time over numerically approximated derivatives. For systems with molecular association (i.e. hydrogen bonding) described by Wertheim's theory, all algorithms require significantly more iterations to converge. For the studied mixture ethanol-hexane, using the functional of Bymaster and Chapman [27] for the associative contribution to the Helmholtz energy functional yields results in better agreement to experimental data than the functional of Yu and Wu [26], however, computation time is up to ten times longer. In cases where the calculation of surface tension γ is the main objective, using a convergence criterion based on γ instead of the norm of the residual $||F(\rho^k)||_2$ can reduce computation time by up to 50%. Parallelization offers a further

potential to significantly speed up the calculations.

Appendix

Molar overall composition of the twenty-component alkane mixture

Table 3.1: Molar overall composition (%) of the twenty-component alkane mixture [46].

Component	%	Component	%	Component	%	Component	%
Methane	80.11	Heptane	0.96	Tridecane	0.44	Nonadecane	0.36
Ethane	8.23	Octane	0.55	Tetradecane	0.41	Eicosane	0.35
Propane	2.11	Nonane	0.49	Pentadecane	0.41		
Butane	1.07	Decane	0.48	Hexadecane	0.39		
Pentane	0.80	Undecane	0.45	Heptadecane	0.38		
Hexane	1.20	Dodecane	0.44	Octadecane	0.37		

Equation of state parameters

The following tables show the parameters for the PC-SAFT equation of state of all components of this study.

Table 3.2: Values of PC-SAFT parameters for non-associating components.

Component	m	σ/Å	ϵ/k/K	Ref
Methane	1.0000	3.7039	150.03	[23]
Ethane	1.6069	3.5206	191.42	[23]
Propane	2.0020	3.6184	208.11	[23]
Butane	2.3316	3.7086	222.88	[23]
Pentane	2.6896	3.7729	231.20	[23]
Hexane	3.0576	3.7983	236.77	[23]
Heptane	3.4831	3.8049	238.40	[23]
Octane	3.8176	3.8373	242.78	[23]
Nonane	4.2079	3.8448	244.51	[23]
Decane	4.6627	3.8384	243.87	[23]
Undecane	4.9082	3.8893	248.82	[23]
Dodecane	5.3060	3.8959	249.21	[23]
Tridecane	5.6877	3.9143	249.78	[23]
Tetradecane	5.9002	3.9396	254.21	[23]
Pentadecane	6.2855	3.9531	254.14	[23]
Hexadecane	6.6485	3.9552	254.70	[23]
Heptadecane	6.9809	3.9675	255.65	[23]
Octadecane	7.3271	3.9668	256.20	[23]
Nonadecane	7.7175	3.9721	256.00	[23]
Eicosane	7.9849	3.9869	257.75	[23]

Table 3.3: Values of PC-SAFT parameters for the associating component.

Component	m	σ/Å	ϵ/k/K	$\epsilon_{A_iB_i}/k$/K	κ_{ii}	Ref
Ethanol	2.3827	3.1771	198.24	2653.4	0.032384	[24]

Bibliography

[1] H. Löwen, "Density functional theory of inhomogeneous classical fluids: recent developments and new perspectives," *Journal of Physics: Condensed Matter*, vol. 14, no. 46, p. 11897, 2002.

[2] J. Wu, "Density functional theory for chemical engineering: From capillarity to soft materials," *AIChE Journal*, vol. 52, no. 3, pp. 1169–1193, 2006.

[3] J. Wu and Z. Li, "Density-functional theory for complex fluids," *Annu. Rev. Phys. Chem.*, vol. 58, pp. 85–112, 2007.

[4] C. P. Emborsky, Z. Feng, K. R. Cox, and W. G. Chapman, "Recent advances in classical density functional theory for associating and polyatomic molecules," *Fluid Phase Equilibria*, vol. 306, no. 1, pp. 15–30, 2011.

[5] J. Gross, "A density functional theory for vapor-liquid interfaces using the PCP-SAFT equation of state," *The Journal of chemical physics*, vol. 131, no. 20, p. 204705, 2009.

[6] C. Klink and J. Gross, "A density functional theory for vapor–liquid interfaces of mixtures using the perturbed-chain polar statistical associating fluid theory equation of state," *Industrial & Engineering Chemistry Research*, vol. 53, no. 14, pp. 6169–6178, 2014.

[7] C. Klink, B. Planková, and J. Gross, "Density functional theory for liquid–liquid interfaces of mixtures using the perturbed-chain polar statistical associating fluid theory equation of state," *Industrial & Engineering Chemistry Research*, vol. 54, no. 16, pp. 4633–4642, 2015.

[8] S. Tripathi and W. G. Chapman, "Microstructure of inhomogeneous polyatomic mixtures from a density functional formalism for atomic mixtures," *The Journal of chemical physics*, vol. 122, no. 9, p. 094506, 2005.

[9] S. Jain, A. Dominik, and W. G. Chapman, "Modified interfacial statistical associating fluid theory: A perturbation density functional theory for inhomogeneous complex fluids," *The Journal of chemical physics*, vol. 127, no. 24, p. 244904, 2007.

[10] Y.-X. Yu and J. Wu, "Density functional theory for inhomogeneous mixtures of polymeric fluids," *The Journal of chemical physics*, vol. 117, no. 5, pp. 2368–2376, 2002.

[11] L. J. D. Frink and A. G. Salinger, "Two-and three-dimensional nonlocal density functional theory for inhomogeneous fluids: I. algorithms and parallelization," *Journal of Computational Physics*, vol. 159, no. 2, pp. 407–424, 2000.

[12] L. Frink, A. Salinger, M. Sears, J. Weinhold, and A. Frischknecht, "Numerical challenges in the application of density functional theory to biology and nanotechnology," *Journal of Physics: Condensed Matter*, vol. 14, no. 46, p. 12167, 2002.

[13] A. L. Frischknecht, J. D. Weinhold, A. G. Salinger, J. G. Curro, L. J. D. Frink, and J. D. McCoy, "Density functional theory for inhomogeneous polymer systems. I. numerical methods," *The Journal of chemical physics*, vol. 117, no. 22, pp. 10385–10397, 2002.

[14] M. P. Sears and L. J. Frink, "A new efficient method for density functional theory calculations of inhomogeneous fluids," *Journal of Computational Physics*, vol. 190, no. 1, pp. 184–200, 2003.

[15] M. A. Heroux, A. G. Salinger, and L. J. Frink, "Parallel segregated schur complement methods for fluid density functional theories," *SIAM Journal on Scientific Computing*, vol. 29, no. 5, pp. 2059–2077, 2007.

[16] M. G. Knepley, D. A. Karpeev, S. Davidovits, R. S. Eisenberg, and D. Gillespie, "An efficient algorithm for classical density functional theory in three dimensions: Ionic solutions," *The Journal of chemical physics*, vol. 132, no. 12, p. 124101, 2010.

[17] M. Oettel, S. Dorosz, M. Berghoff, B. Nestler, and T. Schilling, "Description of hard-sphere crystals and crystal-fluid interfaces: A comparison between density functional approaches and a phase-field crystal model," *Physical review E*, vol. 86, no. 2, p. 021404, 2012.

[18] A. Härtel, M. Oettel, R. E. Rozas, S. U. Egelhaaf, J. Horbach, and H. Löwen, "Tension and stiffness of the hard sphere crystal-fluid interface," *Physical review letters*, vol. 108, no. 22, p. 226101, 2012.

[19] P. Pulay, "Convergence acceleration of iterative sequences. the case of SCF iteration," *Chemical Physics Letters*, vol. 73, no. 2, pp. 393–398, 1980.

[20] R. Roth, "Fundamental measure theory for hard-sphere mixtures: a review," *Journal of Physics: Condensed Matter*, vol. 22, no. 6, p. 063102, 2010.

[21] M. Edelmann and R. Roth, "A numerical efficient way to minimize classical density functional theory," *The Journal of Chemical Physics*, vol. 144, no. 7, p. 074105, 2016.

[22] "MoDeNa EU-Project," 2015. Modelling of Morphology Development of Micro- and Nanostructures. URL: https://github.com/MoDeNa-EUProject.

[23] J. Gross and G. Sadowski, "Perturbed-chain SAFT: An equation of state based on a perturbation theory for chain molecules," *Industrial & engineering chemistry research*, vol. 40, no. 4, pp. 1244–1260, 2001.

[24] J. Gross and G. Sadowski, "Application of the perturbed-chain SAFT equation of state to associating systems," *Industrial & engineering chemistry research*, vol. 41, no. 22, pp. 5510–5515, 2002.

[25] E. Sauer and J. Gross, "Classical density functional theory for liquid-fluid interfaces and confined systems using the perturbed-chain polar statistical associating fluid theory equation of state," *Industrial & engineering chemistry research*, submitted 2016.

[26] Y.-X. Yu and J. Wu, "A fundamental-measure theory for inhomogeneous associating fluids," *The Journal of chemical physics*, vol. 116, no. 16, pp. 7094–7103, 2002.

[27] A. Bymaster and W. G. Chapman, "An iSAFT density functional theory for associating polyatomic molecules," *The Journal of Physical Chemistry B*, vol. 114, no. 38, pp. 12298–12307, 2010.

[28] S. Balay, S. Abhyankar, M. F. Adams, J. Brown, P. Brune, K. Buschelman, L. Dalcin, V. Eijkhout, W. D. Gropp, D. Kaushik, M. G. Knepley, L. C. McInnes, K. Rupp, B. F. Smith, S. Zampini, H. Zhang, and H. Zhang, "PETSc Web page," 2016.

[29] Y. Rosenfeld, "Free-energy model for the inhomogeneous hard-sphere fluid mixture and density-functional theory of freezing," *Physical review letters*, vol. 63, no. 9, p. 980, 1989.

[30] R. Roth, R. Evans, A. Lang, and G. Kahl, "Fundamental measure theory for hard-sphere mixtures revisited: the white bear version," *Journal of Physics: Condensed Matter*, vol. 14, no. 46, p. 12063, 2002.

[31] Y.-X. Yu and J. Wu, "Structures of hard-sphere fluids from a modified fundamental-measure theory," *The Journal of chemical physics*, vol. 117, no. 22, pp. 10156–10164, 2002.

[32] E. Kierlik and M. Rosinberg, "A perturbation density functional theory for polyatomic fluids. II. flexible molecules," *The Journal of chemical physics*, vol. 99, no. 5, pp. 3950–3965, 1993.

[33] C. J. Segura, W. G. Chapman, and K. P. Shukla, "Associating fluids with four bonding sites against a hard wall: density functional theory," *Molecular Physics*, vol. 90, no. 5, pp. 759–772, 1997.

[34] R. S. Dembo, S. C. Eisenstat, and T. Steihaug, "Inexact newton methods," *SIAM Journal on Numerical analysis*, vol. 19, no. 2, pp. 400–408, 1982.

[35] S. C. Eisenstat and H. F. Walker, "Choosing the forcing terms in an inexact newton method," *SIAM Journal on Scientific Computing*, vol. 17, no. 1, pp. 16–32, 1996.

[36] Y. Saad and M. H. Schultz, "Gmres: A generalized minimal residual algorithm for solving nonsymmetric linear systems," *SIAM Journal on scientific and statistical computing*, vol. 7, no. 3, pp. 856–869, 1986.

[37] P. N. Brown and Y. Saad, "Hybrid krylov methods for nonlinear systems of equations," *SIAM Journal on Scientific and Statistical Computing*, vol. 11, no. 3, pp. 450–481, 1990.

[38] L. Hascoet and V. Pascual, "The tapenade automatic differentiation tool: principles, model, and specification," *ACM Transactions on Mathematical Software (TOMS)*, vol. 39, no. 3, p. 20, 2013.

[39] J. Nocedal, "Updating quasi-newton matrices with limited storage," *Mathematics of computation*, vol. 35, no. 151, pp. 773–782, 1980.

[40] D. F. Shanno and K.-H. Phua, "Matrix conditioning and nonlinear optimization," *Mathematical Programming*, vol. 14, no. 1, pp. 149–160, 1978.

[41] M. J. D. Powell, "Restart procedures for the conjugate gradient method," *Mathematical programming*, vol. 12, no. 1, pp. 241–254, 1977.

[42] D. G. Anderson, "Iterative procedures for nonlinear integral equations," *Journal of the ACM (JACM)*, vol. 12, no. 4, pp. 547–560, 1965.

[43] E. W. Lemmon, M. O. McLinden, and D. G. Friend, "Thermophysical properties of fluid systems," in *NIST Chemistry WebBook, NIST Standard Reference Database*

Number 69 (P. J. Linstrom and W. G. Mallard, eds.), Gaithersburg MD, 20899: National Institute of Standards and Technology, 2016. http://webbook.nist.gov, (retrieved July 12, 2016).

[44] B. Giner, A. Villares, S. Martín, H. Artigas, and C. Lafuente, "Study of the temperature dependence of surface tensions of some alkanol + hexane mixtures," *Journal of Chemical & Engineering Data*, vol. 52, no. 5, pp. 1904–1907, 2007.

[45] L.-Z. Zhang, G.-H. Chen, Z.-H. Cao, and S. J. Han, "New double circulation apparatus for vle determination: establishment and applications in the determination of isobars, isotherms, and isoplethes," *Thermochimica Acta*, vol. 169, pp. 247–261, 1990.

[46] A. Danesh, A. Dandekar, A. Todd, and R. Sarkar, "A modified scaling law and parachor method approach for improved prediction of interfacial tension of gas-condensate systems," in *SPE Annual Technical Conference and Exhibition*, Society of Petroleum Engineers, 1991.

Chapter 4

Modeling properties of the one-dimensional vapor-liquid interface: application of classical density functional and density gradient theory

The content of this chapter is a literal quote of the publication

Mairhofer, Gross, Fluid Phase Equilibria, 458, 2018, 243-252.

In comparison to the published work, the abstract is here omitted. Additions or deletions compared to the published work are marked with angular brackets.

Properties of vapor-liquid interfaces play an important role in many industrial applications. Density functional theory (DFT) and density gradient theory (DGT) are two approaches commonly applied to calculate these interfacial properties.
The framework of density functional theory was first developed to study the inhomogeneous electron gas by Hohenberg and Kohn [1] and Mermin [2] and was later applied to classical systems by Ebner et al. [3] [4]. The fundamentals of density gradient theory date back to the work of Van der Waals [5]. Later, Cahn and Hilliard [6] provided a rigoros derivation and extension of the DGT. For a detailed description of the historical development of both theories we refer to the book of Henderson [7].
Applied to a classical, inhomogeneous system of N components at given values of temperature T, volume V and chemical potentials μ_i $(i = 1, ..., N)$, both approaches aim to find the equilibrium species density profiles $\rho_i(\mathbf{r})$ that minimze the grand potential $\Omega = A - \int \sum_i^N \mu_i \rho_i \mathrm{d}\mathbf{r}$ of the system. The fundamental difference between DFT and DGT

as they are applied in this work is the approximate expression for the Helmholtz energy $A[\rho(\mathbf{r})]$ of an inhomogeneous system. In DGT, an approximation of $A[\rho(\mathbf{r})] = \int a[\rho(\mathbf{r})]\mathrm{d}\mathbf{r}$ is obtained by an expansion of the local Helmholtz energy density $a[\rho(\mathbf{r})]$ about the local density approximation $a_0(\mathbf{r}) = a(\rho(\mathbf{r}))$ truncated after the square density gradient term. The prefactor of this gradient term is the so called influence parameter c_{ii}, which is a component specific property. Theoretical approaches [8] [9] [10] and several correlations [11] [12] [13] [14] [15] exist to determine c_{ii}. In most cases however, the value of c_{ii} is adjusted to experimental surface tension data. The appeal of DGT is its ease of implementation: besides the value of c_{ii} only an equation of state to evaluate a_0 is required. For an extensive list of previous studies using various equations of state to evaluate a_0, we refer to a previous study [16] [Chapter 2].

DFT, on the other hand, does not require any additional parameters beyond those of the equation of state to calculate interfacial properties. A is treated as a functional of the spatially varying density profile. Common approximations are derived from perturbation theory for the Helmholtz energy by decomposing the intermolecular potential into a predominantly repulsive part (defining the reference fluid) and an attractive part of the intermolecular potential. Furthermore, the unknown correlation function of the inhomogeneous fluid is approximated by its value for the homogeneous fluid evaluated at averaged densities. As shown by Evans [10], DFT can be seen as a generalization of the DGT approach of Van der Waals. For an overview of current applications of DFT, we refer to the following review articles [17] [18] [19] [20].

The chemical potentials as well as the densities of the coexisting vapor and liquid phases enter the DFT and DGT calculations. Therefore, the first step when DFT or DGT are applied to the one-dimensional vapor-liquid interface, is the calculation of these phase equilibrium properties. This has to be done using the same model that is applied to calculate a_0 in DGT and the model has to be consistent with the Helmholtz energy functional employed in the DFT approach.

In this work, we compare results for the surface tension of pure components and of mixtures obtained from DFT and DGT for non-polar and non-associating compounds, polar molecules and associating components. The PCP-SAFT equation of state [21] [22] [23] [24] is applied to determine the bulk properties at phase equilibrium and to evaluate the local Helmholtz energy density a_0 in DGT. PCP-SAFT has proven to yield accurate results of thermodynamic properties for a wide range of systems. A Helmholtz energy functional consistent with PCP-SAFT has been developed by Gross [25], Klink and Gross [26] and Sauer and Gross [27]. This DFT approach is used here with the modification that associative interactions are treated in a non-local description using the Helmholtz energy functional of Bymaster and Chapman [28], which is a modification of the work of Segura et al. [29]. For mixtures, two algorithms to solve the DGT equations are applied: the path

function approach of Liang et al. [30] which requires the geometrical combining rule for the influence parameter ($c_{ij} = \sqrt{c_{ii}c_{jj}}$) and the stabilized algorithm of Qiao and Sun [31] that allows to use a binary correction parameter β_{ij} ($c_{ij} = \sqrt{c_{ii}c_{jj}}(1-\beta_{ij})$). Limitations of the practical utility of β_{ij} are discussed. Like in most DGT-studies, we treat the pure component influence parameters c_{ii} as temperature-independent and follow the study of Amézquita et al. [32] in applying the constant c_{ii} values unchanged to components which are supercritical at mixture conditions. Both, the DFT or DGT approach, give the same bulk phase properties, which allows us to attribute differences in the interfacial properties to the DFT or DGT approach, respectively.

4.1 Theoretical background of DGT and DFT

In this section, we summarize the basic equations of DFT and DGT for a one-dimensional system with a vapor-liquid interface. For further details on the underlying molecular model of PCP-SAFT, we refer to the original literature [21] [22] [23] [24]. Detailed descriptions of DGT can be found in [6] [33] [34] and more information on the DFT approach applied in this work is available in previous studies [25] [26] [27] [35] [Chapter 3].
The goal of both approaches is to determine the equilibrium density profiles $\rho_i(\mathbf{r})$ across the interface which minimize the value of the grand potential Ω of a system of N components at given values of temperature T, chemical potentials μ_i and volume V.
In the absence of an external field, Ω is given by

$$\Omega[\{\rho_k\}] = A[\{\rho_k\}] - \sum_i^N \int \mu_i \rho_i(\mathbf{r}) \mathrm{d}\mathbf{r} \tag{4.1}$$

where the dependencies of A and Ω on T, μ_i and V are dropped for brevity and the curly brackets denote the dependency on all species-densities.
Eq. 4.1 is the starting point for both DGT and DFT. The main difference between the two approaches is the route to describe the intrinsic Helmholtz energy of the system $A[\{\rho_k\}]$, which is a functional of all species-densities $\rho_i(\mathbf{r})$ (as denoted by the square brackets). In our DFT approach, $A[\{\rho_k\}]$ is modeled as a sum of contributions according to the PCP-SAFT model

$$A[\{\rho_k\}] = A^{ig}[\{\rho_k\}] + A^{hs}[\{\rho_k\}] + A^{chain}[\{\rho_k\}] + A^{disp}[\{\rho_k\}] + A^{assoc}[\{\rho_k\}] + A^{polar}[\{\rho_k\}] \tag{4.2}$$

where the individual contributions to the Helmholtz energy are for the ideal gas, hard sphere interactions, chain formation, dispersion, association (i.e. hydrogen bonding) and polar (dipolar or quadrupolar) interactions. In this work, we use the functionals developed

by Rosenfeld [36] in the modified form of Roth et al. [37] and Yu and Wu [38] for $A^{hs}[\{\rho_k\}]$, Tripathi and Chapman [39] with the adaptations of ref. [25] and [26] for $A^{chain}[\{\rho_k\}]$. Furthermore, for $A^{disp}[\{\rho_k\}]$ and for $A^{polar}[\{\rho_k\}]$ we adopt functionals of Sauer and Gross [27], respectively and for $A^{assoc}[\{\rho_k\}]$ we use functionals proposed by Bymaster and Chapman [28]. The final form of these functionals is presented in [27] and [35] [Chapter 3].
In equilibrium, where $\Omega[\{\rho_k\}]$ reaches its minimum value with respect to density profiles $\rho_i(\mathbf{r})$, the functional derivatives with respect to all species-density profiles $\rho_i(\mathbf{r})$ vanish

$$\frac{\delta\Omega[\{\rho_k\}]}{\delta\rho_i(\mathbf{r})} = \frac{\delta A[\{\rho_k\}]}{\delta\rho_i(\mathbf{r})} - \mu_i = 0 \quad \forall i \tag{4.3}$$

Eqs. 4.3 can be discretized on a one-dimenional grid. As described in a previous study [35] [Chapter 3], a matrix-free inexact Newton method is applied to solve the resulting system of nonlinear equations.

In the DGT approach, $A[\{\rho_k\}]$ is not decomposed into a sum of functionals as for DFT. Instead, the Helmholtz energy density of the inhomogeneous fluid is expanded about the local density approximation $a_0(\{\rho_k\})$ truncated after the square density gradient term

$$A[\{\rho_k\}] = \int a_0(\{\rho_k\}) + \frac{1}{2}\sum_i^N \sum_j^N c_{ij}\nabla\rho_i\nabla\rho_j \mathrm{d}\mathbf{r} \tag{4.4}$$

with the local density gradient $\nabla\rho_i$ and the influence parameter c_{ij}. In this work, we evaluate interfacial properties for the case, where the influence parameter is determined from a geometric combining rule, as $c_{ij} = \sqrt{c_{ii}c_{ij}}$, but also for the case, where c_{ij} is an adjustable parameter. It is convenient therefore to cast the influence parameter in the form

$$c_{ij} = \sqrt{c_{ii}c_{ij}}\,(1-\beta_{ij}) \tag{4.5}$$

where parameter β_{ij} is zero for the geometric combining rule and non-zero for an adjusted value of c_{ij}. The local Helmholtz energy density evaluated at the local density value is then split according to the PCP-SAFT model

$$a_0(\{\rho_k\}) = a_0^{ig}(\{\rho_k\}) + a_0^{hs}(\{\rho_k\}) + a_0^{chain}(\{\rho_k\}) + a_0^{disp}(\{\rho_k\}) + a_0^{assoc}(\{\rho_k\}) + a_0^{polar}(\{\rho_k\}) \tag{4.6}$$

Thus, DGT requires a model for the local Helmholtz energy density $a_0(\{\rho_k\})$ and values of the influence parameters c_{ij}, which are adjusted to reproduce interfacial properties. Whereas for DFT, a description of the Helmholtz energy contributions as functionals of

the density profiles is necessary (compare equations 4.2 and 4.6) without interface-specific adjustable parameters. For a one-dimensional system, inserting eq. 4.4 in eq. 4.1 leads to the following set of Euler-Lagrange equations for the equilibrium density profiles

$$\mu_{i,0}(\{\rho_k\}) - \mu_i = \sum_j^N c_{ij} \frac{\partial^2 \rho_j}{\partial z^2} \quad \forall i \tag{4.7}$$

with μ_i as the constant chemical potential imposed to the system and $\mu_{i,0}(\{\rho_k\}) = \frac{\partial a_0(\{\rho_k\})}{\partial \rho_i}$ as the local value varying across the interface. Far from the flat interface in equilibrium, the two sides of the equation approach zero. For pure components, the resulting equations for the density profile and surface tension γ read

$$z_2 - z_1 = \int_{\rho(z_1)}^{\rho(z_2)} \sqrt{\frac{c_{11}}{2\Delta\omega_0}} \mathrm{d}\rho \tag{4.8}$$

$$\gamma = \int_{\rho^v}^{\rho^l} \sqrt{2c_{11}\Delta\omega_0} \mathrm{d}\rho \tag{4.9}$$

where $\Delta\omega_0$ denotes the difference of the grand potential energy density of the local homogeneous fluid to its bulk value, $\Delta\omega_0 = a_0(\{\rho_k\}) - \sum_i^N \rho_i\mu_i + p$ with equilibrium pressure p, and the vapor and liquid bulk densities, ρ^v and ρ^l, respectively.

To solve eq. 4.7 for mixtures, we apply two different approaches: the path function approach of Liang et al. [30] that requires $\beta_{ij} = 0$ in the combining rule, eq. 4.5, of the influence parameter and the stabilized DGT algorithm first presented by Qiao and Sun [31] using the Peng-Robinson equation of state and applied by Mu et al. [40] using PC-SAFT which allows to set $\beta_{ij} \neq 0$ and thus offers additional adjustable parameters for any pair of substances in a mixture. Compared to the frequently used reference component algorithm, both approaches do not require the a priori choice of a reference component which has to exhibit a monotonic density profile across the interface.

In the path function approach of Liang et al. [30], a variable $s = \sum_i \sqrt{c_i}\rho_i$ is introduced in eq. 4.7, leading to the following set of $N + 1$ equations [30]

$$\mu_{i,0}(\{\rho_k\}) - (\mu_i + \alpha\sqrt{c_i}) = 0 \quad \forall i \tag{4.10}$$

$$s - \sum_j^N \sqrt{c_j}\rho_j = 0 \tag{4.11}$$

that need to be satisfied everywhere in the interface with $N+1$ unknowns (ρ_i ($i = 1, ..., N$) and α). The density profile and the value of surface tension γ follow from [30]

$$z_2 - z_1 = \int_{s(z_1)}^{s(z_2)} \frac{1}{\sqrt{2(s\alpha + \Delta\omega_0)}} \mathrm{d}s \tag{4.12}$$

and

$$\gamma = \int_{s^v}^{s^l} \sqrt{2(s\alpha + \Delta\omega_0)} \mathrm{d}s \tag{4.13}$$

where s^v and s^l correspond to the values of s evaluated at the vapor and liquid bulk densities, respectively.

In the stabilized DGT algorithm, a pseudo time dependence is introduced in eq. 4.7

$$\frac{\partial \rho_i}{\partial t} + \mu_{i,0}(\{\rho_k\}) - \mu_i = \sum_j^N c_{ij} \frac{\partial^2 \rho_j}{\partial z^2} \tag{4.14}$$

with the pseudo time variable t. Eq. 4.14 is solved together with the boundary conditions $\rho_i(t,0) = \rho_i^l$ and $\rho_i(t,D) = \rho_i^v$ where ρ_i^l and ρ_i^v denote the liquid and vapor bulk densities, respectively, and D is the size of the domain that needs to be set a priori. Discretization in time and space as presented in [40] (using n_z grid points) leads to a system of nonlinear equations of dimension $N \cdot n_z$ that have to be solved at every time step and integration in time has to be performed until the steady-state solution (with vanishing pseudo-time derivative) of eq. 4.14 is found. Details of the numerical implementation as well as a comparison of computation time for the different approaches are presented in the Supporting Information.

Once the equilibrium density profiles are obtained, the value of surface tension can be calculated as

$$\gamma = \int_0^D \sum_i^N \sum_j^N c_{ij} \frac{\mathrm{d}\rho_i}{\mathrm{d}z} \frac{\mathrm{d}\rho_j}{\mathrm{d}z} \mathrm{d}z \tag{4.15}$$

In summary, the solution procedures of both DGT approaches can be compared as follows: in the stabilized DGT algorithm, the size of the computation domain D is set a priori and the variables that are discretized are the spacial coordinate z and the pseudo time t. This leads to a system of nonlinear equations of dimension $N \cdot n_z$ solved at every time step. The calculation is stopped, once certain convergence criteria are met (see Supporting Information). In the path function approach of Liang et al. [30], the variable s is discretized between its bulk values, s^l and s^v, using n_s points. For every discrete value of s, the system of $N+1$ equations given by eq. 4.10 and 4.11 has to be solved. Thus, instead of one large system of equations at every time step as in the stabilized DGT algorithm, n_s small systems of dimension $N+1$ have to be solved. Once eq. 4.10

and 4.11 are solved for the unknown densities and α at every discrete value s, the density profile can be generated using eq. 4.12. The size of the computation domain is a result of the calculation (in contrast to the stabilized DGT algorithm). For DFT calculations and for the stabilized DGT algorithm, we use a computation domain of size $D = 100$ Å. As shown in the Supporting Information, the value of D can be chosen over a wide range with neglectable impact on surface tension results. Furthermore, a constant value of 1000 for n_s and n_z is used in all DFT and DGT calculations. We note that for DGT, algorithms have been developed by Larsen et al. [41] and Liang and Michelsen [42] which are more efficient than using a constant number of discretization points.

4.2 Results and discussions

In this section, predictions of DFT and correlated results of DGT for surface tension γ of pure components are compared to experimental data or to results of accurate multi-parameter correlations. Results of non-polar, non-associating species are presented first, results for polar compounds or components that exhibit hydrogen bonds such as alcohols and water follow thereafter. Values of the constant influence parameters c_{ii} as well as the PCP-SAFT parameters are given in the Supporting Information.
For mixtures, results of DFT are compared to results obtained with the path function DGT approach and experimental data. Furthermore, the possibility of improving DGT results by applying the stabilized DGT algorithm and adjusting the value of β_{ij} to experimental data is discussed exemplary for several mixtures.

4.2.1 Pure components

Figure 4.1 shows surface tension results for n-alkanes (fig. 4.1a) and further non-polar, non-associating components (fig. 4.1b). For all components, reference data is available over a wide temperature range. The agreement of DFT and DGT results to the reference data is excellent: the maximal absolute deviation of the DGT correlations takes on a value of 1.52 mN/m for cyclopentene at the lowest evaluated temperature which corresponds to an error of 3.5%. The largest deviation of the values predicted by DFT amounts to 2.85 mN/m (7.9%) for propane at the lowest temperature.

Results for polar compounds are presented in fig. 4.2. DGT correlates the reference data very accurately with a maximum absolute deviation of 1.25 mN/m (3.6%) for dimethylether at the lowest evaluated temperature. For most compounds shown in fig. 4.2, surface tension predictions of DFT are practically indistinguishable from the DGT correlations and agree excellently with the reference data. Only for some components, DFT over-

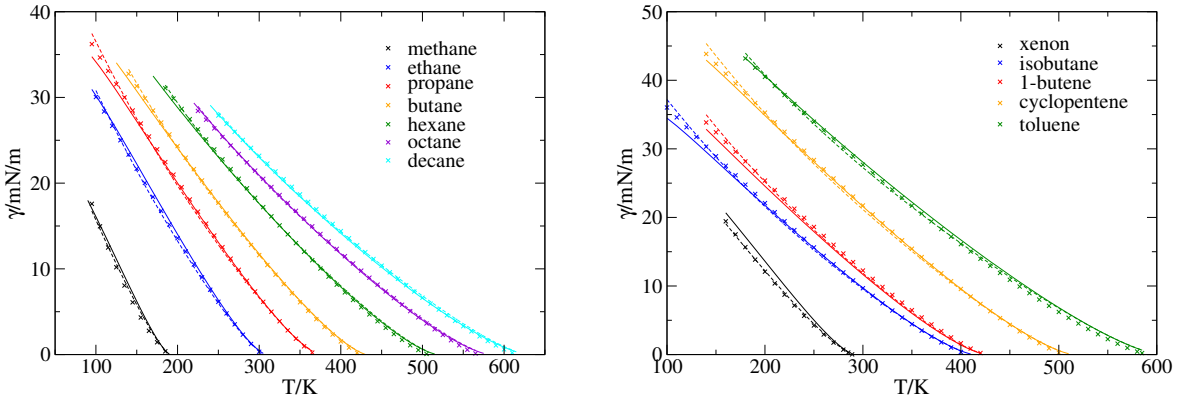

(a) (b)

Figure 4.1: Calculated results of surface tension γ (DFT: solid lines, DGT: dashed lines) and reference data [43] [44] [45] (symbols) for n-alkanes (a) and further non-polar, non-associating components (b).

predicts the value of γ moderately at low temperatures. In the case of methylmethanoate, dimethylether and R23, deviations for state points in the low temperature range rise to around 10%. These deviations cannot be attributed to the magnitude of the polarity of the molecules: the dipole moment densities (squared dipole moment per molecular volume) of R22 and R125 where DFT results of γ agree very well with the reference data are all higher than that of e.g. dimethylether for which notable deviations occur. However, with a deviation averaged over all results shown in fig. 4.2 of only 0.55 mN/m (DGT: 0.19 mN/m), DFT predictions for surface tension of polar molecules can still be considered very accurate.

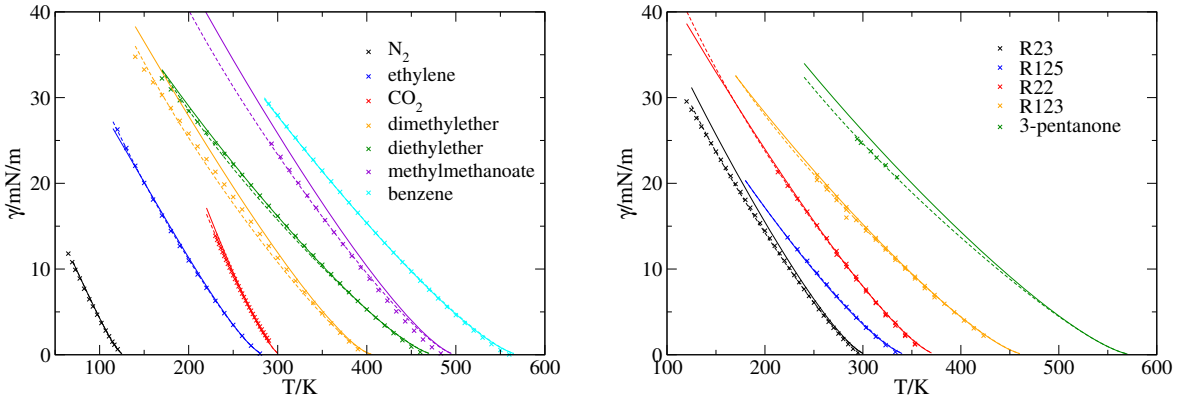

(a) (b)

Figure 4.2: Calculated results of surface tension γ (DFT: solid lines, DGT: dashed lines) and reference data (symbols) for several polar compounds. The references to the reference data are presented in tables 5 and 6 of the Supporting Information.

The ability of DFT and DGT to treat associating components can be studied best using a family of molecules with varying degree of association strength and sufficient reference

data, such as 1-alcohols. Additionaly, results for water will be presented. Surface tension predictions of DFT for 1-alcohols show an interesting trend (fig. 4.3): deviations for methanol are small in the complete temperature range while for 1-propanol the surface tension is strongly overpredicted. For 1-decanol deviations are lower again, although the DFT results do not show the correct curvature of γ with temperature. DGT correlates the reference data closely for methanol and 1-propanol. For 1-decanol, DGT results show a similar behavior as DFT results with better agreement to reference data at low temperatures and larger deviations than DFT at intermediate temperature values.

In the Supporting Information, DFT and DGT results for γ for all 1-alcohols from methanol to 1-decanol are presented and compared to reference data. Furthermore, in the Supporting Information, we compare DFT results obtained with pure component PCP-SAFT parameters taken from Gross and Sadowski [22] to results obtained using pure component parameters of Kontogeorgis et al. [46] where experimental data of monomer fractions were included in the parameter regression. Larger differences occur only for methanol where agreement to reference data is much better using the parameters of ref. [22] and the following discussion is based on results obtained with these pure component parameters.

Figure 4.4 shows the variation of the averaged absolute deviation of γ for 1-alcohols as a function of chain length for both models. For the correlated results of DGT, moderately increasing deviations with chain length can be observed. For the DFT predictions, deviations start at a low level, close to the value of DGT, for methanol but reach a pronounced maximum for 1-propanol. For longer 1-alcohols, deviations show a steady decrease and for 1-decanol they reach a similar level as DGT. These results are unexpected: for the family of 1-alcohols, association strength decreases with increasing chain length (using monomer fraction as the measure of association strength) [46] [47]. Therefore, if the treatment of association *per se* was the weak-point of the model, highest deviations would be expected for the shortest molecule, i.e. methanol, with decreasing deviations for longer molecules. This is in contrast to the very good agreement of results of DFT and DGT for methanol, the stark increase of deviations from methanol to 1-propanol for DFT and the general trend of increasing deviations from methanol to 1-decanol for DGT. One possible explanation for the DFT results could be an insufficient description of the orientation of the molecules at the interface. As shown by sum-frequency generation [48] [49] and in molecular dynamics simulations [50], the non-isotropic orientational distribution is caused by the hydrogen bonding hydroxyl groups that, at the vapor-liquid interface, are preferentially directed towards the liquid phase due to the higher number of potential hydrogen bonding partners. This orientation is expected to be strongest for the shortest molecules while with increasing chain length the orientation of a molecule at the interface becomes increasingly difficult due to steric hinderance. In this light, the comparably good results

for methanol and ethanol are surprising. The steady decrease of deviations for longer alcohol molecules, on the other hand, are in line with this explanation. Furthermore, a comparison of DFT surface tension results for 1-alcohols to results for the corresponding isomers, which do not have the same capability to align themselves at the interface, also supports this view: AAD values for isomers are between 15 (1-pentanol vs. 2-pentanol) and 30% (1-propanol vs. 2-propanol) lower than for 1-alcohols.

A factor that can be ruled out to cause these deviations is the error in the prediction of the critical temperature T_c. An accurate prediction of T_c is important to recover the correct course of γ as a function of temperature because surface tension vanishes at T_c. It can be expected that errors in γ increase for components where PCP-SAFT predictions of T_c show larger deviations. However, the errors in the calculated value of T_c are small and do not follow any trend which could explain the course of the deviations of DFT or DGT for surface tension.

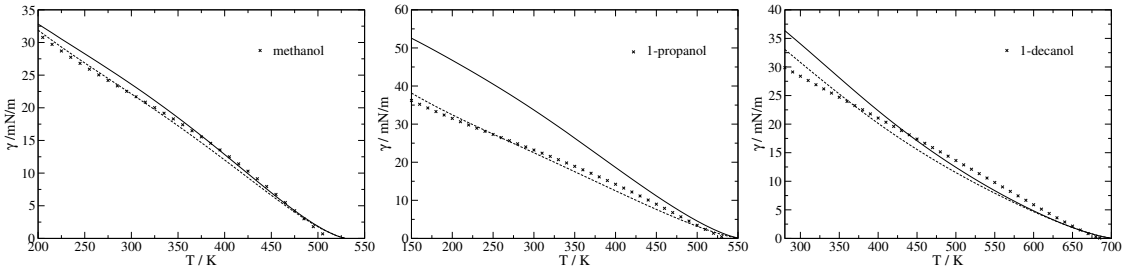

(a) (b) (c)

Figure 4.3: Calculated results of surface tension γ (DFT: solid lines, DGT: dashed lines) and reference data [43] [44] (symbols) for methanol (a), 1-propanol (b) and 1-decanol (c).

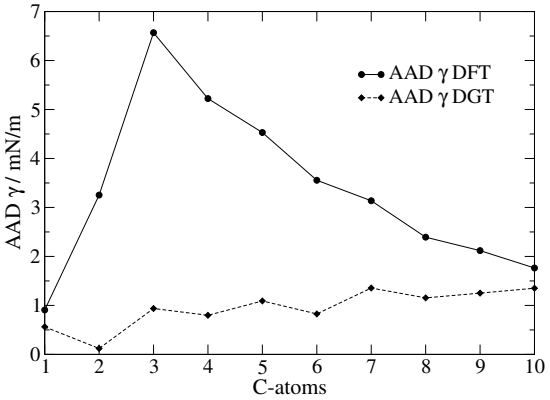

Figure 4.4: Deviations of surface tension γ for 1-alcohols ($AAD = \frac{1}{N_{exp}} \sum_i^{N_{exp}} |\gamma_i^{exp} - \gamma_i^{model}|$) using surface tension results from a reduced temperature of $T_r = T/T_c \approx 0.4$ to the critical temperature T_c for DFT (black solid line) and DGT (black dashed line) as a function of chain length.

For water, the pure component parameters of PCP-SAFT are close to degenerate. Like for other SAFT models, a multitude of different PCP-SAFT parameter gives reasonable vapor pressures and liquid density data. As a consequence several pure component parameters for water were proposed in the literature. In their study, Liang et al. [51] compare nine parameter sets. The comparison shows that the parameter sets were almost exclusively adjusted to reproduce a certain set of bulk properties, first and foremost vapor pressures and liquid densities. The only exception being the set of [52] (labelled *3B_C*) which was adjusted to reproduce the critical point. We performed DFT and DGT calculations using all nine parameter sets evaluated in [51] as well a set of Kontogeorgis et al. [46] (labelled *4C_3*) where experimental data of monomer fraction (besides liquid density and vapor pressure) was used to adjust the parameters. Figure 4.5 shows surface tension results of DFT and DGT for six of the parameter sets (results of the remaining four sets lie between the depicted results but not closer to the reference data) and values from NIST [43] as a reference.

Fig. 4.5a shows that the DFT results for the various parameter sets vary greatly. Parameter set *4C_2* from ref. [53] showed the smallest overall error for the properties studied in ref. [51] but underestimates surface tension significantly over a wide temperature range. Set *3B_1* [52] overestimates surface tension by an even larger amount and results of set *2B_1* [22] run almost in parallel to the reference data in the complete temperature range, overpredicting surface tensions by roughly 10 mN/m. Parameter set *3B_C* [52] that shares the association parameters with *3B_1* but whose remaining parameters were adjusted to reproduce the critical point predicts surface tension well at low temperatures while at higher temperatures surface tension values are moderately too low. The adjustment to the critical point, however, comes at the prize of unacceptable errors in liquid density (the averaged deviation takes on values above 60 % compared to below 7% for the remaining parameter sets [51]). The results of set *4C_3* show that an accurate prediction of T_c does not guarantee surface tension results anywhere close to the reference data. Set *4C_1* of Liang et al.[51] is the only parameter set which gives acceptable errors in surface tension while showing good agreement to other bulk properties. This parameter set was adjusted to vapor pressure, liquid density as well as LLE data of water-hydrocarbon systems.

For DGT, the error in the prediction of T_c seems to be the predominant influence on surface tension results for water (fig. 4.5b). Results of the two data sets that accurately predict T_c (*3B_C* and *4C_3*) show a similar behavior: at low temperatures γ values of both sets are too high while in the high temperature range γ is underpredicted moderately. In general, results obtained with parameter set *4C_3* are in better agreement to the reference data. Results of the remaining sets correlate surface tension accurately in the low temperature range. However, due to the significant overprediction of T_c, agreement to the reference data deteriorates at high temperatures.

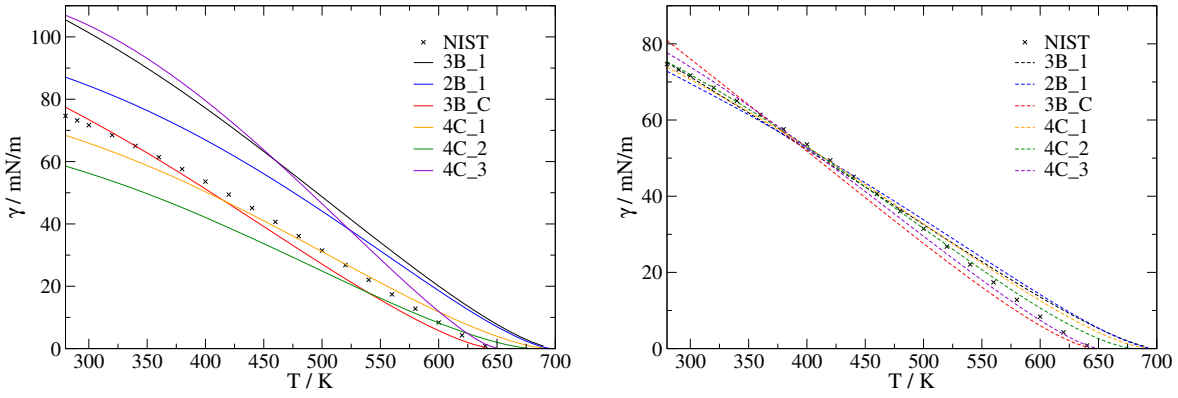

Figure 4.5: Surface tension γ of water. Calculated results of (lines) obtained from different PCP-SAFT parameter sets and reference data [43] (symbols). The parameter sets are taken from: *2B_1* [22], *3B_1* [52], *3B_C* [52], *4C_1* [51], *4C_2* [53] and *4C_3* [46]. Diagram (a): DFT predictions (solid lines). Diagram (b): DGT correlation results (dashed lines).

Summarizing the results for pure components, predictions of DFT and correlations of DGT can both be considered very accurate for non-associating compounds. The averaged absolute deviation of DFT (DGT) for non-polar, non-associating compounds takes on a value of 0.43 mN/m (0.28 mN/m). For polar molecules this value increases only slightly for DFT to 0.55 mN/m (0.19 mN/m). Once associative molecular interactions have to be taken into account, deviations of both models increase (DFT: 3.34 mN/m, DGT: 0.94 mN/m, excluding water). DFT results for water vary greatly depending on the parameter set. Average deviations range from just below 3 mN/m (sets *4C_1* and *3B_C*) to around 20 mN/m (sets *4C_3* and *3B_1*). For DGT, average deviations take on values between 0.8 mN/m (*4C_2*) and 2.8 mN/m (*3B_C*). As shown in the previous sections, deviations of DFT do not correlate with the polarity or association strength of the molecules. In the Supporting Information, it is shown that deviations of DFT and DGT also do not correlate with errors in vapor pressure, liquid density or critical temperature (determination coefficients below 0.3). Furthermore, with a determination coefficient of $R^2 = 0.44$, deviations of DFT predictions do not correlate significantly with deviations of DGT correlations.

4.2.2 Mixtures

In this section, results for mixtures are presented. We follow the same structure as in the pure component paragraph: results of mixtures containing non-polar, non-associating components are shown first and systems including polar and associating species are presented thereafter. For every mixture, predictions of DFT are compared to results of DGT

using the path function approach (which requires $\beta_{ij} = 0$ for eq. 4.5). Furthermore, the possibility to improve DGT results by adjusting a cross-wise influence parameter β_{ij} to experimental mixture surface tension data is discussed for several mixtures. We then apply the stabilized DGT algorithm. A restriction for this procedure is the requirement of a positive definite matrix of influence parameters C [34]. It will be shown that for binary mixtures, violations of this restriction lead to unreliable results or a breakdown of the algorithm. However, for several multicomponent mixtures studied in this work, C is not positive definite even for $\beta_{ij} = 0$ and still both DGT algorithms converge, the density profiles look reasonable and surface tension results agree very well with experimental data.

Alkane mixtures

Fig. 4.6 shows results of DFT and DGT for surface tensions of binary n-alkane mixtures where the molecules differ significantly in size. DFT and DGT results for mixtures containing methane and a longer n-alkane (fig. 4.6a) are very similar and except at the lowest pressure values agreement to experimental data is excellent.
Results of the mixture n-heptane–eicosane for two isotherms are presented in fig. 4.6b. Surface tensions obtained with DFT and DGT agree very closely and underpredict experimental values moderately at both temperatures. In an attempt to improve the results, the stabilized DGT algorithm with values $\beta_{ij} \neq 0$ is applied, however to no avail: it is apparent from fig. 4.6b that positive β_{ij} values increase the deviations at $T = 343.15$ K (the same applies to results at $T = 313.15$ K, see Supporting Information). Negative values on the other hand result in a matrix C that is not positive definite. Ignoring the restriction of positive definiteness of C and performing calculations with negative values of β_{ij} leads to several plateaus of surface tension as a function of 'pseudo time' (see Supporting Information) or to failure of the calculation due to rank deficient Jacobian matrices.
Results of DFT and DGT for a seven-component and a twenty-component alkane mixture are presented in fig. 4.8. The molar overall compositions of these mixtures are given in table 2 of the Supporting Information. For both mixtures, the matrix of influence parameters C is not positive definite even for $\beta_{ij} = 0$. It is therefore somewhat surprising that both DGT algorithms converge without numerical issues. Comparing the results of both DGT algorithms to ensure that the stabilized DGT algorithm has reached the steady-state solution reveals that results of both algorithms only agree for the seven-component mixture and in the low pressure region for the twenty-component mixture. At higher pressures, results of the stabilized DGT algorithm are not in agreement to results of the DGT path function approach as seen in fig. 4.7 and in the Supporting Information. This highly disturbing observation is neither resolved with longer computation time nor with tighter convergence criteria. A possible explanation could be that the non-positive

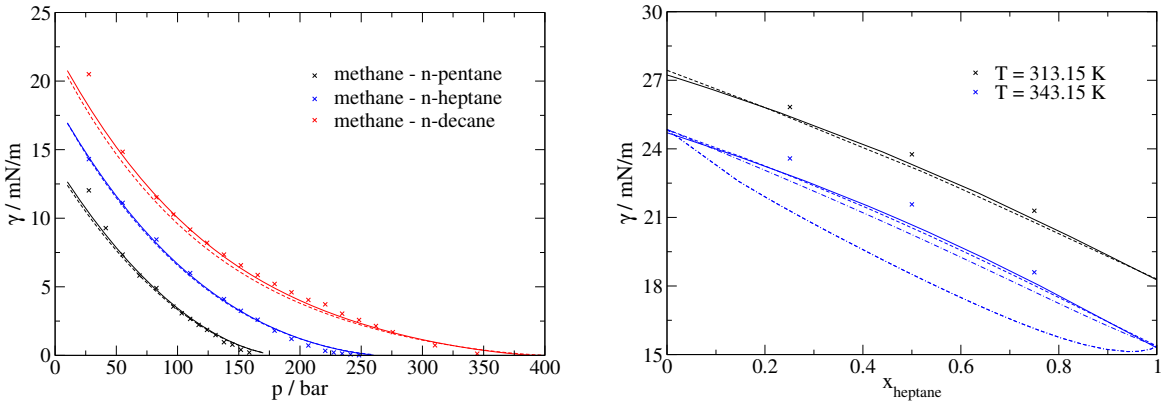

(a) (b)

Figure 4.6: Diagram (a): Surface tension γ of binary mixtures of methane with three n-alkanes at $T = 310.93$ K. Calculated results (DFT: solid lines, DGT: dashed lines) and experimental data [54]. k_{ij} values of 0.024, 0.016 and 0.021 are used for methane – pentane, methane – heptane, and methane – decane, respectively. Diagram (b): Surface tension γ of binary mixture of n-heptane – eicosane. Calculated results (DFT: solid lines, DGT: dashed lines) and experimental data [55]. At $T = 343.15$ K, additional results obtained using the stabilized DGT algorithm and $\beta_{ij} = 0.1$ (dash-dotted line) and $\beta_{ij} = 0.5$ (double-dash-dotted line) are presented. All k_{ij} values are set to zero.

definite matrix C causes these differences between the two algorithms. However, using the same matrix at lower pressures leads to identical results for both algorithms.

As fig. 4.8a shows, surface tensions obtained from DFT and the DGT path function approach for the seven-component mixture are in very good agreement to the experiments. The same applies for DGT results for the twenty-component mixture while in this case DFT results are moderately too low, see fig. 4.8b.

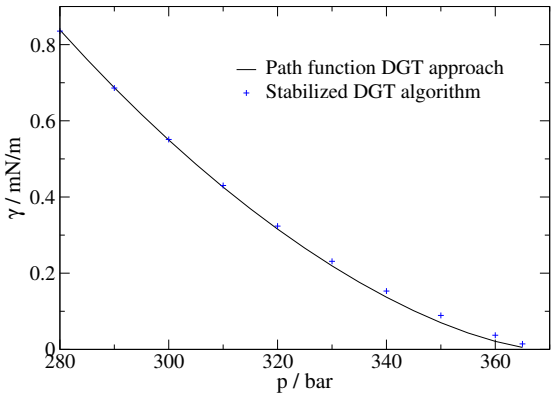

Figure 4.7: Mismatch of DGT-results from two solution methods: the path function approach (black line) and the stabilized DGT algorithm (blue symbols), both using $\beta_{ij} = 0$. Results should be identical, irrespective of the solution method. Both approaches appear to be converged, i.e. the results are independent of longer computation time or tighter convergence criteria. Considered is the surface tension γ of the twenty-component mixture at $T = 366.45$ K.

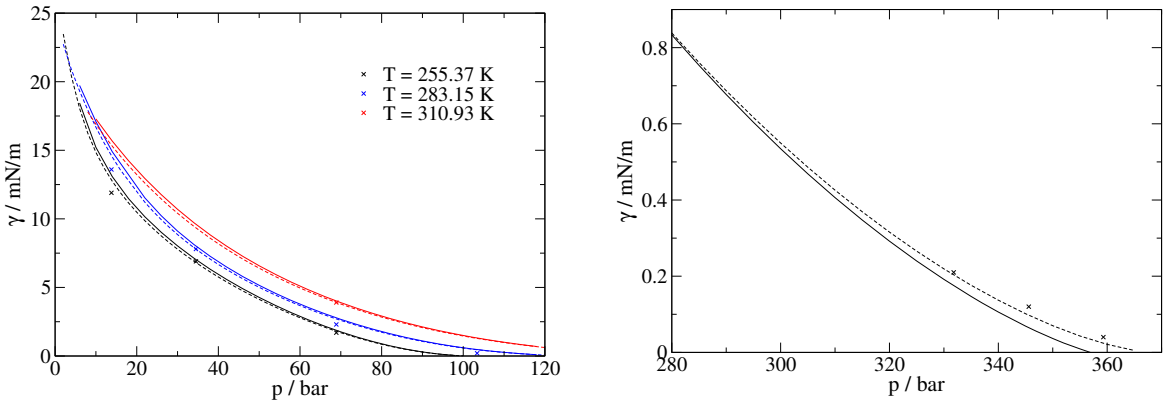

(a) (b)

Figure 4.8: Diagram (a): Seven-component alkane mixture. Calculated results of surface tension γ (DFT: solid lines, DGT path function approach: dashed lines) and experimental data [56] (symbols). No binary interaction parameters were used in the calculations. Diagram (b): Twenty-component alkane mixture at $T = 366.45$ K. Calculated results of surface tension γ (DFT: solid lines, DGT path function approach: dashed lines) and experimental data [57] (symbols). No binary interaction parameters were used in the calculations.

Mixtures including polar compounds

DFT predictions and DGT correlations are both very accurate for the pure polar substances presented in the section on pure component systems. As figures 4.9 and 4.10 show, the same applies to mixtures including one or more polar components. With average deviations of only 0.25 mN/m and 0.43 mN/m, DGT and DFT results, respectively, are very accurate for the mixture CO_2-decane (fig. 4.9a) over a wide temperature and pressure range. For the binary mixture nitrogen-heptane, DFT and DGT results behave similarly and give surface tension results that are moderately too low compared to experimental data with better agreement for DFT results. However, for this mixture, DGT results can be improved by adjusting a binary correction parameter for the influence parameters β_{ij} (fig. 4.9b) and applying the stabilized DGT algorithm. It has to be kept in mind that these DGT results are obtained using two component specific and one mixture specific parameter adjusted to interfacial data while DFT offers no such adjustable parameters. In that light and in view of the very comparable results, we propose using DFT for such systems

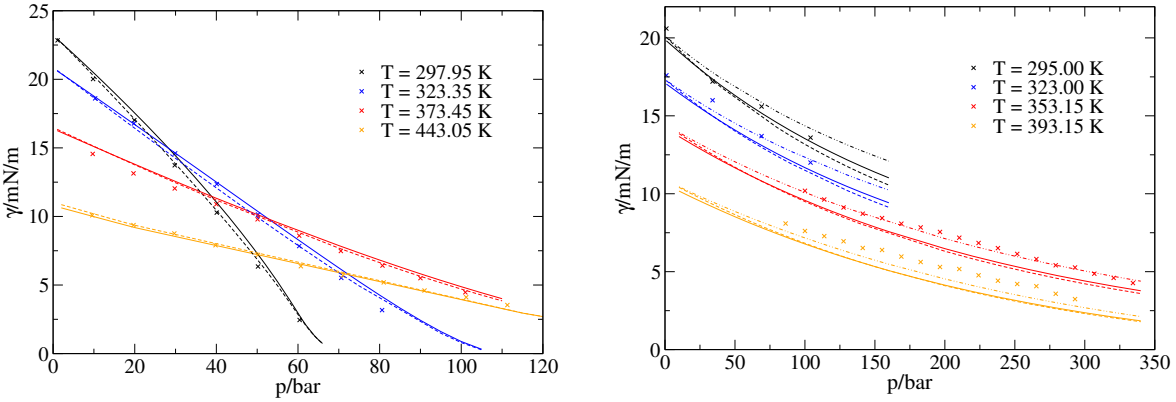

(a) (b)

Figure 4.9: Diagram (a): Surface tension of the binary mixture CO_2 – decane. Calculated results (DFT: solid lines, DGT: dashed lines) using a binary interaction coefficient of $k_{ij} = 0.0681$ and experimental data [58] (symbols). Diagram (b): Surface tension of the binary mixture N_2 – heptane. Calculated results (DFT: solid lines, DGT with $\beta_{ij} = 0$: dashed lines, DGT with $\beta_{ij} = 0.869$: double-dotted dashed line) using a binary interaction coefficient of $k_{ij} = 0.0930$ and experimental data [32] (symbols). The non-zero DGT-parameter of β_{ij} was adjusted simultaneously to experimental data points on all four isotherms.

Results for refrigerant mixtures of up to four polar compounds are exemplified in fig. 4.10. In general, surface tension values of DFT and DGT agree very well at higher temperatures while in the low temperature range DFT predictions are larger than DGT values. Overall agreement to experimental data is excellent for DGT and only slightly worse for DFT.

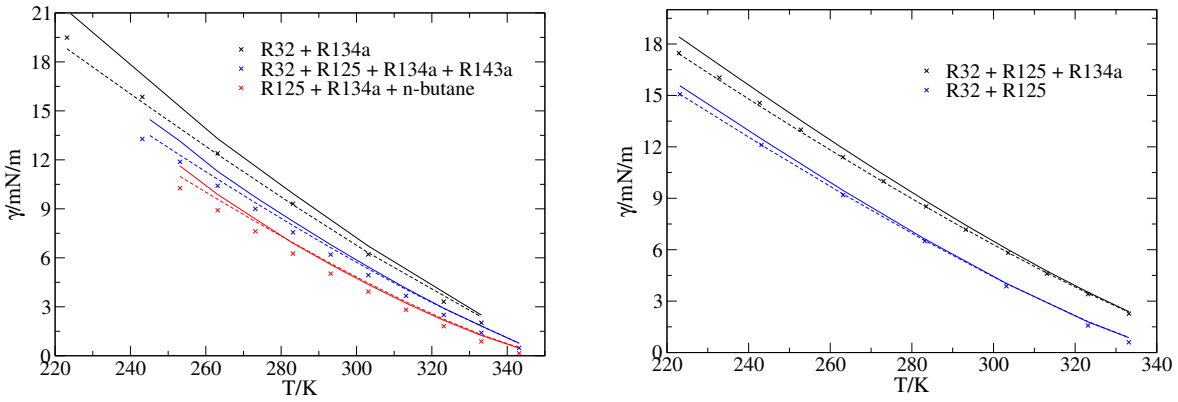

(a) (b)

Figure 4.10: Surface tension γ of several mixtures of polar compounds. Calculated results (DFT: solid lines, DGT: dashed lines) and experimental data [59] [60] [61]. The following k_{ij} values are used: R32-R134a: 0.0104, R32-R125: -0.0102, R125-R134a: -0.00386, R125-butane: 0.0914, R134a-butane: 0.0934, R32-R143a: 0.018, R125-R143a: -0.0107, R143a-R143a: -0.003.

Mixtures including associating compounds

In this section, results of DFT and DGT for mixtures of an associating component with non-associating components are compared to experiments. Figure 4.11a shows results for surface tensions of the binary mixtures n-hexane – ethanol and n-hexane – 1-octanol at $T = 298.15$ K as a function of hexane mole fraction in the liquid phase x_{hexane}. DFT results for γ agree very well with experimental values at high and intermediate values of x_{hexane} while for low composition of hexane γ is overpredicted significantly. Considering DFT results for pure associating components, the deviations toward pure alcohol is anticipated. Deviations of DGT for pure associating components, on the other hand, showed much smaller deviations than DFT results. However, DGT results with $\beta_{ij} = 0$ for both mixtures in fig. 4.11a are too low and with much larger errors than DFT over a wide composition range. Furthermore, as fig. 4.11b shows exemplarily for hexane – ethanol, density profiles obtained from DGT with $\beta_{ij} = 0$ (using the path function approach) are unreasonable: the species-density profile of hexane shows an almost infinitely steep gradient in the interface and the gradient of ethanol is also much steeper than the gradient in the profile obtained by DFT. The DFT profiles can serve as a reference in this case because the comparison is made at a value of x_{hexane} where DFT results for the surface tension are in excellent agreement with experimental data. Density profiles for the remaining binary hexane – alcohol mixtures are presented in the Supporting Information and confirm that DGT leads to sharper interfaces with steeper density gradients. A detailed study of this behavior can be found in the work of Liang et al. [30]. Adjusting β_{ij} (using the stabilized DGT algorithm) yields only a very limited improvement for the correlation of γ (fig. 4.11a): with increasing values of β_{ij} first leads to a shift of γ results towards the

experimental values but beyond a certain value of β_{ij}, the effect is reversed and deviations to the experiments increase (see Supporting Information). Minimizing the sum of squared errors yields optimal values of $\beta_{ij} = 0.07646$ and $\beta_{ij} = 0.08553$ for the mixtures hexane – ethanol and hexane – 1-octanol, respectively. Despite the small influence on γ, the optimized value of β_{ij} causes pronounced changes in the density profiles, see fig. 4.11b. The steep gradient in the density profile of hexane vanishes and the enrichment of hexane in the interface is reduced notably. Furthermore, the enrichment of ethanol in the interface present in the profile of the DGT path function approach vanishes almost completely. In general, the profiles resemble the profiles obtained from DFT more closely.

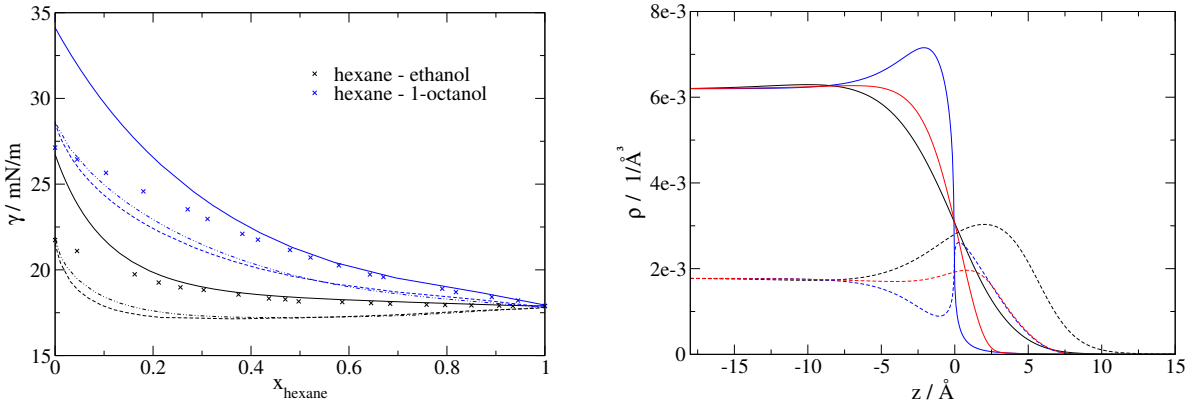

(a) (b)

Figure 4.11: Diagram (a): calculated results of surface tension γ (DFT: solid lines, DGT path function approach: dashed lines, stabilized DGT algorithm: double-dotted dashed lines) and experimental results [62] for the mixtures hexane - ethanol ($k_{ij} = 0.02854$) and hexane - 1-octanol ($k_{ij} = 0.006435$) at 298.15K. The optimized values of β_{ij} used in the calculations with the stabilized DGT algorithm are 0.07646 and 0.08553 for hexane - ethanol and hexane - 1-octanol, respectively. Diagram (b): density profiles for the mixture hexane (dashed lines)-ethanol (solid lines) at $T = 298.15$ K and $x_{hexane} = 0.22$ ($p = 0.236$ bar) obtained from DFT (black), path function DGT approach (blue) and stabilized DGT algorithm using $\beta_{ij} = 0.07646$ (red).

Table 4.1 lists averaged absolute deviations for surface tension as obtained from DFT predictions and from DGT correlations (with $\beta_{ij} = 0$) for several binary mixtures of hexane with alcohols. Depending on the mixture, deviations can be smaller for either method. The corresponding graphical representation of these results are presented in the Supporting Information. In analyzing all mixtures we find that DFT predictions agree very well with experimental results over a wide concentration range but overpredict the surface tension for pure associating components leading to deviations at high alcohol composition. For DGT correlations with $\beta_{ij} = 0$ at intermediate compositions, surface tension is underpredicted and the density profiles show unreasonably steep gradients. It is therefore possible that larger deviations occur for mixtures even though the pure components surface tension is enforced at the correct value by adjusting c_{ii} and c_{jj} for a

mixture of species i and j, respectively. The additional adjustment of β_{ij} results in very limited improvements of surface tension results.

Table 4.1: Average deviations of DFT predictions and DGT correlations ($\beta_{ij} = 0$) for binary mixtures of hexane with different alcohols at $T = 298.15$ K. Experimental results are taken from Jiménez et al. [62] $\left(AAD = \frac{1}{N_{exp}} \sum_1^{N_{exp}} |\gamma_{exp} - \gamma_{calc}|\right)$.

hexane + ...	AAD / (mN/m) DFT prediction	AAD / (mN/m) DGT correlation
ethanol	0.57	0.98
1-propanol	1.28	1.79
1-butanol	1.38	1.22
1-pentanol	1.45	1.72
1-hexanol	1.42	1.29
1-heptanol	1.69	1.23
1-octanol	1.32	1.08

4.3 Conclusion

Interfacial properties are studied by classical density functional theory and density gradient theory. Surface tension predictions of DFT for pure components are found in excellent agreement with experimental data for non-associating non-polar and polar molecules. The DGT with an adjustable parameter per species correlates the surface tension also in very good agreement to the experiments for these pure substances. For hydrogen-bonding substances, where association has to be taken into account, DFT overpredicts surface tensions in the low temperature range while deviations for DGT increase only slightly. A possible explanation for the deviations of DFT could be the insufficient description of the orientation of the molecules at the interface. For water, a large variation of DFT results for surface tensions can be observed for different PCP-SAFT pure component parameter sets.

DFT results for mixtures agree very well to experimental data for systems where surface tension for the constituent components are predicted accurately. This includes multicomponent mixtures of up to twenty components and mixtures of several polar compounds. Mixture results of DGT are excellent for most systems of this study. However, larger deviations may occur even though surface tension of the single components are correlated accurately, e.g. for alkane-alcohol mixtures. In this case, non-physically steep density gradients occur and for some systems deviations of DGT are larger than for DFT despite the much larger errors of DFT for pure alcohols. Adjusting a cross-wise influence parameter to experimental mixture surface tension data has only limited practical use for the studied systems. The requirement of a positive definite matrix of influence parameters C poses a restriction on the value of β_{ij} for binary systems, however, for several multicom-

ponent mixtures C is not positive definite even for $\beta_{ij} = 0$ with no consequences for the solution procedure or validity of the results. However, for one mixture with non-positive definite C, we observed that both applied DGT algorithms converge to different solutions (independent of the convergence criteria), which is a worrying finding.
In view of DFT predictions in very good agreement to experimental data and the difficulties observed for some mixtures using DGT, while requiring adjustable parameters, we see justification for selecting a DGT approach over a DFT approach only in rare cases.

Bibliography

[1] P. Hohenberg and W. Kohn, "Inhomogeneous electron gas," *Physical review*, vol. 136, no. 3B, p. B864, 1964.

[2] N. D. Mermin, "Thermal properties of the inhomogeneous electron gas," *Physical Review*, vol. 137, no. 5A, p. A1441, 1965.

[3] C. Ebner, W. Saam, and D. Stroud, "Density-functional theory of simple classical fluids. I. surfaces," *Physical Review A*, vol. 14, no. 6, p. 2264, 1976.

[4] W. Saam and C. Ebner, "Density-functional theory of classical systems," *Physical Review A*, vol. 15, no. 6, p. 2566, 1977.

[5] J. D. Van Der Waals, "Thermodynamische theorie der capillariteit in de onderstelling van continue dichtheidsverandering," *Verbandelingen der Koninklijke Akademie van Wetenschappen te Amsterdam*, vol. 1, no. 8, 1893.

[6] J. W. Cahn and J. E. Hilliard, "Free energy of a nonuniform system. I. interfacial free energy," *The Journal of chemical physics*, vol. 28, no. 2, pp. 258–267, 1958.

[7] D. Henderson, *Fundamentals of inhomogeneous fluids*. CRC Press, 1992.

[8] V. Bongiorno, L. Scriven, and H. Davis, "Molecular theory of fluid interfaces," *Journal of Colloid and Interface Science*, vol. 57, no. 3, pp. 462–475, 1976.

[9] A. J. Yang, P. D. Fleming III, and J. H. Gibbs, "Molecular theory of surface tension," *The Journal of Chemical Physics*, vol. 64, no. 9, pp. 3732–3747, 1976.

[10] R. Evans, "The nature of the liquid-vapour interface and other topics in the statistical mechanics of non-uniform, classical fluids," *Advances in Physics*, vol. 28, no. 2, pp. 143–200, 1979.

[11] B. Breure and C. Peters, "Modeling of the surface tension of pure components and mixtures using the density gradient theory combined with a theoretically derived influence parameter correlation," *Fluid Phase Equilibria*, vol. 334, pp. 189–196, 2012.

[12] P. Cornelisse, C. Peters, and J. de Swaan Arons, "On the fundamentals of the gradient theory of van der waals," *The Journal of chemical physics*, vol. 106, no. 23, pp. 9820–9834, 1997.

[13] C. Miqueu, B. Mendiboure, A. Graciaa, and J. Lachaise, "Modelling of the surface tension of pure components with the gradient theory of fluid interfaces: a simple and accurate expression for the influence parameters," *Fluid phase equilibria*, vol. 207, no. 1, pp. 225–246, 2003.

[14] H. Lin, Y.-Y. Duan, and Q. Min, "Gradient theory modeling of surface tension for pure fluids and binary mixtures," *Fluid phase equilibria*, vol. 254, no. 1, pp. 75–90, 2007.

[15] J. M. Garrido, A. Mejía, M. M. Piñeiro, F. J. Blas, and E. A. Müller, "Interfacial tensions of industrial fluids from a molecular-based square gradient theory," *AIChE Journal*, 2016.

[16] J. Mairhofer and J. Gross, "Modeling of interfacial properties of multicomponent systems using density gradient theory and PCP-SAFT," *Fluid Phase Equilibria*, vol. 439, pp. 31–42, 2017.

[17] H. Löwen, "Density functional theory of inhomogeneous classical fluids: recent developments and new perspectives," *Journal of Physics: Condensed Matter*, vol. 14, no. 46, p. 11897, 2002.

[18] J. Wu, "Density functional theory for chemical engineering: From capillarity to soft materials," *AIChE journal*, vol. 52, no. 3, pp. 1169–1193, 2006.

[19] J. Wu and Z. Li, "Density-functional theory for complex fluids," *Annu. Rev. Phys. Chem.*, vol. 58, pp. 85–112, 2007.

[20] C. P. Emborsky, Z. Feng, K. R. Cox, and W. G. Chapman, "Recent advances in classical density functional theory for associating and polyatomic molecules," *Fluid Phase Equilibria*, vol. 306, no. 1, pp. 15–30, 2011.

[21] J. Gross and G. Sadowski, "Perturbed-chain SAFT: An equation of state based on a perturbation theory for chain molecules," *Industrial & engineering chemistry research*, vol. 40, no. 4, pp. 1244–1260, 2001.

[22] J. Gross and G. Sadowski, "Application of the perturbed-chain SAFT equation of state to associating systems," *Industrial & engineering chemistry research*, vol. 41, no. 22, pp. 5510–5515, 2002.

[23] J. Gross and J. Vrabec, "An equation-of-state contribution for polar components: Dipolar molecules," *AIChE journal*, vol. 52, no. 3, pp. 1194–1204, 2006.

[24] J. Gross, "An equation-of-state contribution for polar components: Quadrupolar molecules," *AIChE journal*, vol. 51, no. 9, pp. 2556–2568, 2005.

[25] J. Gross, "A density functional theory for vapor-liquid interfaces using the PCP-SAFT equation of state," *The Journal of chemical physics*, vol. 131, no. 20, p. 204705, 2009.

[26] C. Klink and J. Gross, "A density functional theory for vapor–liquid interfaces of mixtures using the perturbed-chain polar statistical associating fluid theory equation of state," *Industrial & Engineering Chemistry Research*, vol. 53, no. 14, pp. 6169–6178, 2014.

[27] E. Sauer and J. Gross, "Classical density functional theory for liquid-fluid interfaces and confined systems using the perturbed-chain polar statistical associating fluid theory equation of state," *Industrial & engineering chemistry research*, submitted 2016.

[28] A. Bymaster and W. G. Chapman, "An iSAFT density functional theory for associating polyatomic molecules," *The Journal of Physical Chemistry B*, vol. 114, no. 38, pp. 12298–12307, 2010.

[29] C. J. Segura, W. G. Chapman, and K. P. Shukla, "Associating fluids with four bonding sites against a hard wall: density functional theory," *Molecular Physics*, vol. 90, no. 5, pp. 759–772, 1997.

[30] X. Liang, M. L. Michelsen, and G. M. Kontogeorgis, "Pitfalls of using the geometric-mean combining rule in the density gradient theory," *Fluid Phase Equilibria*, vol. 415, pp. 75–83, 2016.

[31] Z. Qiao and S. Sun, "Two-phase fluid simulation using a diffuse interface model with peng–robinson equation of state," *SIAM Journal on Scientific Computing*, vol. 36, no. 4, pp. B708–B728, 2014.

[32] O. N. Amézquita, S. Enders, P. Jaeger, and R. Eggers, "Interfacial properties of mixtures containing supercritical gases," *The Journal of Supercritical Fluids*, vol. 55, no. 2, pp. 724–734, 2010.

[33] V. Bongiorno and H. T. Davis, "Modified van der waals theory of fluid interfaces," *Physical Review A*, vol. 12, no. 5, p. 2213, 1975.

[34] P. M. W. Cornelisse, *The Square Gradient Theory Applied*. PhD thesis, TU Delft, 1997.

[35] J. Mairhofer and J. Gross, "Numerical aspects of classical density functional theory for one-dimensional vapor-liquid interfaces," *Fluid Phase Equilibria*, vol. 444, pp. 1–12, 2017.

[36] Y. Rosenfeld, "Free-energy model for the inhomogeneous hard-sphere fluid mixture and density-functional theory of freezing," *Physical review letters*, vol. 63, no. 9, p. 980, 1989.

[37] R. Roth, R. Evans, A. Lang, and G. Kahl, "Fundamental measure theory for hard-sphere mixtures revisited: the white bear version," *Journal of Physics: Condensed Matter*, vol. 14, no. 46, p. 12063, 2002.

[38] Y.-X. Yu and J. Wu, "Structures of hard-sphere fluids from a modified fundamental-measure theory," *The Journal of chemical physics*, vol. 117, no. 22, pp. 10156–10164, 2002.

[39] S. Tripathi and W. G. Chapman, "Microstructure of inhomogeneous polyatomic mixtures from a density functional formalism for atomic mixtures," *The Journal of chemical physics*, vol. 122, no. 9, p. 094506, 2005.

[40] X. Mu, F. Frank, F. O. Alpak, and W. G. Chapman, "Stabilized density gradient theory algorithm for modeling interfacial properties of pure and mixed systems," *Fluid Phase Equilibria*, vol. 435, pp. 118–130, 2017.

[41] P. M. Larsen, B. Maribo-Mogensen, and G. M. Kontogeorgis, "A collocation method for surface tension calculations with the density gradient theory," *Fluid Phase Equilibria*, vol. 408, pp. 170–179, 2016.

[42] X. Liang and M. L. Michelsen, "General approach for solving the density gradient theory in the interfacial tension calculations," *Fluid Phase Equilibria*, vol. 451, pp. 79–90, 2017.

[43] E. W. Lemmon, M. O. McLinden, and D. G. Friend, "Thermophysical properties of fluid systems," in *NIST Chemistry WebBook, NIST Standard Reference Database Number 69* (P. J. Linstrom and W. G. Mallard, eds.), Gaithersburg MD, 20899: National Institute of Standards and Technology, 2016. http://webbook.nist.gov, (retrieved July 12, 2016).

[44] G. Somayajulu, "A generalized equation for surface tension from the triple point to the critical point," *International journal of thermophysics*, vol. 9, no. 4, pp. 559–566, 1988.

[45] A. Mulero, I. Cachadiña, and M. Parra, "Recommended correlations for the surface tension of common fluids," *Journal of Physical and Chemical Reference Data*, vol. 41, no. 4, p. 043105, 2012.

[46] G. M. Kontogeorgis, I. Tsivintzelis, N. von Solms, A. Grenner, D. Bøgh, M. Frost, A. Knage-Rasmussen, and I. G. Economou, "Use of monomer fraction data in the parametrization of association theories," *Fluid Phase Equilibria*, vol. 296, no. 2, pp. 219–229, 2010.

[47] I. Tsivintzelis, D. Bøgh, E. Karakatsani, and G. M. Kontogeorgis, "The role of monomer fraction data in association theories—can we improve the performance for phase equilibrium calculations?," *Fluid Phase Equilibria*, vol. 365, pp. 112–122, 2014.

[48] R. Superfine, J. Huang, and Y. Shen, "Nonlinear optical studies of the pure liquid/vapor interface: Vibrational spectra and polar ordering," *Physical review letters*, vol. 66, no. 8, p. 1066, 1991.

[49] C. Stanners, Q. Du, R. Chin, P. Cremer, G. Somorjai, and Y.-R. Shen, "Polar ordering at the liquid-vapor interface of n-alcohols (c1-c8)," *Chemical physics letters*, vol. 232, no. 4, pp. 407–413, 1995.

[50] M. Matsumoto and Y. Kataoka, "Molecular orientation near liquid–vapor interface of methanol: Simulational study," *The Journal of Chemical Physics*, vol. 90, no. 4, pp. 2398–2407, 1989.

[51] X. Liang, I. Tsivintzelis, and G. M. Kontogeorgis, "Modeling water containing systems with the simplified PC-SAFT and CPA equations of state," *Industrial & Engineering Chemistry Research*, vol. 53, no. 37, pp. 14493–14507, 2014.

[52] S. Aparicio-Martínez and K. R. Hall, "Phase equilibria in water containing binary systems from molecular based equations of state," *Fluid phase equilibria*, vol. 254, no. 1, pp. 112–125, 2007.

[53] N. I. Diamantonis and I. G. Economou, "Evaluation of statistical associating fluid theory (SAFT) and perturbed chain-SAFT equations of state for the calculation of thermodynamic derivative properties of fluids related to carbon capture and sequestration," *Energy & Fuels*, vol. 25, no. 7, pp. 3334–3343, 2011.

[54] R. Amin and T. N. Smith, "Interfacial tension and spreading coefficient under reservoir conditions," *Fluid Phase Equilibria*, vol. 142, no. 1, pp. 231–241, 1998.

[55] A. J. Queimada, F. A. Silva, A. I. Caço, I. M. Marrucho, and J. A. Coutinho, "Measurement and modeling of surface tensions of asymmetric systems: heptane, eicosane, docosane, tetracosane and their mixtures," *Fluid phase equilibria*, vol. 214, no. 2, pp. 211–221, 2003.

[56] H. Ng, S. Taylor, H. Schroeder, and D. Sieben, "High pressure gas separation and conditioning," *GPA Research Report, Rep. No. PR-193*, pp. 1–50, 2008.

[57] A. Danesh, A. Dandekar, A. Todd, and R. Sarkar, "A modified scaling law and parachor method approach for improved prediction of interfacial tension of gas-condensate systems," in *SPE Annual Technical Conference and Exhibition*, Society of Petroleum Engineers, 1991.

[58] A. Georgiadis, F. Llovell, A. Bismarck, F. J. Blas, A. Galindo, G. C. Maitland, J. M. Trusler, and G. Jackson, "Interfacial tension measurements and modelling of (carbon dioxide + n-alkane) and (carbon dioxide + water) binary mixtures at elevated pressures and temperatures," *The Journal of Supercritical Fluids*, vol. 55, no. 2, pp. 743–754, 2010.

[59] R. Heide, "The surface tension of HFC refrigerants and mixtures," *International journal of refrigeration*, vol. 20, no. 7, pp. 496–503, 1997.

[60] A. Heller, M. Rausch, F. Flohr, A. Leipertz, and A. Fröba, "Thermophysical properties of the refrigerant mixtures R417A and R417B from dynamic light scattering (DLS)," *International Journal of Thermophysics*, vol. 33, no. 3, pp. 396–411, 2012.

[61] A. P. Fröba, C. Botero, H. Kremer, and A. Leipertz, "Thermophysical properties of a quaternary refrigerant mixture: comparison of dynamic light scattering measurements with a simple prediction method," *International Journal of Thermophysics*, vol. 28, no. 3, pp. 743–757, 2007.

[62] E. Jiménez, H. Casas, L. Segade, and C. Franjo, "Surface tensions, refractive indexes and excess molar volumes of hexane + 1-alkanol mixtures at 298.15 k," *Journal of Chemical & Engineering Data*, vol. 45, no. 5, pp. 862–866, 2000.

Chapter 5

A classical Density Functional Theory for Vapor-Liquid Interfaces consistent with the heterosegmented group-contribution Perturbed-Chain Polar Statistical Associating Fluid Theory

The content of this chapter is a literal quote of the publication

Mairhofer, Xiao, Gross, Fluid Phase Equilibria, 472, 2018, 117-127.

In comparison to the published work, the abstract is here omitted. Additions or deletions compared to the published work are marked with angular brackets.

In many technical applications, interfacial properties play a determining role. For the calculation of surface tension, many simple methods have been developed [1, 2, 3, 4, 5, 6, 7]. Most of these simple methods are only applicable to certain classes of systems, lack predictive capabilities, especially for mixtures, and require input values for densities or critical properties of the components under study, which need to be known experimentally or provided by auxiliary models. There is a clear need for self-contained, predictive models with a more general range of applicability. Beyond prediction of interfacial tensions, a detailed description of the interface is important for example in the development of theories for interfacial mass transfer beyond the simple two-film model, taking into account implications from the enrichment of certain species at the interface [8].
Density gradient theory (DGT) and classical density functional theory (DFT) are two

methods that can be applied to describe interfacial properties. The fundamental difference between both methods is that DFT is entirely predictive for interfacial properties, whereas DGT requires a component-specific adjustable parameter (referred to as influence parameter), which is usually adjusted to experimental data of surface tensions. In this study we apply DFT without adjustable parameters.

An approximate expression for the Helmholtz energy functional $A[\rho(\mathbf{r})]$, where the square brackets denote a functional dependence on the spatially varying density profile $\rho(\mathbf{r})$, is at the core of any DFT approach. The development of the Statistical Associating Fluid Theory (SAFT) led to equations of state for non-spherical and hydrogen-bonding (i.e. associating) interactions [9]. SAFT models are based on Wertheim's Thermodynamic Perturbation Theory (TPT) [10, 11, 12, 13] and were natively developed in a functional form [14], as worked out by Chapman and coworkers [15, 16, 17] with contributions of Kierlik and Rosinberg [18, 19]. Jain et al. [20] modified the interfacial SAFT (iSAFT) form earlier proposed by Tripathi and Chapman [17] to account for the chain formation of single segments. The theory can be used to build heteronuclear chain fluids with individually tagged segments, which means that the density profile of all segments within a chain can be individually calculated.

In several studies, Helmholtz energy functionals consistent with SAFT-type equations of state have been applied successfully to study vapor-liquid interfaces and predict surface tension or study fluids in confined media. This includes the studies of Jackson and coworkers [21, 22, 23, 24, 24, 25, 26], Schindler et al. [27] and Malheiro et al. [28] who applied Helmholtz energy functionals consistent with the Statistical Associating Fluid Theory for potentials of variable range (SAFT-VR) or Kahl and Winkelmann [29] who applied a functional consistent with Lennard-Jones-SAFT. A review of current DFT applications can be found in the articles of Davis [30], Löwen [31], Wu [32], Emborsky et al. [33] or Landers et al. [34].

A Helmholtz energy functional consistent with the Perturbed-Chain Polar Statistical Associating Fluid Theory (PCP-SAFT) [35] [36] [37] [38] has been developed in our group [39, 40, 41]. Surface tension predictions from DFT calculations using the most recent Helmholtz energy functional are in excellent agreement with experiments [41] [42]. The required input for these calculations are the pure-component PCP-SAFT parameters and possibly binary interaction parameters. These parameters are commonly regressed to pure component and mixture vapor liquid equilibria, respectively, without considering interfacial properties.

In order to further increase the predictive capabilities of the DFT approach, a Helmholtz energy functional consistent with an accurate group-contribution (GC) equation of state is desirable. Group-contribution methods assume that the properties of a molecule can be determined as a function of the distinct functional groups that make up the given

molecule. Such an approach makes the need for component-specific equation of state parameters obsolete. The range of applicability of DFT thus increases to compounds for which no or not enough experimental data is available to retrieve model parameters.
In this study we develop a Helmholtz energy functional consistent with the heterosegmented group-contribution PCP-SAFT equation of state [43] [44], i.e. when applied to a homogeneous system, this functional reduces to the expressions of heterosegmented GC-PCP-SAFT.
The Helmholtz energy functional is based on modified iSAFT to account for the chain formation of single segments. Predictions of the surface tension as obtained from the DFT approach for pure components as well as mixtures for non-polar and non-associating, polar as well as associating compounds are compared to experimental data. Furthermore, it is shown that the level of detail accessible by calculating density profiles for individual segments offers the possibility to qualitatively reproduce the orientation of hydrogen-bonding molecules at the interface. This is exemplified for 1-alcohols.

5.1 Heterosegmented group-contribution PCP-SAFT

In the heterosegmented group-contribution PCP-SAFT equation of state, the Helmholtz energy A is calculated as the sum of several contributions [43] [44]

$$\frac{A}{NkT} = \frac{A^{IG}}{NkT} + \frac{A^{HS}}{NkT} + \frac{A^{HC}}{NkT} + \frac{A^{Disp}}{NkT} + \frac{A^{Assoc}}{NkT} + \frac{A^{Dipole}}{NkT} \tag{5.1}$$

where the summands are the Helmholtz energy of an ideal gas, the contribution of the hard-sphere fluid, of chain formation, of dispersive attraction, of association, and of dipole-dipole interactions. In the following paragraph, we present modifications to the dispersive contribution of eq. 5.1. For details on the remaining Helmholtz energy contributions, we refer to the original work on the group-contribution PCP-SAFT equation of state by Sauer et al. [43] and Gross et al. [44].
The defining advantage of group-contribution methods is their predictive capability: properties of compounds where no experimental data is available to adjust component-specific parameters can be derived from the molecular structure of the compound and parameters for the groups constituting the molecule. A drawback of GC methods, on the other hand, is that methods using compound-specific parameters, where applicable, usually fare better than group-contribution approaches. In an attempt to improve results of heterosegmented GC-PCP-SAFT for compounds with a large body of experimental data we introduce a parameter ϕ_i to the dispersive contribution which is adjusted to experimental vapor pressure data of component i. As a consequence, we improve the representation of well-known substances, while preserving the ability to predict substances with no or

limited experimental characterization, and mixtures thereof. The choice to use vapor pressure data rather than liquid density to regress ϕ_i is based on the results presented in [43] which show that values of heterosegmented GC-PCP-SAFT for liquid density are already convincingly accurate whereas larger deviations occur for vapor pressure. Furthermore, transferable group-group interaction parameters $k_{\alpha\beta}$ are introduced to improve the description of mixtures. The parameters $k_{\alpha\beta}$ have values $\neq 0$ only for segments of unlike types α and β which are located on different chain molecules. The dispersive contribution to the Helmholtz energy for a mixture of N components at temperature T and density ρ is then obtained as

$$\frac{A^{Disp}}{NkT} = a_1 + a_2 \tag{5.2}$$

where

$$a_1 = -2\pi\rho I_1 \sum_{i=1}^{N}\sum_{j=1}^{N} x_i x_j \sum_{\alpha}\sum_{\beta} n_{i\alpha} n_{j\beta} m_\alpha m_\beta \sigma_{\alpha\beta}^3 \epsilon_{i\alpha,j\beta}/kT \tag{5.3}$$

$$a_2 = -\pi\bar{m}\rho I_2 C_1 \sum_{i=1}^{N}\sum_{j=1}^{N} x_i x_j \sum_{\alpha}\sum_{\beta} n_{i\alpha} n_{j\beta} m_\alpha m_\beta \sigma_{\alpha\beta}^3 (\epsilon_{i\alpha,j\beta}/kT)^2 \tag{5.4}$$

The sums with indices α and β run over all group types and $n_{i\alpha}$ denotes the number of segments of type α on molecule i. Furthermore, m_α and σ_α represent the segment number and diameter parameter, respectively, of segments of type α, with the geometric condition $\bar{m} = \sum_i^N x_i \sum_\alpha n_{i\alpha} m_\alpha$, the combining rule $\sigma_{\alpha\beta} = 0.5(\sigma_\alpha + \sigma_\beta)$, and the combining rule for the cross-wise energy parameter

$$\epsilon_{i\alpha,j\beta} = \sqrt{\epsilon_\alpha \phi_i \cdot \epsilon_\beta \phi_j}(1 - k_{\alpha\beta}) \tag{5.5}$$

where $k_{\alpha\beta}$ takes on the values presented in table 5.1 only if $\alpha \neq \beta$ and $i \neq j$, otherwise it is defined as zero. Here ϵ_α is the dispersive energy parameter characterizing the attractive van der Waals interaction between two groups of type α and I_1, I_2 and C_1 are obtained as presented for the original PC-SAFT equation of state [35]. The values of ϕ_i for the compounds studied in this work are presented in the Supporting Information. For most compounds, ϕ_i is very close to unity. Only for short molecules which cannot be represented accurately by a group-contribution method as well as some multi-functional compounds, the value of ϕ_i deviates notably from one and deviations of vapor pressure for these compounds can be reduced significantly. This is shown exemplary for propyne and 2-butenal in fig. 5.1.

The $k_{\alpha\beta}$ parameters are regressed to experimental VLE data of a large set of binary

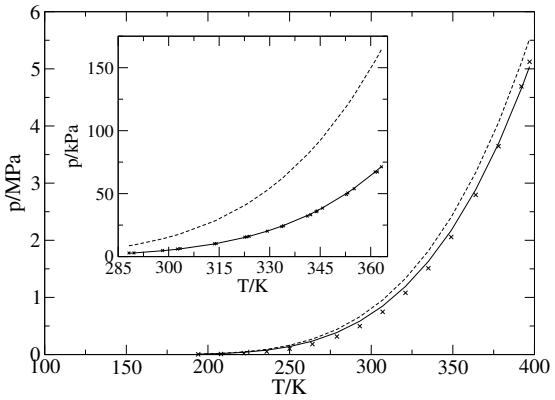

Figure 5.1: Vapor pressure curves for propyne (large graphic) and 2-butenal (small graphic) with adjusted ϕ_i (solid lines) and with $\phi_i = 1$ (dashed lines). Experimental data (symbols) is taken from [45] and [46].

mixtures. Results are presented in table 5.1. Information on the binary mixtures included in the adjustment of $k_{\alpha\beta}$ can be found in the Supporting Information.

Table 5.1: Binary interaction parameters $k_{\alpha\beta}$ for groups of type α and β located on unlike chain molecules. The binary mixtures considered in the adjustment of $k_{\alpha\beta}$ are presented in the Supporting Information.

$\alpha\backslash\beta$	CH_4	CH_3	CH_2	COO	OH
CH_4	0	-0.005	-0.00269	-	-
CH_3	-0.005	0	0.01151	0.0996	-0.0087
CH_2	-0.00269	0.01151	0	-0.015235	0.0489
COO	-	0.0996	-0.015235	0	-
OH	-	-0.0087	0.0489	-	0

Figures 5.2 and 5.3 exemplify for two binary systems how VLE results of n-alkane-ester and n-alkane-1-alcohol mixtures can significantly be improved by applying the $k_{\alpha\beta}$ parameters. For methane-n-alkane or n-alkane-n-alkane mixtures, results with $k_{\alpha\beta} = 0$ are usually already in good agreement with experiments and adjusting $k_{\alpha\beta}$ parameters for these mixtures only leads to minor improvements. Further results, underlining the transferability of the adjusted $k_{\alpha\beta}$ parameters are shown in the Supporting Information. The heterosegmented GC-PCP-SAFT parameters for the single group types used in this study are taken from [43] and are presented in the Supporting Information.

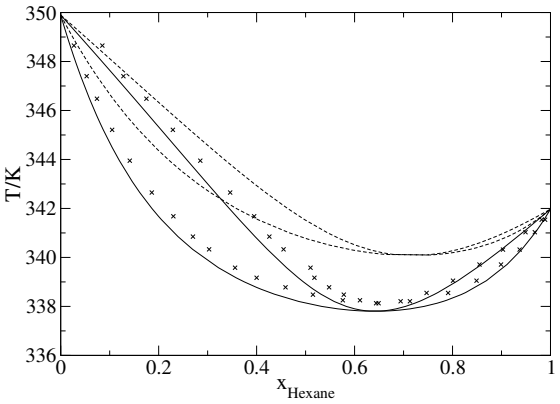

Figure 5.2: Temperature-composition diagram for the binary mixture n-hexane-ethylethanoate at $p = 1.0132$ bar obtained with the adjusted, transferable values of k_{CH_2,CH_3}, $k_{CH_2,COO}$ and $k_{CH_3,COO}$ (solid lines) and without any group-group interaction parameters (dashed line). Experimental results (symbols) are taken from [47].

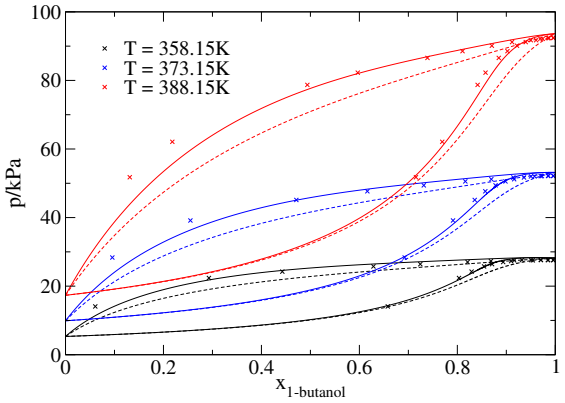

Figure 5.3: Pressure-composition diagram for the binary mixture 1-butanol-decane at three different values of temperature obtained with the adjusted, transferable values of k_{CH_2,CH_3}, $k_{CH_2,OH}$ and $k_{CH_3,OH}$ (solid lines) and without any group-group interaction parameters (dashed line). Experimental results (symbols) are taken from [48].

5.2 Classical density functional theory

In this section, we present the proposed group-contribution density functional theory (GC-DFT) for a mixture of N components. Each component i is modeled as a chain molecule of NS_i segments and in total there are $NS = \sum_1^N NS_i$ segments in the mixture. For a system at given values of temperature T, volume V and chemical potentials μ_{is} ($is = 1, ..., NS$), the grand potential Ω is related to the intrinsic Helmholtz energy of the system A by

$$\Omega[\{\rho_{ks}\}] = A[\{\rho_{ks}\}] - \sum_{is=1}^{NS} \int \rho_{is}(\mathbf{r})\mu_{is}\mathrm{d}\mathbf{r} \tag{5.6}$$

where the square brackets denote a functional dependence on the spatially varying density profiles $\rho_{is}(\mathbf{r})$ and the curly brackets make the dependence on the density profiles of all segments explicit. For brevity, we don't explicitly show that A depends on T and V, nor that Ω is a potential to T, V and $\{\mu_{ks}\}$. The intrinsic Helmholtz energy $A[\{\rho_{ks}\}]$ is approximated as the sum of the same contributions as presented in eq. 5.1. However, now all contributions are functionals of the density profiles

$$A[\{\rho_{ks}\}] = A[\{\rho_{ks}\}]^{IG} + A[\{\rho_{ks}\}]^{HS} + A[\{\rho_{ks}\}]^{HC} + A[\{\rho_{ks}\}]^{Disp} + A[\{\rho_{ks}\}]^{Assoc} + A[\{\rho_{k}\}]^{Dipole} \tag{5.7}$$

Both, the association term $A[\{\rho_{ks}\}]^{Assoc}$ that accounts for short-ranged attractive interactions (hydrogen-bonds) and the chain contribution $A[\{\rho_{ks}\}]^{HC}$, where the association is driven to a limit of connecting spherical interaction sites to chains, are based on the Thermodynamic Perturbation Theory of Wertheim [10, 11, 12, 13]. For details about the theory, we refer to a recent review [14].

At thermodynamic equilibrium, Ω is minimal with respect to the internal degrees of freedom and thus the functional derivatives with respect to all segment-density profiles $\rho_{is}(\mathbf{r})$ vanish

$$\frac{\delta\Omega[\{\rho_{ks}\}]}{\delta\rho_{is}(\mathbf{r})} = 0, \quad \forall\, is = 1, ..., NS \tag{5.8}$$

Eq. 5.8 can be rewritten to arrive at the working equations that are solved iteratively to obtain the equilibrium density profiles $\rho_{is}(\mathbf{r})$ [20]

$$\rho_{is}(\mathbf{r}) = \exp\left(\beta\mu_i\right) \exp\left(D_{is}(\mathbf{r})\right) I_1^{(is)}(\mathbf{r}) I_2^{(is)}(\mathbf{r}) \tag{5.9}$$

where μ_i denotes the equilibrium chemical potential of chain molecule i to which segment (is) is a member, and $\beta = 1/kT$ is the inverse temperature. For every chain molecule i, the integrals $I_1^{(is)}(\mathbf{r})$ and $I_2^{(is)}(\mathbf{r})$ ($is = 1, ..., NS_i$) are calculated as [20]

$$I_1^{(1)}(\mathbf{r}) = 1 \tag{5.10}$$

$$I_1^{(is)}(\mathbf{r}) = \int I_1^{(is-1)}(\mathbf{r'})\exp\left(D_{is-1}(\mathbf{r'})\right)\Delta_{is-1,is}(\mathbf{r'},\mathbf{r})\mathrm{d}\mathbf{r'} \tag{5.11}$$

$$I_2^{(NS_i)}(\mathbf{r}) = 1 \tag{5.12}$$

$$I_2^{(is)}(\mathbf{r}) = \int I_2^{(is+1)}(\mathbf{r'})\exp\left(D_{is+1}(\mathbf{r'})\right)\Delta_{is,is+1}(\mathbf{r'},\mathbf{r})\mathrm{d}\mathbf{r'} \tag{5.13}$$

where [20]

$$D_{is}(\mathbf{r}) = \frac{1}{2}\sum_{js=1}^{NS}\sum_{js'}^{\{js'\}}\int \rho_{js}(\mathbf{r'})\frac{\delta \ln y_{js,js'}^{contact}\left[\{\bar{\rho}_{is}(\mathbf{r'})\},(\mathbf{r},\mathbf{r'})\right]}{\delta\rho_{is}(\mathbf{r})}\mathrm{d}\mathbf{r'} - \frac{\delta\beta A^{HS}}{\delta\rho_{is}(\mathbf{r})} - \frac{\delta\beta A^{Disp}}{\delta\rho_{is}(\mathbf{r})} - \frac{\delta\beta A^{Assoc}}{\delta\rho_{is}(\mathbf{r})} - \frac{\delta\beta A^{Dipole}}{\delta\rho_{is}(\mathbf{r})} \tag{5.14}$$

The second sum in eq. 5.14 runs over all neighbouring segments $\{js'\}$ of segment js. Only linear chain molecules are considered in this study. Thus, end segments have only one neighbouring segment and middle segments have two. Necessary modifications for branched chains or ring molecules are presented in [20] and [49]. The averaged density $\bar{\rho}_{is}(\mathbf{r})$ is defined as [20]

$$\bar{\rho}_{is}(\mathbf{r}) = \frac{3}{4\pi d_{is}^3}\int \rho_{is}(\mathbf{r'})\Theta\left(d_{is} - |\mathbf{r}-\mathbf{r'}|\right)\mathrm{d}\mathbf{r'} \tag{5.15}$$

with the temperature dependent effective segment diameter

$$d_{is} = \sigma_{is}\left(1 - 0.12\exp(-3\epsilon_{is}/kT)\right) \tag{5.16}$$

Here, σ_{is} and ϵ_{is} denote the constant segment diameter parameter and dispersive energy parameter for the group type of segment (is). Analogously, in the following equations we use index (is) for the segment number, m_{is}, as well as to the parameters for association, $\kappa_{is,js}$ and $\epsilon_{Ais,Bjs}$ of groups or pairs of groups.

The cavity correlation function of the inhomogeneous hard-sphere reference fluid at contact distance $y_{is,is'}^{contact}\left[\{\bar{\rho}_{ks}(\mathbf{r'})\},(\mathbf{r},\mathbf{r'})\right]$ is approximated by the corresponding values of the cavity correlation function of the homogeneous fluid at $\mathbf{r}$ and $\mathbf{r'}$ evaluated at the averaged densities $\bar{\rho}_{is}$ calculated from eq. 5.15 [20], as

$$y_{is,is'}^{contact}\left[\{\bar{\rho}_{ks}(\mathbf{r'})\},(\mathbf{r},\mathbf{r'})\right] = \left(y_{is,is'}^{contact}[\{\bar{\rho}_{ks}(\mathbf{r})\}]\cdot y_{is,is'}^{contact}[\{\bar{\rho}_{ks}(\mathbf{r'})\}]\right)^{0.5} \tag{5.17}$$

where $y_{is,is'}^{contact}[\{\bar{\rho}_{ks}(\mathbf{r})\}]$ is calculated [17], as

$$y_{is,is'}^{contact}[\{\bar{\rho}_{ks}(\mathbf{r})\}] = \frac{1}{1-\bar{\xi}_3} + 3\frac{d_{is}d_{is'}}{d_{is}+d_{is'}}\frac{\bar{\xi}_2}{\left(1-\bar{\xi}_3\right)^2} + 2\left(\frac{d_{is}d_{is'}}{d_{is}+d_{is'}}\right)^2\frac{\bar{\xi}_2^2}{\left(1-\bar{\xi}_3\right)^3} \tag{5.18}$$

The moments of density are given by

$$\bar{\xi}_n = \frac{\pi}{6}\sum_{js=1}^{NS} m_{js}\bar{\rho}_{js}(\mathbf{r})d_{js}^n \tag{5.19}$$

and furthermore

$$\Delta_{is,is'}(\mathbf{r'},\mathbf{r}) = \frac{\delta\left(|\mathbf{r'}-\mathbf{r}|-d_{is,is'}\right)}{4\pi(d_{is,is'})^2} y_{is,is'}^{contact}\left[\{\bar{\rho}_{ks}(\mathbf{r'})\},(\mathbf{r},\mathbf{r'})\right] \tag{5.20}$$

where $d_{is,is'} = 0.5(d_{is}+d_{is'})$ and where δ denotes the Dirac delta function.
Minor modifications to the original equations presented in [20] are made in this work to achieve consistency with GC-PCP-SAFT: the average densities $\bar{\rho}_{is}(\mathbf{r})$ are scaled by the segment number m_{is} in the calculation of the density moments, eq. 5.19. Furthermore, the temperature dependent segment diameter d_{is} instead of the constant segment diameter parameter σ_{is} is used in equations 5.15, 5.18, 5.19 and 5.20.
The contribution of hard-sphere interactions, $A^{HS}[\{\rho_{ks}\}]$, is calculated using the Fundamental Measure Theory of Rosenfeld [50] in the modified form of Roth et al. [51] and Yu and Wu [52]

$$\beta A^{HS}[\{\rho_{ks}\}] = \int \Phi(n_\alpha(\mathbf{r}))\mathrm{d}\mathbf{r} \tag{5.21}$$

with the reduced Helmholtz energy density for a hard-sphere fluid given by

$$\Phi(n_\alpha(\mathbf{r})) = -n_0\ln(1-n_3) + \frac{n_1n_2-\mathbf{n}_{v1}\mathbf{n}_{v2}}{1-n_3} + \left(n_2^3-3n_2\mathbf{n}_{v2}\mathbf{n}_{v2}\right)\frac{n_3+(1-n_3)^2\ln(1-n_3)}{36\pi n_3^2(1-n_3)^2} \tag{5.22}$$

and n_α denote the weighted densities obtained as

$$n_\alpha(\mathbf{r}) = \sum_{is=1}^{NS} m_{is}\int \rho_{is}(\mathbf{r\text{-}r'})\omega_{\alpha,is}(\mathbf{r'})\mathrm{d}\mathbf{r'} \tag{5.23}$$

where $\omega_{\alpha,is}(\mathbf{r})$ are the weight functions of Fundamental Measure Theory and the multiplication by m_{is} is introduced for consistency with GC-PCP-SAFT. The final form of eq. 5.23 as well as the functional derivatives of A^{HS} for a planar system where density varies only in z-direction normal to the interface are presented in a previous work of our group [41]. Whereby component-specific values, e.g. ρ_i and m_i, need to be replaced by the corresponding segment-specific values ρ_{is} and m_{is}.

Dispersive contributions and dipolar interactions are treated in a weighted-density approximation analogous to the functional presented by Sauer and Gross [41]

$$A^{Disp}[\{\rho_{ks}\}]/kT = \int \hat{\rho}(\mathbf{r}) \frac{A^{Disp}(\hat{\rho}(\mathbf{r}))}{NkT} \mathrm{d}\mathbf{r} \tag{5.24}$$

$$A^{Dipole}[\{\rho_{k}\}]/kT = \int \hat{\rho}(\mathbf{r}) \frac{A^{Dipole}(\hat{\rho}(\mathbf{r}))}{NkT} \mathrm{d}\mathbf{r} \tag{5.25}$$

where $\frac{A^{Disp}(\hat{\rho}(\mathbf{r}))}{NkT}$ and $\frac{A^{Dipole}(\hat{\rho}(\mathbf{r}))}{NkT}$ correspond to the dispersive and dipolar Helmholtz energy contributions of GC-PCP-SAFT, respectively, evaluated at a weighted density [41]

$$\hat{\rho}(\mathbf{r}) = \sum_{is=1}^{NS} \frac{3}{4\pi\psi^3 d_{is}^3} \int \rho_{is}(\mathbf{r'}) \Theta\left(\psi d_{is} - |\mathbf{r} - \mathbf{r'}|\right) \mathrm{d}\mathbf{r'} \tag{5.26}$$

with the Heaviside step function Θ. The universal model parameter ψ is readjusted for the GC-DFT approach to experimental pure-component surface tension data of n-alkanes from methane to eicosane. The optimal value is $\psi = 1.5357$. The one-dimensional form of eq. 5.26 as well as the functional derivatives $\frac{\delta A^{Disp}[\{\rho_{ks}\}]/kT}{\delta \rho_{is}(\mathbf{r})}$ are presented in ref. [41]

Alternative ways to include dispersive interactions in the DFT framework exist. Gloor et al. [22, 23, 24] proposed an approach based on perturbation theory. This approach was applied e.g. by Gross [39] and Klink and Gross [40] with a local correction term to achieve consistency with PCP-SAFT to accurately predict surface tension for a variety of pure components and mixtures. However, this approach requires the numerical integration of the dispersive perturbation potential and an approximation of the pair correlation function for the inhomogeneous repulsive reference fluid up to a predefined cut-off radius. Neglecting correlations in the fluid structure and assuming a pair correlation function of unity simplifies the calculation but also leads to increased deviations of the predicted surface tension results to experimental values [39]. As shown by Sauer and Gross [41], accuracy of the here employed weighted density approach is comparable to the more rigorous approach applied in [39] and [40] at significantly lower complexity and computation time.

The dipole term of the heterosegmented GC-PCP-SAFT equation of state [43] is different to other Helmholtz energy contributions, because a homosegmented approach is used: the dipolar contribution is averaged over the complete chain molecule instead of being attributed only to that segment carrying the dipole moment. The implication for this study is that functional derivatives of the dipolar contribution are first evaluated with respect to the chain densities ρ_i and the values for the single segments are obtained by applying the chain rule

$$\frac{\delta A^{Dipole}[\{\rho_k\}]/kT}{\delta\rho_{is}(\mathbf{r})} = \frac{\delta A^{Dipole}[\{\rho_k\}]/kT}{\delta\rho_i(\mathbf{r})}\frac{\partial\rho_i(\mathbf{r})}{\partial\rho_{is}(\mathbf{r})} \tag{5.27}$$

From $\rho_i(\mathbf{r}) = \frac{1}{NS_i}\sum_{is=1}^{NS_i}\rho_{is}(\mathbf{r})$, it follows that $\frac{\partial\rho_i(\mathbf{r})}{\partial\rho_{is}(\mathbf{r})} = \frac{1}{NS_i}$, i.e. the value of $\frac{\delta A^{Dipole}[\{\rho_k\}]/kT}{\delta\rho_{is}(\mathbf{r})}$ is the same for all segments (is) on a given chain molecule i, regardless whether segment (is) carries a dipole moment or not. The functional derivatives $\frac{\delta A^{Dipole}[\{\rho_k\}]/kT}{\delta\rho_i(\mathbf{r})}$ are obtained as shown in [41]. Smearing the dipole moment out across a molecule is undesired, because the local character of polar headgroups of molecules, for example, can then not adequately be resolved. It is an aspect that deserves further consideration in future work.

To account for associative interactions, we apply the functional of Bymaster and Chapman [53] which is a modification of the work of Segura et al. [16]

$$\beta A^{Assoc}[\{\rho_{ks}\}] = \int\sum_{is=1}^{NS}\rho_{is}(\mathbf{r})\sum_{A\in\Gamma^{is}}\left(\ln(\chi_A^{is}(\mathbf{r})) - \chi_A^{is}(\mathbf{r})/2 + \frac{1}{2}\right)\mathrm{d}\mathbf{r} \tag{5.28}$$

In eq. 5.28, Γ^{is} represents the set of all association sites on segment (is) and χ_A^{is} denotes the fraction of segments (is) not bonded at their association site A, as introduced in the theory of Wertheim [10, 11, 12, 13, 14]. For a planar interface, χ_A^{is} can be obtained by iteratively solving

$$\chi_A^{is}(z) = \left(1 + \frac{1}{2}\sum_{js=1}^{NS}\kappa_{is,js}\sigma_{is,js}^2\int_{z-\sigma_{is,js}}^{z+\sigma_{is,js}}\rho_{js}(z')\sum_{B\in\Gamma^{js}}\chi_B^{js}(z')\left\{y_{is,js}^{contact}(z,z')\left[\exp(\beta\epsilon_{Ais,Bjs}) - 1\right]\right\}\mathrm{d}z'\right)^{-1} \tag{5.29}$$

where $\sigma_{is,js} = 0.5(\sigma_{is}+\sigma_{js})$, $\epsilon_{Ais,Bjs} = 0.5(\epsilon_{Ais,Ais}+\epsilon_{Bjs,Bjs})$, $\kappa_{is,js} = \sqrt{\kappa_{is,is}\kappa_{js,js}}\sqrt{(\sigma_{is}\sigma_{js})^3}/\sigma_{is,js}^3$ and $y_{is,js}^{contact}(z,z')$ given by eq. 5.17. We note a certain degree of skepticism about employing combining rules for associating interactions, because cross-wise hydrogen-bonds can not generally be expected to scale with hydrogen-bonding interactions of pure substances. In practice, however, combining rules often work surprisingly well [36, 54, 55].

Eq. 5.29 differs slightly from the published form in ref. [53] to account for the fact that the association volume κ is an adjustable parameter in the GC-PCP-SAFT equation of state while in ref. [53] it is treated as a geometric constant defined through the accessibility of associating interaction. The functional derivatives of A^{Assoc} with respect to the segment densities $\rho_{is}(\mathbf{r})$ for a planar interface can be found in the original publication of Bymaster and Chapman [53].

5.3 Numerical settings

In all calculations, the size of the planar, one-dimensional computation domain is set to 160 Å and 1000 equidistant grid points. The system of coupled non-linear equations given by eq. 5.9 is solved by a matrix-free Newton method with numerically approximated directional derivatives, see ref. [56] [Chapter 3] for more details. The linear system for the solution update at every Newton iteration is solved using the *Generalized minimal residual algorithm for solving non-symmetric linear systems* (GMRES) [57] in the implementation of Frayssé et al. [58]. To control the solution update, a standard three point parabola line search method [59] is applied. However, for strongly associating systems as well as for very long molecules (e.g. hexacontane) it was found advantageous to instead apply a simple damping strategy for the solution update using a constant damping factor of 0.2 and reducing the number of GMRES iterations (the default number of GMRES iterations for other systems is set to 15). All numerical integrations are carried out using cubic-spline interpolations.

The initial density profiles for the single segments are set according to [39]

$$\rho_{is}^{0}(z) = \frac{1}{2}\left(\rho_i^{l,bulk} - \rho_i^{v,bulk}\right)\tanh\left(\frac{z}{\sigma_{is}}\left(2.4728 - 2.3625\frac{T}{T_c^{calc}}\right)\right) + \frac{1}{2}\left(\rho_i^{l,bulk} + \rho_i^{v,bulk}\right) \tag{5.30}$$

where i denotes the chain molecule that segment (is) is located on and T_c^{calc} is the calculated critical temperature of the system.

5.4 Results and discussion

As the main results, we compare predicted surface tensions γ obtained from the GC-DFT approach to experimental data. Results for systems of non-polar, non-associating compounds are presented first, results for polar molecules and hydrogen-bonding species follow thereafter.

Before presenting results for predicted surface tensions using the proposed group-contribution DFT approach, we first evaluate the influence of the parameter ϕ_i on vapor pressure and density. In the following sections, if not stated differently, reported deviations for the single compounds or mixtures are averages over deviations for all available experimental data points, N_{exp}, and are either given as relative deviations in percent $\left(\frac{1}{N_{\text{exp}}}\sum_i^{N_{\text{exp}}} |\theta_i^{\text{exp}} - \theta_i^{\text{model}}|/\theta_i^{\text{exp}} \cdot 100\right)$ or as absolute values $\left(\frac{1}{N_{\text{exp}}}\sum_i^{N_{\text{exp}}} |\theta_i^{\text{exp}} - \theta_i^{\text{model}}|\right)$ where θ denotes the considered physical property.

5.4.1 Influence of ϕ_i on vapor pressure and density

A comparison of vapor pressure results before and after the adjustment of ϕ_i to experimental vapor pressure data is shown in fig. 5.4. A significant improvement is achieved for all chemical families by the adjusting ϕ_i-values. The improvement of individualizing the group-contribution approach is particularly pronounced for polar or hydrogen-bonding chemical families. For aldehydes, the very high initial deviation ($\phi_i = 1$) is predominantly caused by one compound, 2-butenal, with high errors in vapor pressure as seen fig. 5.1. The drastic improvement for esters has to be partly attributed to the fact that for many ester compounds only one experimental data point was available to adjust ϕ_i and deviations for these compounds thus reduced to 0%.

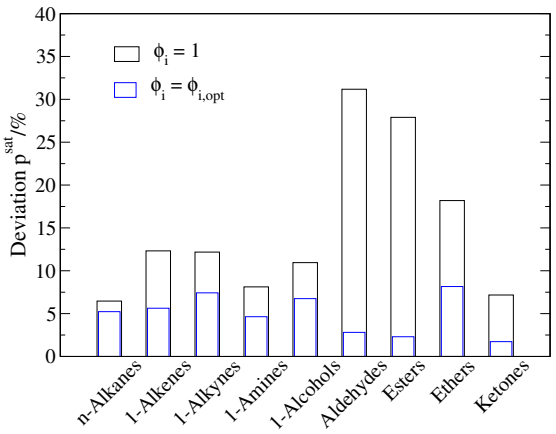

Figure 5.4: Deviations of calculated vapor pressures p^{sat} from quasi-experimental data for several chemical families. Original GC-PCP-SAFT results, corresponding to $\phi_i = 1$, (black) and individualized GC-PCP-SAFT results, with ϕ_i adjusted to experimental vapor pressure data (blue). The considered compounds and their ϕ_i values are presented in the Supporting Information.

The implications of ϕ_i on liquid saturated densities is only mild. Even for substances like methanol and methylamine, where ϕ_i deviates notably from unity and deviations of vapor pressure reduce significantly (from 30% to 8% and from 26% to 4%, respectively), the improvement in the description of saturated liquid densities is below 3%.

The following section discusses the influence of parameter ϕ_i and also the impact of the binary interaction parameter $k_{\alpha\beta}$ on predicted values of surface tensions for several mixtures. A detailed comparison of all results for surface tensions obtained with and without these additional parameters is presented in the Supporting Information.

5.4.2 Non-polar, non-associating substances: pure components and mixtures

Results for pure n-alkanes, 1-alkenes and 1-alkynes are presented in figs. 5.5 and 5.6. The general agreement of the GC-DFT predictions with experiments is very good. Deviations of predicted surface tensions from experimental values tend to increase for long molecules such as eicosane, hexacontane or 1-eicosene. In the case of hexacontane, no experimental vapor pressure data is available to regress pure-component equation of state parameters. One has to apply group-contribution methods or rely on correlations for these parameters. For PCP-SAFT, such correlations are available e.g. for n-alkanes and polyethylene [35]. Furthermore, correlations for the influence parameter of n-alkanes as a function of carbon atoms [60] or molecular mass [61] [Chapter 2] exist for DGT using PCP-SAFT as the local model. Surface tension results for hexacontane can then be used to compare GC-DFT predictions to results of an alternative approach applicable to polymeric molecules with scarce experimental data: DGT with pure-component PCP-SAFT parameters calculated from the correlations given in ref. [35] and influence parameters extrapolated using the correlations presented in refs. [60] and [61] [Chapter 2]. This comparison shows a clear superiority of GC-DFT: deviations take on values of 1.92 mN/m for the presented GC-DFT approach but 3.73 mN/m and 3.56 mN/m for DGT with the correlations for the influence parameter of [60] and [61] [Chapter 2], respectively.

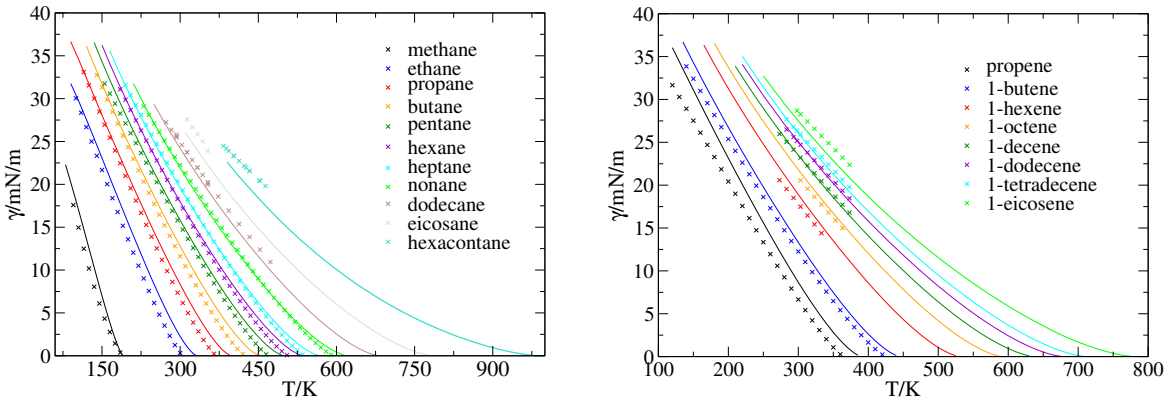

(a) (b)

Figure 5.5: Surface tension of n-alkanes (a) and 1-alkenes (b). Comparison of predicted values (lines) to (quasi)-experimental data [62] [63] [64] [65] [66] (symbols).

Figures 5.7 and 5.8 exemplify that very good results can also be obtained for mixtures of simple molecules. Values for different binary methane-n-alkane mixtures are in very good agreement with experiments over a wide pressure range. Surface tension deviations for two ternary n-alkane mixtures depicted in fig. 5.8 confirm the accurate results for medium-sized molecules and the trend of growing errors for increasing numbers of segments: deviations for a mixture of hexane, octane and tetradecane are on the order of 2%. This value

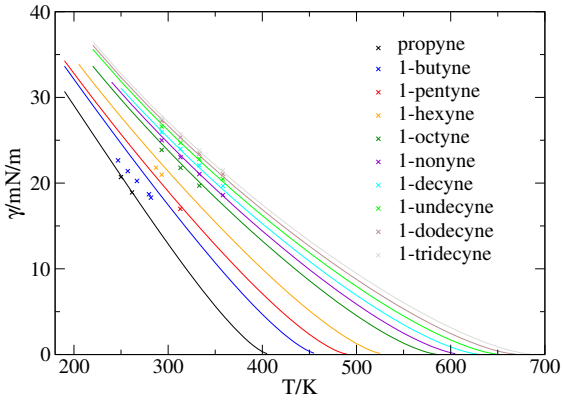

Figure 5.6: Surface tension of 1-alkynes. Comparison of predicted values (lines) to experimental data [65] [67] [68] [69] [70] (symbols).

increases to up to 7% for a mixture including longer alkane molecules (decane, eicosane and tetracosane). Furthermore, for both mixtures, a moderate increase of deviations with increasing temperature can be observed. As expected from the marginal implications on VLE results (see Supporting Information), the influence of the group-group interaction parameters k_{CH_4,CH_3}, k_{CH_4,CH_2} and k_{CH_3,CH_2} on surface tension results is neglectable for the mixtures shown in figs. 5.7 and 5.8.

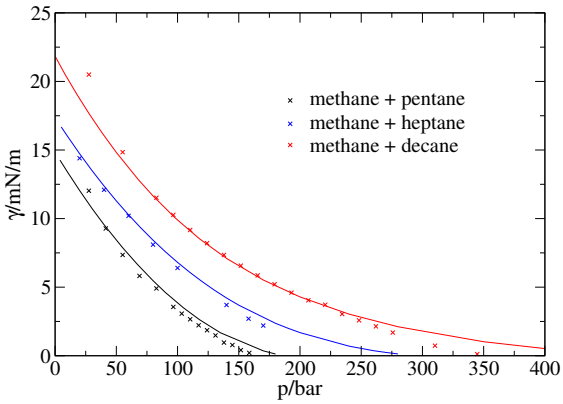

Figure 5.7: Surface tension of the binary mixtures methane + pentane ($T = 310.928$ K), methane + heptane ($T = 323.0$ K) and methane + decane ($T = 310.928$ K). Comparison of predicted of surface tensions (lines) to experimental data [71] (symbols).

5.4.3 Polar substances: pure components and mixtures

In this section, results for esters, ethers, aldehydes and ketones are presented. Deviations of predicted surface tensions from experimental data for ester molecules are shown in table 5.2. The overall agreement is remarkable with average deviations across all considered substances of 3.7% and a maximum error of any of the listed compounds at any given state point of 11%. For the methyl and ethyl esters of 2-butenoic acid as well as for 3-butenoic methyl ester, the adjustment of ϕ_i to experimental vapor pressure data leads

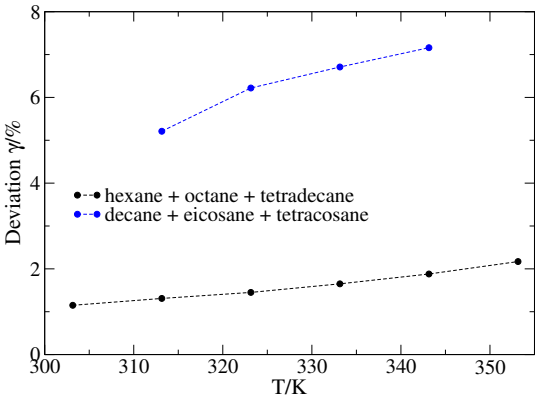

Figure 5.8: Deviations of predicted surface tensions from experimental data [72, 73] for various temperatures of two ternary n-alkane mixtures. Deviations are averages of results for different liquid phase compositions at a given temperature.

to a significant improvement of surface tension results, see Supporting Information. For the remaining ester molecules, for which experimental data is available to adjust ϕ_i, the influence on surface tension is marginal. Furthermore, surface tension values for many compounds, for which no adjustment of ϕ_i is possible, are already in very good agreement with experiments for $\phi_i = 1$, e.g. the propyl, butyl and pentyl esters of 3-butenoic acid or 4-pentynoic acid ethyl ester. Table 5.2 allows a comparison between results for butanoic acid and butenoic acid and also between pentanoic acid and pentynoic acid. It can thereby be observed that deviations increase with an increasing number of different functional groups on a molecule. That is not surprising because, first, multi-functional molecules were not considered in the adjustment of the group parameters of the equation of state, and second, the specifics of intramolecular interactions between functional groups are not explicitly accounted for in the group-contribution method.

Table 5.2: Deviations of predicted surface tensions for ester compounds from experimental data [74, 75, 76, 77, 78].

Compound	dev./%	Compound	dev./%
butanoic acid methyl ester	1.82	2-butenoic acid pentyl ester	6.98
butanoic acid ethyl ester	2.43	3-butenoic acid methyl ester	1.03
butanoic acid propyl ester	1.74	3-butenoic acid ethyl ester	3.48
butanoic acid butyl ester	1.01	3-butenoic acid propyl ester	3.63
pentanoic acid methyl ester	2.84	3-butenoic acid butyl ester	3.26
2-butenoic acid methyl ester	2.89	3-butenoic acid pentyl ester	3.05
2-butenoic acid ethyl ester	3.37	4-pentynoic acid methyl ester	8.70
2-butenoic acid propyl ester	8.37	4-pentynoic acid ethyl ester	1.59
2-butenoic acid butyl ester	7.25		

In addition to the ester compounds shown in table 5.2, results for several fatty acid methyl esters are presented in table 5.3, using the common notation of $\{$*number of carbon atoms*$\}$:

{*number of double-bonds*}. These molecules are important constituents of biodiesel fuels and knowledge of their surface tension is essential for modelling the atomization and subsequent combustion process in the diesel engine. Due to lack of experimental data for vapor pressures for many of these compounds, a value of $\phi_i = 1$ is used in all cases. Predicted values for surface tension γ are in very good agreement with experiments, with errors ranging from 1.7% for the shortest compound to 4.7% for the longest molecule. Results for binary and ternary mixtures of fatty acid ethyl esters can also be predicted with high accuracy: errors stay well below 2%, see table 5.4. The use of group-group interaction parameters $k_{\alpha\beta}$ has a minor but decreasing influence on errors of surface tension for these mixtures.

For fatty acid methyl and ethyl ester systems, the strength of the group-contribution DFT approach becomes apparent: obtaining surface tension results for these systems using alternative methods such as density gradient theory would only be possible with considerable additional effort, including the establishment of a group-contribution prescription to calculate the influence parameter, or, in case a non-group-contribution approach is preferred, developing correlations for the pure-component equation of state parameters and influence parameters for the different ester types.

Table 5.3: Surface tensions γ of pure organic acid methyl esters at $T = 313.15$ K. Predicted values γ and deviations from experimental data [79].

Compound	γ/mN/m	dev./%
8:0 ME	24.98	1.7
10:0 ME	25.78	2.0
12:0 ME	26.40	2.9
14:0 ME	26.90	3.6
16:0 ME	27.30	3.9
18:0 ME	27.64	4.7

Table 5.4: Surface tensions γ of four binary and ternary mixtures of fatty acid ethyl esters at $T = 298.15$ K. Predicted values γ and deviations from experimental results [79]. The mixture composition w is given in mass fractions. No value for pressure was reported [79]. We assume the feed-composition to be the liquid composition, i.e. we assume the experimentally observed amount of vapor as being small compared with the amount of liquid.

	$w_{8:0\ \mathrm{EE}}$	$w_{10:0\ \mathrm{EE}}$	$w_{12:0\ \mathrm{EE}}$	γ/mN/m	dev./%
1	0.48	0.52	-	26.895	1.49
2	0.46	-	0.54	27.198	0.73
3	-	0.75	0.25	27.495	0.38
4	0.33	0.33	0.34	27.100	0.73

Results for ketones, aldehydes and ethers are presented in table 5.5. For most studied

Table 5.5: Ketones, aldehydes and ethers: deviations of predicted surface tensions from experimental data [80, 81, 75, 82, 83, 84, 85, 86, 87, 88, 89, 90, 91].

Compound	dev./%	Compound	dev./%	Compound	dev./%
Ketones		Aldehydes		dioctyl ether	4.28
2-butanone	4.86	2-butenal	13.63	methyl butyl ether	4.05
2-hexanone	2.13	butanal	12.32	methyl hexyl ether	5.68
2-octanone	1.75	pentanal	11.65	ethyl butyl ether	1.73
3-pentanone	1.52	hexanal	9.79	ethyl hexyl ether	3.29
3-heptanone	0.85	heptanal	6.40	ethyl hexadecal ether	5.96
3-nonanone	1.96	dodecanal	13.41		
4-heptanone	1.20	Ethers			
4-nonanone	0.69	diethyl ether	5.19		
6-undecanone	0.60	dibutyl ether	1.98		
3-heptene-2-on	6.73	dihexyl ether	1.12		

ketones, predictions of the model are in excellent agreement with experimental data showing deviations of less than 2%. Results of 3-heptanone and 3-heptene-2-on reconfirm the observation of growing deviations with increasing number of group types per molecule. Aldehydes exhibit larger deviations, in order of 10%, than the other polar families. Finally, surface tension for ether compounds can be predicted accurately with deviations usually below 5%.

Figure 5.9 exemplifies results for two binary n-alkane-ester mixtures. The surface tension is predicted accurately for the mixture heptane and ethanoic acid pentyl ester over the complete concentration range, considering that no parameters are adjusted, neither component-specific pure component parameters nor binary parameters. For pentane and ethanoic acid methyl ester, very small deviations are observed for the pentane rich side but results are underpredicted moderately elsewhere.

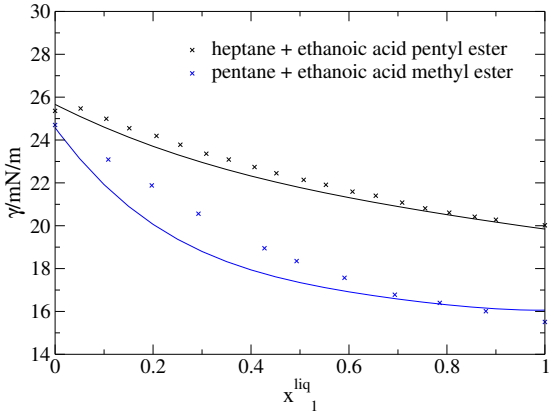

Figure 5.9: Surface tension of the binary mixtures heptane (1) + ethanoic acid pentyl ester (2) and pentane (1) + ethanoic acid methyl ester (2) at $T = 298.15$ K. Comparison of predicted values (lines) to experimental data [92] [93] (symbols).

5.4.4 Associating substances: pure components and mixtures

1-Alcohols and 1-amines are considered as hydrogen-bonding compounds in this study. As a general finding, surface tensions of short associating molecules are overestimated significantly. With increasing chain length decreases the impact of the hydrogen-bonding group on the components' properties and predicted surface tensions become more accurate. This is shown in figs. 5.10 and 5.11 where results of ethanol and 1-decanol as well as ethylamine and 1-hexylamine are displayed.

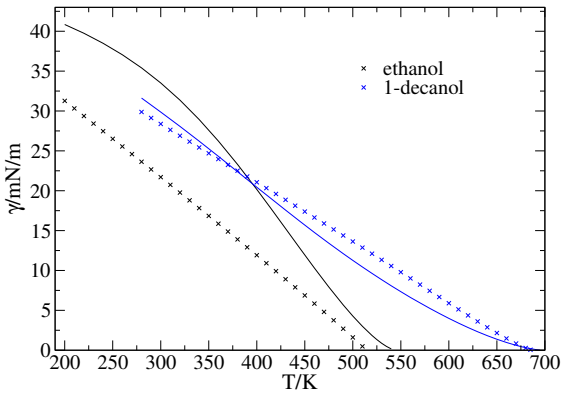

Figure 5.10: Surface tension of ethanol and 1-decanol. Comparison of predicted values (lines) to (quasi)-experimental data [94] [64] (symbols).

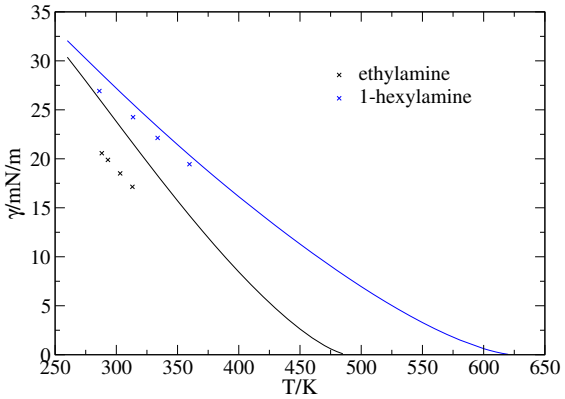

Figure 5.11: Surface tension of ethylamine and 1-hexylamine. Comparison of predicted values (lines) to experimental data [65] [95] (symbols).

Deviations of predicted surface tensions from experimental data for pure 1-alcohols from methanol to 1-decanol are depicted in fig. 5.12. Results obtained from a non-group-contribution DFT consistent with PCP-SAFT and from density gradient theory correlations using PCP-SAFT as the model for the local Helmholtz energy published in a previous study [42] [Chapter 4] are also included. It is apparent that the group-contribution DFT approach leads to high deviations for methanol and ethanol. The properties of the smallest molecules of a chemical family are usually represented insufficiently by group-

contribution methods. From 1-propanol on, the proposed GC-DFT outperforms the non-group-contribution DFT and for molecules longer than 1-hexanol, surface tension predictions reach the same level of accuracy as DGT correlations (where for every substance, a parameter is optimized to the here considered experimental data).

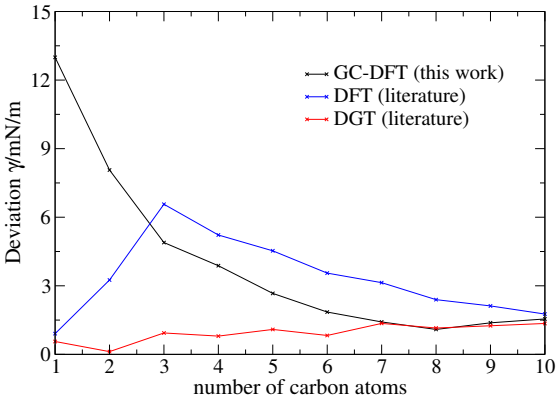

Figure 5.12: Results for pure 1-alcohols from methanol to 1-decanol from a reduced temperature of $T_r = T/T_c \approx 0.4$ to the critical temperature T_c: deviations of surface tensions γ as predicted from the proposed group-contribution DFT (black) from experimental data. Results from a non-group-contribution DFT (blue) and correlation results from a density gradient theory with adjustable parameters (red) are also included for comparison (both, earlier reported in ref. [42] [Chapter 4]).

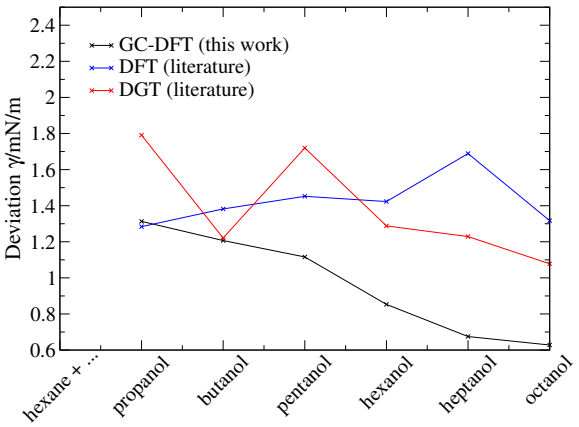

Figure 5.13: Results for binary mixtures of hexane with different 1-alcohol compounds at $T = 298.15$ K: deviations of surface tensions γ as predicted from the proposed group-contribution DFT (black) from experimental data of Jiménez et al. [96]. Results from a non-group-contribution DFT (blue) and correlation results from a density gradient theory with adjustable parameters (red) are also included for comparison (both, earlier reported in ref. [42] [Chapter 4]).

For binary 1-alcohol-n-alkane mixtures, where the 1-alcohols of medium size (1-propanol) to rather long (1-octanol) are considered, the GC-DFT approach predicts the surface tension in very good agreement to experimental data, as fig. 5.13 confirms. Deviations of the GC-DFT model are notably smaller than for the non-group-contribution DFT or DGT

approaches. In comparison to the non-group-contribution DFT model, that is understood because the pure alcohols are well predicted by the GC-DFT model. To illustrate two of these mixtures, fig. 5.14 shows the surface tension for the binary mixtures of hexane and 1-propanol as well as of hexane and 1-octanol. The results are rather satisfying for a predictive approach. We note, for all considered alkane-1-alcohol mixtures, the use of group-group interaction parameters k_{CH_3,CH_2}, $k_{CH_3,OH}$ and $k_{CH_2,OH}$ reduces deviations of surface tension to experiments as shown in the Supporting Information.

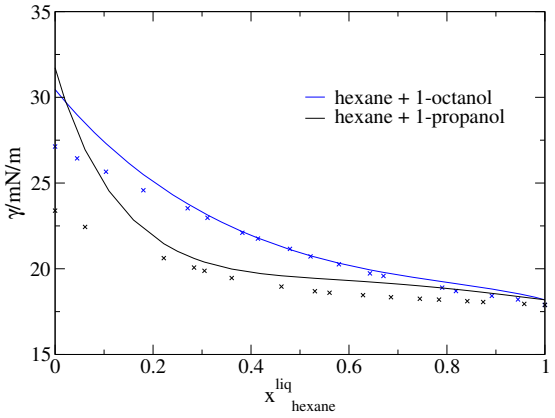

Figure 5.14: Surface tension γ of binary mixtures hexane + 1-propanol and hexane + 1-octanol at $T = 298.15$ K. Comparison of predicted values (lines) to experimental data [96] (symbols).

An interesting question is whether the group-contribution DFT approach is capable of reproducing the orientation of hydrogen-bonding molecules at the vapor-liquid interface. As shown by Stanners et al. [97] from spectroscopic measurements, 1-alcohols have a preferred orientation at the interface in order to maximize the number of hydrogen bonds: the hydroxyl group is more likely to face towards the liquid phase while the non-polar hydrocarbon tail preferentially faces towards the vapor phase. This orientation was reported to be present to a similar extent for all studied 1-alcohols from methanol to octanol [97]. In our DFT formalism orientational distribution functions are not considered. But the GC-DFT approach does resolve density profiles on a segment level and it thus offers enough detail to predict some aspects of the orientation, namely the density profile of the hydroxyl group with a peak on the liquid side of the interface. Fig. 5.15 shows the density profiles of the single segments of 1-pentanol at $T = 345$ K. A peak of the hydroxyl group density profile on the liquid side of the interface is clearly observed. Furthermore, the CH_2 segment bonded to the hydroxyl group also shows the expected accumulation while segments located on the opposite side of the chain molecule are depleted.

A quantitative comparison to orientation angles reported in [97] is not possible because these angles cannot be inferred from our DFT model. For a qualitative comparison, a simple measure for the orientation at the interface is introduced. We define the integral

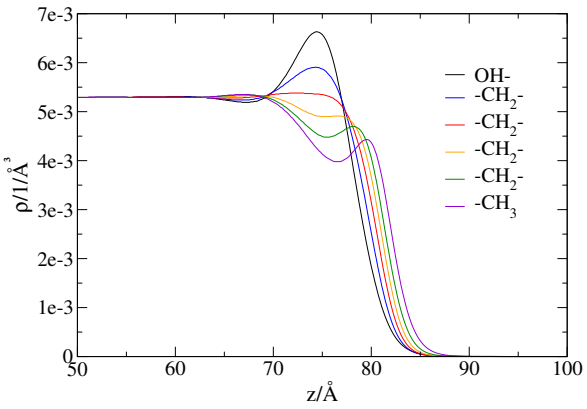

Figure 5.15: Density profiles of the single segments of 1-pentanol at $T = 345$ K. Stoichiometry for chain formation requires the number of the different segments present in the system to be equal. This is ensured for the depicted density profiles by evaluating the integrals $\int \rho_{is}(z)\mathrm{d}z$ which give the same result for all segments (0.426 Å^{-2}).

of the difference between the local densities of the two end segments, $\rho_{OH}(z)$ and $\rho_{CH_3}(z)$, of the 1-alcohol molecules

$$\delta_{OH,CH_3} = \int |\rho_{OH}(z) - \rho_{CH_3}(z)|/\rho(z)\mathrm{d}z \tag{5.31}$$

with the local density of the chain molecule $\rho(z)$. Eq. 5.31 is evaluated only on the liquid side of the interface (defined as the region where $\rho(z) > 0.95\rho^{bulk,liquid}$) where the accumulation of the hydroxyl group occurs. The integrand of eq. 5.31 takes on values $\neq 0$ only where there is a preferred orientation (accumulation) and thus the average densities of the two end segments of the alcohol molecules differ. Fig. 5.16 shows the value of δ_{OH,CH_3} as a function of reduced temperature for several 1-alcohols. Parameter δ_{OH,CH_3} shows the expected decay with increasing temperature and vanishes close to the critical temperature. We further observe a similar degree of orientation for 1-alcohol compounds of different chain lengths, in agreement to what has previously been reported by Stanners et al. [97] from spectroscopic investigations.

The ability of the proposed method to calculate density profiles at the level of chemical functional groups and the observation that the orientation of the molecules at the interface is qualitatively captured by the model also encourages the study of surfactant molecules and furthermore offers the perspective of optimizing the molecular structure of surfactants by screening the influence of different functional groups on the structure at the interface and the surface tension of the system.

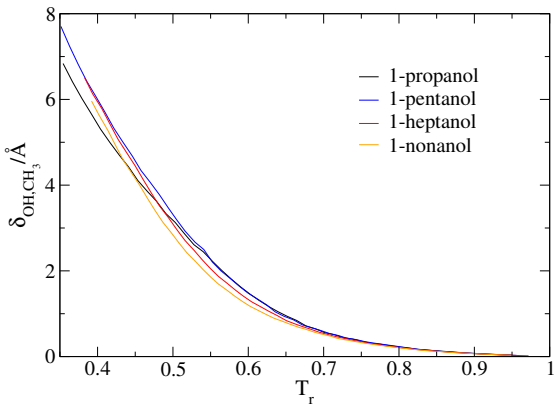

Figure 5.16: Degree of orientation at the interface for different alcohol compounds measured by the value of δ_{OH,CH_3} as a function of reduced temperature $T_r = T/T_c$.

5.5 Conclusion

In this study, a group-contribution density functional theory consistent with the heterosegmented group-contribution PCP-SAFT equation of state is developed. A component-specific parameter ϕ_i as well as transferable group-group interaction parameters $k_{\alpha\beta}$ are introduced to the dispersive contribution of GC-PCP-SAFT in order to improve results for vapor pressure especially for small and multi-functional compounds and VLE results for alkane-ester and alkane-alcohol systems, respectively. The effect of ϕ_i and $k_{\alpha\beta}$ on surface tension are small in general. Predictions of the surface tension for non-polar, non-associating compounds as well as for polar, non-associating species are in very good agreement with experiments, both, for pure component systems as well as for mixtures. The advantages of the group-contribution DFT are demonstrated for very long alkane compounds and biodiesel systems where alternative methods such as density gradient theory have to rely on correlations (if available) for the pure-component equation of state parameters and the influence parameter. Small hydrogen-bonding compounds pose a challenge to the proposed GC-DFT approach. However, except for methanol and ethanol, better results for surface tension of 1-alcohols were obtained with the group-contribution DFT than with a non-group-contribution DFT and with increasing chain length, deviations for 1-alcohols decrease to the same level as for DGT correlations (where component-specific parameters were adjusted). Furthermore, deviations for binary hexane-alcohol mixtures are significantly smaller than for the non-group-contribution DFT or DGT.
The presented method calculates density profiles on a segment level which allows a detailed description of the interface and it is shown that the GC-DFT method can qualitatively capture the orientation of hydrogen-bonding compounds at the vapor-liquid interface. These features suggest a study of surfactant molecules or even the use of GC-DFT to design surfactant molecules with desired properties.

Bibliography

[1] D. Macleod, "On a relation between surface tension and density," *Transactions of the Faraday Society*, vol. 19, no. July, pp. 38–41, 1923.

[2] S. Sugden, "CXLII.—a relation between surface tension, density, and chemical composition," *Journal of the Chemical Society, Transactions*, vol. 125, pp. 1177–1189, 1924.

[3] E. A. Guggenheim, "The principle of corresponding states," *The Journal of Chemical Physics*, vol. 13, no. 7, pp. 253–261, 1945.

[4] A. Queimada, L. Rolo, A. Caço, I. Marrucho, E. H. Stenby, and J. Coutinho, "Prediction of viscosities and surface tensions of fuels using a new corresponding states model," *Fuel*, vol. 85, no. 5, pp. 874–877, 2006.

[5] L. Girifalco and R. Good, "A theory for the estimation of surface and interfacial energies. I. derivation and application to interfacial tension," *The Journal of Physical Chemistry*, vol. 61, no. 7, pp. 904–909, 1957.

[6] F. M. Fowkes, "Determination of interfacial tensions, contact angles, and dispersion forces in surfaces by assuming additivity of intermolecular interactions in surfaces," *The Journal of Physical Chemistry*, vol. 66, no. 2, pp. 382–382, 1962.

[7] P. Winterfeld, L. Scriven, and H. Davis, "An approximate theory of interfacial tensions of multicomponent systems: Applications to binary liquid-vapor tensions," *AIChE Journal*, vol. 24, no. 6, pp. 1010–1014, 1978.

[8] C. Klink, C. Waibel, and J. Gross, "Analysis of interfacial transport resistivities of pure components and mixtures based on density functional theory," *Industrial & Engineering Chemistry Research*, vol. 54, no. 45, pp. 11483–11492, 2015.

[9] W. G. Chapman, G. Jackson, and K. E. Gubbins, "Phase equilibria of associating fluids: chain molecules with multiple bonding sites," *Molecular Physics*, vol. 65, no. 5, pp. 1057–1079, 1988.

[10] M. Wertheim, "Fluids with highly directional attractive forces. I. statistical thermodynamics," *Journal of statistical physics*, vol. 35, no. 1, pp. 19–34, 1984.

[11] M. Wertheim, "Fluids with highly directional attractive forces. II. thermodynamic perturbation theory and integral equations," *Journal of statistical physics*, vol. 35, no. 1-2, pp. 35–47, 1984.

[12] M. Wertheim, "Fluids with highly directional attractive forces. III. multiple attraction sites," *Journal of statistical physics*, vol. 42, no. 3, pp. 459–476, 1986.

[13] M. Wertheim, "Fluids with highly directional attractive forces. IV. equilibrium polymerization," *Journal of statistical physics*, vol. 42, no. 3, pp. 477–492, 1986.

[14] W. Zmpitas and J. Gross, "Detailed pedagogical review and analysis of wertheim's thermodynamic perturbation theory," *Fluid Phase Equilibria*, vol. 428, pp. 121–152, 2016.

[15] W. G. Chapman. PhD thesis, Cornell University, 1988.

[16] C. J. Segura, K. P. Shukla, and W. G. Chapman, "Associating fluids with four bonding sites against a hard wall: density functional theory," *Molecular Physics*, vol. 90, no. 5, pp. 759–772, 1997.

[17] S. Tripathi and W. G. Chapman, "Microstructure of inhomogeneous polyatomic mixtures from a density functional formalism for atomic mixtures," *The Journal of chemical physics*, vol. 122, no. 9, p. 094506, 2005.

[18] E. Kierlik and M. Rosinberg, "The classical fluid of associating hard rods in an external field," *Journal of statistical physics*, vol. 68, no. 5, pp. 1037–1063, 1992.

[19] E. Kierlik and M. Rosinberg, "A perturbation density-functional theory for polyatomic fluids. I. rigid molecules," *The Journal of chemical physics*, vol. 97, no. 12, pp. 9222–9239, 1992.

[20] S. Jain, A. Dominik, and W. G. Chapman, "Modified interfacial statistical associating fluid theory: A perturbation density functional theory for inhomogeneous complex fluids," *The Journal of chemical physics*, vol. 127, no. 24, p. 244904, 2007.

[21] F. J. Blas, E. M. Del Río, E. De Miguel, and G. Jackson, "An examination of the vapour-liquid interface of associating fluids using a SAFT-DFT approach," *Molecular Physics*, vol. 99, no. 22, pp. 1851–1865, 2001.

[22] G. J. Gloor, F. J. Blas, E. M. del Río, E. de Miguel, and G. Jackson, "A SAFT-DFT approach for the vapour–liquid interface of associating fluids," *Fluid phase equilibria*, vol. 194, pp. 521–530, 2002.

[23] G. J. Gloor, G. Jackson, F. J. Blas, E. M. del Río, and E. de Miguel, "An accurate density functional theory for the vapor-liquid interface of associating chain molecules based on the statistical associating fluid theory for potentials of variable range," *The Journal of chemical physics*, vol. 121, no. 24, pp. 12740–12759, 2004.

[24] G. J. Gloor, G. Jackson, F. Blas, E. M. Del Rio, and E. De Miguel, "Prediction of the vapor- liquid interfacial tension of nonassociating and associating fluids with the SAFT-VR density functional theory," *The Journal of Physical Chemistry C*, vol. 111, no. 43, pp. 15513–15522, 2007.

[25] F. Llovell, A. Galindo, F. J. Blas, and G. Jackson, "Classical density functional theory for the prediction of the surface tension and interfacial properties of fluids mixtures of chain molecules based on the statistical associating fluid theory for potentials of variable range," *The Journal of chemical physics*, vol. 133, no. 2, p. 024704, 2010.

[26] F. Llovell, N. Mac Dowell, F. J. Blas, A. Galindo, and G. Jackson, "Application of the SAFT-VR density functional theory to the prediction of the interfacial properties of mixtures of relevance to reservoir engineering," *Fluid Phase Equilibria*, vol. 336, pp. 137–150, 2012.

[27] B. J. Schindler, L. A. Mitchell, C. McCabe, P. T. Cummings, and M. D. LeVan, "Adsorption of chain molecules in slit-shaped pores: development of a SAFT-FMT-DFT approach," *The Journal of Physical Chemistry C*, vol. 117, no. 41, pp. 21337–21350, 2013.

[28] C. Malheiro, B. Mendiboure, F. Plantier, F. J. Blas, and C. Miqueu, "Density functional theory for the description of spherical non-associating monomers in confined media using the SAFT-VR equation of state and weighted density approximations," *The Journal of chemical physics*, vol. 140, no. 13, p. 134707, 2014.

[29] H. Kahl and J. Winkelmann, "Modified PT-LJ-SAFT density functional theory: I. prediction of surface properties and phase equilibria of non-associating fluids," *Fluid Phase Equilibria*, vol. 270, no. 1-2, pp. 50–61, 2008.

[30] H. T. Davis, *Statistical mechanics of phases, interfaces, and thin films*. Wiley-VCH, 1996.

[31] H. Löwen, "Density functional theory of inhomogeneous classical fluids: recent developments and new perspectives," *Journal of Physics: Condensed Matter*, vol. 14, no. 46, p. 11897, 2002.

[32] J. Wu, "Density functional theory for chemical engineering: From capillarity to soft materials," *AIChE Journal*, vol. 52, no. 3, pp. 1169–1193, 2006.

[33] C. P. Emborsky, Z. Feng, K. R. Cox, and W. G. Chapman, "Recent advances in classical density functional theory for associating and polyatomic molecules," *Fluid Phase Equilibria*, vol. 306, no. 1, pp. 15–30, 2011.

[34] J. Landers, G. Y. Gor, and A. V. Neimark, "Density functional theory methods for characterization of porous materials," *Colloids and Surfaces A: Physicochemical and Engineering Aspects*, vol. 437, pp. 3–32, 2013.

[35] J. Gross and G. Sadowski, "Perturbed-chain SAFT: An equation of state based on a perturbation theory for chain molecules," *Industrial & engineering chemistry research*, vol. 40, no. 4, pp. 1244–1260, 2001.

[36] J. Gross and G. Sadowski, "Application of the perturbed-chain SAFT equation of state to associating systems," *Industrial & engineering chemistry research*, vol. 41, no. 22, pp. 5510–5515, 2002.

[37] J. Gross and J. Vrabec, "An equation-of-state contribution for polar components: Dipolar molecules," *AIChE journal*, vol. 52, no. 3, pp. 1194–1204, 2006.

[38] J. Gross, "An equation-of-state contribution for polar components: Quadrupolar molecules," *AIChE journal*, vol. 51, no. 9, pp. 2556–2568, 2005.

[39] J. Gross, "A density functional theory for vapor-liquid interfaces using the PCP-SAFT equation of state," *The Journal of chemical physics*, vol. 131, no. 20, p. 204705, 2009.

[40] C. Klink and J. Gross, "A density functional theory for vapor–liquid interfaces of mixtures using the perturbed-chain polar statistical associating fluid theory equation of state," *Industrial & Engineering Chemistry Research*, vol. 53, no. 14, pp. 6169–6178, 2014.

[41] E. Sauer and J. Gross, "Classical density functional theory for liquid-fluid interfaces and confined systems: A new functional for the perturbed-chain polar statistical associating fluid theory equation of state," *Industrial & Engineering Chemistry Research*, vol. 56, no. 14, pp. 4119–4135, 2017.

[42] J. Mairhofer and J. Gross, "Modeling properties of the one-dimensional vapor-liquid interface: application of classical density functional and density gradient theory," *Fluid Phase Equilibria*, vol. 458, pp. 243–252, 2018.

[43] E. Sauer, M. Stavrou, and J. Gross, "Comparison between a homo-and a heterosegmented group contribution approach based on the perturbed-chain polar statistical

associating fluid theory equation of state," *Industrial & Engineering Chemistry Research*, vol. 53, no. 38, pp. 14854–14864, 2014.

[44] J. Gross, O. Spuhl, F. Tumakaka, and G. Sadowski, "Modeling copolymer systems using the perturbed-chain SAFT equation of state," *Industrial & engineering chemistry research*, vol. 42, no. 6, pp. 1266–1274, 2003.

[45] B. D. Smith and R. Srivastava, *Thermodynamic Data for Pure Compounds: Hydrocarbons and Ketones*, vol. 1. Elsevier Science Limited, 1986.

[46] Y. Van-Chin-Syan, V. Kochubei, V. Sergeev, Y. A. Raevskii, S. Gerasimchuk, and K. Z. Kotovich, "Thermodynamic properties of some acids and aldehydes of the acrylic series," *Russian journal of physical chemistry*, vol. 70, no. 11, pp. 1789–1794, 1996.

[47] L. Fernández, E. Pérez, J. Ortega, J. Canosa, and J. Wisniak, "Measurements of the excess properties and vapor- liquid equilibria at 101.32 kPa for mixtures of ethyl ethanoate + alkanes (from c5 to c10)," *Journal of Chemical & Engineering Data*, vol. 55, no. 12, pp. 5519–5533, 2010.

[48] S. Bernatová, J. Linek, and I. Wichterle, "Vapour-liquid equilibrium in the butyl alcohol-n-decane system at 85, 100 and 115°C," *Fluid phase equilibria*, vol. 74, pp. 127–132, 1992.

[49] B. D. Marshall and W. G. Chapman, "Higher order classical density functional theory for branched chains and rings," *The Journal of Physical Chemistry B*, vol. 115, no. 50, pp. 15036–15047, 2011.

[50] Y. Rosenfeld, "Free-energy model for the inhomogeneous hard-sphere fluid mixture and density-functional theory of freezing," *Physical review letters*, vol. 63, no. 9, p. 980, 1989.

[51] R. Roth, R. Evans, A. Lang, and G. Kahl, "Fundamental measure theory for hard-sphere mixtures revisited: the white bear version," *Journal of Physics: Condensed Matter*, vol. 14, no. 46, p. 12063, 2002.

[52] Y.-X. Yu and J. Wu, "Structures of hard-sphere fluids from a modified fundamental-measure theory," *The Journal of chemical physics*, vol. 117, no. 22, pp. 10156–10164, 2002.

[53] A. Bymaster and W. G. Chapman, "An iSAFT density functional theory for associating polyatomic molecules," *The Journal of Physical Chemistry B*, vol. 114, no. 38, pp. 12298–12307, 2010.

[54] Y.-H. Fu and S. I. Sandler, "A simplified SAFT equation of state for associating compounds and mixtures," *Industrial & engineering chemistry research*, vol. 34, no. 5, pp. 1897–1909, 1995.

[55] G. M. Kontogeorgis, M. L. Michelsen, G. K. Folas, S. Derawi, N. von Solms, and E. H. Stenby, "Ten years with the CPA (cubic-plus-association) equation of state. part 2. cross-associating and multicomponent systems," *Industrial & Engineering Chemistry Research*, vol. 45, no. 14, pp. 4869–4878, 2006.

[56] J. Mairhofer and J. Gross, "Numerical aspects of classical density functional theory for one-dimensional vapor-liquid interfaces," *Fluid Phase Equilibria*, vol. 444, pp. 1–12, 2017.

[57] Y. Saad and M. H. Schultz, "Gmres: A generalized minimal residual algorithm for solving nonsymmetric linear systems," *SIAM Journal on scientific and statistical computing*, vol. 7, no. 3, pp. 856–869, 1986.

[58] V. Frayssé, L. Giraud, S. Gratton, and J. Langou, "Algorithm 842: A set of gmres routines for real and complex arithmetics on high performance computers," *ACM Transactions on Mathematical Software (TOMS)*, vol. 31, no. 2, pp. 228–238, 2005.

[59] C. T. Kelley, "Iterative methods for linear and nonlinear equations," *Society for Industrial and Applied Mathematics*, 1995.

[60] O. G. Nino-Amezquita, S. Enders, P. T. Jaeger, and R. Eggers, "Measurement and prediction of interfacial tension of binary mixtures," *Industrial & Engineering Chemistry Research*, vol. 49, no. 2, pp. 592–601, 2009.

[61] J. Mairhofer and J. Gross, "Modeling of interfacial properties of multicomponent systems using density gradient theory and PCP-SAFT," *Fluid Phase Equilibria*, vol. 439, pp. 31–42, 2017.

[62] E. W. Lemmon, M. O. McLinden, and D. G. Friend, "Thermophysical properties of fluid systems," in *NIST Chemistry WebBook, NIST Standard Reference Database Number 69* (P. J. Linstrom and W. G. Mallard, eds.), Gaithersburg MD, 20899: National Institute of Standards and Technology, 2016. http://webbook.nist.gov, (retrieved July 12, 2016).

[63] G. Korosi and E. S. Kovats, "Density and surface tension of 83 organic liquids," *Journal of Chemical and Engineering Data*, vol. 26, no. 3, pp. 323–332, 1981.

[64] G. Somayajulu, "A generalized equation for surface tension from the triple point to the critical point," *International journal of thermophysics*, vol. 9, no. 4, pp. 559–566, 1988.

[65] J. J. Jasper, "The surface tension of pure liquid compounds," *Journal of physical and chemical reference data*, vol. 1, no. 4, pp. 841–1010, 1972.

[66] J. J. Jasper and E. R. Kerr, "The orthobaric surface tensions and thermodynamic properties of the liquid surfaces of a series of 1-alkenes, c6 to c16, and of n-decylcyclopentane, n-decylcyclohexane and n-decylbenzene," *Journal of the American Chemical Society*, vol. 76, no. 10, pp. 2659–2661, 1954.

[67] F. Morehouse and O. Maass, "The preparation and physical properties of ethyl and methyl acetylene," *Canadian Journal of Research*, vol. 5, no. 3, pp. 306–312, 1931.

[68] F. R. Morehouse and O. Maass, "The preparation and physical properties of aliphatic acetylenes," *Canadian Journal of Research*, vol. 11, no. 5, pp. 637–643, 1934.

[69] R. Grzeskowiak, G. H. Jeffery, and A. I. Vogel, "919. physical properties and chemical constitution. part XXIX. acetylenic compounds," *Journal of the Chemical Society (Resumed)*, pp. 4719–4722, 1960.

[70] W. D. Harkins and Y. Cheng, "The orientation of molecules in surfaces. VI. cohesion, adhesion, tensile strength, tensile energy, negative surface energy, interfacial tension, and molecular attraction.," *Journal of the American Chemical Society*, vol. 43, no. 1, pp. 35–53, 1921.

[71] R. Amin and T. N. Smith, "Interfacial tension and spreading coefficient under reservoir conditions," *Fluid phase equilibria*, vol. 142, no. 1, pp. 231–241, 1998.

[72] P. Pugachevich and A. Cherkasskaya, "The surface properties of ternary solutions of normal alkanes," *Russian J. Phys. Chem*, vol. 54, pp. 328–1330, 1980.

[73] A. J. Queimada, A. I. Caco, I. M. Marrucho, and J. A. Coutinho, "Surface tension of decane binary and ternary mixtures with eicosane, docosane, and tetracosane," *Journal of Chemical & Engineering Data*, vol. 50, no. 3, pp. 1043–1046, 2005.

[74] A. T. Gros and R. Feuge, "Surface and interfacial tensions, viscosities, and other physical properties of some n-aliphatic acids and their methyl and ethyl esters," *Journal of the American Oil Chemists' Society*, vol. 29, no. 8, pp. 313–317, 1952.

[75] S. Mumford and J. Phillips, "19. the physical properties of some aliphatic compounds," *Journal of the Chemical Society (Resumed)*, pp. 75–84, 1950.

[76] A. I. Vogel, "130. physical properties and chemical constitution. part XIII. aliphatic carboxylic esters," *Journal of the Chemical Society (Resumed)*, pp. 624–644, 1948.

[77] G. H. Jeffery and A. I. Vogel, "133. physical properties and chemical constitution. part XVI. ethylenic compounds," *Journal of the Chemical Society (Resumed)*, pp. 658–673, 1948.

[78] G. H. Jeffery and A. I. Vogel, "134. physical properties and chemical constitution. part XVII. acetylenic compounds and cyanides," *Journal of the Chemical Society (Resumed)*, pp. 674–683, 1948.

[79] C. A. Allen, K. C. Watts, and R. G. Ackman, "Predicting the surface tension of biodiesel fuels from their fatty acid composition," *Journal of the American Oil Chemists' Society*, vol. 76, no. 3, pp. 317–323, 1999.

[80] S. Bi, G. Zhao, and J. Wu, "Surface tension of diethyl ether, diisopropyl ether, and dibutyl ether," *Journal of Chemical & Engineering Data*, vol. 55, no. 4, pp. 1523–1526, 2009.

[81] A. I. Vogel, "129. physical properties and chemical constitution. part XII. ethers and acetals," *Journal of the Chemical Society (Resumed)*, pp. 616–624, 1948.

[82] K. Habrdová, Š. Hovorka, and L. Bartovská, "Concentration dependence of surface tension for very dilute aqueous solutions of organic nonelectrolytes," *Journal of Chemical & Engineering Data*, vol. 49, no. 4, pp. 1003–1007, 2004.

[83] R. Wanchoo and J. Narayan, "Some physical properties of binary liquid systems:(2-butanone + n-propionic acid or n-butyric acid)," *Physics and Chemistry of Liquids*, vol. 27, no. 3, pp. 159–167, 1994.

[84] D. M. Cowan, G. H. Jeffery, and A. I. Vogel, "31. physical properties and chemical constitution. part V. alkyl ketones," *Journal of the Chemical Society (Resumed)*, pp. 171–176, 1940.

[85] K. Owen, O. R. Quayle, and W. J. Clegg, "A study of organic parachors. V. constitutive variations of the parachors of a series of normal ketones," *Journal of the American Chemical Society*, vol. 64, no. 6, pp. 1294–1296, 1942.

[86] A. Baglai, L. Gurarii, and G. G. Kuleshov, "Physical properties of compounds used in vitamin synthesis," *Journal of Chemical and Engineering Data*, vol. 33, no. 4, pp. 512–518, 1988.

[87] N. G. Tsierkezos and I. E. Molinou, "Conductivity studies of n-tetrabutylammonium tetraphenylborate in 3-pentanone in the temperature range from 283.15 to 329.15K," *Journal of solution chemistry*, vol. 36, no. 2, pp. 153–170, 2007.

[88] A. I. Vogel, "128. physical properties and chemical constitution. part XI. ketones," *Journal of the Chemical Society (Resumed)*, pp. 610–615, 1948.

[89] A. Doeuvre, "About mesityl oxide and some halogen derivatives," *Bull. Soc. Chim. Fr.*, pp. 1594–1600, 1926.

[90] R. Grzeskowiak, G. H. Jeffery, and A. I. Vogel, "919. physical properties and chemical constitution. part XXIX. acetylenic compounds," *Journal of the Chemical Society (Resumed)*, pp. 4719–4722, 1960.

[91] W. D. Harkins and Y. Cheng, "The orientation of molecules in surfaces. VI. cohesion, adhesion, tensile strength, tensile energy, negative surface energy, interfacial tension, and molecular attraction.," *Journal of the American Chemical Society*, vol. 43, no. 1, pp. 35–53, 1921.

[92] M. L. De Soria, J. L. Zurita, M. A. Postigo, and M. Katz, "Excess thermodynamic properties of the n-pentane + methylacetate system at 298.15K," *Thermochimica acta*, vol. 130, pp. 249–258, 1988.

[93] A. A. Rafati and E. Ghasemian, "Experimental and theoretical study of surface tension of binary mixtures of (n-alkyl acetates + heptane, benzene, and toluene)," *The Journal of Chemical Thermodynamics*, vol. 41, no. 3, pp. 386–391, 2009.

[94] A. Mulero, I. Cachadiña, and M. Parra, "Recommended correlations for the surface tension of common fluids," *Journal of Physical and Chemical Reference Data*, vol. 41, no. 4, p. 043105, 2012.

[95] A. I. Vogel, "368. physical properties and chemical constitution. part XXII. some primary, secondary, and tertiary amines," *Journal of the Chemical Society (Resumed)*, pp. 1825–1833, 1948.

[96] E. Jiménez, H. Casas, L. Segade, and C. Franjo, "Surface tensions, refractive indexes and excess molar volumes of hexane + 1-alkanol mixtures at 298.15K," *Journal of Chemical & Engineering Data*, vol. 45, no. 5, pp. 862–866, 2000.

[97] C. Stanners, Q. Du, R. Chin, P. Cremer, G. Somorjai, and Y.-R. Shen, "Polar ordering at the liquid-vapor interface of n-alcohols (c1-c8)," *Chemical physics letters*, vol. 232, no. 4, pp. 407–413, 1995.

Chapter 6

Identifying pure component parameters of an analytic equation of state using experimental surface tension or molecular simulations with a transferable force field

The content of this chapter is a literal quote of the publication

Mairhofer, Gross, Industrial & Engineering Chemistry Research, 2018, submitted.

In comparison to the published work, the abstract is here omitted. Additions or deletions compared to the published work are marked with angular brackets.

The parametrization of equations of state is an important step in modelling thermodynamic properties. Different routes exist to retrieve these model parameters for a given compound depending on the equation of state and the body of experimental data available for this compound. Information of the critical properties and the azentric factor for the molecule under study is sufficient to parametrize an equation of state. It is common for cubic equations of state such as the Peng-Robinson [1] or Soave-Redlich-Kwong [2] equation to take these quantities as input for obtaining pure component parameters. The pure-component parameters of SAFT-type (statistical associating fluid theory) equations of state are more commonly regressed to experimental data for vapor pressures and liquid densities in a range of temperatures. The most valuable thermodynamic properties for regression are those which exhibit the largest sensitivity to the model parameters. Some authors include supercritical densities or subcooled densities in the regression[3], or further properties such as speed of sound [4, 5]. Only few studies exist where other

properties, such as the fraction of unbonded hydrogen bonding sites are used during parameter regression[6].

An alternative for compounds with scarce experimental data is the use of group-contribution (GC) methods. The concept of GC methods is that the properties of a molecule can be estimated as a function of the (hypothetical) properties of the functional groups which make up the molecule. Once the parameters of all functional groups of a target compound have been determined e.g. by adjusting them for similar compounds with sufficient experimental data, the properties of the target compound can be approximated. For polymeric compounds, hardly any experimental data for properties describing the vapor-liquid equilibrium of the pure component such as vapor pressure or enthalpy of evaporation is available and alternative schemes to obtain pure-component parameters are required. For homologous series of polymers an approach similar to the group-contribution method exists where parameters of lower-mass molecules are extrapolated to higher-mass compounds [7, 3, 8]. The shortcomings of this route are discussed in ref. [9] where pure-component parameters for polymers are instead adjusted to liquid density and binary phase equilibrium data.

In this work, we explore two different routes for retrieving meaningful pure-component parameters of the PCP-SAFT model[3, 10, 11, 12, 13]. In the first scheme, we use experimental data for liquid density and for surface tension. This is achieved by applying a density functional theory (DFT) consistent with PCP-SAFT recently developed by Gross [14], Klink and Gross [15] and refined by Sauer and Gross [16]. Only the equation of state parameters are required for DFT calculations. Interfacial properties such as surface tension are obtained in a completely predictive manner and show excellent agreement to experimental results [17] [Chapter 4]. It therefore seems promising to reverse the procedure by using surface tension data as input for the parameter regression. In the second scheme, we use results for liquid density and enthalpy from molecular dynamics simulations using a transferable force field. We show that for polymeric compounds with 'vanishing' vapor pressure, the need for experimental data is thereby removed, and is replaced by the requirement of a suitable force fields for the considered component. We apply the transferable anisotropic Mie force field (TAMie)[18, 19, 20], which is developed with emphasis on phase equilibrium properties and thermodynamic properties. Results for vapor pressure, saturated liquid density, enthalpy of evaporation as well as surface tension calculated with parameters obtained from both schemes are evaluated for compounds of three chemical groups: n-alkanes, 1-alkenes and ethers.

6.1 Fundamentals of classical density functional theory

This section summarizes the basic equations of classical density functional theory. A more detailed description of the DFT approach applied in this work can be found in previous studies of our group [14, 15, 16]. In this work, DFT is applied to determine the value of surface tension γ for pure component systems during parameter optimization.

The single steps to obtain the value of surface tension for a pure component in a DFT calculation are the following: first, the vapor-liquid equilibrium is determined for the specified temperature. That delivers the value of vapor pressure p^{sat}, the densities of the coexisting vapor and liquid phases, ρ^v and ρ^l, as well as the equilibrium value of the chemical potential μ at vapor liquid equilibrium. Second, the equilibrium interfacial density profile $\rho(r)$ is determined by a DFT calculation with ρ^v and ρ^l as the boundary conditions for the density profile $\rho(r)$ across the vapor-liquid interface.

The equilibrium density profile minimizes the grand potential Ω of the system, which in the absence of an external field is defined as

$$\Omega[\rho] = A[\rho] - \int \mu\rho(\mathbf{r})\mathrm{d}\mathbf{r} \tag{6.1}$$

where the square brackets make the functional dependency on the density profile $\rho(r)$ explicit and the dependencies of Ω and A on temperature, volume and chemical potential are dropped for brevity.

In this work, a Helmholtz energy functional $A[\rho]$ consistent with PCP-SAFT is applied. $A[\rho]$ is then obtained as the sum of several contributions according to the PCP-SAFT model

$$A[\rho] = A^{ig}[\rho] + A^{hs}[\rho] + A^{chain}[\rho] + A^{disp}[\rho] + A^{dipolar}[\rho] \tag{6.2}$$

The hard-sphere contribution ($A^{hs}[\rho]$) is determined from Rosenfeld's Fundamental Measure Theory [21] in the modified form of Roth at al. [22] and Yu and Wu [23]. Chain formation ($A^{chain}[\rho]$) is treated using the iSAFT functional of Tripathi and Chapman [24] with the adaptations of Gross [14] and Klink and Gross [15]. The weighted-density approximation developed by Sauer and Gross [16] is applied for dispersive ($A^{disp}[\rho]$) as well as dipolar ($A^{dipolar}[\rho]$) contributions.

For the imposed variables $\{\mu, T, V\}$, the density profile $\rho(r)$ is the internal degree of freedom of the considered system. The minimum of Ω is characterized by a vanishing functional derivative with respect to the systems internal degree of freedom, i.e. the density profile $\rho(r)$

$$\frac{\delta\Omega[\rho]}{\delta\rho(r)} = \frac{\delta A[\rho]}{\delta\rho(r)} - \mu = 0 \tag{6.3}$$

For the flat vapor-liquid interface, eq. 6.3 can be discretized on a one-dimensional grid which results in a coupled set of nonlinear equations. An efficient algorithm to solve this set of equations is essential here because many DFT calculations are required during parameter optimization. We use a matrix-free Newton method which proved to be a suitable algorithm in a previous study [25] [Chapter 3].
The value of surface tension γ can be obtained once the equilibrium density profile across the interface is determined as

$$\gamma = \int a[\rho(z)] - \mu\rho(z) + p^{sat}\mathrm{d}z \tag{6.4}$$

where z denotes the coordinate normal to the interface and the Helmholtz energy density a is defined as $A[\rho] = \int a[\rho(z)]S\mathrm{d}z$ with surface area S.

6.2 Molecular dynamics simulations

Results for enthalpy from molecular simulations cannot be used directly for parameter optimization of PCP-SAFT. That is because PCP-SAFT can only determine residual enthalpy $h^{res}(T,p) \equiv h(T,p) - h^{ig}(T)$ where h^{ig} denotes the enthalpy of an ideal gas. To calculate the total enthalpy $h(T,p)$ from PCP-SAFT, the ideal gas isobaric heat capacity of the compound is required as additional input to evaluate h^{ig} (and a standard state enthalpy). Molecular simulations with classical force fields, of course, also don't provide the ideal gas contribution, but the enthalpies most easily obtained include intramolecular energy contributions. It is easier, therefore, to derive other properties from the enthalpy values of molecular simulations which only require the residual part h^{res}. One such property is enthalpy of evaporation

$$\Delta h^{lv}(T) = h^{vap}(T, p^{sat}(T)) - h^{liq}(T, p^{sat}(T)) \tag{6.5}$$

$$= h^{vap,res}(T, p^{sat}(T)) - h^{liq,res}(T, p^{sat}(T)) \tag{6.6}$$

To calculate Δh^{lv} according to eq. 6.6, simulations of the vapor and liquid phases coexisting at temperature T and vapor pressure $p^{sat}(T)$ have to be performed. A common simplification at this point is to approximate the gas phase as an ideal gas [26, 27]

$$\Delta h^{lv}(T) \approx h^{ig}(T) - h^{liq}(T, p^{sat}(T)) = -h^{liq,res}(T, p^{sat}(T)) \tag{6.7}$$

In molecular simulations, the vapor enthalpy h^{ig} can be obtained by simulating a single

molecule. However, the sampling of intramolecular configurations is greatly improved by simulating a larger number of molecules and specifying a large simulation box in order to marginalize intermolecular interactions between the molecules [26, 27].

An alternative property suited for the parameter optimization of the PCP-SAFT model is the residual enthalpy of the liquid phase

$$h^{liq,res}(T,p) \equiv h^{liq}(T,p) - h^{ig}(T) \tag{6.8}$$

The value of $h^{liq,res}$ can be obtained from a simulation of the liquid phase at specified values of temperature T, pressure p and particle number N to obtain $h^{liq}(T,p)$ as well as a simulation of the vapor phase at specified temperature T, particle number N and a volume V, which has to be chosen large enough to ensure the system is in the ideal gas state, to determine h^{ig}.

Choosing $h^{liq,res}$ over Δh^{lv} offers several advantages: firstly, using Δh^{lv} one is bound to thermodynamic states at vapor-liquid phase equilibrium, i.e. simulations have to be performed for subcritical temperatures at the corresponding value of vapor pressure. Enthalpy values $h^{res,liq}$, on the other hand, can be obtained for arbitrary (stable) liquid states. Secondly, as shown in Fig. 6.1a for n-butane, results for Δh^{lv} with the ideal gas approximation for the vapor phase deteriorate with increasing temperature due to the increasing value of vapor pressure p^{sat}. Only if the gas phase is simulated at the correct value of p^{sat}, accurate results can be obtained for Δh^{lv} over a wider temperature range, Fig. 6.1a.

The definition of $h^{liq,res}$, eq. 6.8, is valid regardless of the system temperature or pressure and simulation results for the identical state points as in Fig. 6.1a follow the reference data closely also for higher temperatures, Fig. 6.1b.

Therefore, to adjust the PCP-SAFT parameters we use values for $h^{liq,res}$ and for liquid densities as obtained from molecular simulations using the TAMie force field[18, 19, 20]. We will show that for polymeric compounds it is a valid approximation to assume zero pressure in the molecular simulation of the liquid phase.

6.2.1 Simulation details

All molecular dynamics simulations are performed using the DL_POLY_4 software package [30] and the transferable anisotropic Mie force field (TAMie) [18, 19, 20] with analytical long range corrections for energy and pressure. In the gas and liquid phase, for every compound simulations are performed at eight subcritical isotherms for reduced temperatures between 0.55 and 0.9.

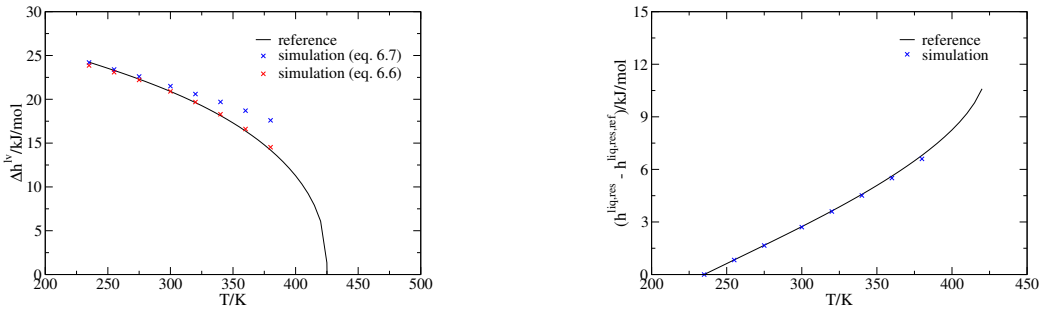

(a) (b)

Figure 6.1: Diagram (a): enthalpy of evaporation Δh^{lv} for n-butane as a function of temperature. Comparison of simulation results where the gas phase is approximated as an ideal gas (blue symbols) to simulation results where the gas phase is simulated at the correct value of vapor pressure (red symbols) as well as reference data (solid line) [28]. Diagram (b): residual liquid enthalpy for n-butane as a function of temperature. Results are calculated as $h^{liq,res}(T, p^{sat}(T)) - h^{liq,res,ref}\left(T^{ref}, p^{sat}(T^{ref})\right)$. The reference temperature is set to $T^{ref} = 235$ K. Comparison of simulation results (symbols) to reference data (solid line) [28, 29].

Simulation details liquid phase

For liquid phase simulations, 512 molecules are placed in a cubic box using packmol [31]. All simulations of a given compound are started from the same initial box, which has a density close to the average of the expected densities at the lowest and highest simulated temperatures. The system is equilibrated for 100,000 time steps in the microcanonical ensemble and the velocities are scaled to the desired simulation temperature every 10 time steps. Subsequently, the simulations are continued in the isothermal-isobaric ensemble for 5 million (10 million for the longest molecules of each chemical family) time steps and samples are taken over the last 4 million (9 million for the longest molecules of each chemical family) steps. The value of pressure is set to the experimental vapor pressure corresponding to the specified temperature. For polymeric compounds, additional simulations are performed at zero pressure to validate the approach of obtaining equation of state parameters from a scheme which does not require experimental data as input. Pressure and temperature are controlled by a Martyna-Tuckerman-Klein barostat [32, 33]. The relaxation constants of the thermostat and barostat, τ_T and τ_p, respectively, are set to $\tau_T = 0.1$ ps and $\tau_p = 1$ ps. In all simulations, the equations of motion are integrated by a velocity-verlet integration scheme using a time step of 1 fs. The tolerance for the SHAKE algorithm is set to 10^{-5} and a cut-off radius of 14Å is used for van der Waals interactions.

The standard Ewald summation is applied to evaluate Coulombic interactions between charged particles. The parameters of the Ewald summation are set automatically by DL_POLY by specifying a global tolerance. From a comparison of different values for this

tolerance, a value of 10^{-6} was found to be a suitable choice. Tighter tolerances did not lead to significant changes of simulation results, see Appendix.

Using results of molecular simulations with the TAMie force field as input for optimizing pure component parameters of the PCP-SAFT model is only sensible, if the TAMie force field gives sufficiently accurate estimates of the considered properties. Table 6.1 lists deviations of liquid densities from the TAMie force field to reference data. Across all studied compounds, deviations are usually around 1 to 2%. Furthermore, it can be observed that assuming zero vapor pressure for polymeric molecules still leads to accurate density results.

Table 6.1: Deviations of liquid saturated density evaluated at eight reduced temperatures $T_r = T/T_c$ between 0.55 and 0.9. Experimental data from NIST [28] and the Korean Thermophysical Properties Data Bank [34].

compound	Dev.%	compound	Dev. %	compound	Dev. %
butane	0.84	1-butene	1.62	methylbutylether	1.14
heptane	1.22	1-heptene	2.24	dimethylether	1.22
decane	1.39	1-decene	1.60	dipropylether	1.88
heptadecane	2.32	1-hexadecene	1.98	dipentylether	1.77
heptadecane (p=0)	2.22	1-hexadecene (p=0)	1.84	dipentylether (p=0)	1.63

Simulation details vapor phase

The vapor phase simulations are performed with the same number of molecules as the liquid phase simulations. In order to obtain simulation conditions which resemble the ideal gas state, i.e. negligible intermolecular interactions, for every compound the final simulation box of the liquid phase simulation at highest temperature is expanded by a factor of ten in every direction. The molecules are then placed inside this box with a minimal initial distance between any two molecules of 40Å using packmol [31]. The system is equilibrated in the microcanonical ensemble for 500000 steps scaling the velocities every 10 time steps to the desired temperature, followed by a simulation run at constant particle number N, temperature T and volume V using the Langevin thermostat with a friction constant of $\tau = 2\text{ps}^{-1}$ and a time step of 1 fs. The equations of motion are integrated by the velocity-verlet scheme. These simulations are continued for 8 million steps and samples are taken from the last 7 million. The same tolerances for the SHAKE algorithm and Ewald summation are applied as in the liquid phase simulations. However, the long-range contribution to the Coulomb interactions is never evaluated.

6.3 Results and discussion

In this section, the PCP-SAFT parameter sets adjusted to experimental results for saturated liquid density and surface tension (labelled *set Surface Tension*) and to saturated liquid density and residual liquid enthalpy from molecular simulations (labelled *set TAMie*) are evaluated. Results obtained with both parameters sets are compared to quasi-experimental data. We thereby assess four thermodynamic properties: liquid saturated density, vapor pressure, enthalpy of evaporation, and surface tension. Special attention is given to results for those properties which were not included in the parameter optimization and thus represent predictions. The evaluation is carried out for compounds of three different chemical families: n-alkanes, 1-akenes and ethers. For the largest studied molecules of each chemical family, the approach of performing molecular simulations of the liquid phase at zero pressure and using the results of these simulations for parameter adjustment is discussed. For comparison, results obtained from parameter sets adjusted in the conventional manner, to liquid density and to vapor pressure are also regarded for comparison (labelled *reference set*). All parameter sets are listed in the Appendix.
Deviations presented in this section are averaged values calculated according to $\frac{1}{N^{exp}} \sum_{i=1}^{N^{exp}} \frac{|\phi_i^{exp} - \phi_i^{calc}|}{\phi_i^{exp}}$ with the number of evaluated data points N^{exp} and the with the calculated result ϕ^{calc} and the quasi-experimental value ϕ^{exp} of the studied property ϕ. In all cases, eight data points at reduced temperatures between 0.55 and 0.9 are considered.

6.3.1 Results for n-alkanes

Results obtained from the different parameter sets for butane, heptane, decane and heptadecane are shown in Figs. 6.2 and 6.3. The reference parameter sets are taken from the original PC-SAFT publication of Gross and Sadowski [3].

Set Surface Tension correlates liquid density equally well as the *reference set*. Deviations range from 0.2% for butane to 1.5% for heptadecane which is only slightly worse than the *reference set* (0.3% for butane and 0.5% for heptadecane). From results of liquid density for heptadecane (Figs. 6.2 (B)), it is apparent that the critical temperature T_c is obtained more accurately from parameter *set Surface Tension* than from the *reference set*. A possible explanation is that surface tension (included for parameter optimization for *set Surface Tension*) contains more information on the value of T_c (where surface tension vanishes) than vapor pressure (which has gone into *reference set*) that does not in itself imply any peculiar value of T_c.

Surface tension results are correlated very accurately by *set Surface Tension* for all studied n-alkanes. Notable deviations to quasi-experimental data only occur at the lowest temperatures. Results predicted by the *reference set* are also in excellent agreement to quasi-experimental results. Vapor pressures and enthalpies of evaporation are not included in the parameter optimization of *set Surface Tension*. Predictions of p^{sat} from *set Surface Tension* are in very good agreement to quasi-experimental data and only for heptadecane, where vapor pressure is overpredicted at high temperatures, notable differences to correlations of the *reference set* become apparent. Predictions of *set Surface Tension* for enthalpy of evaporation tend to overpredict the experimental data at low temperatures with increasing molecular mass. At elevated temperatures, predictions of *set Surface Tension* and the *reference set* agree closely. Only for heptadecane the more accurate value of T_c leads to better agreement of predictions from *set Surface Tension* to quasi-experimental results. In general, only small deviations below 6% occur for Δh^{lv} with *set Surface Tension*.

Results obtained with *set TAMie* for n-butane agree very well with quasi-experimental data for all studied thermodynamic properties. Deviations range from below 1% for liquid density to 8% for surface tension. For longer n-alkane molecules, a growing overestimation of the critical temperature is observed. This causes increased deterioration of the results for all properties depicted in Figs. 6.2 and 6.3 at elevated temperatures. For heptadecane, the longest studied n-alkane, deviations increase to 1.5% for liquid density, 4% for enthalpy of evaporation, 10% for vapor pressure and 17% for surface tension. In the low temperature range, on the other hand, results for surface tension and liquid density obtained with *set TAMie* agree very well with results from the *reference set* and quasi-experimental data.

Table 6.2 presents results for heptadecane. The table lists deviations of calculated proper-

ties from experimental values achieved with all parameter sets. With averaged deviations across all four properties of 2.9% and 3%, the *reference set* and *set Surface Tension* show similar accuracy. As expected, both parameter sets show larger deviations for predicted properties, surface tension for the *reference set* and vapor pressure for *set Surface Tension*, while correlated results are very accurate. Enthalpy of evaporation, a property not included in the parameter optimization of any of the two parameter sets, is predicted with almost identical deviation by both sets.

Parameter *set TAMie* leads to average deviations of 8.5% across all properties of heptadecane listed in Table 6.2. Additionally, deviations for a modified *set TAMie* are presented in Table 6.2 which is adjusted to results of molecular simulations where in the liquid phase simulations the vapor pressure is assumed to be zero. Deviations for the single properties do not deviate substantially from values of the regular *set TAMie* and the overall deviation across all properties takes on a value of 8.1%. That is a rather satisfactory result considering that no experimental information about the compound is necessary to perform the required molecular simulations. The result, of course, critically relies on a suitable transferable force field.

Table 6.2: Deviations for vapor pressure, liquid density, enthalpy of evaporation as well as surface tension for the different parameter sets for n-heptadecane.

	Dev. p^{sat} %	Dev. ρ^{l} %	Dev. Δh^{lv} %	Dev. γ %
reference set	1.65	0.49	2.45	7.12
set Surface Tension	7.80	1.49	2.43	0.30
set TAMie	10.46	1.54	4.49	17.35
mod. *set TAMie*	9.87	1.51	4.41	16.63

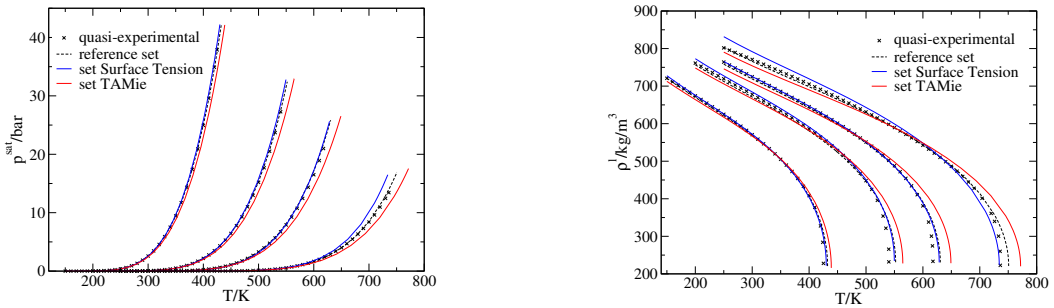

(a) (b)

Figure 6.2: Results for vapor pressure (a) and saturated liquid density (b) for butane, heptane, decane and heptadecane (from left to right) obtained from the different PCP-SAFT parameter sets as well as quasi-experimental results [28, 35].

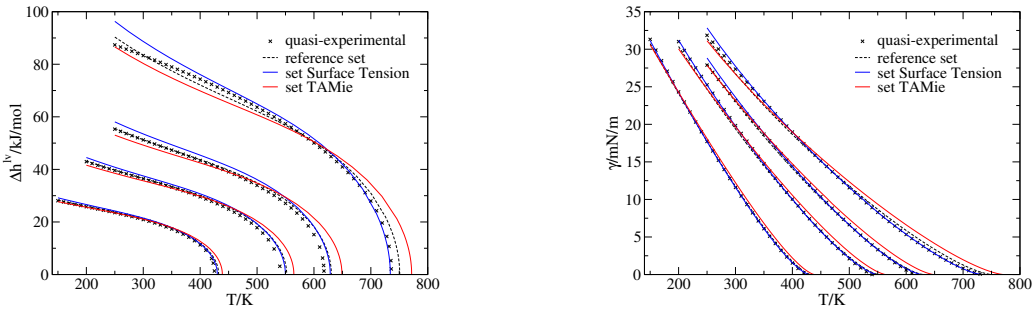

(a) (b)

Figure 6.3: Results for enthalpy of evaporation (a) and surface tension (b) for butane, heptane, decane and heptadecane (from left to right) obtained from the different PCP-SAFT parameter sets as well as quasi-experimental results [28, 35].

6.3.2 Results for 1-alkenes

Results for 1-butene, 1-heptene, 1-decene as well as 1-hexadecene are exemplified in Figs. 6.4 and 6.5. Reference parameter sets are taken from Gross and Sodowski [3] and Kontogeorgis and Folas [36].

Correlations for liquid density of *set Surface Tension* agree very well with quasi-experimental data (and with results of the *reference set*). Correlations of surface tension obtained from *set Surface Tension* as well as predictions from the *reference set* agree very well with quasi-experimental results. Except for 1-hexadecene, where deviations increase for both parameter sets, errors stay below 1% for *set Surface Tension* and below 4% for the *reference set*. Results of *set Surface Tension* for both predicted properties show a similar trend: deviations for vapor pressure as well as enthalpy of evaporation are in the order of 2% for 1-butene which is practically identical to the *reference set* (where vapor pressure is correlated) and increase to 15% for p^{sat} and 7% for Δh^{lv} for 1-hexadecene. For 1-decene and 1-hexadecene, predictions for Δh^{lv} of *set Surface Tension* show larger deviations than the other parameter sets at low and intermediate temperatures while in the vicinity of the critical point, results are more accurate due to the more accurate prediction of T_c.

Results obtained from *set TAMie* for 1-alkenes show similar trends as the corresponding results for 1-alkanes: with growing molecular weight, the growing overprediction of T_c leads to increasing deviations for all studied properties at elevated temperatures. On the other hand, accurate results (comparable to the results of the *reference set*) are obtained for the correlated as well as the predicted properties at low temperatures.

Table 6.3 summarizes the deviations of all parameter sets for all properties of 1-hexadecene. With a deviation across all four properties of 3.3%, results of the *reference set* are the most accurate. Unlike in the case of heptadecane (Table 6.2), deviations of *set TAMie* are smaller (7.1%) than of *set Surface Tension* (8.4%). This is mainly caused by lower deviations of *set TAMie* for enthalpy of evaporation and surface tension. The latter is

very surprising as results for γ from *set Surface Tension* are correlated values while for *set TAMie* they represent predictions. Presented deviations for the modified *set TAMie*, where molecular simulations of the liquid phase are performed at zero vapor pressure, are again very close to the figures of *set TAMie* and confirm the validity of this approach to obtain equation of state parameters for polymeric molecules.

Table 6.3: Deviations for vapor pressure, liquid density, enthalpy of evaporation as well as surface tension for the different parameter sets for 1-hexadecene.

	Dev. p^{sat} %	Dev. ρ^{l} %	Dev. Δh^{lv} %	Dev. γ %
reference set	2.63	1.07	2.49	6.85
set Surface Tension	14.76	0.44	7.34	10.99
set TAMie	13.24	1.93	4.38	7.06
mod. *set TAMie*	12.51	1.88	4.29	6.71

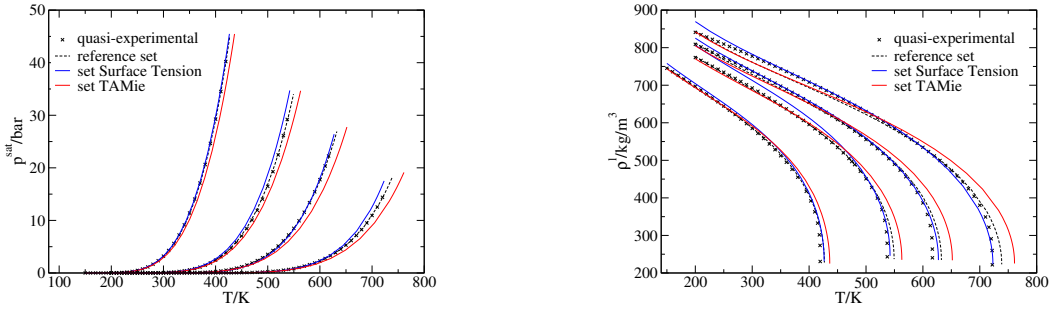

(a) (b)

Figure 6.4: Results for vapor pressure (a) and saturated liquid density (b) for 1-butene, 1-heptene, 1-decene and 1-hexadecene (from left to right) obtained from the different PCP-SAFT parameter sets as well as quasi-experimental results [35].

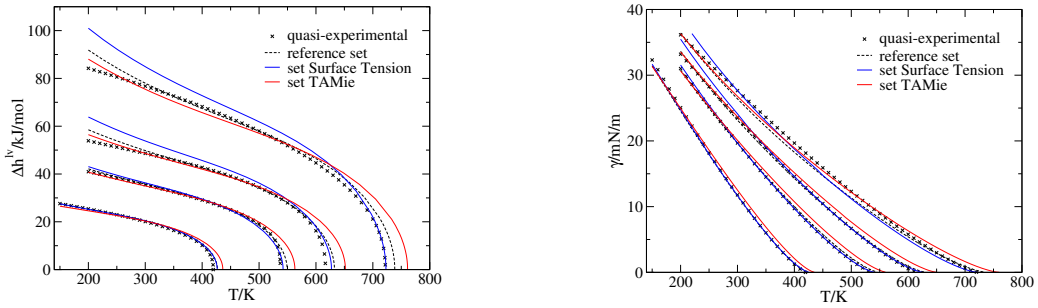

(a) (b)

Figure 6.5: Results for enthalpy of evaporation (a) and surface tension (b) for 1-butene, 1-heptene, 1-decene and 1-hexadecene (from left to right) obtained from the different PCP-SAFT parameter sets as well as quasi-experimental results [35].

6.3.3 Results for ethers

Results obtained from the different parameter sets for dimethylether, methylbutylether as well as dipentylether are presented in Figs. 6.6 and 6.7. Furthermore, results for dipropylether (not shown in Figs. 6.6 and 6.7) will be discussed. Reference parameters for dimethylether are taken from Gross and Vrabec [11]. For the remaining ether compounds, they are adjusted in this work and presented in the Appendix.

For ethers we recognize a similar pattern as observed for alkanes, namely very good agreement of correlated liquid densities and surface tensions obtained from *set Surface Tension* to quasi-experimental data and to results of the *reference set*. Significant differences between both parameter sets only occur for dimethylether, where a clear improvement of *set Surface Tension* surface tension correlations (deviation: 1.3%) over predictions of the *reference set* (deviation: 7%) can be observed as well as for dipentylether. For this compound, the critical temperature is obtained more accurately by *set Surface Tension* than by the *reference set* and liquid density results are correlated more accurately at elevated temperatures by *set Surface Tension*. Vapor pressure predictions for ethers obtained with *set Surface Tension* agree very well with quasi-experimental data and to the correlated values of the *reference set* (Fig. 6.6a). For dimethylether, dipropylether and dipentylether, higher deviations occur at very low temperatures which cause the averaged deviation of *set Surface Tension* predictions to rise to up to 21%. For higher temperatures, on the other hand, vapor pressure predictions of *set Surface Tension* for dipentylether agree more closely with quasi-experimental data than correlations of the *reference set*. Enthalpy of evaporation is predicted very accurately for methylbutylether by *set Surface Tension* (deviation: 2%). For the remaining ether molecules, deviations take on values between 5% for dipropylether and 8% for dipentylether.

Vapor pressure predictions of *set TAMie* show increasing errors with molecular size: deviations start at 11% for dimethylether and increase to 16 and 18% for methylbutylether and dipentylether, respectively. Results for liquid density are convincingly accurate on the other hand, with deviations below 2% for all four ether compounds. Only at elevated temperatures, results deteriorate due to the overshoot of critical temperature. This also causes increased deviations of *set TAMie* for enthalpy of evaporation and surface tension in the high temperature range. At low temperatures however, predictions of *set TAMie* for Δh^{lv} and γ agree well with results of the *reference set* and with quasi-experimental data.

In Table 6.4, deviations for dipentylether obtained with the different parameter sets are presented. Deviations across all four thermodynamic properties are lowest for the reference set (2.8%). *Set Surface Tension* and *set TAMie* show similar overall deviations of 7.7 and 8.2%. In the temperature range for which deviations are calculated, enthalpy of evaporation results of *set TAMie* are remarkably accurate compared to results of the

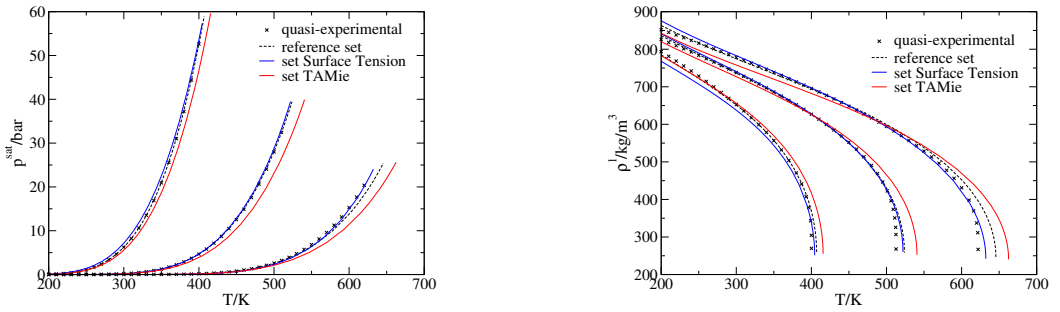

(a) (b)

Figure 6.6: Results for vapor pressure (a) and saturated liquid density (b) for dimethylether, methylbutylether and dipentylether (from left to right) obtained from the different PCP-SAFT parameter sets as well as quasi-experimental results [35].

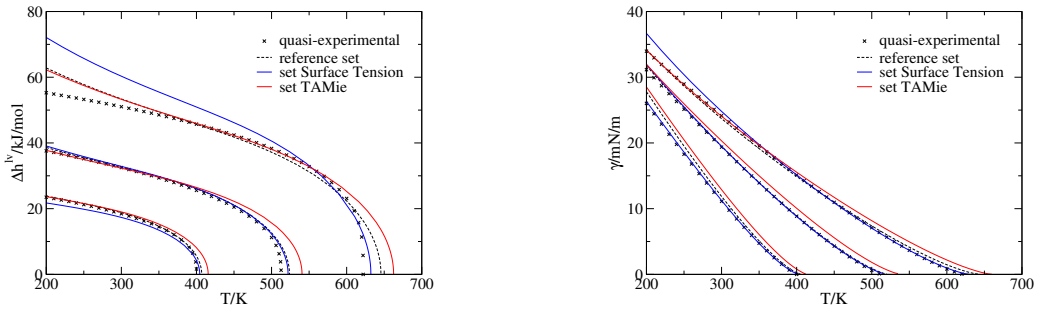

(a) (b)

Figure 6.7: Results for enthalpy of evaporation (a) and surface tension (b) for dimethylether, methylbutylether and dipentylether (from left to right) obtained from the different PCP-SAFT parameter sets as well as quasi-experimental results [35].

other sets. Figures for the modified *set TAMie* are again convincingly accurate (overall deviations: 7.9%) to reconfirm this route of obtaining meaningful equations of state parameters for polymeric compounds.

Table 6.4: Deviations for vapor pressure, liquid density, enthalpy of evaporation as well as surface tension for the different parameter sets for dipentylether.

	Dev. p^{sat} %	Dev. ρ^l %	Dev. Δh^{lv} %	Dev. γ %
reference set	3.53	0.75	2.29	4.43
set Surface Tension	21.33	0.34	8.30	0.74
set TAMie	17.66	1.68	0.76	12.80
mod. *set TAMie*	16.98	1.66	0.77	11.97

6.4 Conclusion

In this study we mimic the situation, where experimental data for vapor pressure of a considered substance is absent. Two schemes to adjust PCP-SAFT pure-component parameters for such a case are presented. The first scheme makes use of classical density functional theory that allows to include experimental surface tension data besides liquid density data for parameter optimization. The second scheme uses results for saturated liquid density as well as residual liquid enthalpy from molecular dynamics simulations using a suitable transferable force field. We apply the TAMie force field in this study. Results from both routes are evaluated for four thermodynamic properties (saturated liquid density, vapor pressure, enthalpy of evaporation and surface tension) for several n-alkanes, 1-alkenes as well as ethers. Very satisfactory results are observed for both schemes. Results obtained with the first scheme exhibit larger deviations only at low temperatures. At elevated temperatures agreement to experimental data is excellent. The reverse holds true for the second scheme: accurate results are obtained at low temperatures while deviations increase with increasing temperature due to overprediction of the critical temperature. The second scheme allows to obtain pure-component equation of state parameters of polymeric compounds with 'vanishing' vapor pressure without experimental data.

Appendix

Choosing the global tolerance for the Ewald summation

Fig. 6.8 shows the results of a parameter study to identify a suitable value for the global Ewald summation tolerance as discussed in the main text.

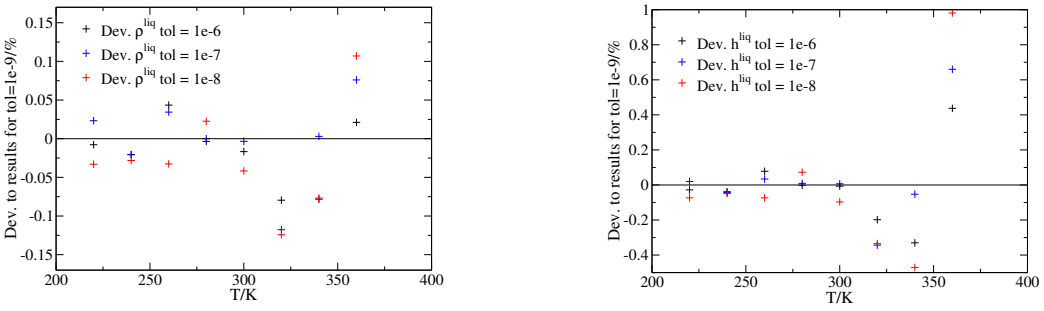

(a) (b)

Figure 6.8: Deviations of liquid density (a) and liquid enthalpy (b) for simulations of dimethylether at different temperatures using different values for the global tolerance of the Ewald summation. Results obtained with a tolerance of 10^{-9} are used as the reference.

Parameter sets

Table 6.5: PCP-SAFT parameters of the different parameter sets used in this work for n-alkanes and 1-alkenes. Reference parameter sets are taken from Gross and Sadowski [3] and Kontogeorgis and Folas [36].

set label	m	σ/Å	$\epsilon/k/K$	set label	m	σ/Å	$\epsilon/k/K$
butane				1-butene			
reference set	2.332	3.709	222.88	*reference set*	2.286	3.643	222.00
set Surface Tension	2.530	3.595	213.37	*set Surface Tension*	2.273	3.632	222.47
set TAMie	2.133	3.841	236.10	*set TAMie*	1.958	3.851	244.71
heptane				1-heptene			
reference set	3.483	3.805	238.40	*reference set*	3.364	3.790	240.62
set Surface Tension	3.740	3.686	230.77	*set Surface Tension*	3.638	3.640	230.09
set TAMie	3.041	4.007	258.04	*set TAMie*	2.939	3.987	261.11
decane				1-decene			
reference set	4.663	3.838	243.87	*reference set*	4.370	3.891	250.35
set Surface Tension	5.092	3.712	235.90	*set Surface Tension*	5.180	3.651	234.05
set TAMie	3.960	4.092	266.55	*set TAMie*	3.817	4.096	271.40
heptadecane				1-hexadecene			
reference set	6.981	3.968	255.65	*reference set*	6.500	3.975	256.70
set Surface Tension	8.086	3.724	240.29	*set Surface Tension*	7.830	3.688	238.63
set TAMie	6.140	4.177	272.82	*set TAMie*	5.717	4.165	275.04
mod. *set TAMie*	6.173	4.170	271.96	mod. *set TAMie*	5.750	4.157	274.10

Table 6.6: PCP-SAFT parameters of the different parameter sets used in this work for ethers. The reference parameter set of dimethylether is taken from [11]. The *reference sets* of the remaining compounds are adjusted to saturated liquid densities and densities of the subcooled liquid as well as vapor pressure data [35, 37, 38]. Dipole moments μ are taken from the DIPPR database [35].

set label	m	σ/Å	$\epsilon/k/K$	μ/D
methylbutylether				
reference set	3.196	3.616	234.10	1.25
set Surface Tension	3.308	3.566	229.95	1.25
set TAMie	2.789	3.822	256.22	1.25
dimethylether				
reference set	2.263	3.272	210.29	1.3
set Surface Tension	1.794	3.571	233.68	1.3
set TAMie	2.062	3.390	224.55	1.3
dipropylether				
reference set	3.470	3.704	234.71	1.2
set Surface Tension	3.988	3.527	221.36	1.2
set TAMie	3.083	3.904	253.30	1.2
dipentylether				
reference set	4.712	3.876	248.77	1.2
set Surface Tension	6.206	3.506	222.77	1.2
set TAMie	4.368	4.017	262.25	1.2
mod. *set TAMie*	4.400	4.008	261.07	1.2

Bibliography

[1] D.-Y. Peng and D. B. Robinson, "A new two-constant equation of state," *Industrial & Engineering Chemistry Fundamentals*, vol. 15, no. 1, pp. 59–64, 1976.

[2] G. Soave, "Equilibrium constants from a modified redlich-kwong equation of state," *Chemical Engineering Science*, vol. 27, no. 6, pp. 1197–1203, 1972.

[3] J. Gross and G. Sadowski, "Perturbed-chain SAFT: An equation of state based on a perturbation theory for chain molecules," *Industrial & engineering chemistry research*, vol. 40, no. 4, pp. 1244–1260, 2001.

[4] T. Lafitte, D. Bessieres, M. M. Piñeiro, and J.-L. Daridon, "Simultaneous estimation of phase behavior and second-derivative properties using the statistical associating fluid theory with variable range approach," *The Journal of chemical physics*, vol. 124, no. 2, p. 024509, 2006.

[5] T. Lafitte, A. Apostolakou, C. Avendaño, A. Galindo, C. S. Adjiman, E. A. Müller, and G. Jackson, "Accurate statistical associating fluid theory for chain molecules formed from Mie segments," *The Journal of chemical physics*, vol. 139, no. 15, p. 154504, 2013.

[6] G. M. Kontogeorgis, I. Tsivintzelis, N. von Solms, A. Grenner, D. Bøgh, M. Frost, A. Knage-Rasmussen, and I. G. Economou, "Use of monomer fraction data in the parametrization of association theories," *Fluid Phase Equilibria*, vol. 296, no. 2, pp. 219–229, 2010.

[7] T. Sako, A. H. Wu, and J. M. Prausnitz, "A cubic equation of state for high-pressure phase equilibria of mixtures containing polymers and volatile fluids," *Journal of applied polymer science*, vol. 38, no. 10, pp. 1839–1858, 1989.

[8] I. A. Kouskoumvekaki, N. von Solms, T. Lindvig, M. L. Michelsen, and G. M. Kontogeorgis, "Novel method for estimating pure-component parameters for polymers: application to the PC-SAFT equation of state," *Industrial & engineering chemistry research*, vol. 43, no. 11, pp. 2830–2838, 2004.

[9] J. Gross and G. Sadowski, "Modeling polymer systems using the perturbed-chain statistical associating fluid theory equation of state," *Industrial & engineering chemistry research*, vol. 41, no. 5, pp. 1084–1093, 2002.

[10] J. Gross and G. Sadowski, "Application of the perturbed-chain SAFT equation of state to associating systems," *Industrial & engineering chemistry research*, vol. 41, no. 22, pp. 5510–5515, 2002.

[11] J. Gross and J. Vrabec, "An equation-of-state contribution for polar components: Dipolar molecules," *AIChE journal*, vol. 52, no. 3, pp. 1194–1204, 2006.

[12] J. Gross, "An equation-of-state contribution for polar components: Quadrupolar molecules," *AIChE journal*, vol. 51, no. 9, pp. 2556–2568, 2005.

[13] J. Vrabec and J. Gross, "Vapor-liquid equilibria simulation and an equation of state contribution for dipole-quadrupole interactions," *The Journal of Physical Chemistry B*, vol. 112, no. 1, pp. 51–60, 2008.

[14] J. Gross, "A density functional theory for vapor-liquid interfaces using the PCP-SAFT equation of state," *The Journal of chemical physics*, vol. 131, no. 20, p. 204705, 2009.

[15] C. Klink and J. Gross, "A density functional theory for vapor–liquid interfaces of mixtures using the perturbed-chain polar statistical associating fluid theory equation of state," *Industrial & Engineering Chemistry Research*, vol. 53, no. 14, pp. 6169–6178, 2014.

[16] E. Sauer and J. Gross, "Classical density functional theory for liquid–fluid interfaces and confined systems: A functional for the perturbed-chain polar statistical associating fluid theory equation of state," *Industrial & Engineering Chemistry Research*, vol. 56, no. 14, pp. 4119–4135, 2017.

[17] J. Mairhofer and J. Gross, "Modeling properties of the one-dimensional vapor-liquid interface: Application of classical density functional and density gradient theory," *Fluid Phase Equilibria*, 2017.

[18] A. Hemmen and J. Gross, "Transferable anisotropic united-atom force field based on the Mie potential for phase equilibrium calculations: n-alkanes and n-olefins," *The Journal of Physical Chemistry B*, vol. 119, no. 35, pp. 11695–11707, 2015.

[19] A. Hemmen, A. Z. Panagiotopoulos, and J. Gross, "Grand canonical monte carlo simulations guided by an analytic equation of state transferable anisotropic Mie potentials for ethers," *The Journal of Physical Chemistry B*, vol. 119, no. 23, pp. 7087–7099, 2015.

[20] D. Weidler and J. Gross, "Transferable anisotropic united-atom force field based on the Mie potential for phase equilibria: Aldehydes, ketones, and small cyclic alkanes," *Industrial & Engineering Chemistry Research*, vol. 55, no. 46, pp. 12123–12132, 2016.

[21] Y. Rosenfeld, "Free-energy model for the inhomogeneous hard-sphere fluid mixture and density-functional theory of freezing," *Physical review letters*, vol. 63, no. 9, p. 980, 1989.

[22] R. Roth, R. Evans, A. Lang, and G. Kahl, "Fundamental measure theory for hard-sphere mixtures revisited: the white bear version," *Journal of Physics: Condensed Matter*, vol. 14, no. 46, p. 12063, 2002.

[23] Y.-X. Yu and J. Wu, "Structures of hard-sphere fluids from a modified fundamental-measure theory," *The Journal of chemical physics*, vol. 117, no. 22, pp. 10156–10164, 2002.

[24] S. Tripathi and W. G. Chapman, "Microstructure of inhomogeneous polyatomic mixtures from a density functional formalism for atomic mixtures," *The Journal of chemical physics*, vol. 122, no. 9, p. 094506, 2005.

[25] J. Mairhofer and J. Gross, "Numerical aspects of classical density functional theory for one-dimensional vapor-liquid interfaces," *Fluid Phase Equilibria*, vol. 444, pp. 1–12, 2017.

[26] C. Oostenbrink, A. Villa, A. E. Mark, and W. F. Van Gunsteren, "A biomolecular force field based on the free enthalpy of hydration and solvation: the gromos force-field parameter sets 53a5 and 53a6," *Journal of computational chemistry*, vol. 25, no. 13, pp. 1656–1676, 2004.

[27] L. D. Schuler and W. F. Van Gunsteren, "On the choice of dihedral angle potential energy functions for n-alkanes," *Molecular Simulation*, vol. 25, no. 5, pp. 301–319, 2000.

[28] E. W. Lemmon, M. O. McLinden, and D. G. Friend, "Thermophysical properties of fluid systems," in *NIST Chemistry WebBook, NIST Standard Reference Database Number 69* (P. J. Linstrom and W. G. Mallard, eds.), Gaithersburg MD, 20899: National Institute of Standards and Technology, 2016. http://webbook.nist.gov, (retrieved July 12, 2016).

[29] B. E. Poling, J. M. Prausnitz, J. P. O'connell, *et al.*, *The properties of gases and liquids*, vol. 5. Mcgraw-hill New York, 2001.

[30] I. T. Todorov, W. Smith, K. Trachenko, and M. T. Dove, "Dl_poly_3: new dimensions in molecular dynamics simulations via massive parallelism," *Journal of Materials Chemistry*, vol. 16, no. 20, pp. 1911–1918, 2006.

[31] L. Martínez, R. Andrade, E. G. Birgin, and J. M. Martínez, "Packmol: a package for building initial configurations for molecular dynamics simulations," *Journal of computational chemistry*, vol. 30, no. 13, pp. 2157–2164, 2009.

[32] G. J. Martyna, D. J. Tobias, and M. L. Klein, "Constant pressure molecular dynamics algorithms," *The Journal of Chemical Physics*, vol. 101, no. 5, pp. 4177–4189, 1994.

[33] G. J. Martyna, M. E. Tuckerman, D. J. Tobias, and M. L. Klein, "Explicit reversible integrators for extended systems dynamics," *Molecular Physics*, vol. 87, no. 5, pp. 1117–1157, 1996.

[34] "Korean thermophysical properties data bank," 2017. https://www.cheric.org/research/kdb/ (accessed Oct 11, 2017).

[35] Design Institute for Physical Properties, 2017, www.aiche.org/dippr.

[36] G. M. Kontogeorgis and G. K. Folas, *Thermodynamic models for industrial applications: from classical and advanced mixing rules to association theories*. John Wiley & Sons, 2009.

[37] M. Obama, Y. Oodera, N. Kohama, T. Yanase, Y. Saito, and K. Kusano, "Densities, molar volumes, and cubic expansion coefficients of 78 aliphatic ethers," *Journal of Chemical and Engineering Data*, vol. 30, no. 1, pp. 1–5, 1985.

[38] M. Safarov, K. Madzhidov, and R. S. Asoev, "Generalized equation of state for liquid simple ethers," *Zhurnal Fizicheskoi Khimii*, vol. 66, no. 10, pp. 2595–2603, 1992.

Chapter 7

Conclusion

In this thesis, interfacial properties of the vapor-liquid interface for a variety of systems are studied using classical density functional theory (DFT) and density gradient theory (DGT). PCP-SAFT is used as the local model for density gradient theory and the Helmholtz energy functional applied in classical density functional theory is also consistent with PCP-SAFT.

Strengths and weaknesses of both models are identified: pure component surface tension is correlated accurately by DGT using constant influence parameters adjusted to experimental surface tension data. Excellent results for mixtures are obtained with the geometric combining rule for the cross-influence parameters as long as the attractive interactions (such as van der Waals attraction, polar interactions, or hydrogen bonds) among the considered substances are sufficiently symmetric. This is demonstrated for several systems including multicomponent model reservoir fluids and mixtures of polar refrigerants. Problems arise for mixtures of components with strongly differing attractive interactions. This is the case e.g. for alkane-alcohol mixtures where alkane molecules only exhibit attractive interactions of the van der Waals type while alcohol compounds also form hydrogen bonds. Depending on the algorithm applied to solve the Euler-Lagrange equations of density gradient theory, no or inaccurate surface tension results are obtained over a wide concentration range and unphysically steep gradients can occur in the interfacial density profiles. It is shown that the introduction of a binary correction parameter in the combining rule for the cross influence parameters, which is adjusted to mixture surface tension data, only has a marginal positive impact on surface tension results for the studied systems and does not solve the problems arising for alkane-alcohol mixtures.

Classical density functional theory is a purely predictive approach to determine interfacial properties which requires no adjustable parameter such as the influence parameter of density gradient theory. For most studied systems, surface tension results predicted by DFT are remarkably accurate and deviations to experimental data are similar to values of density gradient theory. This is true for pure components as well as multicomponent

mixtures of non-associating compounds. Pure associating compounds such as alcohols, amines or water are the only type of molecules for which significant differences occur between DFT predictions and DGT correlations of surface tension. Surface tension obtained from classical density functional theory shows a systematic overprediction of experimental results. On the other hand, DFT does not suffer from the same shortcomings as density gradient theory for mixtures including associating and non-associating compounds such as alkane-alcohol systems. Despite the larger deviations for the pure alcohol, average deviations for many binary alcohol-alkane mixtures are lower for classical density functional theory than for density gradient theory. The proposed explanation for the increasing deviations for DFT surface tension predictions for associating compounds, the insufficient description of the orientation of hydrogen bonds forming molecules at the vapor-liquid interface, has to be further investigated e.g. by explicitly treating the orientation of a molecule as a further degree of freedom.

The group-contribution classical density functional theory developed in this work allows predicting surface tension also for compounds for which not enough experimental data for bulk properties is available to adjust component-specific equation of state parameters. Very accurate surface tension predictions are obtained from this group-contribution DFT. The practical use of this approach is demonstrated e.g. for biodiesel systems where no component-specific equation of state parameters can be regressed for most molecules due to missing experimental data. Furthermore, a detailed picture of the interface can be obtained from the group-contribution DFT because density profiles are determined for the individual functional groups that make up the molecules. This allows to study the orientation of molecules made up of distinct functional groups at the interface. For 1-alcohols, the model predicts a pronounced orientation of the hydroxyl group towards the liquid phase which is in line with experimental and molecular dynamics studies. The additional degree of freedom that allows distinguishing between density profiles of individual functional groups of a given molecule across the interface also has a positive impact on the accuracy of surface tension predictions for hydrogen-bonding compounds: for 1-alcohols and mixtures thereof, deviations are notably reduced compared to the non-group-contribution DFT.

A drawback of classical density functional theory compared to density gradient theory is the increased computational demand which limits its applicability in process simulations. Efficient algorithms are identified in this work which significantly speed up the calculations compared to the simple and frequently applied Picard iteration. However, especially for systems including associating compounds, DFT still requires considerably longer computation time than DGT. A possible remedy in this special case may be to simultaneously solve for the fraction of non-bonded association sites and the density profile instead of solving for the fraction of non-bonded association sites in an inner loop for

every intermediate iterate of the density profile. The extensive use of fast Fourier transformation to calculate the convolution integrals appearing in the equations of classical density functional theory offers further potential to increase computational performance which was not exploited in this work.

Appendices

Appendix A

Supporting Information to Chapter 4

A.1 Numerical aspects to calculate the equilibrium density profile using the stabilized DGT algorithm

In the stabilized DGT algorithm, the following equation has to be integrated in time until the steady-state solution is reached

$$\frac{\partial \rho_i}{\partial t} + \mu_{i,0}(\{\rho_k\}) - \mu_i = \sum_j^N c_{ij} \frac{\partial^2 \rho_j}{\partial z^2} \tag{A.1}$$

To speed up simulations, we follow [1] and [2] and decompose $\mu_{i,0}(\{\rho_k\})$ in a convex part (including the ideal gas and all repulsive contributions) that is integrated in time using an implicit Euler method and a concave part (including all attractive contributions) for which an explicit Euler method is applied. In contrast to [2], we do not start from a linear density profile but use the same initial profiles as for the DFT calculations as presented in [3] [Chapter 3] which usually is an excellent starting point for the calculation. Discretizing eq. A.1 in time and space as presented in [2] yields

$$f_{i,k} = \rho_{i,k}^{n+1} - \Delta t \sum_j^N c_{ij} \frac{\rho_{j,k-1}^{n+1} - 2\rho_{j,k}^{n+1} + \rho_{j,k+1}^{n+1}}{\Delta z^2} + \Delta t \mu_{i,0}^{convex}(\rho_{1,k}^{n+1}, ..., \rho_{N,k}^{n+1}) + \Delta t \mu_{i,0}^{concave}(\rho_{1,k}^{n}, ..., \rho_{N,k}^{n}) - \Delta t \mu_i - \rho_{i,k}^{n} = 0 \tag{A.2}$$

where $i = 1, ..., N$ denotes the component index and $k = 1, ..., n_z$ denotes a certain grid point in the interface. Eq. A.2 has to be solved at every time step n to obtain the density profile at the next time step $n + 1$. We use Newton's method to this end and exploit the structure of the Jacobi matrix J: the residual $f_{i,k}$ depends on the unknown new densities

ρ_i^{n+1} of all components at grid points $k-1, k, k+1$. J thus has a banded structure with $2N-1$ lower and upper diagonals. To increase performance, only the entries of J on these lower and upper diagonals are computed and stored. The single entries of J are approximated using finite-differences. To solve the system of linear equations at every Newton iteration, we apply the LAPACK [4] routine DGBSV that is specifically designed for matrices with a banded structure. Undamped Newton updates performed best in our calculations. Therefore, no line search or trust region algorithm is used to control the solution update and always the whole Newton step is accepted. A simple strategy is adopted to adjust the step length Δt during calculation: at every time step n, we allow 10 Newton iterations to reach a specified tolerance of $||f||_2 = 10^{-8}$. If this tolerance is reached in 8 successive time steps, Δt is increased by a factor of 1.4. If the tolerance is not met at a given time step, Δt is reduced to half its size and the calculation for this time step is repeated. The initial value of Δt is set to 10^{-4} and during calculation it levels off at values between 10^{-2} to 10^{-1}. These parameter values did not undergo any optimization but proved suitable in all calculations. A calculation is considered converged, once two successive density profiles differ (measured by the Euclidean norm) by less than 10^{-14} or a maximal number of time steps is reached (set to 2000 in this work). To ensure that the steady-state solution is found with these settings, results with $\beta_{ij} = 0$ are compared to corresponding results obtained with the DGT path function approach.

Table A.1 shows the required computation time of DFT and both DGT algorithms for three different mixtures. The binary mixture ethanol and hexane requires the evaluation of associative contributions, which increases computation time, especially for DFT (see [3] [Chapter 3] for an explanation). Polar contributions on the other hand do not increase computation time significantly as the results of the four-component mixture reveal. The long computation time of the stabilized DGT approach for the seven-component mixture can be attributed to the fact that the tolerance for two successive density profiles to stop the calculation cannot be satisfied anymore and the calculation runs for the complete 2000 time steps. Alternative convergence criteria that take the number of components into account or use the change of surface tension between successive time steps may be more appropriate in this case.

A.2 Impact of the size of the computation domain on surface tension results

In DFT calculations as well as for the stabilized DGT algorithm, the size of the computation domain D has to be set a priori. As fig. A.1 shows, surface tension results are not sensitive to the value of D over a wide range of values.

Table A.1: Computation time in seconds for three different mixtures: the binary mixture ethanol and hexane at $T = 298.15$ K and a liquid composition of $x_{hexane} = 0.4$, the quaternary mixture consisting of R32, R125, R134a and R143a at $T = 248.15$ K and a specified liquid composition ($x_{R134a} = 0.2$, $x_{R125} = 0.14112$, $x_{R32} = 0.37673$, $x_{R143a} = 0.28215$) as well as a seven-component mixture (methane, ethane, propane, butane, heptane, toluene and methylcycylohexane) at $T = 283.15$ K and $p = 40$ bar. In the DFT and stabilized DGT calculations, the computation domain is discretized using $n_z = 1000$ grid points. In the calculations with the path function DGT approach, the variable s is discretized using $n_s = 1000$ points. The calculation time is averaged over ten calculations.

N	DFT	DGT path fcn.	Stab. DGT
2	94.90	0.09	62.01
4	15.42	0.38	34.37
7	26.79	0.49	262.63

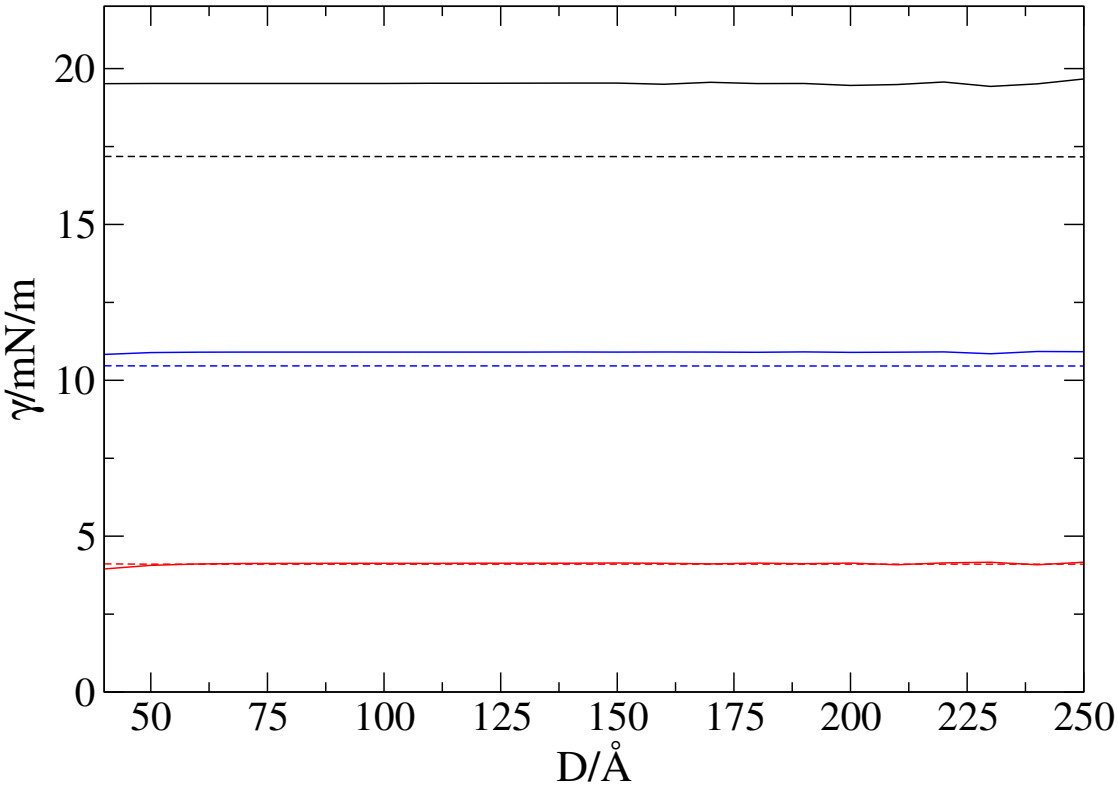

Figure A.1: Surface tension results from DFT (solid lines) as well as from the stabilized DGT algorithm (dashed lines) as a function of the size of the computation domain D for three different systems: the binary mixture n-hexane - ethanol at $T = 298.15$ K and $p = 0.236$ bar, ($x_{hexane} = 0.222$) with $k_{ij} = 0.02854$ (black), a seven-component alkane mixture with overall composition as presented in table A.2 at $T = 255.37$ K and $p = 20$ bar (all $k_{ij} = 0$) (blue) and the binary mixture n-heptane - nitrogen at $T = 393.15$ K and $p = 200$ bar using $k_{ij} = 0.0930$. All β_{ij} are set to 0 in calculations with the stabilized DGT algorithm. In all calculations, the number of discretization points is fixed to $n_z = 1000$.

A.3 Results for 1-alcohols

The following figures show surface tension results of DFT (solid lines) and DGT (dashed lines) for 1-alcohols from methanol to 1-decanol. The pure component PCP-SAFT parameters are taken from Gross and Sadowski [5] (black lines) and Kontogeorgis et al. [6] (blue lines, only DFT results).

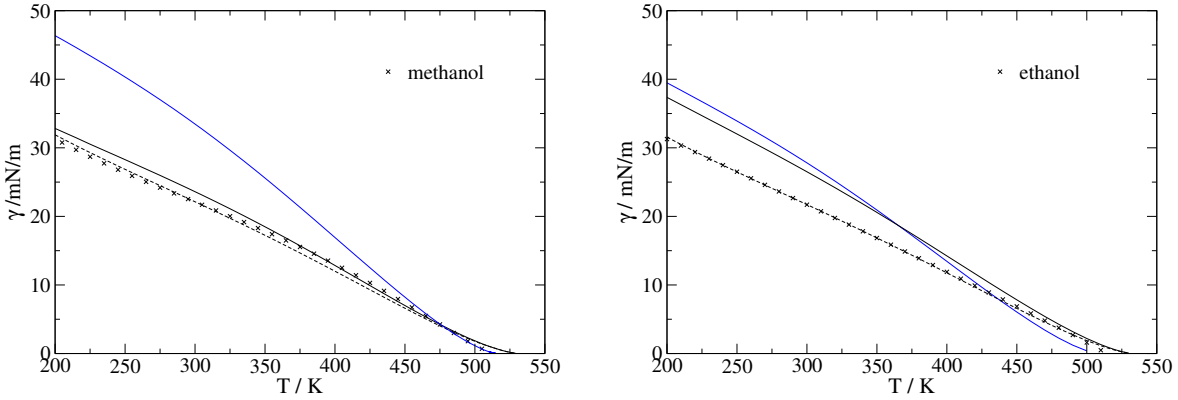

Figure A.2: Calculated surface tension results (DFT: solid lines, DGT: dashed lines) and reference data for methanol (a) and ethanol (b). Reference data is taken from [7] (methanol) and [8] (ethanol). The blue lines represent DFT results obtained with PCP-SAFT parameters of [6], the remaining results are obtained using PCP-SAFT parameters of [5].

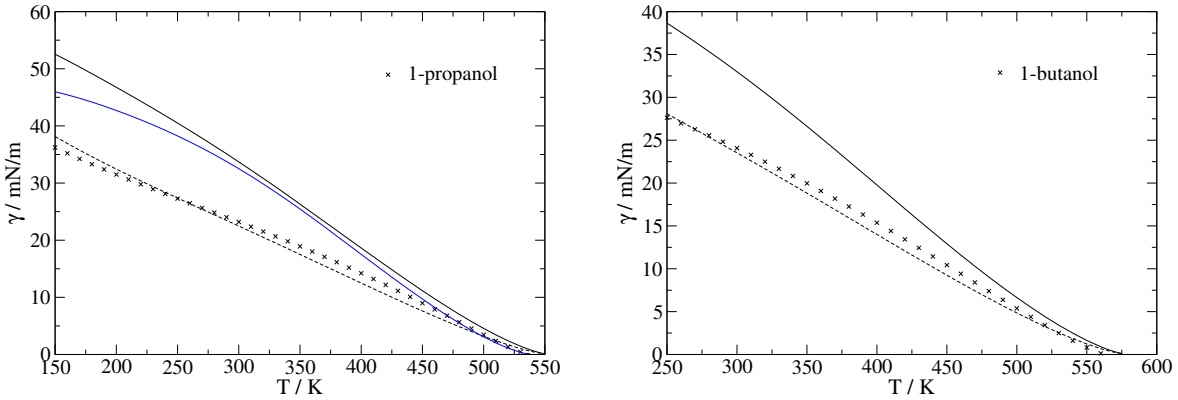

Figure A.3: Calculated surface tension results (DFT: solid lines, DGT: dashed lines) and reference data [9] for 1-propanol (a) and 1-butanol (b). The blue lines represent DFT results obtained with PCP-SAFT parameters of [6], the remaining results are obtained using PCP-SAFT parameters of [5].

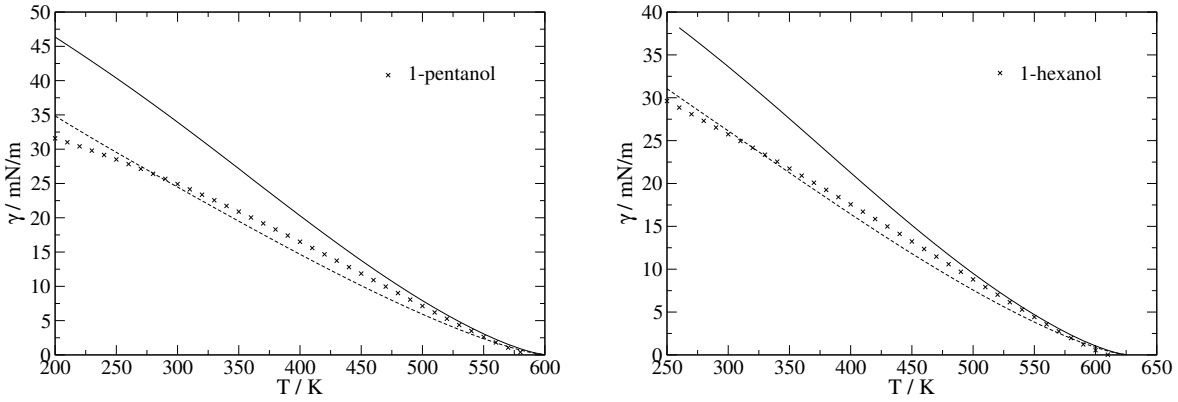

(a) (b)

Figure A.4: Calculated surface tension results (DFT: solid lines, DGT: dashed lines) and reference data [9] for 1-pentanol (a) and 1-hexanol (b).

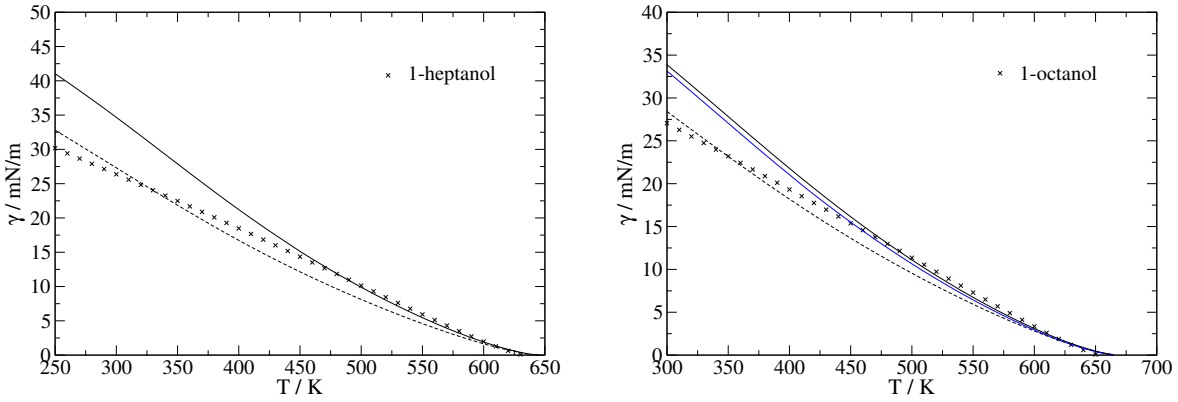

(a) (b)

Figure A.5: Calculated surface tension results (DFT: solid lines, DGT: dashed lines) and reference data [9] for 1-heptanol (a) and 1-octanol (b). The blue lines represent DFT results obtained with PCP-SAFT parameters of [6], the remaining results are obtained using PCP-SAFT parameters of [5].

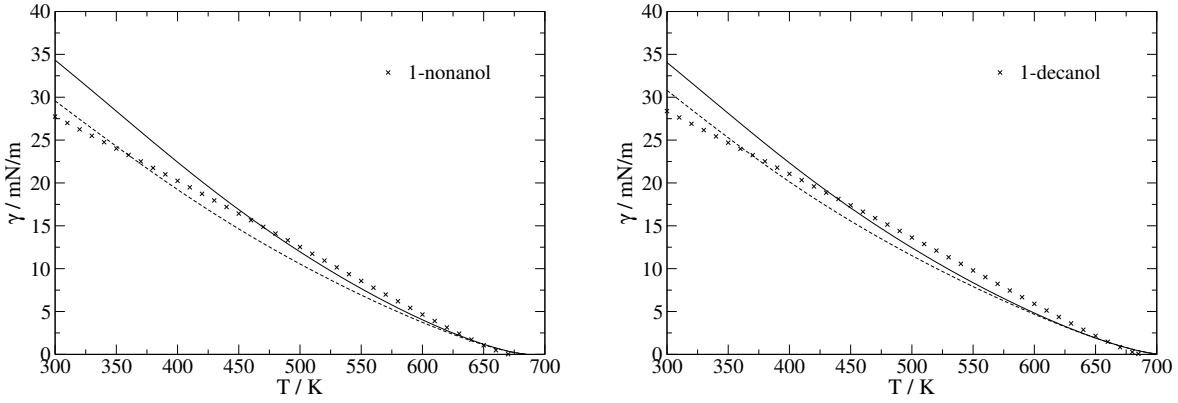

(a) (b)

Figure A.6: Calculated surface tension results (DFT: solid lines, DGT: dashed lines) and reference data [9] for 1-nonanol (a) and 1-decanol (b).

A.4 Correlations of deviations for calculated surface tension with further properties

Figures A.7 and A.8 show the deviations of calculated surface tension values as function of the average errors for vapor pressure p^s, liquid density ρ^l and critical temperature T_c for the compounds studied in this work.
For DFT (DGT) results, the coefficients of determination take on values of $R^2 = 0.09$ (0.28) for the correlation of errors in surface tension γ and errors in p^s, $R^2 = 0.04$ (0.02) for errors in γ and ρ^l and $R^2 = 0.31$ (0.18) for errors in γ and T_c. Furthermore, fig. A.9 visualizes the correlation of deviations of DFT and DGT. The coefficient of determination for this correlation is $R^2 = 0.44$.

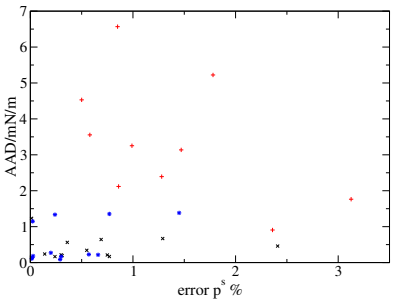

(a)

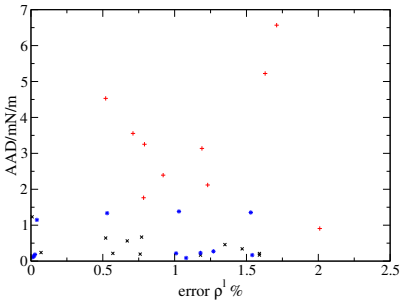

(b)

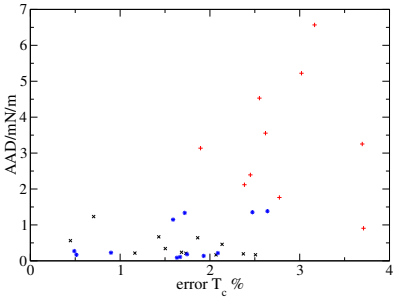

(c)

Figure A.7: Correlations of the average absolute deviation (AAD) for surface tension calculated by DFT with the average error of vapor pressure p^s, liquid density ρ^l and critical temperature T_c for all compounds of this study except water (black crosses: non-polar, non-associating compounds, blue stars: polar compounds, red plus-signs: associating compounds). The average errors of p^s and ρ^l are taken from the original studies where the PCP-SAFT parameters were published.

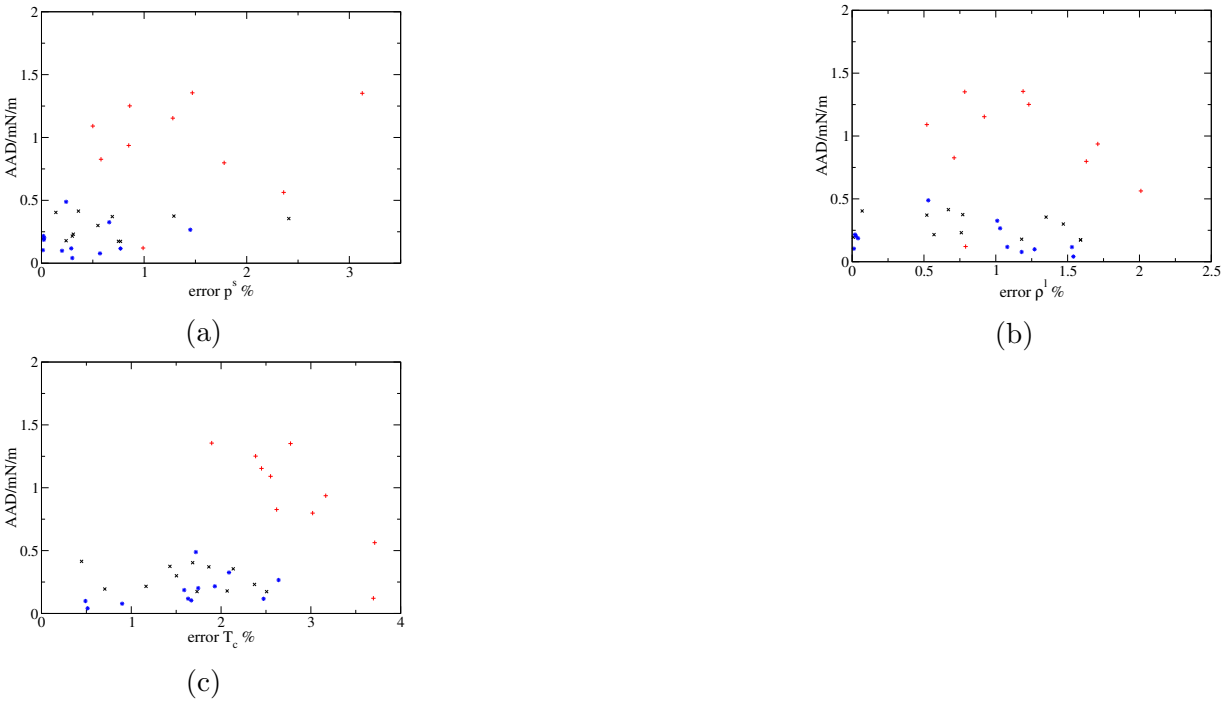

Figure A.8: Correlations of the average absolute deviation (AAD) for surface tension calculated by DGT with the average error of vapor pressure p^s, liquid density ρ^l and critical temperature T_c for all compounds of this study except water (black crosses: non-polar, non-associating compounds, blue stars: polar compounds, red plus-signs: associating compounds). The average errors of p^s and ρ^l are taken from the original studies where the PCP-SAFT parameters were published.

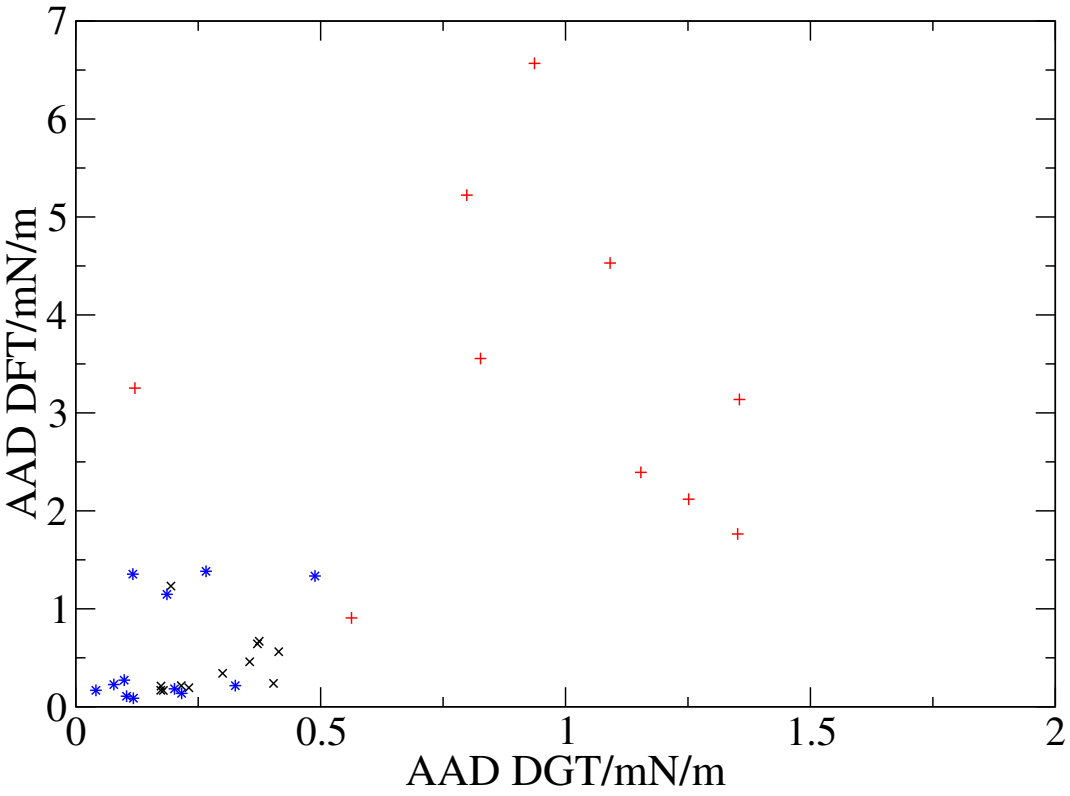

Figure A.9: Correlation of the average absolute deviation (AAD) calculated with DFT and DGT for all compounds of this study except water (black crosses: non-polar, non-associating compounds, blue stars: polar compounds, red plus-signs: associating compounds).

A.5 Alkane mixtures

Figure A.10 shows surface tension results obtained with the stabilized DGT algorithm and different values of β_{ij} for the mixture n-heptane-eicosane at $T = 313.15$ K as a function of the mole fraction of n-heptane in the liquid phase.

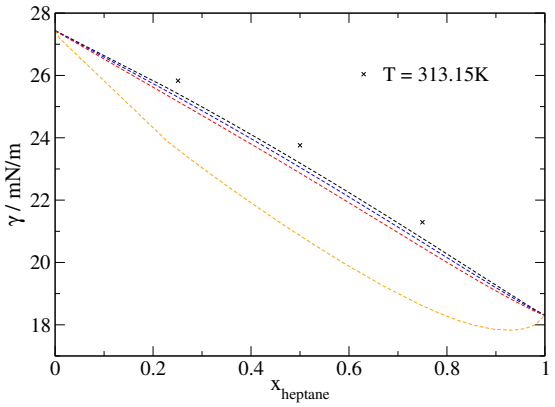

Figure A.10: Surface tension results of the mixture n-heptane-eicosane at $T = 313.15$ K as a function of the mole fraction of n-heptane in the liquid phase obtained with the stabilized DGT algorithm (dashed lines) for different values of β_{ij}: 0 (black), 0.05 (blue), 0.1 (red) and 0.5 (orange). Experimental data (symbols) from [10].

Figure A.11 shows the progression of the value of surface tension for the mixture n-heptane-eicosane at $T = 343.15$ K and $p = 0.1$ bar obtained with the stabilized DGT algorithm for $\beta_{ij} = 0$ and $\beta_{ij} = -0.0001$. For $\beta_{ij} = 0$, the matrix of the influence parameters C is positive definite (eigen values: $5.403 \cdot 10^{-35}$ and $4.253 \cdot 10^{-18}$) while for $\beta_{ij} = -0.0001$ C is not positive definite (eigen values: $-8.718 \cdot 10^{-23}$ and $4.253 \cdot 10^{-18}$). As fig. A.11 shows, the calculation using $\beta_{ij} = 0$ reaches the steady-state solution, indicated by a value of γ that is constant over time, fast. Using $\beta_{ij} = -0.0001$, the calculation shows an almost identical behaviour at the beginning. However, after the value of γ has plateaued for some time at a similar value as obtained with $\beta_{ij} = 0$, surface tension takes another course and converges to a much higher value of γ. Considering that a value of $\beta_{ij} = +0.0001$ leads to a value of $\gamma = 22.5439$ mN/m which is almost identical to the value of $\beta_{ij} = 0$ ($\gamma = 22.544$ mN/m), the result obtained with $\beta_{ij} = -0.0001$ ($\gamma = 24.051$ mN/m) is unexpectedly high. This shows, that in the case of n-heptane-eicosane, ignoring the restriction of positive definiteness of C leads to undesirable results.

Fig. A.12 shows surface tension results for the seven-component mixture obtained with the DGT path function approach as well as the stabilized DGT algorithm. Results of both DGT algorithms are practically identical for $\beta_{ij} = 0$ (fig. A.12a). This confirms that calculations with the stabilized DGT algorithm were indeed carried out long enough to arrive at the steady-state solution. Figure A.12b shows the progression of the value of

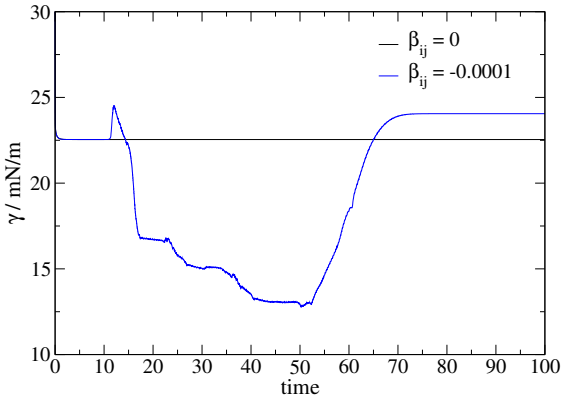

Figure A.11: Progression of surface tension γ during calculation for the mixture n-heptane-eicosane at $T = 343.15$ K and $p = 0.1$ bar obtained with the stabilized DGT algorithm for $\beta_{ij} = 0$ (black) and $\beta_{ij} = -0.0001$ (blue).

Table A.2: Molar overall compositions (%) of the twenty-component mixture studied by Danesh et al. [11] and the seven-component mixture studied by Ng et al. [12].

Component	$N = 20$	$N = 7$
Methane	80.11	67.670
Ethane	8.23	19.171
Propane	2.11	7.683
Butane	1.07	3.880
Pentane	0.80	-
Hexane	1.20	-
Heptane	0.96	0.532
Octane	0.55	-
Nonane	0.49	-
Decane	0.48	-
Undecane	0.45	-
Dodecane	0.44	-
Tridecane	0.44	-
Tetradecane	0.41	-
Pentadecane	0.41	-
Hexadecane	0.39	-
Heptadecane	0.38	-
Octadecane	0.37	-
Nonadecane	0.36	-
Eicosane	0.35	-
Methylcyclohexane	-	0.531
Toluene	-	0.533

γ during calculation with the stabilized DGT algorithm. Eventhough C is not positive definite even for $\beta_{ij} = 0$, no numerical problems occur. Fig. A.13 shows the corresponding results for the twenty-component mixture. Despite the fact that C is not positive definite for $\beta_{ij} = 0$ (half of the eigen values are negative), no numerical problems arise in the

calculation of the stabilized DGT algorithm, see fig. A.13b. However, at high pressure values, the two DGT algorithms do not yield the same surface tension results anymore (fig. A.13a). Increasing computation time or setting stricter convergence criteria does not resolve the issue.

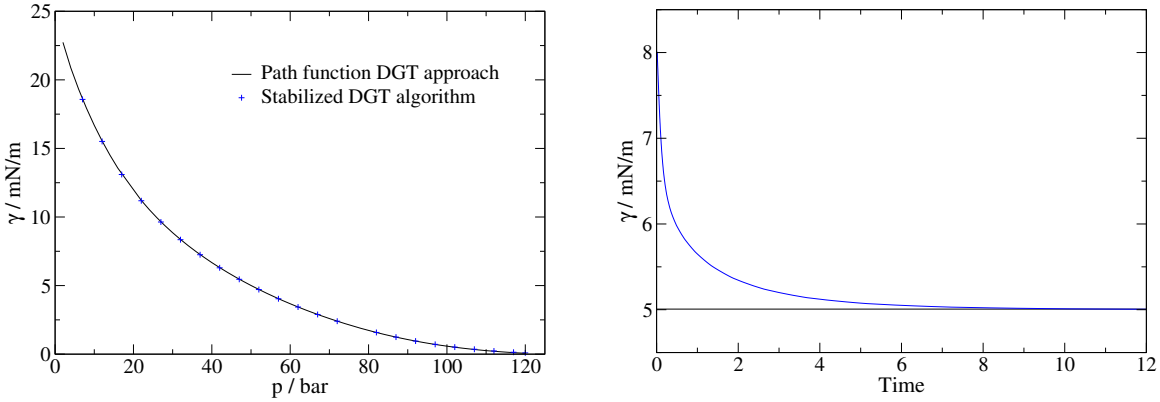

(a) (b)

Figure A.12: Diagram (a): results of surface tension γ for the seven-component mixture at $T = 283.15$ K as a function of pressure obtained with the path function approach (black line) and the stabilized DGT algorithm (blue symbols) using $\beta_{ij} = 0$. Diagram (b): progression of γ during calculation for the seven-component mixture at $T = 283.15$ K and $p = 50$ bar obtained with the stabilized DGT algorithm for $\beta_{ij} = 0$ (blue). As a reference, the value of γ obtained with the path function approach (black) is shown.

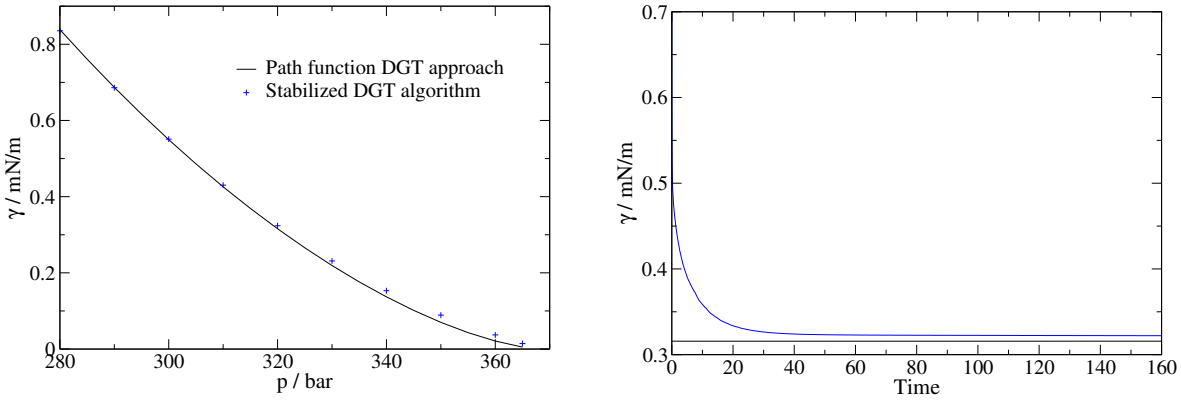

(a) (b)

Figure A.13: Diagram (a): results of surface tension γ for the twenty-component mixture at $T = 366.45$ K as a function of pressure obtained with the path function approach (black line) and the stabilized DGT algorithm (blue symbols) using $\beta_{ij} = 0$. Diagram (b): progression of γ during calculation for the twenty-component mixture at $T = 366.45$ K and $p = 320$ bar obtained with the stabilized DGT algorithm for $\beta_{ij} = 0$ (blue). As a reference, the value of γ obtained with the path function approach (black) is shown.

A.6 Mixtures with one associating component

Figure A.14 shows the variation of surface tension obtained with the stabilized DGT algorithm with the value of β_{ij} for the mixture hexane-ethanol. Initially, values $\beta_{ij} > 0$ lead to decreasing deviations. However, once a certain value is passed, errors start to grow. The value of β_{ij} which minimizes the sum of squared errors is found to be $\beta_{ij} = 0.07646$.

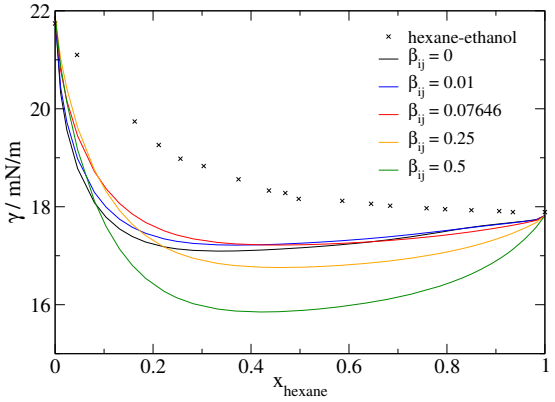

Figure A.14: Surface tension as a function of hexane mole fraction in the liquid phase for the mixture hexane-ethanol at $T = 343.15$ K using the stabilized DGT algorithm (lines). Experimental data (symbols) from [13].

Figure A.15 exemplifies the course of surface tension γ during calculation with the stabilized DGT algorithm for different values of β_{ij} for the mixture hexane-ethanol. For $\beta_{ij} = 0$ and $\beta_{ij} = 0.05$ the matrix of influence parameters C is positive definite and γ smoothly approaches its steady-state value. For $\beta_{ij} = -0.001$, on the other hand, C is not positive definite and the progression of γ resembles the one of the mixture n-heptane-eicosane with $\beta_{ij} = -0.0001$ shown in fig. A.11. However, in this case, no constant value of γ is attained. Thus, the violation of the requirement of a positive definite C leads to a failed calculation.

Figures A.16 to A.21 show surface tension results as a function of mole fraction of n-hexane in the liquid phase x_{hexane} and density profiles obtained with DFT and the path function approach for DGT for binary mixtures of n-hexane with 1-alcohols at $T = 298.15$ K.

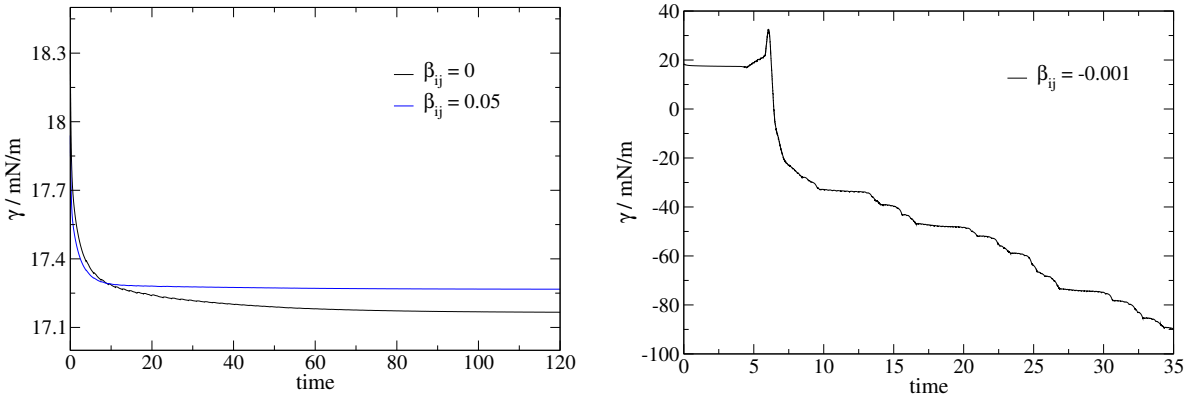

(a) (b)

Figure A.15: Development of surface tension γ during calculation for the mixture ethanol-hexane at $T = 298.15$ K and $x_{hexane} = 0.507$ ($p = 0.254$ bar) obtained with the stabilized DGT algorithm. Diagram (a): using $\beta_{ij} = 0$ (black) and $\beta_{ij} = 0.05$ (blue). Diagram (b): using $\beta_{ij} = -0.001$.

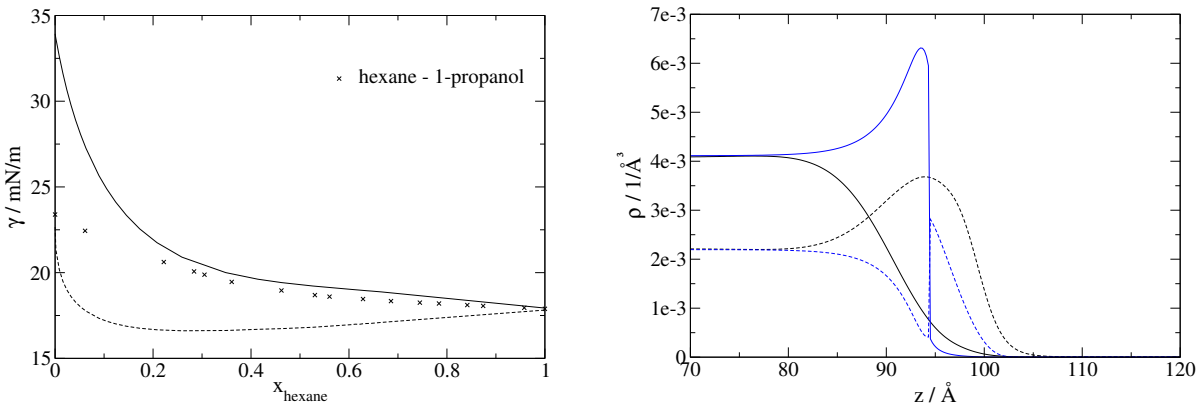

(a) (b)

Figure A.16: Diagram (a): calculated results of surface tension (DFT: solid lines, DGT path function approach: dashed lines) and experimental data [13] (symbols) for the binary mixtures n-hexane - 1-propanol ($k_{ij} = 0.0162233$). Diagram (b): density profiles for the mixtures hexane (dashed lines) and 1-propanol (solid lines) at $x_{hexane} = 0.348$ ($p = 0.19$ bar) obtained from DFT (black) and DGT (blue).

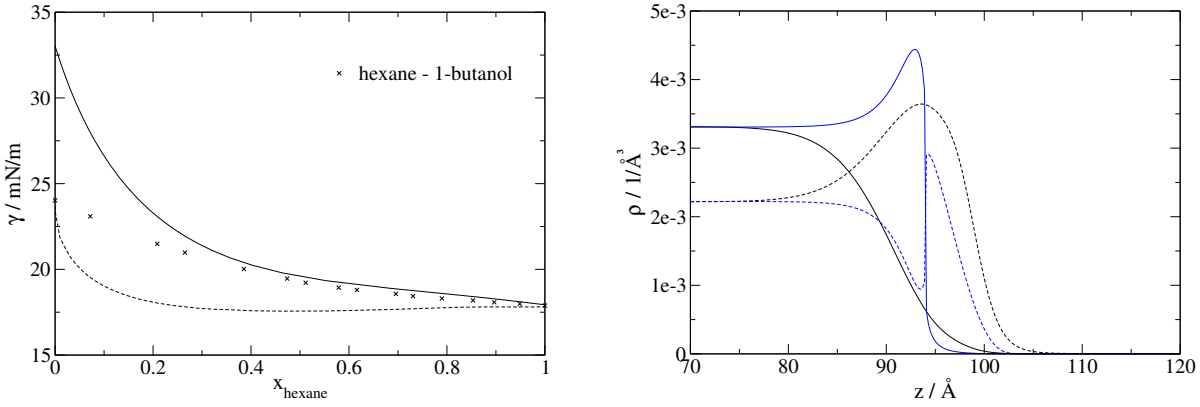

(a) (b)

Figure A.17: Diagram (a): calculated results of surface tension (DFT: solid lines, DGT path function approach: dashed lines) and experimental data [13] (symbols) for the binary mixtures n-hexane - 1-butanol ($k_{ij} = 0.010689$). Diagram (b): density profiles for the mixtures hexane (dashed lines) and 1-butanol (solid lines) at $x_{hexane} = 0.402$ ($p = 0.175$ bar) obtained from DFT (black) and DGT (blue).

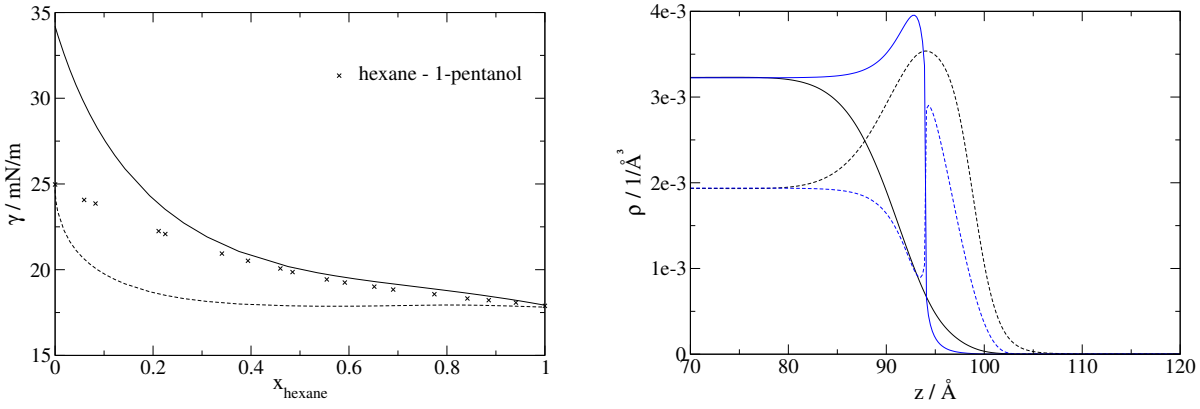

(a) (b)

Figure A.18: Diagram (a): calculated results of surface tension (DFT: solid lines, DGT path function approach: dashed lines) and experimental data [13] (symbols) for the binary mixtures n-hexane - 1-pentanol ($k_{ij} = 0.010754$). Diagram (b): density profiles for the mixtures hexane (dashed lines) and 1-pentanol (solid lines) at $x_{hexane} = 0.375$ ($p = 0.16$ bar) obtained from DFT (black) and DGT (blue).

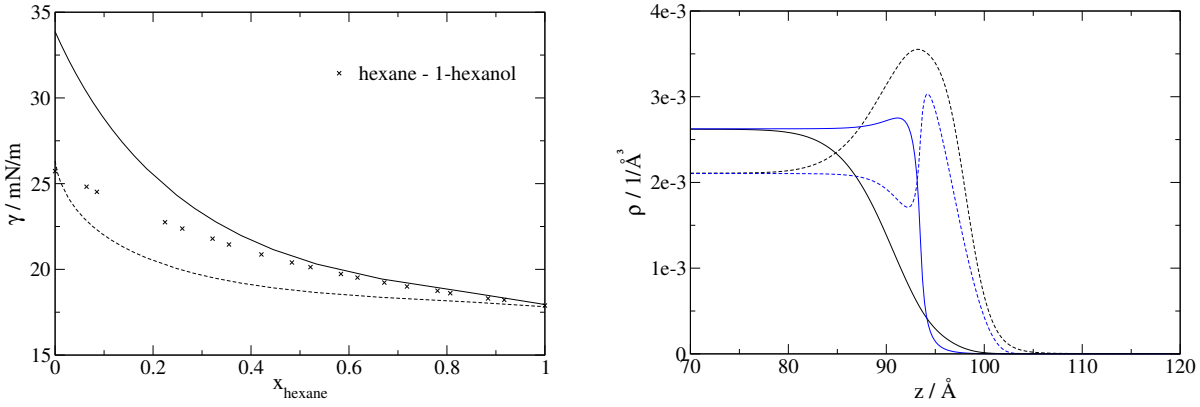

(a) (b)

Figure A.19: Diagram (a): calculated results of surface tension (DFT: solid lines, DGT path function approach: dashed lines) and experimental data [13] (symbols) for the binary mixtures n-hexane - 1-hexanol ($k_{ij} = 0.0051568$). Diagram (b): density profiles for the mixtures hexane (dashed lines) and 1-hexanol (solid lines) at $x_{hexane} = 0.445$ ($p = 0.16$ bar) obtained from DFT (black) and DGT (blue).

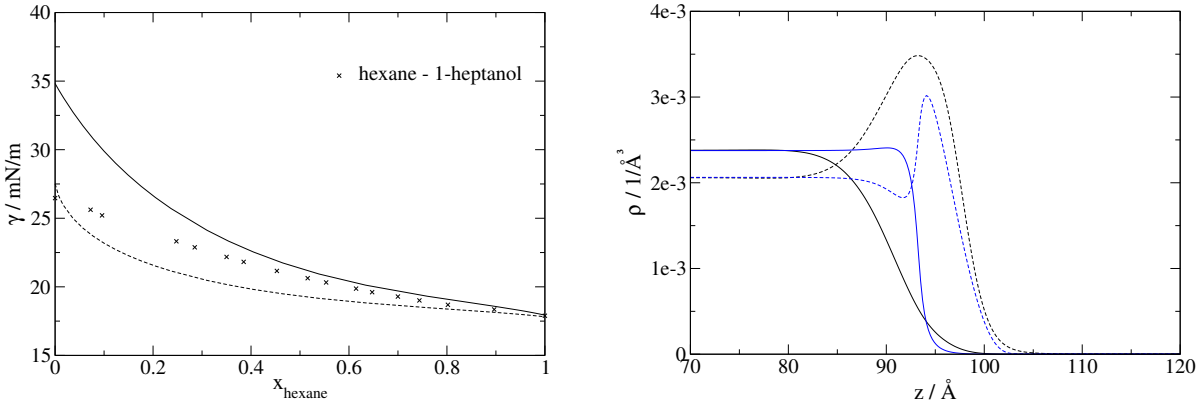

(a) (b)

Figure A.20: Diagram (a): calculated results of surface tension (DFT: solid lines, DGT path function approach: dashed lines) and experimental data [13] (symbols) for the binary mixtures n-hexane - 1-heptanol ($k_{ij} = 0$). Diagram (b): density profiles for the mixtures hexane (dashed lines) and 1-heptanol (solid lines) at $x_{hexane} = 0.465$ ($p = 0.15$ bar) obtained from DFT (black) and DGT (blue).

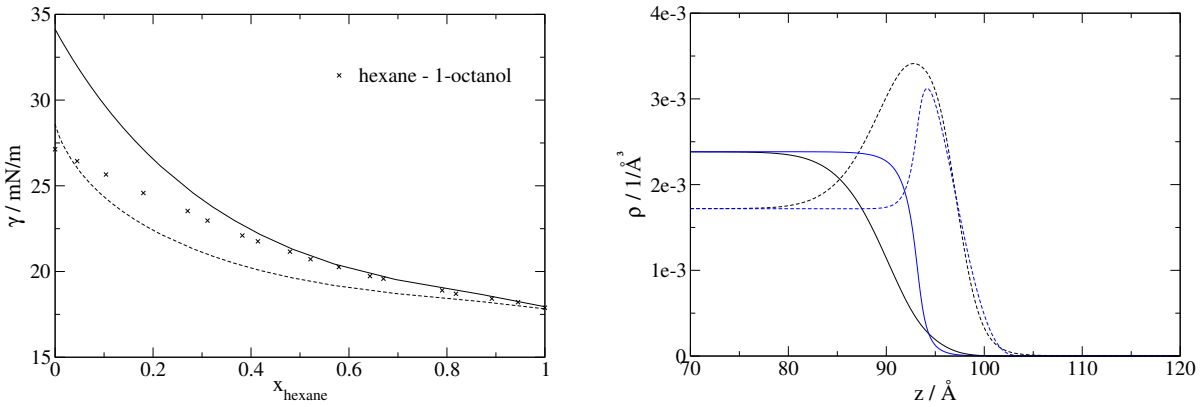

(a) (b)

Figure A.21: Diagram (a): calculated results of surface tension (DFT: solid lines, DGT path function approach: dashed lines) and experimental data [13] (symbols) for the binary mixtures n-hexane - 1-octanol ($k_{ij} = 0.006435$). Diagram (b): density profiles for the mixtures hexane (dashed lines) and 1-octanol (solid lines) at $x_{hexane} = 0.419$ ($p = 0.15$ bar) obtained from DFT (black) and DGT (blue).

A.7 PCP-SAFT parameters and influence parameters

Table A.3: Values of PCP-SAFT parameters and influence parameters for n-alkanes. All PCP-SAFT parameters are taken from [14].

Compound	m	σ/Å	ϵ/k/K	$c_{ii}/10^{-19}/Jm^5/mol^2$	T/K	Ref.
methane	1.0000	3.7039	150.03	0.1917554	105 - 180	[7]
ethane	1.6069	3.5206	191.42	0.4972791	105 - 285	[7]
propane	2.0020	3.6184	208.11	1.0300755	100 - 340	[7]
butane	2.3316	3.7086	222.88	1.7228683	150 - 390	[7]
pentane	2.6896	3.7729	231.20	2.5651212	160 - 460	[7]
hexane	3.0576	3.7983	236.77	3.6444985	195 - 495	[7]
heptane	3.4831	3.8049	238.40	4.9391699	200 - 500	[7]
octane	3.8176	3.8373	242.78	6.0933095	230 - 560	[7]
nonane	4.2079	3.8448	244.51	7.5417139	235 - 580	[7]
decane	4.6627	3.8384	243.87	9.3629705	260 - 590	[7]
undecane	4.9082	3.8893	248.82	11.508127	273 - 373	[15] [16]
dodecane	5.3060	3.8959	249.21	13.769134	273 - 473	[15] [17]
tridecane	5.6877	3.9143	249.78	16.4519049	273 - 443	[15] [18]
tetradecane	5.9002	3.9396	254.21	18.2103532	273 - 353	[15]
pentadecane	6.2855	3.9531	254.14	21.5025322	273 - 359	[15] [19]
hexadecane	6.6485	3.9552	254.70	24.1825590	273 - 353	[15]
heptadecane	6.9809	3.9675	255.65	27.5240777	273 - 473	[15] [17]
octadecane	7.3271	3.9668	256.20	30.0556228	273 - 443	[15] [18]
nonadecane	7.7175	3.9721	256.00	33.7122254	293 - 353	[20]
eicosane	7.9849	3.9869	257.75	37.5930577	293 - 353	[21] [20]

Table A.4: Values of PCP-SAFT parameters and influence parameters for non-polar, non-associating compounds.

Compound	m	σ/Å	ϵ/k/K	Ref.	$c_{ii}/10^{-19}/Jm^5/mol^2$	T/K	Ref.
xenon	0.9147	4.0747	237.68	[22]	0.4010264	160 - 289	[9]
isobutane	2.2616	3.7574	216.53	[14]	1.6542057	100 - 400	[9]
1-butene	2.2864	3.6431	222.00	[14]	1.5842637	140 - 420	[9]
cyclopentene	2.2934	3.6668	267.76	[14]	1.8539574	140 - 500	[9]
toluene	2.8149	3.7169	285.69	[14]	3.1517615	220 - 570	[7]
methylcyclohexane	2.6637	3.9993	282.33	[14]	4.1604730	180 - 555	[23]

Table A.5: Values of PCP-SAFT parameters and influence parameters for polar compounds: dipolar molecules.

Compound	m	σ/Å	ϵ/k/K	μ/D	Ref.	$c_{ii}/10^{-19}/Jm^5/mol^2$	T/K	Ref.
dimethylether	2.2634	3.2723	210.29	1.30	[24]	0.6887794	130 - 390	[9]
diethylether	2.9726	3.5127	219.53	1.15	[24]	2.0321485	160 - 460	[9]
methylmethanoate	2.6225	3.1095	239.05	1.77	[24]	0.8275164	293 - 483	[25]
3-pentanone	3.2786	3.5159	248.69	2.82	[24]	2.7213002	294 - 323	[26] [27]
R22	2.4270	3.1535	186.29	1.458	[28]	0.7036013	213 - 353	[29] [30]
R23	2.5795	2.8514	140.64	1.649	[28]	0.3217159	120 - 295	[31]
R32	2.4719	2.7971	161.66	1.978	[28]	0.3062920	222 - 343	[32] [33]
R123	2.9853	3.4812	213.81	1.356	[28]	1.9408674	253 - 423	[32] [34]
R125	3.1105	3.1200	153.70	1.563	[28]	0.9248322	223 - 333	[33]
R134a	3.1470	3.0455	165.34	2.058	[28]	0.8435321	223 - 368	[33] [35]
R143a	2.4819	3.2817	162.10	2.3	[36] [37]	0.8036647	223 - 333	[33]

Table A.6: Values of PCP-SAFT parameters and influence parameters for polar compounds: quadrupolar molecules.

Compound	m	σ/Å	ϵ/k/K	$\lvert Q\rvert$/DÅ	Ref.	$c_{ii}/10^{-20}/Jm^5/mol^2$	T/K	Ref.
nitrogen	1.1879	3.3353	90.99	1.1151	[38]	1.0525907	65 - 120	[39] [40]
carbon dioxide	1.6298	3.0867	163.34	3.9546	[38]	2.7699291	230 - 290	[7]
ethylene	1.5477	3.4475	179.19	1.9155	[38]	4.2424354	110 - 280	[9]
benzene	2.2463	3.7852	296.24	5.5907	[38]	24.4932827	270 - 560	[8]

Table A.7: Values of PCP-SAFT parameters and influence parameters for associating compounds. All PCP-SAFT parameters are taken from [5] (except decanol [36]) and use the 2B association scheme.

Compound	m	σ/Å	ϵ/k/K	$\epsilon^{A_iB_i}/k$/K	$\kappa^{A_iB_i}$	$c_{ii}/10^{-20}$/Jm^5/mol^2	T/K	Ref.
methanol	1.5255	3.2300	188.90	2899.5	0.035176	2.9493507	195-505	[7]
ethanol	2.3827	3.1771	198.24	2653.4	0.32384	5.2806722	200-505	[8]
1-propanol	2.9997	3.2522	233.40	2276.8	0.015268	7.3296870	150-530	[9]
1-butanol	2.7515	3.6139	259.59	2544.6	0.006692	13.0503410	190-560	[9]
1-pentanol	3.6260	3.4508	247.28	2252.1	0.010319	17.9404645	200-580	[9]
1-hexanol	3.5146	3.6735	262.32	2538.9	0.005747	28.1068925	240-610	[9]
1-heptanol	4.3985	3.5450	253.46	2878.5	0.001155	37.2780311	260-630	[9]
1-octanol	4.3555	3.7145	262.74	2754.8	0.002197	53.8963851	270-670	[9]
1-nonanol	4.6839	3.7292	263.64	2941.9	0.001427	67.5064875	280-685	[9]
1-decanol	5.0949	3.7526	263.36	2979.2	0.000994	91.1880353	280 - 685	[9]

Table A.8: Values of PCP-SAFT parameters and influence parameters for water. All influence parameters are adjusted to pure component surface tension data from NIST [7] in the temperature range 280 K - 640 K.

Set	m	σ/Å	ϵ/k/K	$\epsilon^{A_iB_i}/k$/K	$\kappa^{A_iB_i}$	scheme	Ref.	$c_{ii}/10^{-20}$/Jm^5/mol^2
2B_1	1.0656	3.0007	366.51	2500.70	0.034868	2B	[5]	1.3279471
3B_1	1.7960	2.4697	327.62	1558.40	0.068277	3B	[41]	0.9324370
3B_C	2.3753	2.5609	275.81	1558.40	0.068277	3B	[41]	3.7707134
4C_1	2.0	2.3449	171.67	1704.06	0.159593	4C	[42]	1.2747846
4C_2	2.1945	2.2290	141.66	1804.17	0.2039	4C	[43]	1.4411646
4C_3	0.8148	3.366	388.51	1552.34	0.009634	4C	[44]	1.1389453

Bibliography

[1] Z. Qiao and S. Sun, "Two-phase fluid simulation using a diffuse interface model with peng–robinson equation of state," *SIAM Journal on Scientific Computing*, vol. 36, no. 4, pp. B708–B728, 2014.

[2] X. Mu, F. Frank, F. O. Alpak, and W. G. Chapman, "Stabilized density gradient theory algorithm for modeling interfacial properties of pure and mixed systems," *Fluid Phase Equilibria*, vol. 435, pp. 118–130, 2017.

[3] J. Mairhofer and J. Gross, "Numerical aspects of classical density functional theory for one-dimensional vapor-liquid interfaces," *Fluid Phase Equilibria*, vol. 444, pp. 1–12, 2017.

[4] E. Anderson, Z. Bai, C. Bischof, S. Blackford, J. Demmel, J. Dongarra, J. Du Croz, A. Greenbaum, S. Hammarling, A. McKenney, and D. Sorensen, *LAPACK Users' Guide*. Philadelphia, PA: Society for Industrial and Applied Mathematics, third ed., 1999.

[5] J. Gross and G. Sadowski, "Application of the perturbed-chain SAFT equation of state to associating systems," *Industrial & Engineering Chemistry Research*, vol. 41, no. 22, pp. 5510–5515, 2002.

[6] G. M. Kontogeorgis, I. Tsivintzelis, N. von Solms, A. Grenner, D. Bøgh, M. Frost, A. Knage-Rasmussen, and I. G. Economou, "Use of monomer fraction data in the parametrization of association theories," *Fluid Phase Equilibria*, vol. 296, no. 2, pp. 219–229, 2010.

[7] E. W. Lemmon, M. O. McLinden, and D. G. Friend, "Thermophysical properties of fluid systems," in *NIST Chemistry WebBook, NIST Standard Reference Database Number 69* (P. J. Linstrom and W. G. Mallard, eds.), Gaithersburg MD, 20899: National Institute of Standards and Technology, 2016. http://webbook.nist.gov, (retrieved July 12, 2016).

[8] A. Mulero, I. Cachadiña, and M. Parra, "Recommended correlations for the surface tension of common fluids," *Journal of Physical and Chemical Reference Data*, vol. 41, no. 4, p. 043105, 2012.

[9] G. Somayajulu, "A generalized equation for surface tension from the triple point to the critical point," *International Journal of Thermophysics*, vol. 9, no. 4, pp. 559–566, 1988.

[10] A. J. Queimada, F. A. Silva, A. I. Caço, I. M. Marrucho, and J. A. Coutinho, "Measurement and modeling of surface tensions of asymmetric systems: heptane, eicosane, docosane, tetracosane and their mixtures," *Fluid Phase Equilibria*, vol. 214, no. 2, pp. 211–221, 2003.

[11] A. Danesh, A. Dandekar, A. Todd, R. Sarkar, *et al.*, "A modified scaling law and parachor method approach for improved prediction of interfacial tension of gas-condensate systems," in *SPE Annual Technical Conference and Exhibition*, Society of Petroleum Engineers, 1991.

[12] H. Ng, S. Taylor, H. Schroeder, and D. Sieben, "High pressure gas separation and conditioning," *GPA Research Report, Rep. No. PR-193*, pp. 1–50, 2008.

[13] E. Jiménez, H. Casas, L. Segade, and C. Franjo, "Surface tensions, refractive indexes and excess molar volumes of hexane + 1-alkanol mixtures at 298.15K," *Journal of Chemical & Engineering Data*, vol. 45, no. 5, pp. 862–866, 2000.

[14] J. Gross and G. Sadowski, "Perturbed-chain SAFT: An equation of state based on a perturbation theory for chain molecules," *Industrial & Engineering Chemistry Research*, vol. 40, no. 4, pp. 1244–1260, 2001.

[15] J. J. Jasper, E. R. Kerr, and F. Gregorich, "The orthobaric surface tensions and thermodynamic properties of the liquid surfaces of the nalkanes, c5 to c28," *Journal of the American Chemical Society*, vol. 75, no. 21, pp. 5252–5254, 1953. In Dortmund Data Bank, 2015, www.ddbst.com.

[16] P. P. Pugachevich and Y. A. Khvorov, "The surface tensions of heptane, undecane, hexadecane and their mixtures," *Deposited Doc. VINITI*, vol. 3893–77, pp. 1–14, 1977. In Dortmund Data Bank, 2015, www.ddbst.com.

[17] P. P. Pugachevich and B. B. Zhalsabon, "Experimental determination of surface tension of dodecane, heptadecane and tricosane binary and ternary mixtures in a wide temperature and concentration region," *Deposited Doc. VINITI*, vol. 2644–81, pp. 1–17, 1981. In Dortmund Data Bank, 2015, www.ddbst.com.

[18] P. P. Pugachevich and V. A. Dozorov, "Experimental study of surface tension of decane, tridecane, octadecane and their solutions," *Deposited Doc. VINITI*, vol. 1282–81, pp. 1–34, 1981. In Dortmund Data Bank, 2015, www.ddbst.com.

[19] A. I. Vogel, "38. physical properties and chemical constitution. part IX. aliphatic hydrocarbons," *Journal of the Chemical Society (Resumed)*, pp. 133–139, 1946. In Dortmund Data Bank, 2015, www.ddbst.com.

[20] G. Korosi and E. S. Kovats, "Density and surface tension of 83 organic liquids," *Journal of Chemical and Engineering Data*, vol. 26, no. 3, pp. 323–332, 1981. In Dortmund Data Bank, 2015, www.ddbst.com.

[21] A. J. Queimada, A. I. Caco, I. M. Marrucho, and J. A. Coutinho, "Surface tension of decane binary and ternary mixtures with eicosane, docosane, and tetracosane," *Journal of Chemical & Engineering Data*, vol. 50, no. 3, pp. 1043–1046, 2005. In Dortmund Data Bank, 2015, www.ddbst.com.

[22] V. Vins and V. Vacek, "Effect of gas impurities on the throttling process of fluorocarbon refrigerants: estimation of the henry's law constant," *Journal of Chemical & Engineering Data*, vol. 54, no. 9, pp. 2395–2403, 2009.

[23] K. Stephan and H. Hildwein, "Recommended data of selected compounds and binary mixtures," *Chemistry Data Series Vol. IV, Pts. 1+2, DECHEMA*, 1987. In Surface tension of pure liquids and binary liquid mixtures, M.D. Lechner, Ch. Wohlfarth, B. Wohlfarth, 2015, Springer.

[24] J. Gross and J. Vrabec, "An equation-of-state contribution for polar components: Dipolar molecules," *AIChE Journal*, vol. 52, no. 3, pp. 1194–1204, 2006.

[25] W. Ramsay and J. Shields, "Association in flussigkeiten," *Z. Phys. Chem*, vol. 12, pp. 433–438, 1893. In Dortmund Data Bank, 2015, www.ddbst.com.

[26] K. Owen, O. R. Quayle, and W. J. Clegg, "A study of organic parachors. V. constitutive variations of the parachors of a series of normal ketones1," *Journal of the American Chemical Society*, vol. 64, no. 6, pp. 1294–1296, 1942. In Dortmund Data Bank, 2015, www.ddbst.com.

[27] D. Cowan, G. Jeffery, and A. Vogel *Journal of the Chemical Society London*, pp. 171–176, 1940. In Dortmund Data Bank, 2015, www.ddbst.com.

[28] V. Vinš and J. Hrubỳ, "Solubility of nitrogen in one-component refrigerants: Prediction by PC-SAFT EoS and a correlation of henry's law constants," *International Journal of Refrigeration*, vol. 34, no. 8, pp. 2109–2117, 2011.

[29] R. Heide, "The surface tension of halogenated refrigerants," *Luft-Kaltetech*, vol. 9, pp. 125–127, 1973. In Dortmund Data Bank, 2015, www.ddbst.com.

[30] M. Okada, T. Arima, M. Hattori, and K. Watanabe, "Measurements of the surface tension of three refrigerants, R22, R115, and R502," *Journal of Chemical & Engineering Data*, vol. 33, no. 4, pp. 399–401, 1988. In Dortmund Data Bank, 2015, www.ddbst.com.

[31] V. Zheleznyi and L. Lyasota *Kholod. Tekh. Teknol.*, vol. 40, pp. 53–58, 1985. In Dortmund Data Bank, 2015, www.ddbst.com.

[32] A. Fröba, S. Will, and A. Leipertz, "Saturated liquid viscosity and surface tension of alternative refrigerants," *International Journal of Thermophysics*, vol. 21, no. 6, pp. 1225–1253, 2000. In Dortmund Data Bank, 2015, www.ddbst.com.

[33] R. Heide, "The surface tension of HFC refrigerants and mixtures," *International Journal of Refrigeration*, vol. 20, no. 7, pp. 496–503, 1997.

[34] H. B. Chae, J. W. Schmidt, and M. R. Moldover, "Surface tension of refrigerants R123 and R134a," *Journal of Chemical and Engineering Data*, vol. 35, no. 1, pp. 6–8, 1990. In Dortmund Data Bank, 2015, www.ddbst.com.

[35] G. Zhao, S. Bi, A. P. Fröba, and J. Wu, "Liquid viscosity and surface tension of R1234yf and R1234ze under saturation conditions by surface light scattering," *Journal of Chemical & Engineering Data*, vol. 59, no. 4, pp. 1366–1371, 2014. In Dortmund Data Bank, 2015, www.ddbst.com.

[36] Dortmund Data Bank, 2015, www.ddbst.com.

[37] B. E. Poling, J. M. Prausnitz, J. P. O'connell, *et al.*, *The Properties of Gases and Liquids*, vol. 5. Mcgraw-hill New York, 2001.

[38] J. Gross, "An equation-of-state contribution for polar components: Quadrupolar molecules," *AIChE Journal*, vol. 51, no. 9, pp. 2556–2568, 2005.

[39] V. Baidakov, K. Khvostov, and G. Muratov, "Surface-tension of nitrogen, oxygen and methane in a wide temperature-range," *Zhurnal Fizicheskoi Khimii*, vol. 56, no. 4, pp. 814–817, 1982. In Dortmund Data Bank, 2015, www.ddbst.com.

[40] V. Ostromoukhov and M. Ostronov, "Surface-tension of O2-N2 liquid solutions at 54-77K," *Zhurnal Fizicheskoi Khimii*, vol. 68, no. 1, pp. 39–43, 1994. In Dortmund Data Bank, 2015, www.ddbst.com.

[41] S. Aparicio-Martínez and K. R. Hall, "Phase equilibria in water containing binary systems from molecular based equations of state," *Fluid Phase Equilibria*, vol. 254, no. 1, pp. 112–125, 2007.

[42] X. Liang, I. Tsivintzelis, and G. M. Kontogeorgis, "Modeling water containing systems with the simplified PC-SAFT and CPA equations of state," *Industrial & Engineering Chemistry Research*, vol. 53, no. 37, pp. 14493–14507, 2014.

[43] N. I. Diamantonis and I. G. Economou, "Evaluation of statistical associating fluid theory (SAFT) and perturbed chain-SAFT equations of state for the calculation of thermodynamic derivative properties of fluids related to carbon capture and sequestration," *Energy & Fuels*, vol. 25, no. 7, pp. 3334–3343, 2011.

[44] G. M. Kontogeorgis, I. Tsivintzelis, N. von Solms, A. Grenner, D. Bøgh, M. Frost, A. Knage-Rasmussen, and I. G. Economou, "Use of monomer fraction data in the parametrization of association theories," *Fluid Phase Equilibria*, vol. 296, no. 2, pp. 219–229, 2010.

Appendix B

Supporting Information to Chapter 5

B.1 Group parameters of heterosegmented GC-PCP-SAFT

Table B.1 lists the group parameters of the heterosegmented GC-PCP-SAFT equation of state used in this study.

Table B.1: The GC-PCP-SAFT group parameters used in this study are taken from [1]. For all associating groups the 2B scheme according to Huang and Radosz [2] is applied.

	m	σ/Å	ϵ/k/K	μ/D	$\epsilon^{A_iB_i}/k$/K	$\kappa^{A_iB_i}$
CH_4	1	3.7039	150.03	-	-	-
-CH_3	0.77247	3.6937	181.49	-	-	-
-CH-$_2$	0.79120	3.0207	157.23	-	-	-
=CH_2	0.70581	3.1630	171.34	-	-	-
=CH-	0.90182	2.8864	158.90	-	-	-
-C $\equiv$ CH	1.16145	3.3187	255.13	-	-	-
-COO-	1.28692	3.0643	273.90	3.343	-	-
-CH=O	1.18893	3.2948	316.91	2.413	-	-
-OCH2-	1.18167	3.0090	203.11	2.695	-	-
-OH	1.02306	2.7702	334.29	-	0.009583	2575.88
-NH_2	0.82284	3.1129	309.93	-	0.005769	1471.51

B.2 Individualization parameters ϕ_i

The values of the individualization parameter ϕ_i for compounds used in this study are listed in tables B.2 and B.3. Where no experimental vapor pressure data was available to regress ϕ_i, the value is set to $\phi_i = 1$.

Table B.2: Individualization parameters ϕ_i for n-alkanes, 1-alkenes, 1-alkines, 1-amines and 1-alcohols.

compound	ϕ_i	compound	ϕ_i	compound	ϕ_i
n-alkanes		tetratetracontane	1	1-octyne	0.9988576024
methane	1.0001236	hexatetracontane	1	1-nonyne	0.9994595774
ethane	1.0021311962	hexacontane	1	1-decyne	0.9986231443
propane	0.999097438	1-alkenes		1-undecyne	1.0012472422
butane	0.9994940843	ethylene	1.0329715013	1-dodecyne	1.0022541343
pentane	0.9993240124	propylene	1.0005207425	1-tridecyne	1.0031051651
hexane	0.9983601914	1-butene	0.9985810621	1-amines	
heptane	0.9985191669	1-pentene	1	methylamine	1.0377797572
octane	0.9988058205	1-hexene	1.0019685062	ethylamine	0.9940089521
nonane	0.9989212181	1-heptene	1.0025504004	1-propylamine	0.9985675956
decane	0.9991658666	1-octene	1.0021959807	1-butylamine	0.9880229093
undecane	1.0013619971	1-nonene	1.0029462293	1-pentylamine	0.998722886
dodecane	1.0012160226	1-decene	1	1-hexylamine	1.0010455757
tridecane	1.001772749	1-undecene	1.0028379017	1-heptylamine	1
tetradecane	1.0019491105	1-dodecene	1.0038114081	1-octylamine	0.9979793318
pentadecane	1.0022862814	1-tridecene	1.0046440538	1-alcohols	
hexadecane	1.002105049	1-tetradecene	1.0049143653	methanol	1.042815562
heptadecane	1.0018584753	1-pentadecene	1.0052043746	ethanol	1.0001329848
octadecane	1.0016250416	1-hexadecene	1.0030302061	1-propanol	0.9963672697
nonadecane	1.0013521279	1-heptadecene	0.9940423948	1-butanol	0.9997325502
eicosane	1.001410999	1-octadecene	1.0035460911	1-pentanol	1.0014429915
docosane	1.0047566656	1-nonadecene	1	1-hexanol	1.0022971899
tricosane	0.9988614709	1-eicosene	1	1-heptanol	1.0030503819
tetracosane	1.0006749947	1-alkynes		1-octanol	1.0014193595
octacosane	0.9996067314	propyne	1.0161577153	1-nonanol	1.0038608453
dotriacontane	0.9479948794	1-butyne	1.0133132993	1-decanol	0.996049928
hexatriacontane	0.9856158298	1-pentyne	0.9955678641	1-undecanol	0.9983034523
octatriacontane	0.9866236655	1-hexyne	1.0004325219	1-dodecanol	1.0001855421
tetracontane	1	1-heptyne	1.004330569	1-tetradecanol	1.00009885

Table B.3: Individualization parameters ϕ_i for esters, ethers, ketones and aldehydes.

compound	ϕ_i	compound	ϕ_i
esters		pentyl-3-butenoate	1
methylethanoate	0.9995647736	methyl-4-pentynotae	1
ethylethanoate	0.9991585869	ethyl-4-pentynoate	1
propylethanoate	1.0026850084	ethers	
butylethanoate	1.0084313803	methylbutylether	1.021100927
pentylethanoate	1	methyl hexyl ether	1
methylpropanoate	1.0072901014	ethylbutylether	1.001426515
ethylpropanoate	1.0047332063	ethylhexylether	1
propylpropanoate	0.998499054	ethyl hexadecylether	1
butylpropanoate	1.0000079649	diethylether	1.0000000075
methylbutanoate	1.0076986212	dibutylether	1.0002843897
ethylbutanoate	0.9951791782	dihexylether	1.0074423792
propylbutanoate	0.9950215603	dioctylether	1
methylpentanoate	1.0142672099	ketones	
methyldecanoate	1.0115580169	2-butanone	1.0022825047
methyldodecanoate	1.0110421288	2-hexanone	1.0082266601
methyltetradecanoate	1.0104443039	2-octanone	1.0092553739
ethyltetradecanoate	1.0010535718	3-pentanone	0.9983292939
methylhexadecanoate	1.0099481784	3-heptanone	1.0012357671
methyloctadecanoate	1.0087802266	3-nonanone	1
butyloctadecanoate	0.9708240271	4-heptanone	0.9924203109
methyldocosanoate	1	4-nonanone	1
methyl-2-butenoate	1.0628292395	6-undecanone	0.9979174243
ethyl-2-butenoate	1.0408320291	3-heptene-2-on	1
propyl-2-butenoate	1	aldehydes	
butyl-2-butenoate	1	butanal	0.9987522272
pentyl-2-butenoate	1	pentanal	1.0019768018
methyl-3-butenoate	1.0342764984	hexanal	1.0056470704
ethyl-3-butenoate	0.9997336024	heptanal	1.0012258544
propyl-3-butenoate	1	dodecanal	0.9957997667
butyl-3-butenoate	1	2-butenal	1.0775392182

B.3 Group-group interaction parameters $k_{\alpha\beta}$

B.3.1 methane - n-alkanes

The values of the group-group interaction parameters k_{CH_4,CH_3} and k_{CH_4,CH_2} were adjusted to 971 experimental vapor-liquid equilibria (VLE) data points for 14 binary mixtures. These mixtures are listed in table B.4. The optimal values are $k_{CH_4,CH_3} = -0.005$ and $k_{CH_4,CH_2} = -0.00269$.
As fig. B.1 exemplary shows for the mixtures methane and butane as well as methane and decane, the implications of k_{CH_4,CH_3} and k_{CH_4,CH_2} on VLE results are marginal.

Table B.4: Experimental VLE data for binary mixtures of methane and the following n-alkanes was used to adjust the values of k_{CH_4,CH_3} and k_{CH_4,CH_2}.

ethane	pentane	octane	tridecane	eicosane
propane	hexane	nonane	tetradecane	hexatriacontane
butane	heptane	decane	hexadecane	

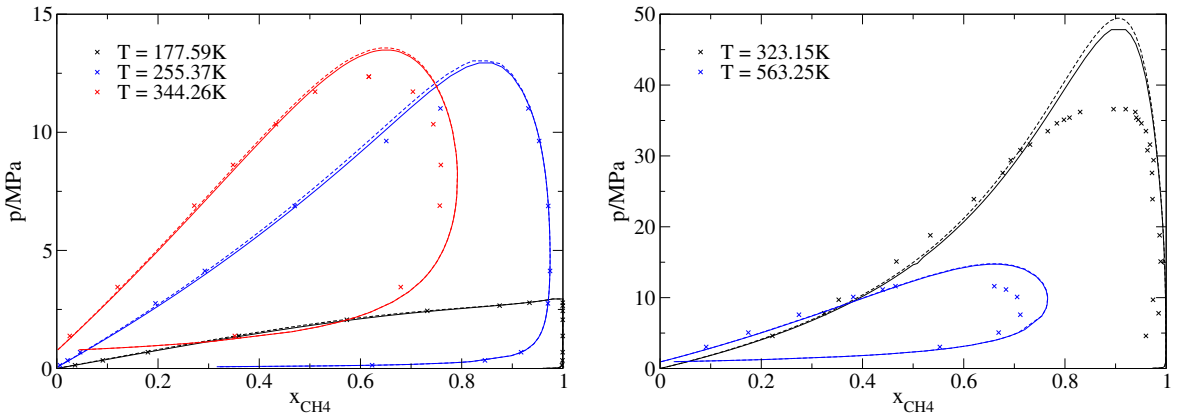

(a) (b)

Figure B.1: Pressure-composition diagrams of the binary mixtures methane + n-butane (a) and methane + n-decane (b) at different temperatures. Results obtained with the adjusted values of k_{CH_4,CH_3} and k_{CH_4,CH_2} (solid lines) are compared to results with $k_{\alpha\beta} = 0$ (dashed lines) and experimental data [3] [4] [5] [6] (symbols).

B.3.2 n-alkanes - n-alkanes

The value of the group-group interaction parameter k_{CH_3,CH_2} was adjusted to 2513 experimental VLE data points for 60 binary n-alkane mixtures. These mixtures are listed in table B.5. The optimal value is $k_{CH_3,CH_2} = 0.01151$. As figs. B.2 and B.3 exemplary show for several binary mixtures, the implication of k_{CH_3,CH_2} on VLE result is marginal.

Table B.5: Experimental VLE data for the following binary n-alkane mixtures was used to regress the value of k_{CH_3,CH_2}.

Ethane+...	docosane	octacosane	octacosane	nonane
propane	tetracosane	Butane+...	Hexane+...	dodecane
butane	Propane+...	pentane	heptane	nonadecane
pentane	butane	hexane	octane	tricosane
hexane	pentane	heptane	decane	Octane+...
heptane	hexane	octane	undecane	decane
octane	heptane	decane	dodecane	dodecane
decane	octane	tetradecane	hexadecane	hexadecane
dodecane	nonane	Pentane+...	tetracosane	Decane+...
tetradecane	decane	octane	octacosane	dodecane
hexadecane	dodecane	octadecane	hexatriacontane	
octadecane	tetradecane	tricosane	Heptane+...	
eicosane	hexadecane	tetracosane	octane	

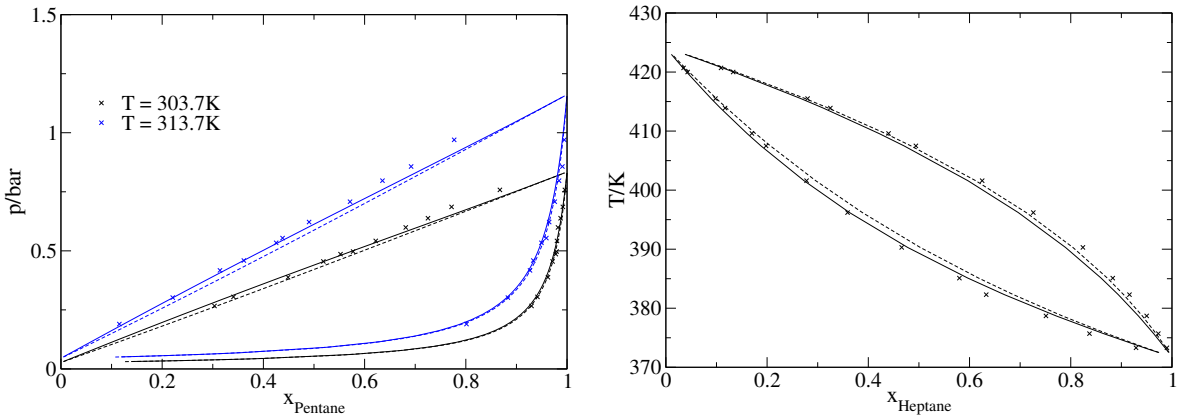

(a) (b)

Figure B.2: Comparison of results obtained with the adjusted value of k_{CH_3,CH_2} (solid lines) to results with $k_{CH_3,CH_2} = 0$ (dashed lines) and experimental data [7] [8] (symbols). Diagram (a): pressure-composition diagram for the binary mixture n-pentane + n-octane. Diagram (b): temperature-composition diagram for the binary mixture n-heptane + n-nonane at $p = 1.013$ bar.

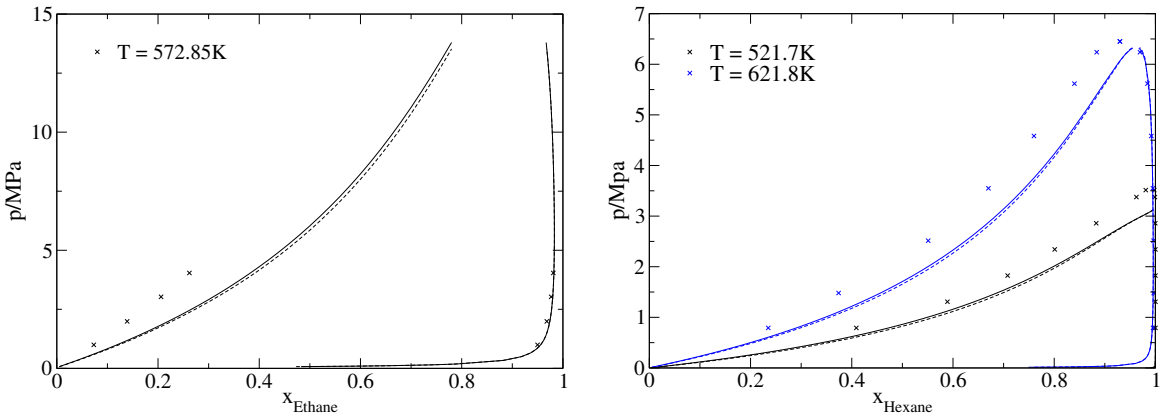

(a) (b)

Figure B.3: Comparison of results obtained with the adjusted value of k_{CH_3,CH_2} (solid lines) to results with $k_{CH_3,CH_2} = 0$ (dashed lines) and experimental data [9] [10] (symbols). Diagram (a): pressure-composition diagram for the binary mixture ethane + n-eicosane. Diagram (b): pressure-composition diagram for the binary mixture n-hexane + n-hexatriacontane.

B.3.3 n-alkanes - esters

The values of the group-group interaction parameters $k_{CH_3,COO}$ and $k_{CH_2,COO}$ were adjusted to 1451 experimental VLE data points for 40 binary mixtures of n-alkane and ester compounds. These mixtures are listed in table B.6. The optimal values are $k_{CH_3,COO} = 0.0996$ and $k_{CH_2,COO} = -0.015235$. Figure B.4 exemplifies for the binary mixtures heptane and butylethanoate as well as hexane and ethylbutanoate the improvement of VLE results due to the adjustment of $k_{CH_3,COO}$ and $k_{CH_2,COO}$.

Table B.6: Experimental VLE data for binary mixtures of the following n-alkane and ester compounds was used to adjust the values of $k_{CH_3,COO}$ and $k_{CH_2,COO}$.

Ethane+...	Butane+...	Heptane+...	methylpentanoate	Decane+...
methylethanoate	ethylethanoate	methylethanoate	Octane+...	ethylethanoate
ethylethanoate	Pentane+...	ethylethanoate	ethylethanoate	Dodecane+...
methyldecanoate	ethylethanoate	propylethanoate	Nonane+...	methylethanoate
methyldodecanoate	Hexane+...	butylethanoate	ethylethanoate	ethylethanoate
methyltetradecanoate	methylethanoate	methylpropanoate	propylethanoate	
methylhexadecanoate	ethylethanoate	ethylpropanoate	pentylethanoate	
methyloctadecanoate	butylethanoate	propylpropanoate	propylpropanoate	
methyldocosanoate	ethylbutanoate	butylpropanoate	methylbutanoate	
Propane+...	butyloctadecanoate	methylbutanoate	ethylbutanoate	
methyltetradecanoate		ethylbutanoate	propylbutanoate	
ethyltetradecanoate		propylbutanoate		

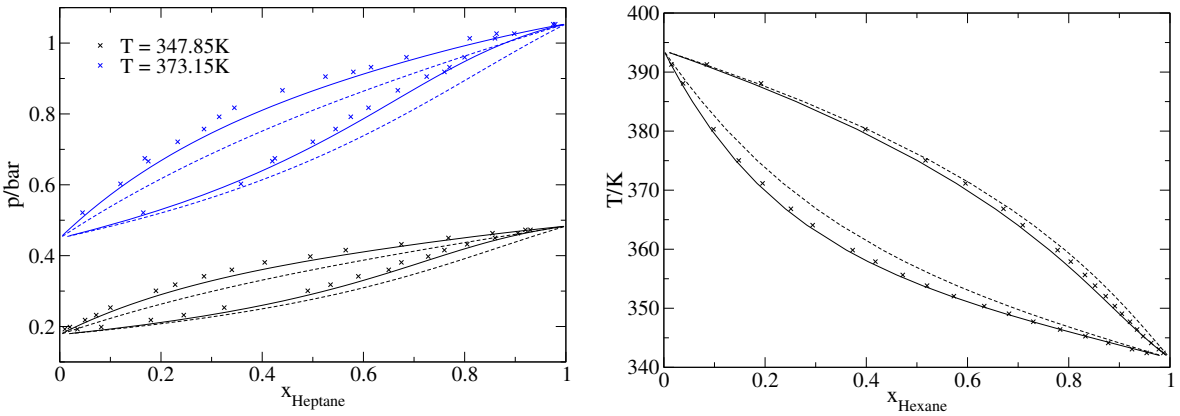

(a) (b)

Figure B.4: Comparison of results obtained with the adjusted values of $k_{CH_3,COO}$ and $k_{CH_2,COO}$ (solid lines) to results with $k_{\alpha\beta} = 0$ (dashed lines) and experimental data [11] [12] (symbols). Diagram (a): pressure-composition diagram for the binary mixture heptane + butylethanoate. Diagram (b): temperature-composition diagram for the binary mixture hexane + ethylbutanoate at $p = 1$ bar.

B.3.4 n-alkanes - 1-alcohols

The values of the group-group interaction parameters $k_{CH_3,OH}$ and $k_{CH_2,OH}$ were adjusted to 2175 experimental VLE data points for 33 binary mixtures of n-alkane and 1-alcohol compounds. These mixtures are listed in table B.7. The optimal values are $k_{CH_3,OH} = -0.0087$ and $k_{CH_2,OH} = 0.0489$. Figure B.5 exemplifies for the binary mixtures 1-propanol and heptane as well as 1-tetradecanol and undecane the improvement of VLE results due to the adjustment of the parameters $k_{CH_3,OH}$ and $k_{CH_2,OH}$.

Table B.7: Experimental VLE data for binary mixtures of the following n-alkane and 1-alcohol compounds was used to adjust the values of $k_{CH_3,OH}$ and $k_{CH_2,OH}$.

Butane+...	butanol	butanol	Nonane+...	dodecanol
ethanol	pentanol	pentanol	ethanol	Undecane+...
Pentane+...	hexanol	octanol	propanol	propanol
ethanol	octanol	Octane+...	butanol	tetradecanol
butanol	decanol	ethanol	Decane+...	Tridecane+...
pentanol	dodecanol	propanol	propanol	dodecanol
Hexane+...	Heptane+...	butanol	butanol	Tetradecane+...
ethanol	ethanol	pentanol	pentanol	dodecanol
propanol	propanol		heptanol	

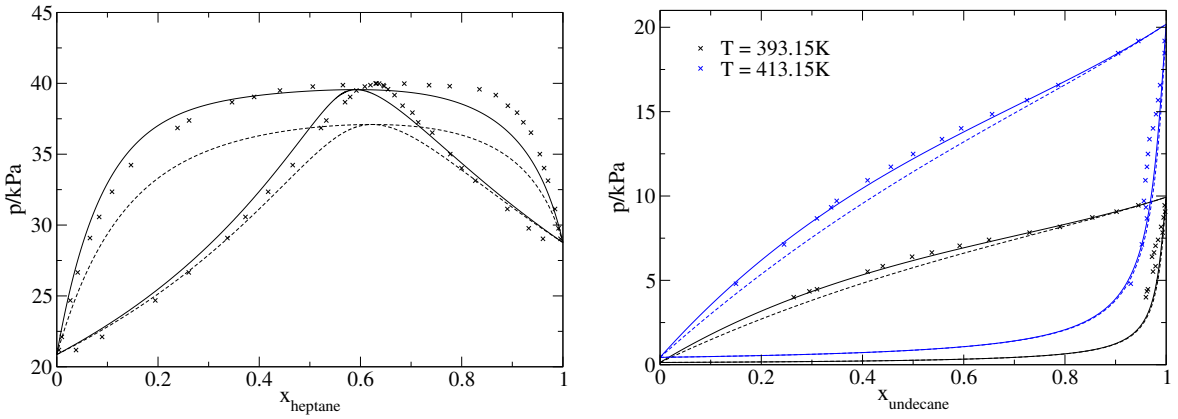

(a) (b)

Figure B.5: Comparison of results obtained with the adjusted values of $k_{CH_3,OH}$ and $k_{CH_2,OH}$ (solid lines) to results with $k_{\alpha\beta} = 0$ (dashed lines) and experimental data [13] [14] (symbols). Diagram (a): pressure-composition diagram for the binary mixture 1-propanol + heptane at $T = 333.15$ K. Diagram (b): pressure-composition diagram for the binary mixture 1-tetradecanol + undecane.

B.4 Influence of ϕ_i on the value of surface tension for pure components

In the following figures, results for surface tension obtained with the adjusted value of ϕ_i are compared to results calculated with $\phi_i = 1$ and to experimental data. The adjusted values of ϕ_i are presented in tables B.2 and B.3.

B.4.1 Pure n-alkanes

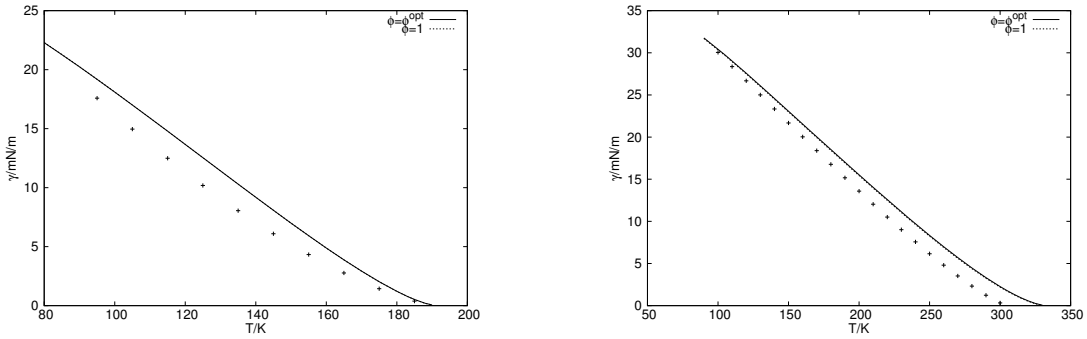

(a) (b)

Figure B.6: Calculated values of surface tension (lines) and reference data [15] (symbols) for methane (a) and ethane (b).

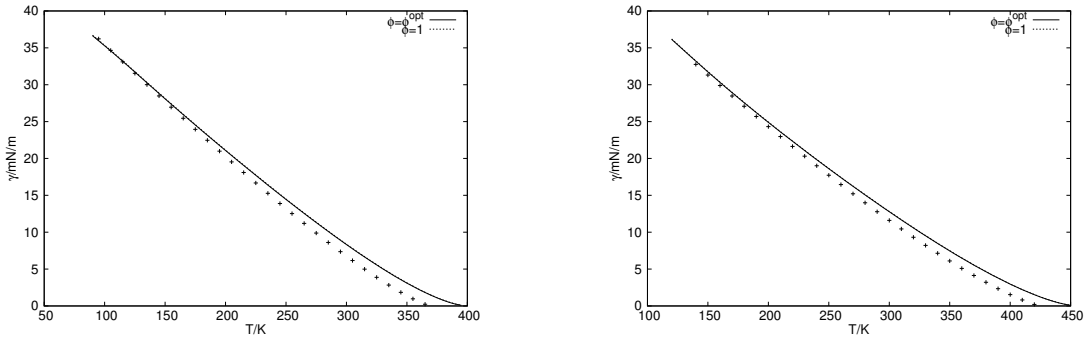

(a) (b)

Figure B.7: Calculated values of surface tension (lines) and reference data [15] (symbols) for propane (a) and butane (b).

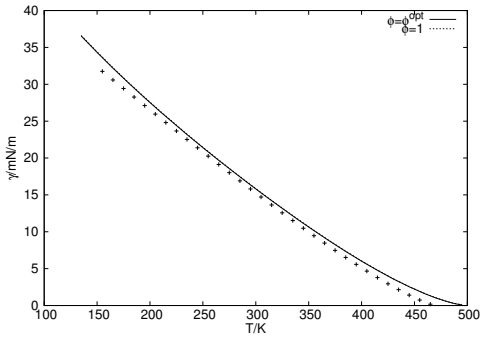

(a)

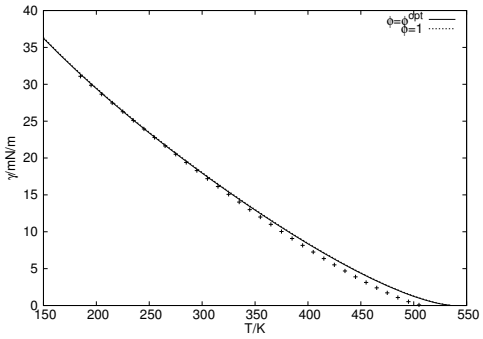

(b)

Figure B.8: Calculated values of surface tension (lines) and reference data [15] (symbols) for pentane (a) and hexane (b).

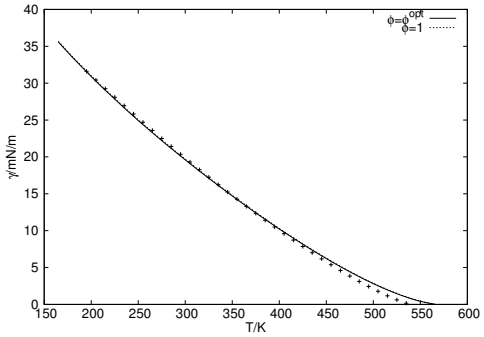

(a)

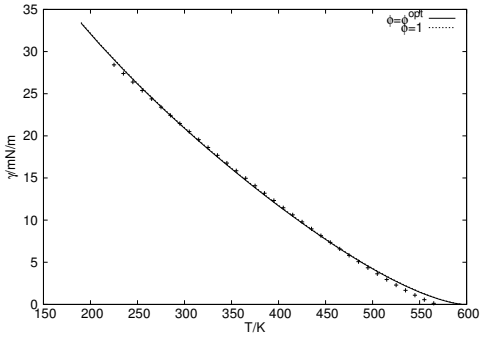

(b)

Figure B.9: Calculated values of surface tension (lines) and reference data [15] (symbols) for heptane (a) and octane (b).

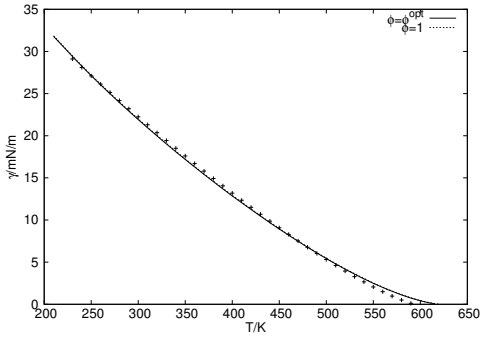

(a)

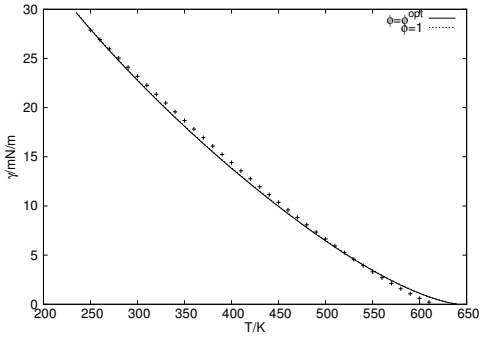

(b)

Figure B.10: Calculated values of surface tension (lines) and reference data [15] (symbols) for nonane (a) and decane (b).

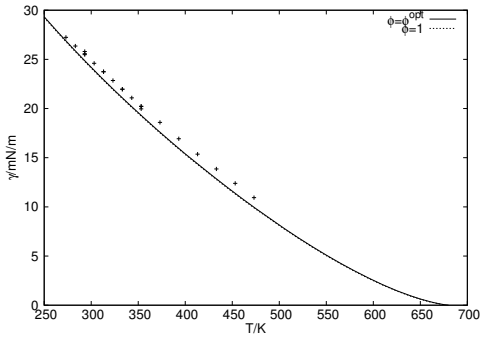

(a)

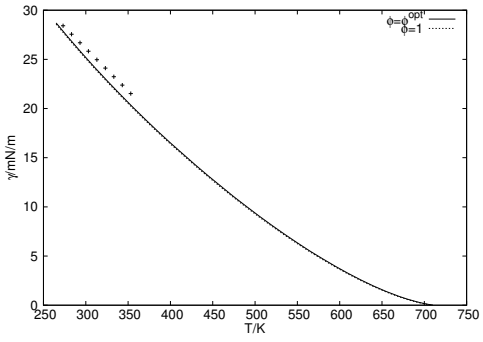

(b)

Figure B.11: Calculated values of surface tension (lines) and reference data [16] (symbols) for dodecane (a) and tetradecane (b).

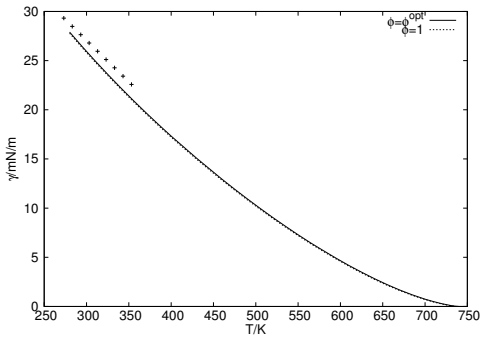

(a)

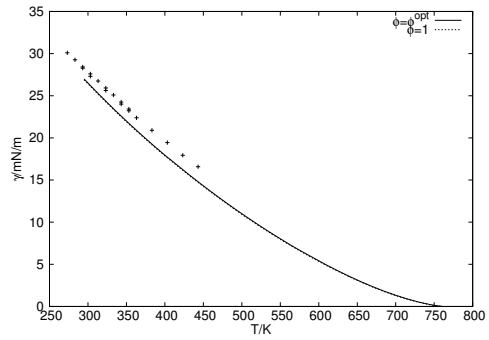

(b)

Figure B.12: Calculated values of surface tension (lines) and reference data [16] [17] [18] (symbols) for hexadecane (a) and octadecane (b).

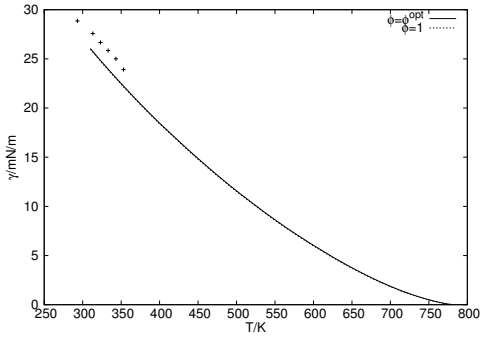

Figure B.13: Calculated values of surface tension (lines) and reference data [19] [20] (symbols) for eicosane.

B.4.2 Pure 1-alkenes

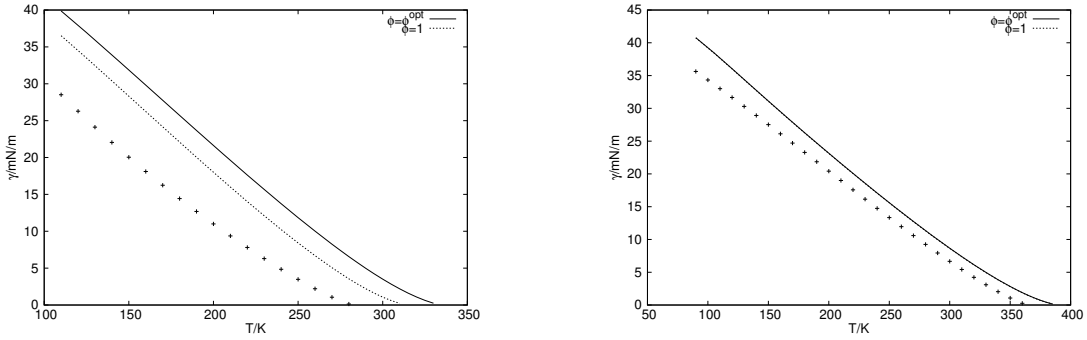

(a) (b)

Figure B.14: Calculated values of surface tension (lines) and reference data [21] (symbols) for ethylene (a) and propylene (b).

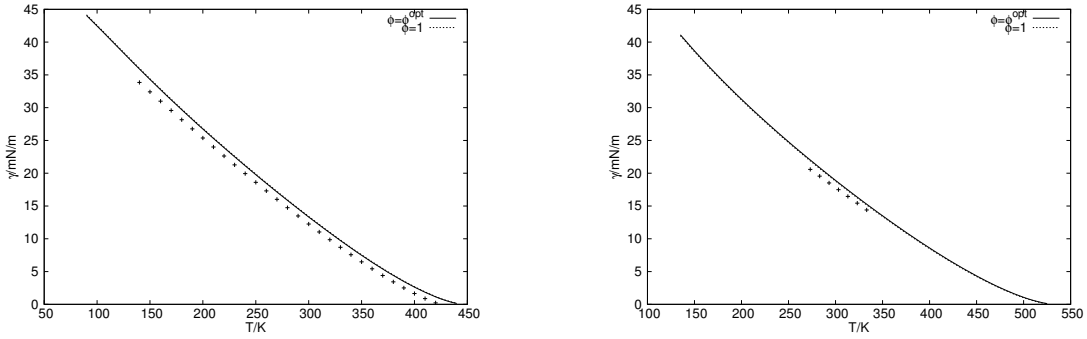

(a) (b)

Figure B.15: Calculated values of surface tension (lines) and reference data [16] [21] (symbols) for 1-butene (a) and 1-hexene (b).

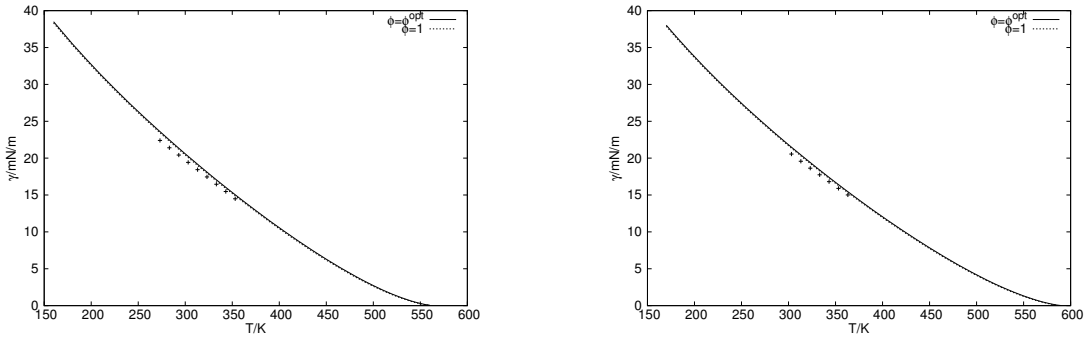

(a) (b)

Figure B.16: Calculated values of surface tension (lines) and reference data [16] (symbols) for 1-heptene (a) and 1-octene (b).

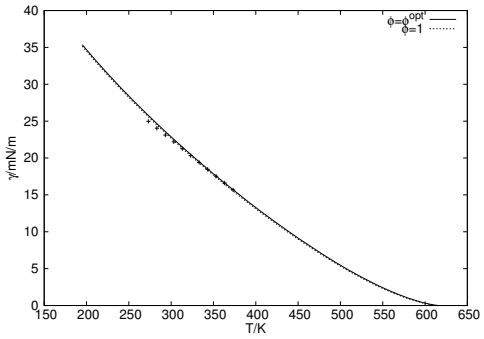

(a)

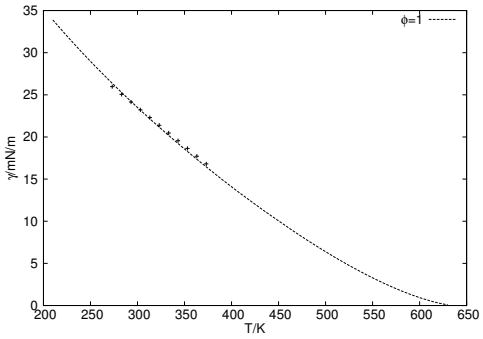

(b)

Figure B.17: Calculated values of surface tension (lines) and reference data [16] (symbols) for 1-nonene (a) and 1-decene (b).

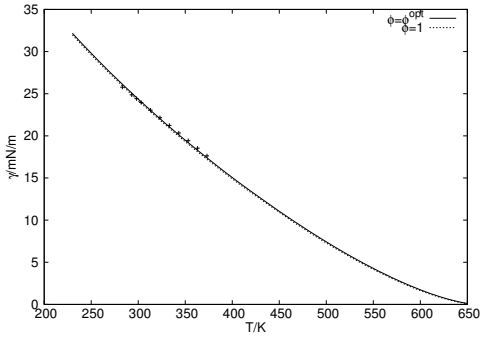

(a)

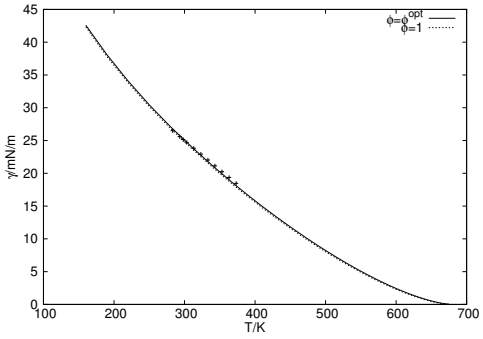

(b)

Figure B.18: Calculated values of surface tension (lines) and reference data [16] (symbols) for 1-undecene (a) and 1-dodecene (b).

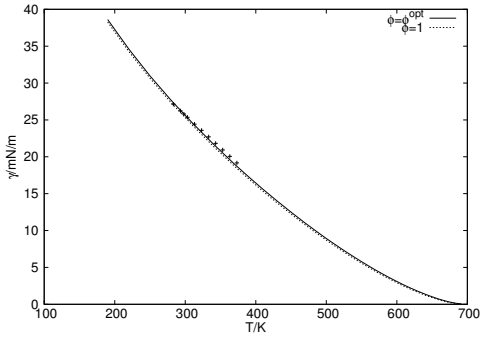

(a)

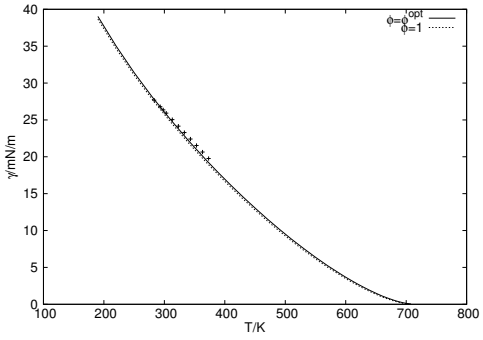

(b)

Figure B.19: Calculated values of surface tension (lines) and reference data [16] (symbols) for 1-tridecene (a) and 1-tetradecene (b).

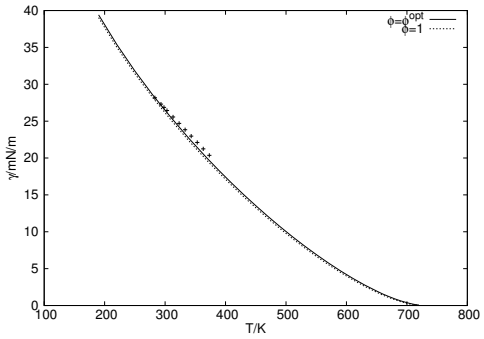

(a)

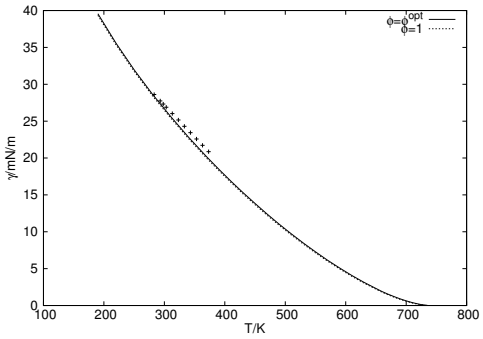

(b)

Figure B.20: Calculated values of surface tension (lines) and reference data [16] (symbols) for 1-pentadecene (a) and 1-hexadecene (b).

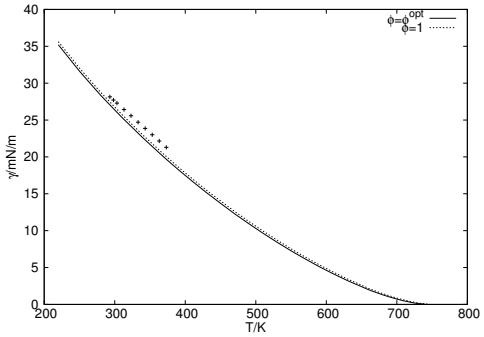

(a)

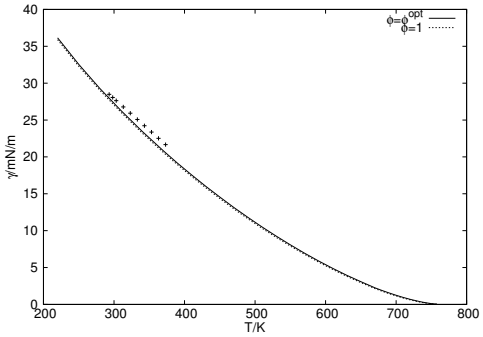

(b)

Figure B.21: Calculated values of surface tension (lines) and reference data [16] (symbols) for 1-heptadecene (a) and 1-octadecene (b).

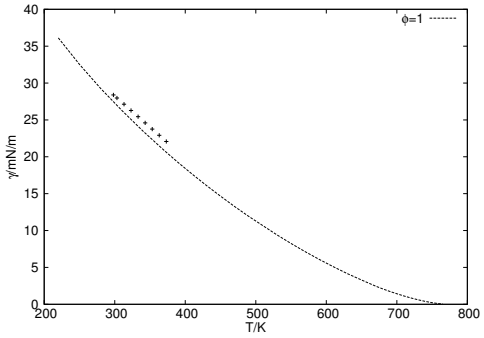

(a)

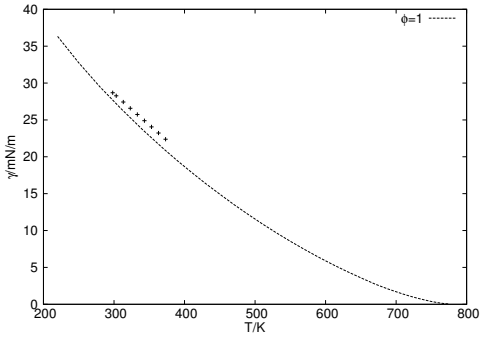

(b)

Figure B.22: Calculated values of surface tension (lines) and reference data [16] (symbols) for 1-nonadecene (a) and 1-eicosene (b).

B.4.3 Pure 1-alkynes

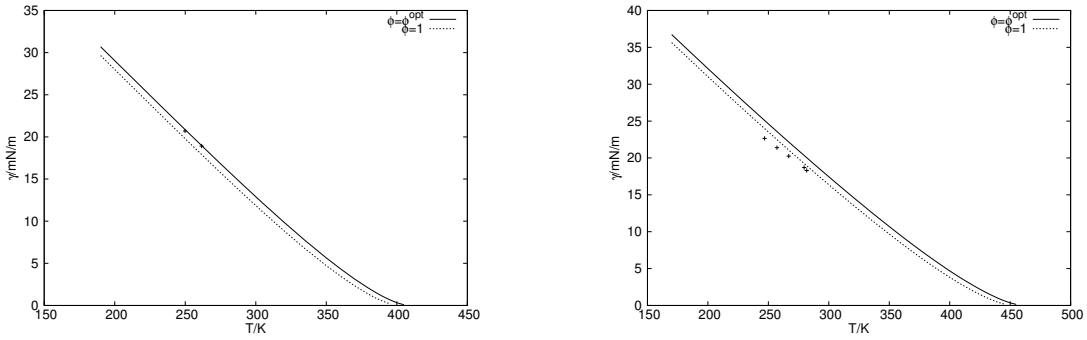

(a) (b)

Figure B.23: Calculated values of surface tension (lines) and reference data [22] (symbols) for propyne (a) and 1-butyne (b).

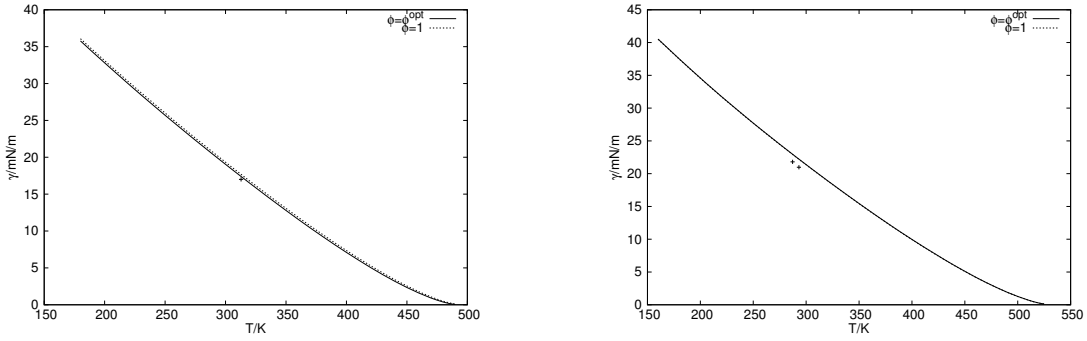

(a) (b)

Figure B.24: Calculated values of surface tension (lines) and reference data [22] [23] (symbols) for 1-pentyne (a) and 1-hexyne (b).

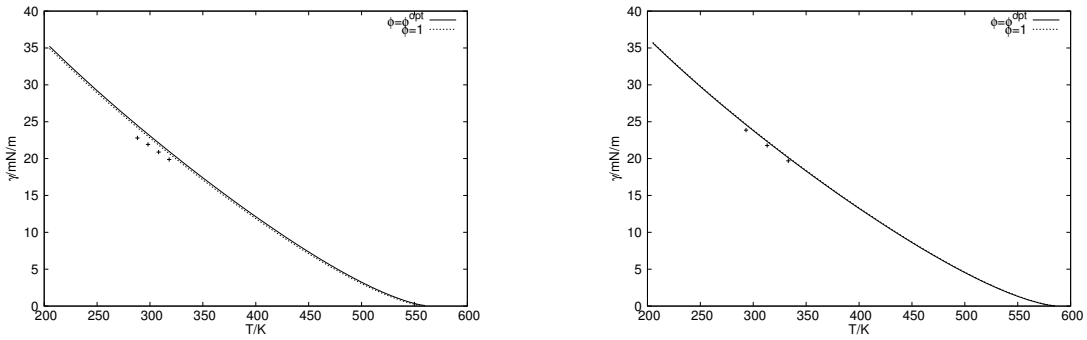

(a) (b)

Figure B.25: Calculated values of surface tension (lines) and reference data [24] [23] (symbols) for 1-heptyne (a) and 1-octyne (b).

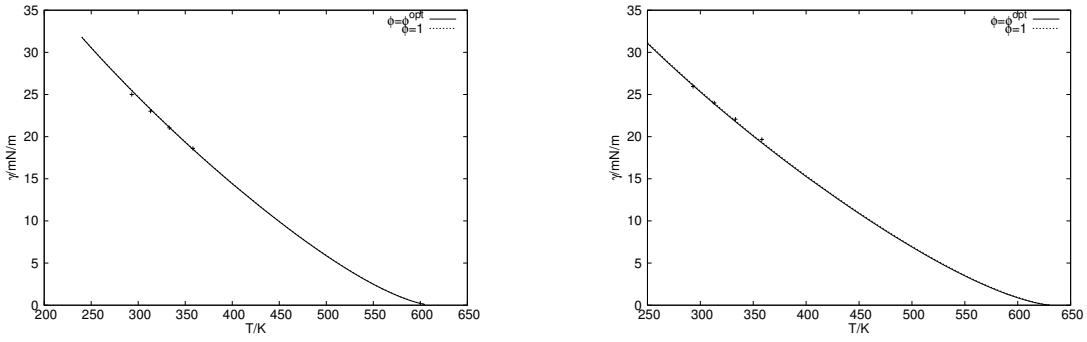

(a) (b)

Figure B.26: Calculated values of surface tension (lines) and reference data [23] (symbols) for 1-nonyne (a) and 1-decyne (b).

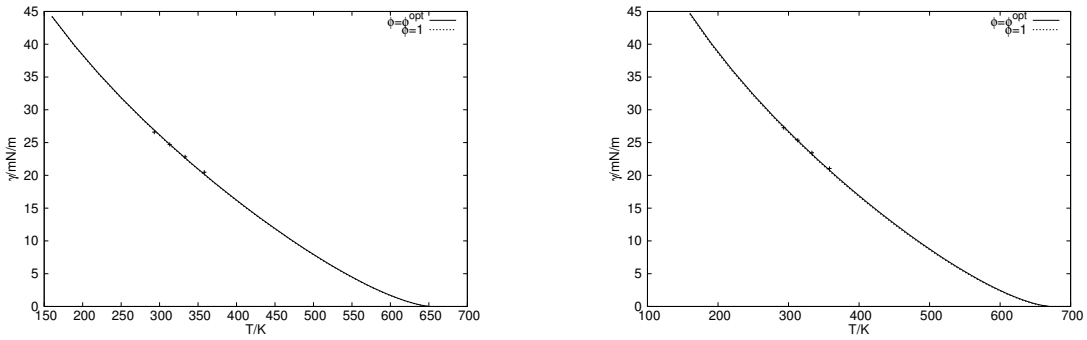

(a) (b)

Figure B.27: Calculated values of surface tension (lines) and reference data [16] (symbols) for 1-undecyne (a) and 1-dodecyne (b).

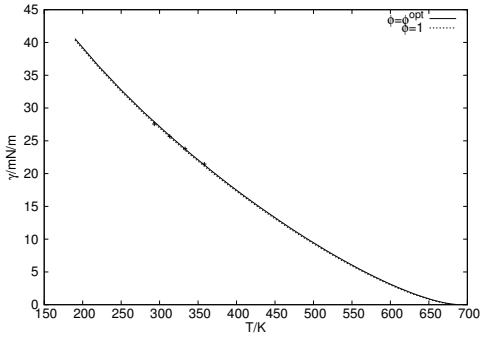

Figure B.28: Calculated values of surface tension (lines) and reference data [16] (symbols) for 1-tridecyne.

B.4.4 Pure 1-amines

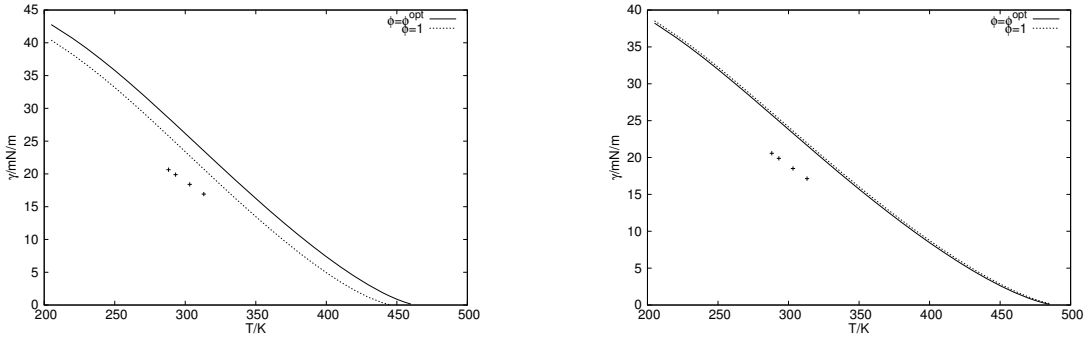

(a) (b)

Figure B.29: Calculated values of surface tension (lines) and reference data [16] (symbols) for methylamine (a) and ethylamine (b).

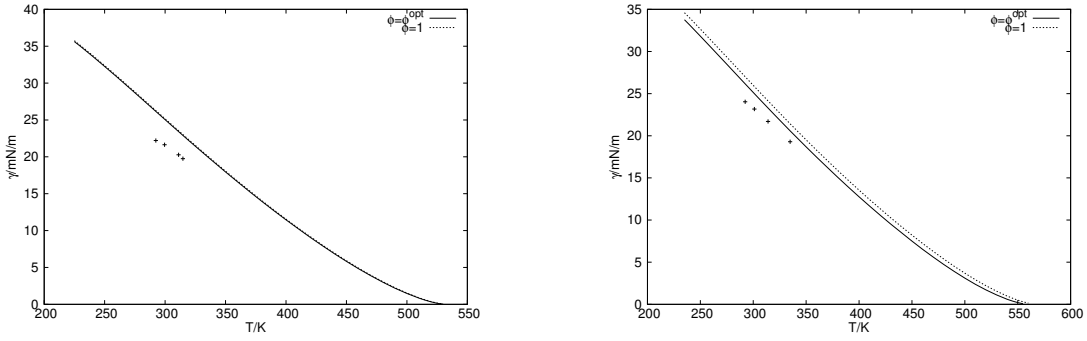

(a) (b)

Figure B.30: Calculated values of surface tension (lines) and reference data [25] (symbols) for 1-propylamine (a) and 1-butylamine (b).

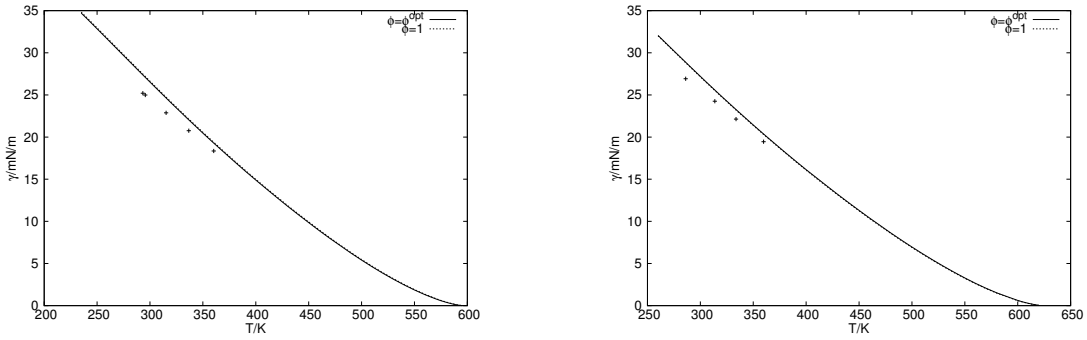

(a) (b)

Figure B.31: Calculated values of surface tension (lines) and reference data [25] (symbols) for 1-pentylamine (a) and 1-hexylamine (b).

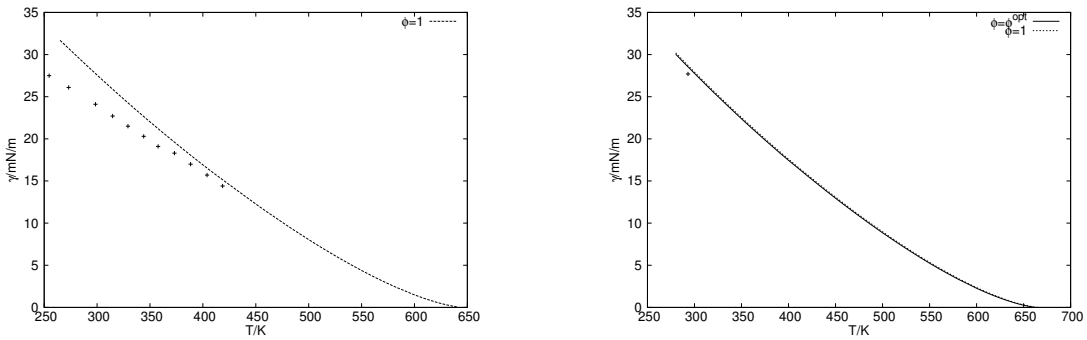

(a) (b)

Figure B.32: Calculated values of surface tension (lines) and reference data [26] [27] (symbols) for 1-heptylamine (a) and 1-octylamine (b).

B.4.5 Pure 1-alcohols

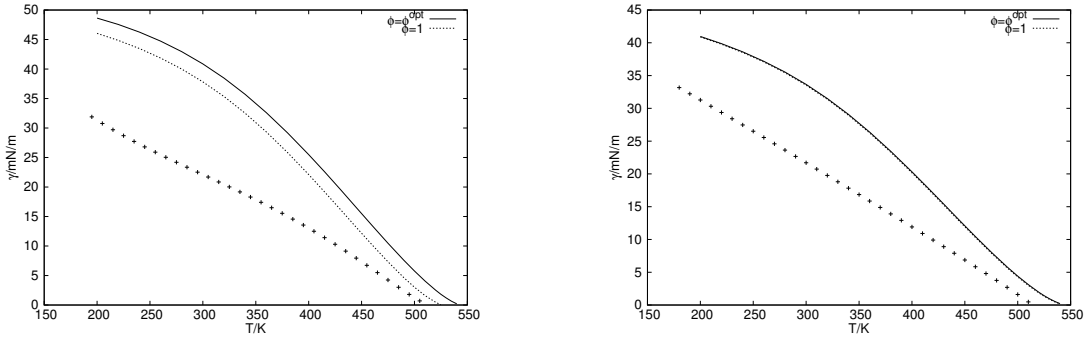

(a) (b)

Figure B.33: Calculated values of surface tension (lines) and reference data [15] [28] (symbols) for methanol (a) and ethanol (b).

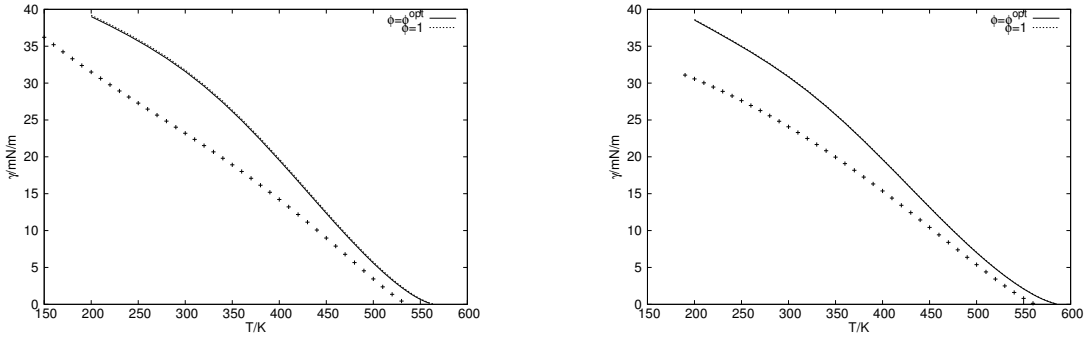

(a) (b)

Figure B.34: Calculated values of surface tension (lines) and reference data [21] (symbols) for 1-propanol (a) and 1-butanol (b).

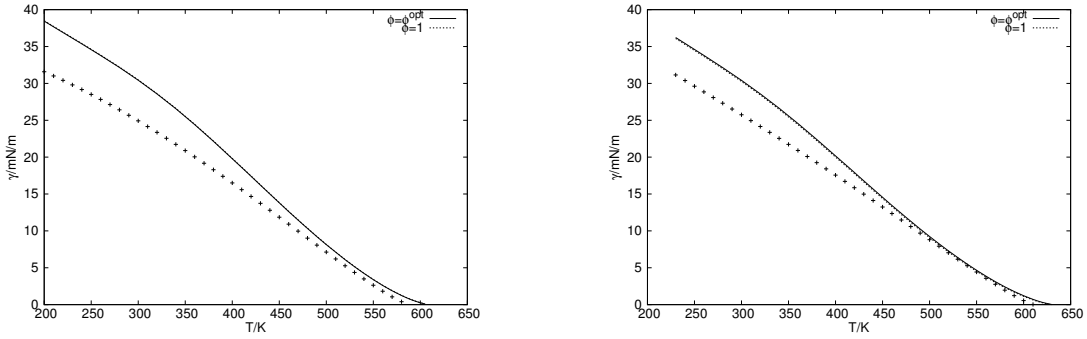

(a) (b)

Figure B.35: Calculated values of surface tension (lines) and reference data [21] (symbols) for 1-pentanol (a) and 1-hexanol (b).

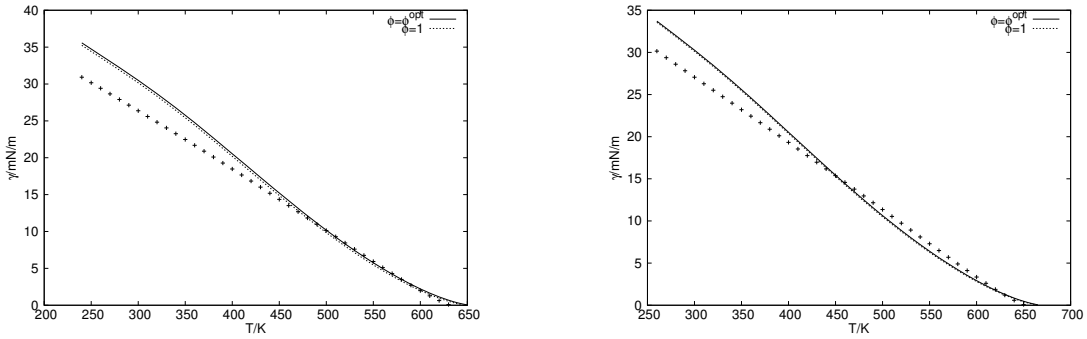

(a) (b)

Figure B.36: Calculated values of surface tension (lines) and reference data [21] (symbols) for 1-heptanol (a) and 1-octanol (b).

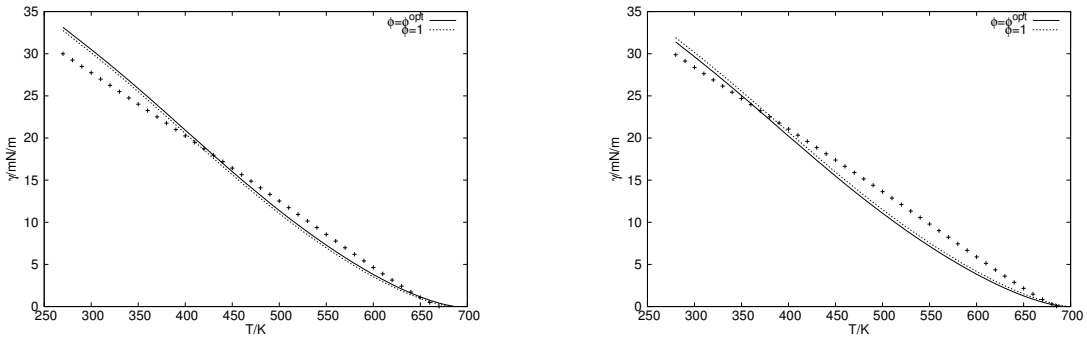

(a) (b)

Figure B.37: Calculated values of surface tension (lines) and reference data [21] (symbols) for 1-nonanol (a) and 1-decanol (b).

B.4.6 Pure esters

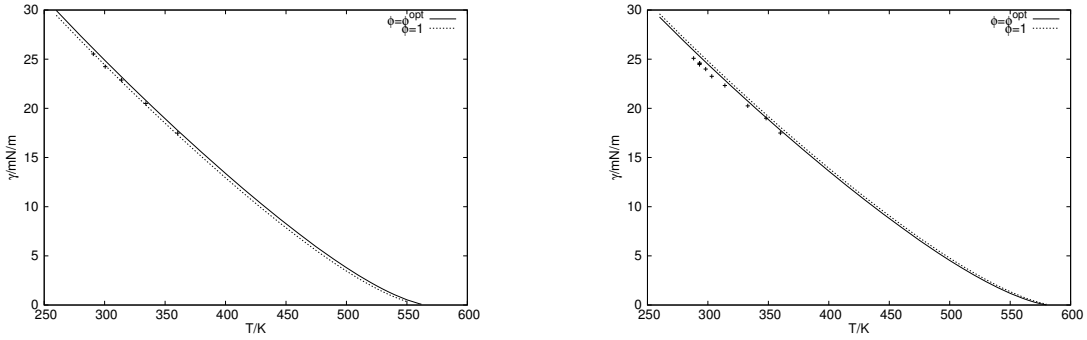

(a) (b)

Figure B.38: Calculated values of surface tension (lines) and reference data [29] [30] (symbols) for butanoic acid methyl ester (a) and butanoic acid ethyl ester (b).

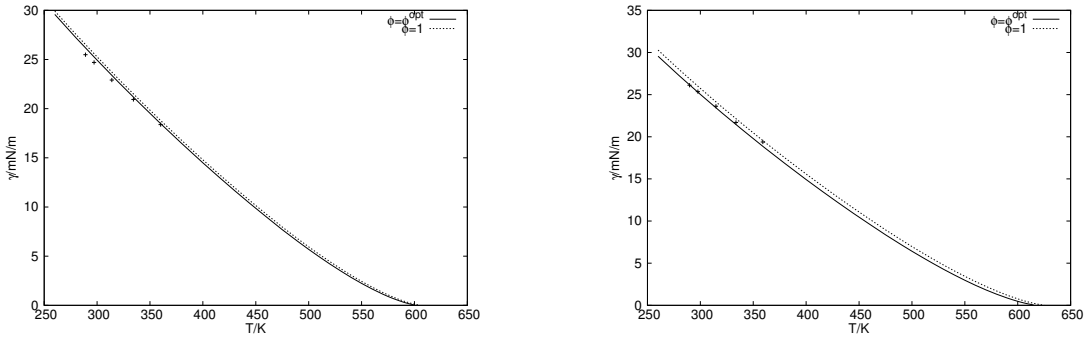

(a) (b)

Figure B.39: Calculated values of surface tension (lines) and reference data [31] (symbols) for butanoic acid propyl ester (a) and butanoic acid butyl ester (b).

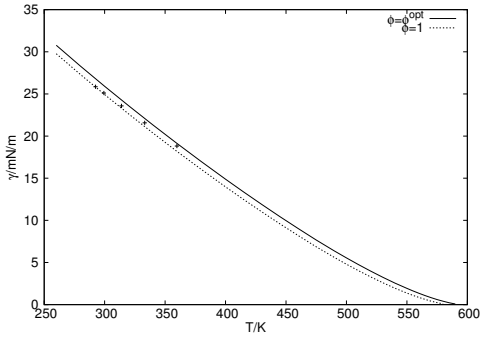

Figure B.40: Calculated values of surface tension (lines) and reference data [31] (symbols) for pentanoic acid methyl ester.

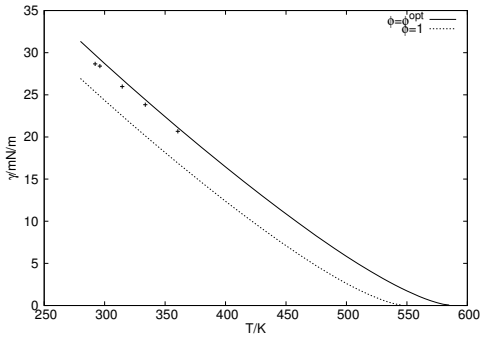

(a)

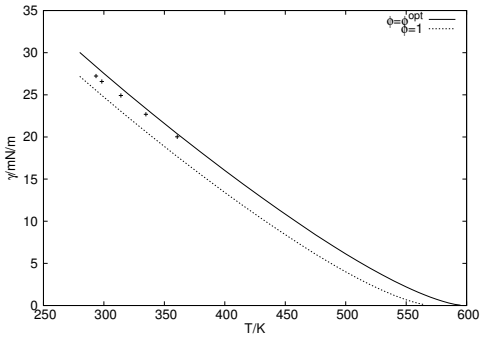

(b)

Figure B.41: Calculated values of surface tension (lines) and reference data [32] (symbols) for 2-butenoic acid methyl ester (a) and 2-butenoic acid ethyl ester (b).

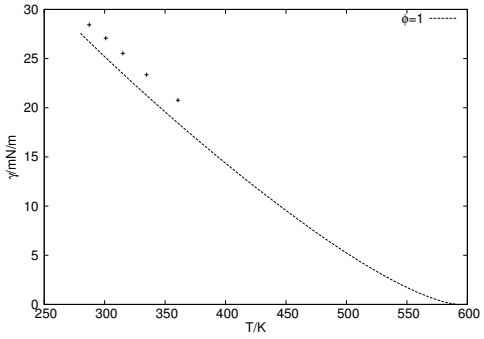

(a)

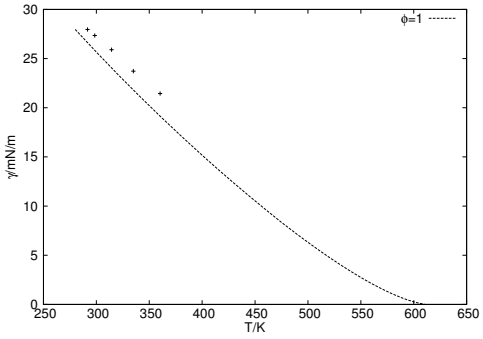

(b)

Figure B.42: Calculated values of surface tension (lines) and reference data [32] (symbols) for 2-butenoic acid propyl ester (a) and 2-butenoic acid butyl ester (b).

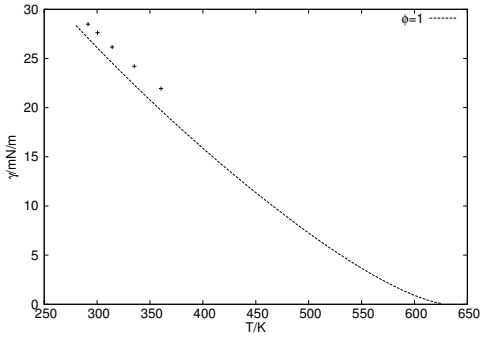

(a)

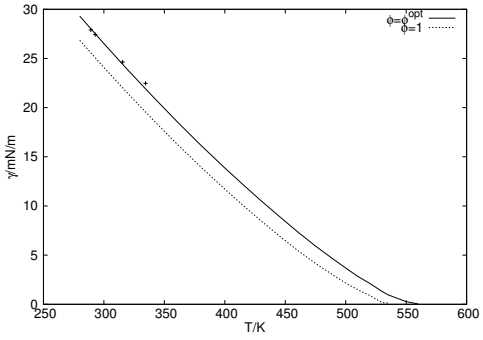

(b)

Figure B.43: Calculated values of surface tension (lines) and reference data [32] (symbols) for 2-butenoic acid pentyl ester (a) and 3-butenoic acid methyl ester (b).

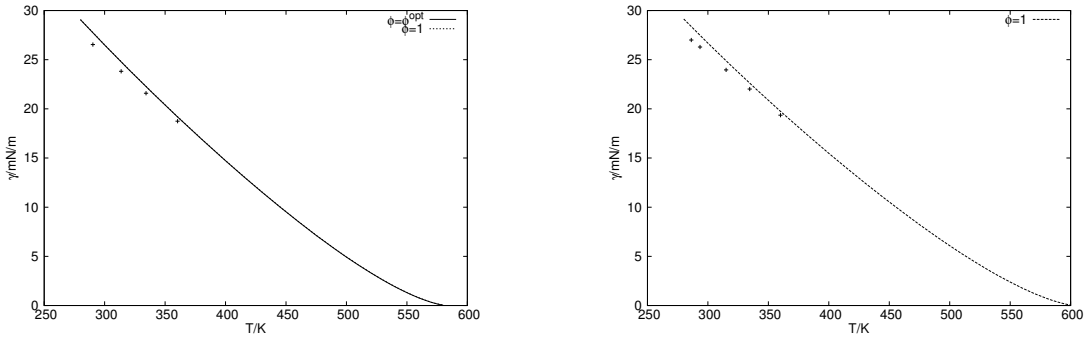

(a) (b)

Figure B.44: Calculated values of surface tension (lines) and reference data [32] (symbols) for 3-butenoic acid ethyl ester (a) and 3-butenoic acid propyl ester (b).

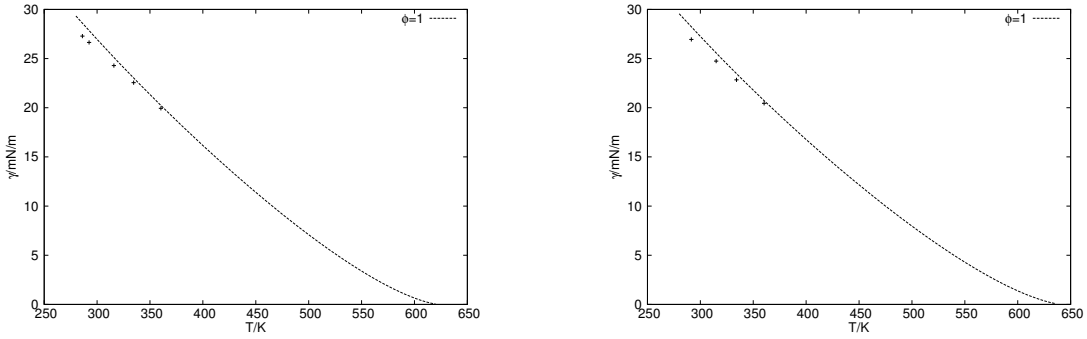

(a) (b)

Figure B.45: Calculated values of surface tension (lines) and reference data [32] (symbols) for 3-butenoic acid butyl ester (a) and 3-butenoic acid pentyl ester (b).

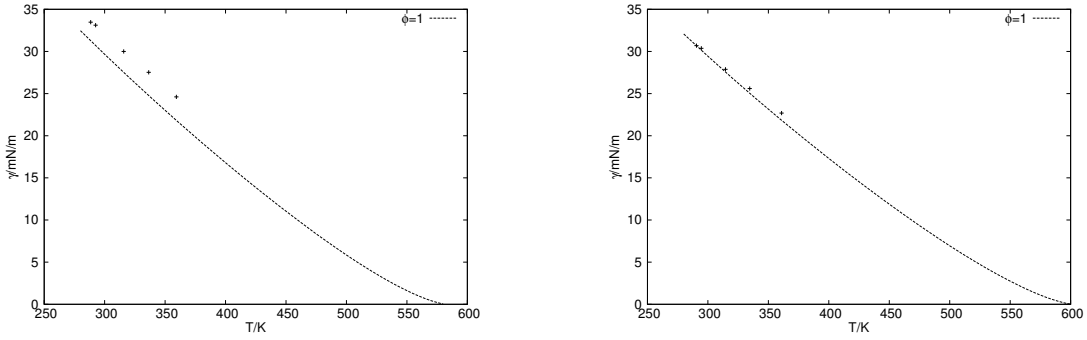

(a) (b)

Figure B.46: Calculated values of surface tension (lines) and reference data [33] (symbols) for 4-pentynoic acid methyl ester (a) and 4-pentynoic acid ethyl ester (b).

B.4.7 Pure ethers

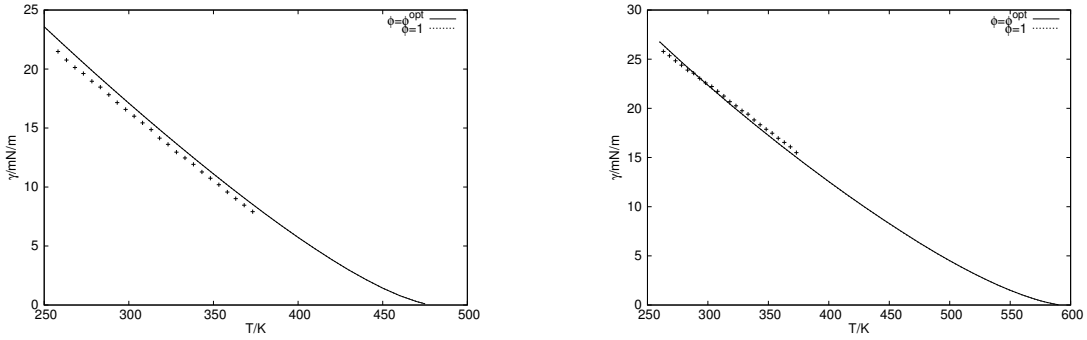

(a) (b)

Figure B.47: Calculated values of surface tension (lines) and reference data [34] (symbols) for diethyl ether (a) and dibutyl ether (b).

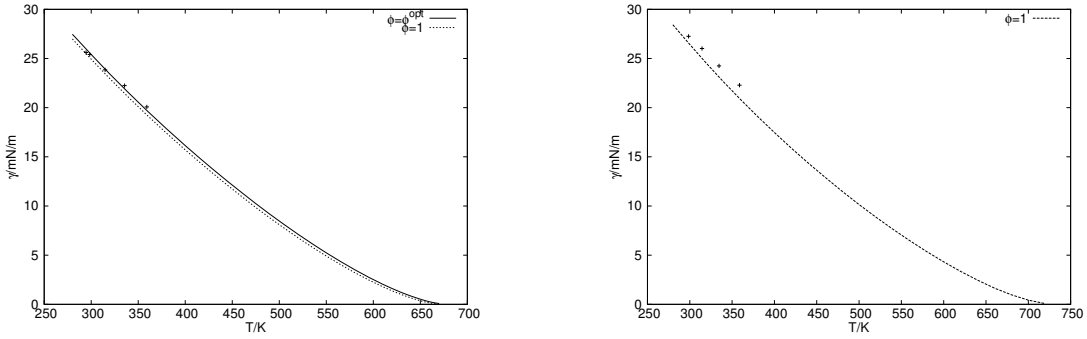

(a) (b)

Figure B.48: Calculated values of surface tension (lines) and reference data [35] (symbols) for dihexyl ether (a) and dioctyl ether (b).

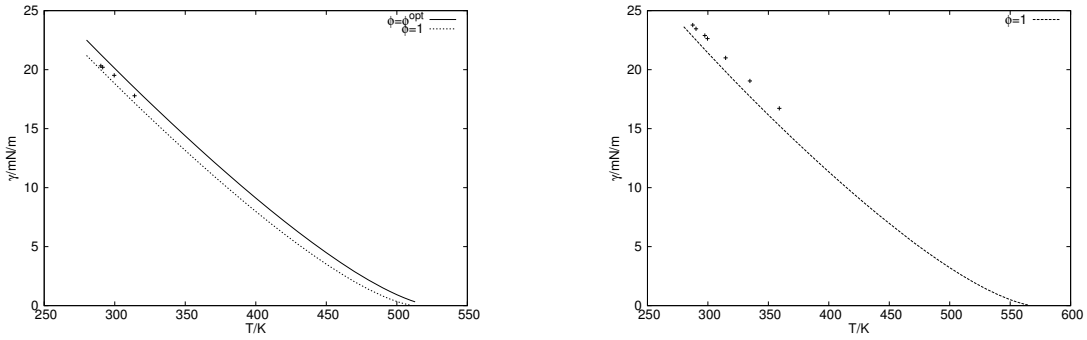

(a) (b)

Figure B.49: Calculated values of surface tension (lines) and reference data [35] (symbols) for methyl butyl ether (a) and methyl hexyl ether (b).

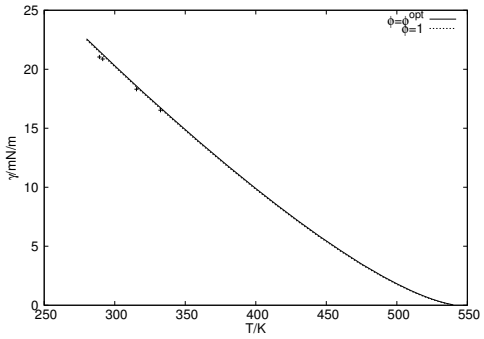

(a)

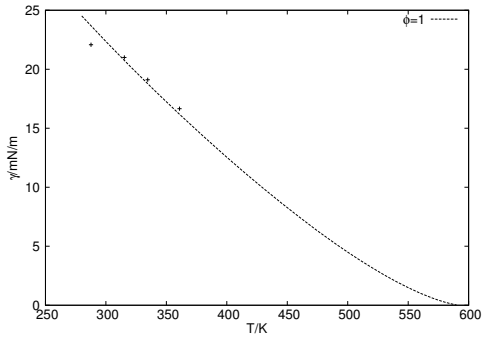

(b)

Figure B.50: Calculated values of surface tension (lines) and reference data [35] (symbols) for ethyl butyl ether (a) and ethyl hexyl ether (b).

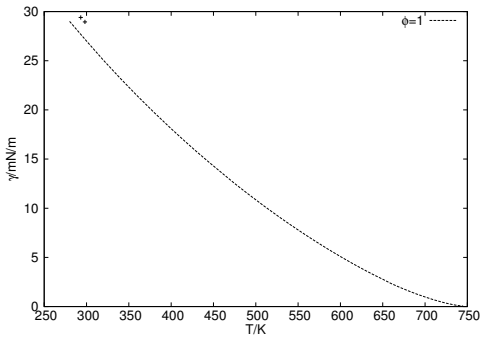

(a)

Figure B.51: Calculated values of surface tension (lines) and reference data [30] (symbols) for ethyl hexadecyl ether.

B.4.8 Pure ketones

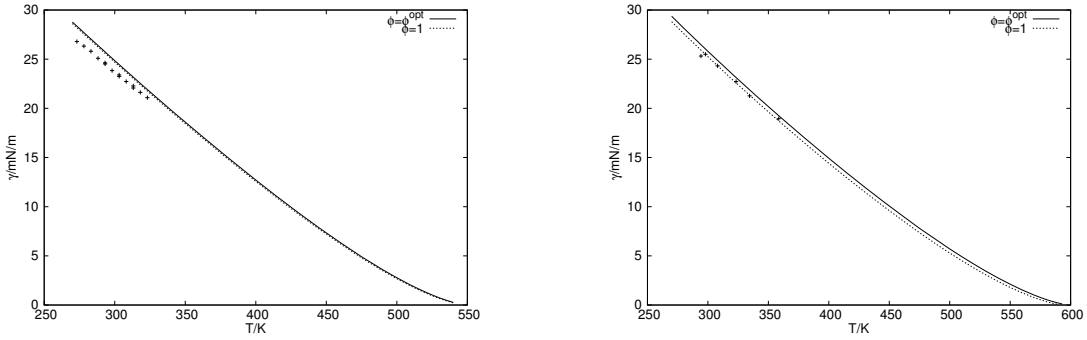

(a) (b)

Figure B.52: Calculated values of surface tension (lines) and reference data [36] [37] [38] [39] (symbols) for 2-butanone (a) and 2-hexanone (b).

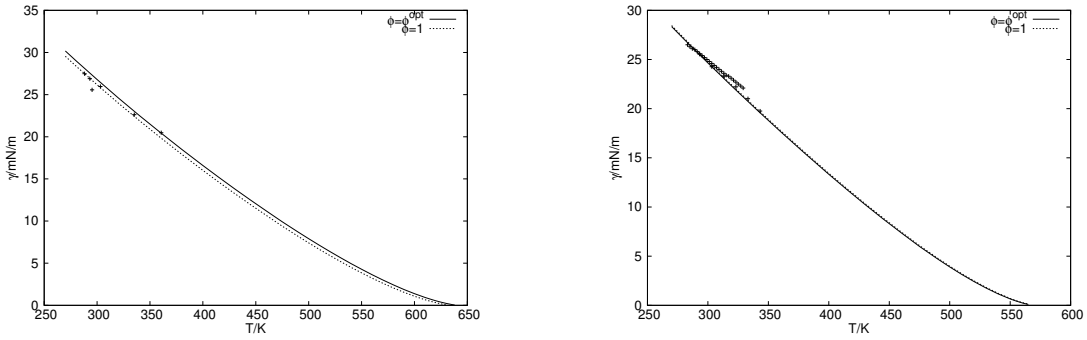

(a) (b)

Figure B.53: Calculated values of surface tension (lines) and reference data [38] [40] [41] (symbols) for 2-octanone (a) and 3-pentanone (b).

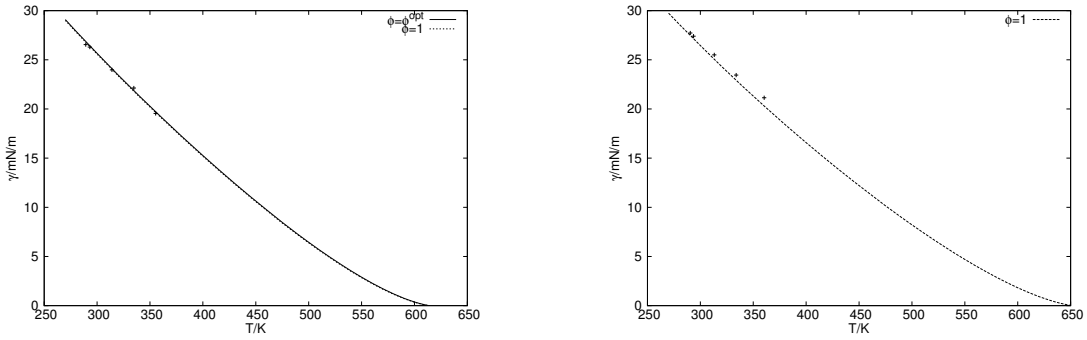

(a) (b)

Figure B.54: Calculated values of surface tension (lines) and reference data [42] (symbols) for 3-heptanone (a) and 3-nonanone (b).

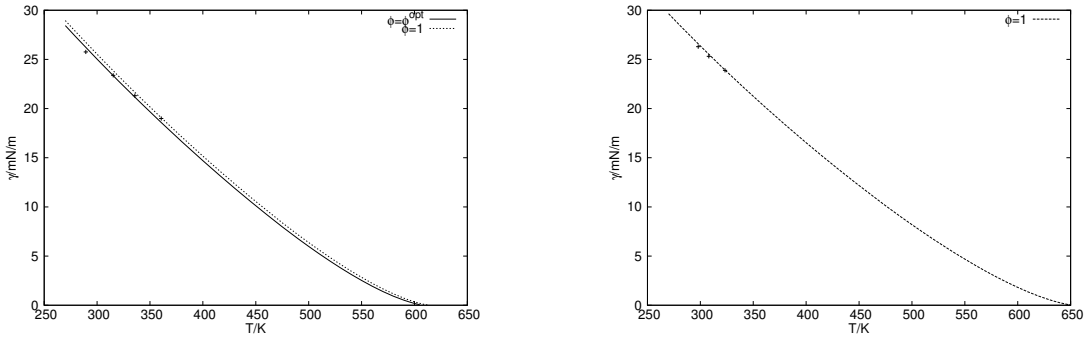

(a) (b)

Figure B.55: Calculated values of surface tension (lines) and reference data [38] [39] (symbols) for 4-heptanone (a) and 4-nonanone (b).

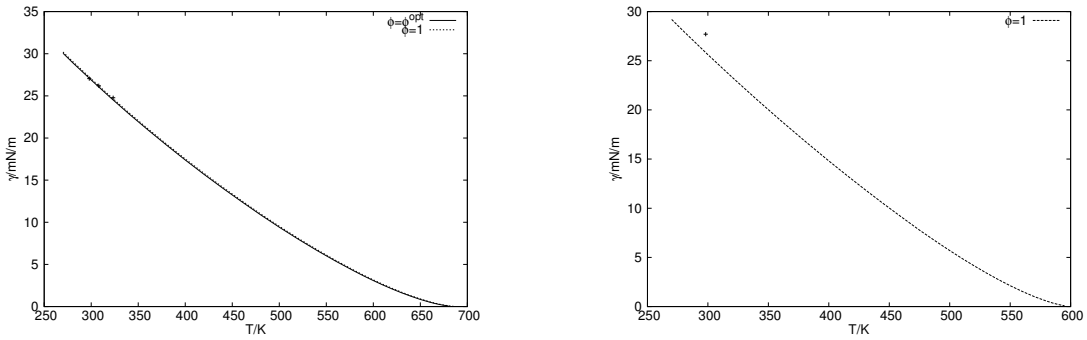

(a) (b)

Figure B.56: Calculated values of surface tension (lines) and reference data [39] [43] (symbols) for 6-undecanone (a) and 3-heptene-2-on (b).

B.4.9 Pure aldehydes

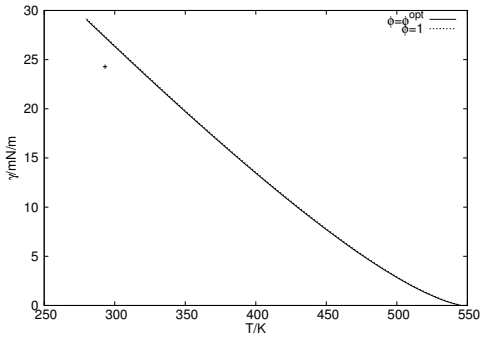

(a)

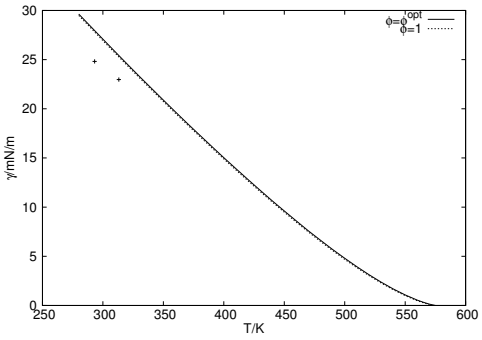

(b)

Figure B.57: Calculated values of surface tension (lines) and reference data [23] (symbols) for butanal (a) and pentanal (b).

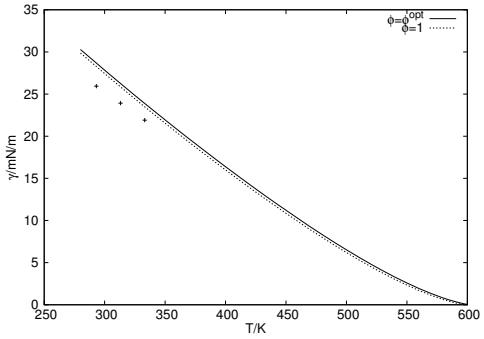

(a)

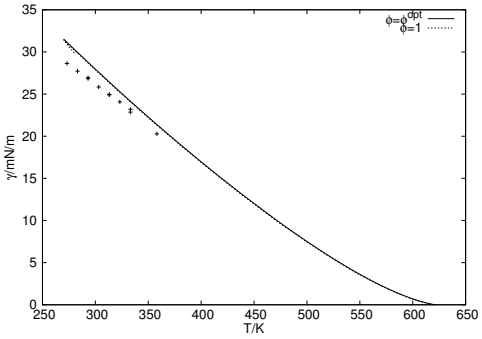

(b)

Figure B.58: Calculated values of surface tension (lines) and reference data [24] [23] (symbols) for hexanal (a) and heptanal (b).

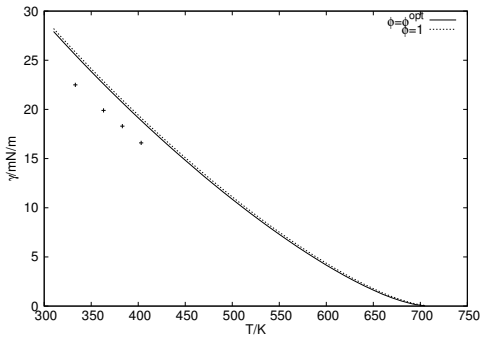

(a)

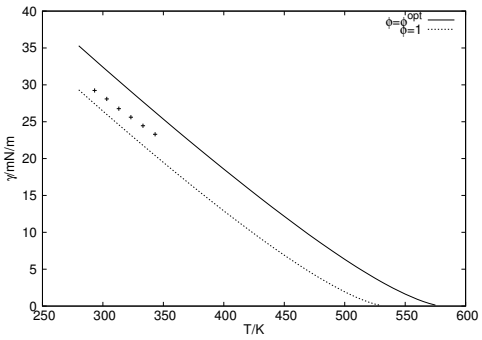

(b)

Figure B.59: Calculated values of surface tension (lines) and reference data [40] (symbols) for dodecanal (a) and 2-butenal (b).

B.5 Influence of $k_{\alpha\beta}$ parameters on the value of surface tension for mixtures

The influence of the group-group interaction parameters on surface tension results for mixtures of methane and n-alkanes as well as n-alkane mixtures is neglectable and, therfore, a graphical comparison is made only for mixtures of n-alkane and ester compounds as well as for mixtures of n-alkane and 1-alcohol compounds.

B.5.1 n-alkanes - esters

For the studied mixtures of n-alkane and ester compounds, the use of group-group interaction parameters moderately increases surface tension deviations, see fig. B.60.

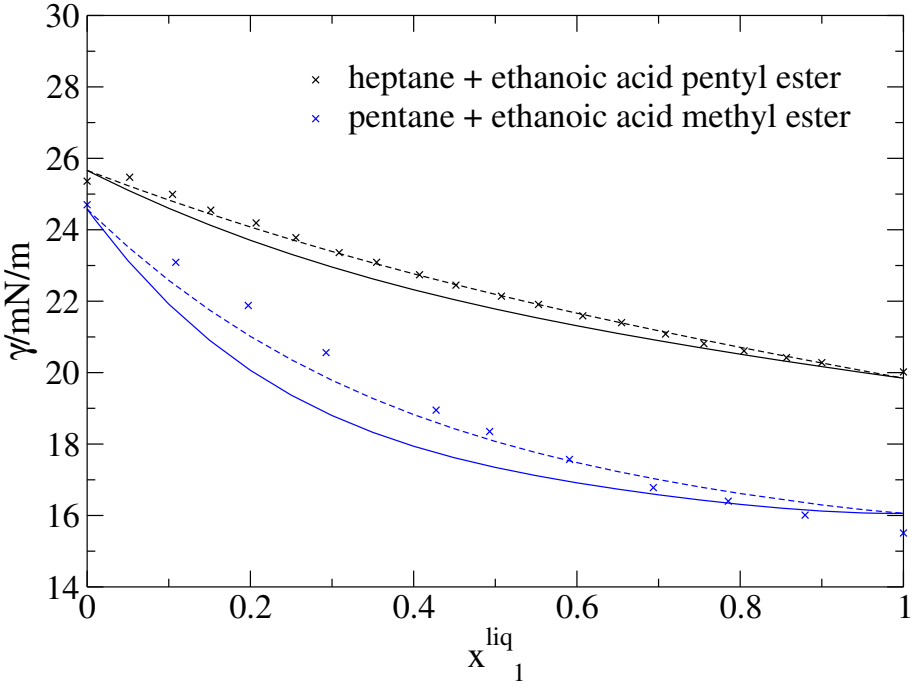

Figure B.60: Calculated values of surface tension obtained with the adjusted values of $k_{CH_3,COO}$ and $k_{CH_2,COO}$ (solid lines) and with $k_{\alpha\beta} = 0$ (dashed lines) as well as experimental data [44] [45] (symbols) for the binary mixtures heptane (1) + ethanoic acid pentyl ester (2) and pentane (1) + ethanoic acid methyl ester (2) at $T = 298.15$ K.

B.5.2 n-alkanes - 1-alcohols

For all studied n-alkane - 1-alcohol mixtures, deviations of surface tension decrease when the adjusted values of $k_{CH_3,OH}$ and $k_{CH_2,OH}$ are used, see figs. B.61, B.62 and B.63.

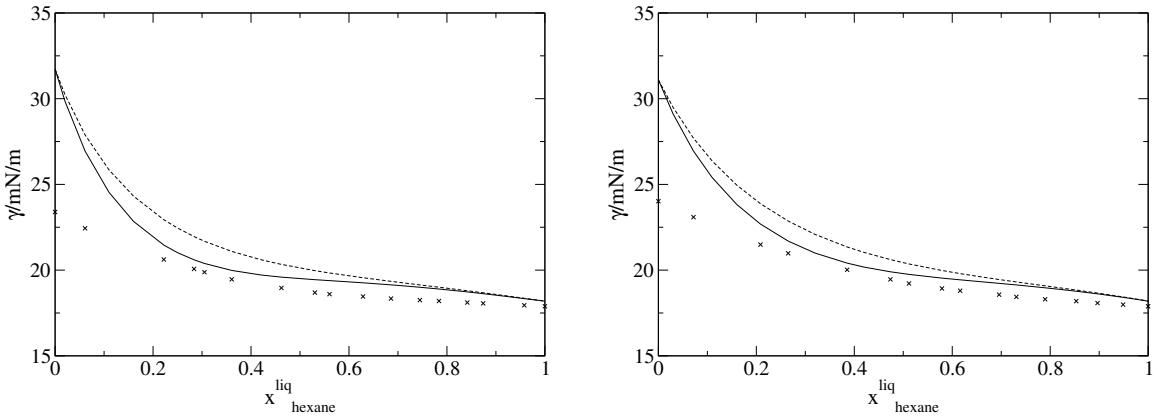

Figure B.61: Calculated values of surface tension obtained with the adjusted values of $k_{CH_3,OH}$ and $k_{CH_2,OH}$ (solid lines) and with $k_{\alpha\beta} = 0$ (dashed lines) as well as experimental data [46] (symbols) for the binary mixtures hexane + 1-propanol (a) and hexane + 1-butanol (b) at $T = 298.15$ K.

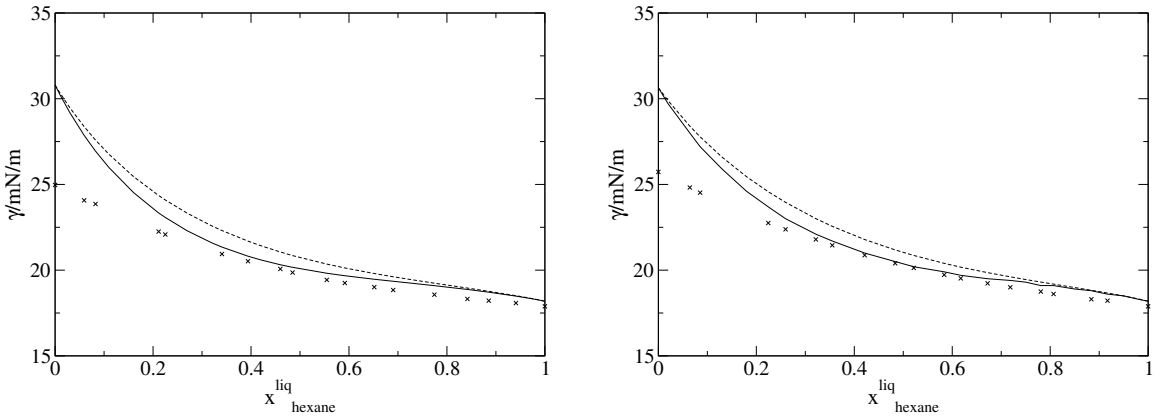

Figure B.62: Calculated values of surface tension obtained with the adjusted values of $k_{CH_3,OH}$ and $k_{CH_2,OH}$ (solid lines) and with $k_{\alpha\beta} = 0$ (dashed lines) as well as experimental data [46] (symbols) for the binary mixtures hexane + 1-pentanol (a) and hexane + 1-hexanol (b) at $T = 298.15$ K.

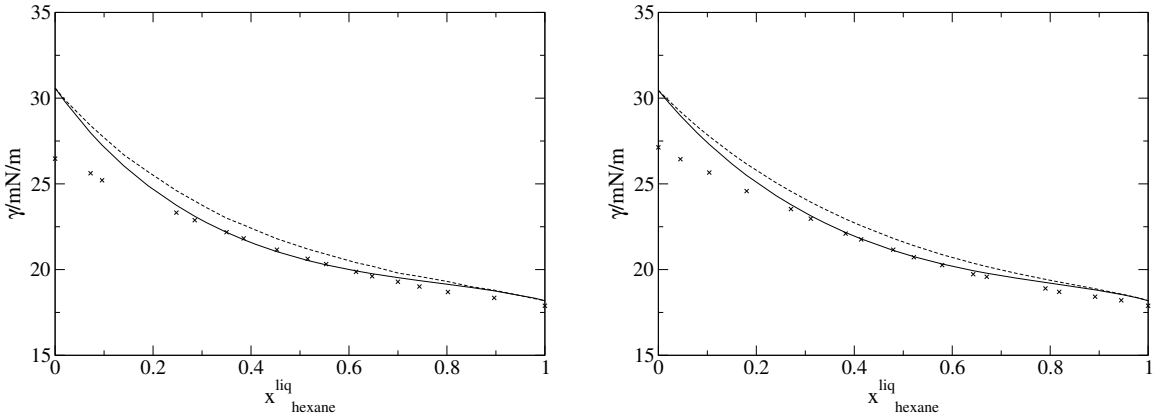

Figure B.63: Calculated values of surface tension obtained with the adjusted values of $k_{CH_3,OH}$ and $k_{CH_2,OH}$ (solid lines) and with $k_{\alpha\beta} = 0$ (dashed lines) as well as experimental data [46] (symbols) for the binary mixtures hexane + 1-heptanol (a) and hexane + 1-octanol (b) at $T = 298.15$ K.

Bibliography

[1] E. Sauer, M. Stavrou, and J. Gross, "Comparison between a homo- and a heterosegmented group contribution approach based on the perturbed-chain polar statistical associating fluid theory equation of state," *Industrial & Engineering Chemistry Research*, vol. 53, no. 38, pp. 14854–14864, 2014.

[2] S. H. Huang and M. Radosz, "Equation of state for small, large, polydisperse, and associating molecules," *Industrial & Engineering Chemistry Research*, vol. 29, no. 11, pp. 2284–2294, 1990.

[3] L. C. Kahre, "Low-temperature K data for methane-butane," *Journal of Chemical and Engineering Data*, vol. 19, no. 1, pp. 67–71, 1974.

[4] H. Wiese, J. Jacobs, and B. Sage, "Phase equilibriums in the hydrocarbon systems. phase behavior in the methane-propane-n-butane system," *Journal of Chemical and Engineering Data*, vol. 15, no. 1, pp. 82–91, 1970.

[5] H.-M. Lin, H. M. Sebastian, J. J. Simnick, and K.-C. Chao, "Gas-liquid equilibrium in binary mixtures of methane with n-decane, benzene, and toluene," *Journal of Chemical and Engineering Data*, vol. 24, no. 2, pp. 146–149, 1979.

[6] K. Bett, B. Juren, and R. Reynolds, "Physical properties of liquids and gases for plant and process design: proceedings of a symposium held at the national engineering laboratory, east kilbride, glasgow, in collaboration with the scottish branch of the institution of chemical engineers, 20th and 21st march, 1968, hm stationary office, 1970, pp," *A53–A76*, 1970.

[7] P. Rice and A. El-Nikheli, "Isothermal vapour-liquid equilibrium data for the systems n-pentane with n-hexane, n-octane and n-decane," *Fluid phase equilibria*, vol. 107, no. 2, pp. 257–267, 1995.

[8] B. S. Gupta and M.-J. Lee, "Isobaric vapor–liquid equilibrium for binary systems of toluene + o-xylene, benzene + o-xylene, nonane + benzene and nonane + heptane at 101.3kPa," *Fluid Phase Equilibria*, vol. 352, pp. 86–92, 2013.

[9] S. H. Huang, H. M. Lin, and K. C. Chao, "Solubility of carbon dioxide, methane, and ethane in n-eicosane," *Journal of Chemical and Engineering Data*, vol. 33, no. 2, pp. 145–147, 1988.

[10] P. C. Joyce, J. Gordon, and M. C. Thies, "Vapor–liquid equilibria for the hexane + tetracosane and hexane + hexatriacontane systems at elevated temperatures and pressures," *Journal of Chemical & Engineering Data*, vol. 45, no. 3, pp. 424–427, 2000.

[11] W. A. Scheller, A. R. Torres-Soto, and K. J. Daphtary, "Isothermal vapor–liquid equilibrium data for the heptane-butyl acetate system at 74.7. deg. C and 100. deg. C," *Journal of Chemical and Engineering Data*, vol. 14, no. 1, pp. 17–19, 1969.

[12] B. Marrufo, B. Rigby, J. Pla-Franco, and S. Loras, "Solvent effects on vapor–liquid equilibria of the binary system 1-hexene + n-hexane," *Journal of Chemical & Engineering Data*, vol. 57, no. 12, pp. 3721–3729, 2012.

[13] M. D. Pena and D. R. Cheda, "Liquid-vapor equilibrium. III. systems of n-propanol-n-hexane at 50. deg. and n-propanol-n-heptane at 60. deg.," *An. Quim*, vol. 66, pp. 747–755, 1970.

[14] J. Schmelzer, I. Lieberwirth, M. Krug, and R. Pfestorf, "Vapour-liquid equilibria and heats of mixing in alkane-alcohol (1) systems. I. vapour-liquid equilibria in 1-alcohol-undecane systems," *Fluid Phase Equilibria*, vol. 11, no. 2, pp. 187–200, 1983.

[15] E. W. Lemmon, M. O. McLinden, and D. G. Friend, "Thermophysical properties of fluid systems," in *NIST Chemistry WebBook, NIST Standard Reference Database Number 69* (P. J. Linstrom and W. G. Mallard, eds.), Gaithersburg MD, 20899: National Institute of Standards and Technology, 2016. http://webbook.nist.gov, (retrieved July 12, 2016).

[16] J. J. Jasper, "The surface tension of pure liquid compounds," *Journal of physical and chemical reference data*, vol. 1, no. 4, pp. 841–1010, 1972.

[17] P. P. Pugachevich and Y. A. Khvorov, "The surface tensions of heptane, undecane, hexadecane and their mixtures," *Deposited Doc. VINITI*, vol. 3893–77, pp. 1–14, 1977. In Dortmund Data Bank, 2015, www.ddbst.com.

[18] P. P. Pugachevich and V. A. Dozorov, "Experimental study of surface tension of decane, tridecane, octadecane and their solutions," *Deposited Doc. VINITI*, vol. 1282–81, pp. 1–34, 1981. In Dortmund Data Bank, 2015, www.ddbst.com.

[19] A. J. Queimada, A. I. Caco, I. M. Marrucho, and J. A. Coutinho, "Surface tension of decane binary and ternary mixtures with eicosane, docosane, and tetracosane," *Journal of Chemical & Engineering Data*, vol. 50, no. 3, pp. 1043–1046, 2005.

[20] G. Korosi and E. S. Kovats, "Density and surface tension of 83 organic liquids," *Journal of Chemical and Engineering Data*, vol. 26, no. 3, pp. 323–332, 1981.

[21] G. Somayajulu, "A generalized equation for surface tension from the triple point to the critical point," *International journal of thermophysics*, vol. 9, no. 4, pp. 559–566, 1988.

[22] F. R. Morehouse and O. Maass, "The preparation and physical properties of aliphatic acetylenes," *Canadian Journal of Research*, vol. 11, no. 5, pp. 637–643, 1934.

[23] R. Grzeskowiak, G. H. Jeffery, and A. I. Vogel, "919. physical properties and chemical constitution. part XXIX. acetylenic compounds," *Journal of the Chemical Society (Resumed)*, pp. 4719–4722, 1960.

[24] W. D. Harkins and Y. Cheng, "The orientation of molecules in surfaces. VI. cohesion, adhesion, tensile strength, tensile energy, negative surface energy, interfacial tension, and molecular attraction.," *Journal of the American Chemical Society*, vol. 43, no. 1, pp. 35–53, 1921.

[25] A. I. Vogel, "368. physical properties and chemical constitution. part XXII. some primary, secondary, and tertiary amines," *Journal of the Chemical Society (Resumed)*, pp. 1825–1833, 1948.

[26] F. Jäger, "Über die temperaturabhängigkeit der molekularen freien oberflächenenergie von flüssigkeiten im temperaturbereich von -80 bis +1650°C," *Z. Anorg. Allg. Chem.*, vol. 101, pp. 1–214, 1917.

[27] E. Shafrin and W. Zisman, "The adsorption on platinum and wettability of monolayers of terminally fluorinated octadecyl derivatives," *The Journal of Physical Chemistry*, vol. 61, no. 8, pp. 1046–1053, 1957.

[28] A. Mulero, I. Cachadiña, and M. Parra, "Recommended correlations for the surface tension of common fluids," *Journal of Physical and Chemical Reference Data*, vol. 41, no. 4, p. 043105, 2012.

[29] A. T. Gros and R. Feuge, "Surface and interfacial tensions, viscosities, and other physical properties of some n-aliphatic acids and their methyl and ethyl esters," *Journal of the American Oil Chemists' Society*, vol. 29, no. 8, pp. 313–317, 1952.

[30] S. Mumford and J. Phillips, "19. the physical properties of some aliphatic compounds," *Journal of the Chemical Society (Resumed)*, pp. 75–84, 1950.

[31] A. I. Vogel, "130. physical properties and chemical constitution. part XIII. aliphatic carboxylic esters," *Journal of the Chemical Society (Resumed)*, pp. 624–4644, 1948.

[32] G. H. Jeffery and A. I. Vogel, "133. physical properties and chemical constitution. part XVI. ethylenic compounds," *Journal of the Chemical Society (Resumed)*, pp. 658–673, 1948.

[33] G. H. Jeffery and A. I. Vogel, "134. physical properties and chemical constitution. part XVII. acetylenic compounds and cyanides," *Journal of the Chemical Society (Resumed)*, pp. 674–683, 1948.

[34] S. Bi, G. Zhao, and J. Wu, "Surface tension of diethyl ether, diisopropyl ether, and dibutyl ether," *Journal of Chemical & Engineering Data*, vol. 55, no. 4, pp. 1523–1526, 2009.

[35] A. I. Vogel, "129. physical properties and chemical constitution. part XII. ethers and acetals," *Journal of the Chemical Society (Resumed)*, pp. 616–624, 1948.

[36] K. Habrdová, Š. Hovorka, and L. Bartovská, "Concentration dependence of surface tension for very dilute aqueous solutions of organic nonelectrolytes," *Journal of Chemical & Engineering Data*, vol. 49, no. 4, pp. 1003–1007, 2004.

[37] R. Wanchoo and J. Narayan, "Some physical properties of binary liquid systems:(2-butanone + n-propionic acid or n-butyric acid)," *Physics and Chemistry of Liquids*, vol. 27, no. 3, pp. 159–167, 1994.

[38] D. M. Cowan, G. H. Jeffery, and A. I. Vogel, "31. physical properties and chemical constitution. part V. alkyl ketones," *Journal of the Chemical Society (Resumed)*, pp. 171–176, 1940.

[39] K. Owen, O. R. Quayle, and W. J. Clegg, "A study of organic parachors. V. constitutive variations of the parachors of a series of normal ketones," *Journal of the American Chemical Society*, vol. 64, no. 6, pp. 1294–1296, 1942.

[40] A. Baglai, L. Gurarii, and G. G. Kuleshov, "Physical properties of compounds used in vitamin synthesis," *Journal of Chemical and Engineering Data*, vol. 33, no. 4, pp. 512–518, 1988.

[41] N. G. Tsierkezos and I. E. Molinou, "Conductivity studies of n-tetrabutylammonium tetraphenylborate in 3-pentanone in the temperature range from 283.15 to 329.15K," *Journal of solution chemistry*, vol. 36, no. 2, pp. 153–170, 2007.

[42] A. I. Vogel, "128. physical properties and chemical constitution. part XI. ketones," *Journal of the Chemical Society (Resumed)*, pp. 610–615, 1948.

[43] A. Doeuvre, "About mesityl oxide and some halogen derivatives," *Bull. Soc. Chim. Fr.*, pp. 1594–1600, 1926.

[44] A. A. Rafati and E. Ghasemian, "Experimental and theoretical study of surface tension of binary mixtures of (n-alkyl acetates + heptane, benzene, and toluene)," *The Journal of Chemical Thermodynamics*, vol. 41, no. 3, pp. 386–391, 2009.

[45] M. L. De Soria, J. L. Zurita, M. A. Postigo, and M. Katz, "Excess thermodynamic properties of the n-pentane + methylacetate system at 298.15K," *Thermochimica acta*, vol. 130, pp. 249–258, 1988.

[46] E. Jiménez, H. Casas, L. Segade, and C. Franjo, "Surface tensions, refractive indexes and excess molar volumes of hexane + 1-alkanol mixtures at 298.15K," *Journal of Chemical & Engineering Data*, vol. 45, no. 5, pp. 862–866, 2000.